

ความสัมพันธ์ระหว่างโครงสร้างและหน้าที่ของแอมิโลมอลเทส
จาก *Corynebacterium glutamicum*

นางสาวสุทิพาพรรณ ตุ่มหอม



จุฬาลงกรณ์มหาวิทยาลัย

CHULALONGKORN UNIVERSITY

บทคัดย่อและแฟ้มข้อมูลฉบับเต็มของวิทยานิพนธ์ตั้งแต่ปีการศึกษา 2554 ที่ให้บริการในคลังปัญญาจุฬาฯ (CUIR)
เป็นแฟ้มข้อมูลของนิสิตเจ้าของวิทยานิพนธ์ ที่ส่งผ่านทางบัณฑิตวิทยาลัย

The abstract and full text of theses from the academic year 2011 in Chulalongkorn University Intellectual Repository (CUIR)
are the thesis authors' files submitted through the University Graduate School.

วิทยานิพนธ์นี้เป็นส่วนหนึ่งของการศึกษาตามหลักสูตรปริญญาวิทยาศาสตรดุษฎีบัณฑิต

สาขาวิชาชีวเคมีและชีววิทยาโมเลกุล ภาควิชาชีวเคมี

คณะวิทยาศาสตร์ จุฬาลงกรณ์มหาวิทยาลัย

ปีการศึกษา 2559

ลิขสิทธิ์ของจุฬาลงกรณ์มหาวิทยาลัย

STRUCTURE AND FUNCTION RELATIONSHIP OF AMYLOMALTASE FROM

Corynebacterium glutamicum

Miss Suthipapun Tumhom



A Dissertation Submitted in Partial Fulfillment of the Requirements
for the Degree of Doctor of Philosophy Program in Biochemistry and Molecular
Biology

Department of Biochemistry

Faculty of Science

Chulalongkorn University

Academic Year 2016

Copyright of Chulalongkorn University

Thesis Title	STRUCTURE AND FUNCTION RELATIONSHIP OF AMYLOMALTASE FROM <i>Corynebacterium glutamicum</i>
By	Miss Suthipapun Tumhom
Field of Study	Biochemistry and Molecular Biology
Thesis Advisor	Professor Piamsook Pongsawasdi, Ph.D.
Thesis Co-Advisor	Assistant Professor Kuakarun Krusong, Ph.D.

Accepted by the Faculty of Science, Chulalongkorn University in Partial
Fulfillment of the Requirements for the Doctoral Degree

..... Dean of the Faculty of Science
(Associate Professor Polkit Sangvanich, Ph.D.)

THESIS COMMITTEE

..... Chairman
(Associate Professor Teerapong Buaboocha, Ph.D.)

..... Thesis Advisor
(Professor Piamsook Pongsawasdi, Ph.D.)

..... Thesis Co-Advisor
(Assistant Professor Kuakarun Krusong, Ph.D.)

..... Examiner
(Assistant Professor Rath Pichyangkura, Ph.D.)

..... Examiner
(Assistant Professor Kanoktip Packdibamrung, Ph.D.)

..... External Examiner
(Associate Professor Jarunee Kaulpiboon, Ph.D.)

สุทิพาพรหม ตุ่มหอม : ความสัมพันธ์ระหว่างโครงสร้างและหน้าที่ของแอมิโลมอลเตสจาก *Corynebacterium glutamicum* (STRUCTURE AND FUNCTION RELATIONSHIP OF AMYLOMALTASE FROM *Corynebacterium glutamicum*) อ.ที่ปรึกษาวิทยานิพนธ์หลัก: ศ. ดร. เปี่ยมสุข พงษ์สวัสดิ์, อ.ที่ปรึกษาวิทยานิพนธ์ร่วม: ผศ. ดร. เกื้อการุณย์ ครูส่ง, 212 หน้า.

แอมิโลมอลเตส (EC 2.4.1.25) เร่งปฏิกิริยาการโยกย้ายหมู่กลูโคซิลภายในหรือระหว่างสายโมเลกุลของกลูแคนทำให้เกิดไซโคลเดกซ์ทรินวงใหญ่ (LR-CD) และออลิโกแซ็กคาไรด์สายตรงตามลำดับ งานวิจัยนี้ต้องการศึกษาความสัมพันธ์ระหว่างโครงสร้างและหน้าที่ของแอมิโลมอลเตสจาก *Corynebacterium glutamicum* (CgAM) โดยทำการกลายพันธุ์เฉพาะตำแหน่งที่กรดอะมิโน Y418 (อยู่บริเวณปลาย loop 410s ที่ปกคลุมบริเวณเร่ง) ตำแหน่ง H461 (ในบริเวณเร่ง) และตำแหน่ง 287 (ในบริเวณ second glucan binding) จากการเปรียบเทียบสมบัติทางชีวเคมีของเอนไซม์กลายที่ทำให้บริสุทธิ์กับเอนไซม์ดั้งเดิม (WT) พบว่าเอนไซม์ทุกรูปแบบมีขนาด 84 kDa มีภาวะเหมาะสมที่ 40 °C pH 6.0 และ 30 °C pH 6.0 สำหรับปฏิกิริยาคิสพอร์พอร์ชันเนชันและไซโคลเซชันตามลำดับ เอนไซม์ WT เอนไซม์กลาย Y418 และ N287 มีความจำเพาะต่อซับสเตรดเหมือนกัน คือ ซอบมอลโทไทรโอส ในขณะที่เอนไซม์กลาย H461 ซอบมอลโทส โดยการกลายเฉพาะตำแหน่ง ทำให้ทรานส์กลูโคซิลเอชันแอกทิวิตีของเอนไซม์กลายลดลงอย่างเห็นได้ชัด โดยเฉพาะไซโคลเซชันแอกทิวิตีของเอนไซม์กลาย H461 หายไป โดยประสิทธิภาพในการเร่งปฏิกิริยา, k_{cat}/K_m ของเอนไซม์กลายทุกชนิดต่ำกว่า WT จากการลดลงของ k_{cat} ในปฏิกิริยาคิสพอร์พอร์ชันเนชันและไซโคลเซชัน ในขณะที่ K_m ของเอนไซม์กลาย Y418 ไม่แตกต่างจาก WT แต่ค่า K_m ของเอนไซม์กลาย H461 และ N287 สูงกว่า WT ในปฏิกิริยาคิสพอร์พอร์ชันเนชัน และเมื่อใช้แป้งถั่วเป็นซับสเตรดในปฏิกิริยาไซโคลเซชันพบว่า K_m ของเอนไซม์กลาย Y418 และ N287 สูงกว่า WT และมีการเปลี่ยนแปลงขนาดและผลผลิตผลิตภัณฑ์ LR-CD โดยพบว่าเอนไซม์กลายทุกตัวให้ปริมาณ LR-CD ที่ลดลงด้วยเมื่อเทียบกับ WT และเอนไซม์กลาย Y418A/S/D ให้ขนาดผลิตภัณฑ์ที่ใหญ่ขึ้น (CD36 - CD40) เอนไซม์กลาย Y418R และ W ให้ช่วงขนาดผลิตภัณฑ์ที่กว้าง ขณะที่เอนไซม์กลาย N287A/S/D/R และ W ให้ขนาดผลิตภัณฑ์ CD ที่เล็กลง (CD26 - CD28) เมื่อเทียบกับ WT (CD29-CD33) จากการวิเคราะห์ CD spectra พบว่าการกลายไม่มีผลเปลี่ยนแปลงโครงสร้างทุติยภูมิของเอนไซม์ เมื่อทำการศึกษาสมบัติชีวฟิสิกส์ของเอนไซม์ด้วยวิธี ITC และ DSC พบว่า เอนไซม์ WT ผลิตความร้อนได้มากกว่าเอนไซม์กลาย Y418A/W ในปฏิกิริยาคิสพอร์พอร์ชันเนชันและเกิดภาวะการยับยั้งด้วยผลิตภัณฑ์เมื่อเพิ่มความเข้มข้นของมอลโทไทรโอส จากการศึกษารายละเอียดความร้อนของเอนไซม์ด้วยเทคนิค DSC พบว่าเอนไซม์ WT และ Y418A มีค่า Peak temperature (T_p) ที่คล้ายกัน ในขณะที่เอนไซม์กลาย Y418W มีค่า T_p ต่ำกว่า 4 °C นั่นคือ เอนไซม์ WT และ Y418A มีความเสถียรต่ออุณหภูมิมากกว่าเอนไซม์กลาย Y418W เราได้สร้างโครงสร้างจำลองของเอนไซม์กลายโดยใช้โครงสร้างผลึกเอนไซม์ WT เป็นต้นแบบ เพื่อใช้ช่วยอธิบายสมบัติของเอนไซม์ที่เปลี่ยนไปเมื่อทำการกลาย จากผลการทดลองทั้งหมด สรุปได้ว่า ทั้ง 3 ตำแหน่งสำคัญต่อแอกทิวิตีของเอนไซม์ในระดับที่ต่างกัน โดยตำแหน่ง Y418 ต้องคงปฏิสัมพันธ์ไฮโดรโฟบิกและขนาดทางเข้าที่เหมาะสมของซับสเตรดในบริเวณ loop ส่วนตำแหน่ง N287 ต้องคงโซ่ข้างประจุบวก โดยทั้ง 2 ตำแหน่งนี้ควบคุมขนาดผลิตภัณฑ์และปริมาณ LR-CDs ด้วย ในขณะที่ H461 มีความจำเป็นต่อการเร่งปฏิกิริยาโดยเฉพาะปฏิกิริยาไซโคลเซชัน

ภาควิชา ชีวเคมี

ลายมือชื่อผู้นิสิต

สาขาวิชา ชีวเคมีและชีววิทยาโมเลกุล

ลายมือชื่อ อ.ที่ปรึกษาหลัก

ปีการศึกษา 2559

ลายมือชื่อ อ.ที่ปรึกษาร่วม

5472910723 : MAJOR BIOCHEMISTRY AND MOLECULAR BIOLOGY

KEYWORDS: AMYLOMALTASE / 410S LOOP / ACTIVE SITE / SECOND BINDING GLUCAN / SITE-DIRECTED MUTAGENESIS / TRANSGLUCOSYLATION / LARGE-RING CYCLODEXTRIN

SUTHIPAPUN TUMHOM: STRUCTURE AND FUNCTION RELATIONSHIP OF AMYLOMALTASE FROM *Corynebacterium glutamicum*. ADVISOR: PROF. PIAMSOOK PONGSAWASDI, Ph.D., CO-ADVISOR: ASST. PROF. KUAKARUN KRUSONG, Ph.D., 212 pp.

Amylomaltase (EC 2.4.1.25) catalyzes intramolecular and intermolecular transglucosylation reactions of glucan to yield large-ring cyclodextrin (LR-CD) and linear oligosaccharide products, respectively. The aim of this work is to investigate structure and function relationship of amylomaltase from *Corynebacterium glutamicum* (CgAM). Three target amino acid residues of CgAM, Y418 (at the tip of 410s loop which lies over the active site), H461 (in active site) and N287 (in second glucan binding site) were selected for site-directed mutagenesis. Biochemical characterization of all purified mutated CgAMs were compared to wild-type (WT). All enzymes had an approximate size of 84 kDa on SDS-PAGE, the same optimum temperature and pH of 40 °C, pH 6.0 and 30 °C, pH 6.0 for disproportionation and cyclization reactions, respectively. For substrate specificity in disproportionation reaction of WT, Y418 and N287 mutated CgAMs preferred maltotriose while maltose was suitable for H461 mutants. Significant decrease in transglucosylation activities of mutated CgAMs was observed especially cyclization activity which was lost in H461 mutants. The catalytic efficiency, k_{cat}/K_m values of all mutated CgAMs were lower than that of WT, mainly due to the significant decrease in k_{cat} for disproportionation and cyclization reactions. K_m values of Y418 mutants were not changed much while values of H461 and N287 mutants were higher than WT. In addition, K_m values of Y418 and N287 mutants were higher than WT with pea starch substrate in cyclization reaction. The changes in size and yield of LR-CD products were observed as the result of Y418 and N287 mutations. Y418A/S/D mutated CgAMs gave a larger CD size (CD36 - CD40), Y418R/W showed a broad product pattern while N287A/S/D/R/W gave a smaller size (CD26 - CD28), all mutated enzymes showed lower product yield in comparison to WT with CD29-CD33 as main products. The secondary structure of all enzymes as analyzed was not significantly changed upon mutations. Biophysical properties of WT and Y418A/W CgAMs were determined by ITC and DSC techniques. Heat production of WT was higher than those of Y418A/W in disproportionation reaction. The product inhibition was occurred as a result of increase in maltotriose concentration. The heat capacity profile from DSC showed that peak temperatures (T_p) of WT and Y418A were similar while a shift of T_p of Y418W towards 4 °C lower was observed. The results indicated that WT and Y418A showed higher stability than Y418W CgAM. The model structures of mutated CgAMs were constructed using WT X-ray structure as template in order to help explain change in properties upon mutation. The overall results suggested that all three residues of CgAM are important for enzyme activity to a different extent. Y418 has to retain hydrophobic interactions and the suitable distance of loop channel for substrate entering, N287 should remain positively charge side chain. Both positions are also involved in controlling the amount and size of LR-CD products. While H461 is essential for enzyme catalysis especially in cyclization reaction.

Department: Biochemistry

Field of Study: Biochemistry and Molecular Biology

Academic Year: 2016

Student's Signature

Advisor's Signature

Co-Advisor's Signature

ACKNOWLEDGEMENTS

I would like to express my greatest gratitude to my advisor, Professor Dr. Piamsook Pongsawasdi for her kindness, generous advices, guidance, attention, stimulating discussion and support throughout this thesis, she is the best supervisor a student could ask for. She consistently exceeded my expectations and I consider myself lucky to have had the opportunity working with her. My gratitude is also extended to Assistant Professor Dr. Kaukarun Krusong; my co-advisor for her valuable comments. Sincere thanks and appreciation are due to Associated Professor Dr. Teerapong Buaboocha, Assistant Professor Dr. Kanoktip Pakdeebungrung, Assistant Professor Dr. Rath Pichyangkura and Associated Professor Dr. Jarunee Kaulpiboon for their valuable suggestions and comments and also dedicating valuable time for thesis examination. Special thanks to my collaborators, Professor Dr. Etsuko Katoh at Advanced Analysis Center, National Agriculture and Food Research Organization, Japan and Professor Dr. Shun-ichi Kidokoro at Department of Bioengineering, Faculty of Engineering, Nagaoka University of Technology, Japan for ITC and DSC instruments in biophysical part and also their technical advices and training. My appreciated is also expressed to all members not only in the Starch and Cyclodextrin Research Unit especially to Dr. Pitchanan Nimpiboon but also other laboratory members; Dr. Apiradee Potipongsa, Dr. Aporn Bualuang and Miss Khanistha Samasil for their supports and understanding throughout the study.

Finally, the greatest gratitude was dedicated to my family, especially to my brother who passed away for their infinite love, encouragement, understanding and everything giving to my life. ST was supported by Science Achievement Scholarship of Thailand (SAST). Financial supports from the IIAC of CU Centenary Academic Development Project, the TRF Grant IRG 5780008, the 90th anniversary of Ratchadaphiseksomphot Endowment Fund and the Oversea Research Experience Scholarship form Graduate school and Faculty of Science, Chulalongkorn University are acknowledged.

CONTENTS

	Page
THAI ABSTRACT	iv
ENGLISH ABSTRACT.....	v
ACKNOWLEDGEMENTS	vi
CONTENTS.....	vii
LIST OF TABLES	xiii
LIST OF FIGURES	xv
LIST OF ABBREVIATIONS.....	xxi
CHAPTER I INTRODUCTION.....	1
1.1 Starch converting enzymes	1
1.2 The 4- α glucanotransferase.....	2
1.3 Amylomaltase (AM).....	3
1.4 Large-ring cyclodextrins (LR-CDs)	4
1.5 Applications of LR-CDs and amylomaltase	5
1.6 <i>Corynebacterium glutamicum</i>	7
1.7 Structure of Amylomaltase from <i>C. glutamicum</i>	16
1.7.1 Structural comparison of CgAM with other amylomaltases	18
1.8 Objectives	21
CHAPTER II MATERIALS AND METHODS.....	27
2.1 Equipments	27
2.2 Chemicals	29
2.3 Enzymes, Restriction enzymes and Bacterial strains.....	32
2.4 Construction of mutated amylomaltase gene from <i>C. glutamicum</i>	32
2.4.1 Selection of target amino acid residues	32
2.4.2 Site-directed mutagenesis of CgAM gene	33
2.4.3 Preparation of competent cells for electroporation	34
2.4.4 Plasmid transformation.....	38
2.4.5 Selection of mutated transformant clones	38
2.4.6 Nucleotide sequencing	38

	Page
2.5 Expression and purification of recombinant amyloamylase.....	39
2.5.1 Expression of amyloamylase in <i>E. coli</i>	39
2.5.2 Purification of amyloamylases	40
2.6 Polyacrylamide gel electrophoresis (PAGE)	40
2.6.1 SDS-Polyacrylamide gel electrophoresis (SDS-PAGE)	40
2.6.2 Detection of protein bands by Coomassie blue staining	41
2.7 Protein determination.....	41
2.8 Enzyme assay.....	41
2.8.1 Starch transglucosylation activity	41
2.8.2 Disproportionation activity.....	42
2.8.3 Starch degrading activity.....	42
2.8.4 Cyclization activity.....	43
2.8.5 Coupling activity	44
2.8.6 Hydrolytic activity.....	44
2.9 Characterization of amyloamylase	45
2.9.1 Effect of temperature on amyloamylase activity.....	45
2.9.2 Effect of pH on amyloamylase activity.....	45
2.9.3 Effect of temperature on amyloamylase stability.....	45
2.9.4 Effect of pH on amyloamylase stability	46
2.9.5 Substrate specificity	46
2.9.6 Determination of kinetic parameters	46
2.9.6.1 Disproportionation reaction.....	46
2.9.6.2 Cyclization reaction.....	47
2.9.7 Analysis of pattern of LR-CD products	47
2.9.7.1 Effect of incubation time on LR-CD profile	47
2.9.7.2 Effect of the amount of enzyme on LR-CD profile.....	47
2.9.8 Circular dichroism spectra.....	48
2.10 Biophysical characterization of amyloamylase	49

	Page
2.10.1 Isothermal titration calorimetry (ITC).....	49
2.10.2 Kinetic measurements by ITC	50
2.10.3 Differential scanning calorimetry (DSC)	50
2.11 Structural Modeling	51
CHAPTER III RESULTS	52
3.1 Construction of mutated amyloamylase gene from <i>C. glutamicum</i>	52
3.1.1 Selection of target amino acid residues of CgAM	52
3.1.2 Extraction of recombinant plasmid pET - 19b - CgAM	53
3.1.3 Site-directed mutagenesis of CgAM gene	53
3.1.4 Transformation	54
3.1.5 Nucleotide sequencing	54
3.2 Expression and purification of Y418 mutated amyloamylases	78
3.3 Effect of Y418 mutation on enzyme characteristics.....	82
3.3.1 Various amyloamylase activities.....	82
3.3.2 Optimum conditions and stability	82
3.3.2.1 Effect of temperature on CgAM activity.....	82
3.3.2.2 Effect of pH on CgAM activity	83
3.3.2.3 Effect of temperature stability of CgAM	83
3.3.2.4 Effect of pH stability of CgAM.....	84
3.3.3 Substrate specificity	84
3.3.4 Determination of kinetic parameters	84
3.3.4.1 Kinetic study of disproportionation reaction.....	84
3.3.4.2 Kinetic study of cyclization reaction.....	85
3.3.5 Analysis of pattern of LR-CDs products.....	85
3.3.5.1 Effect of incubation time	85
3.3.5.2 Effect of unit enzyme	86
3.3.6 Enzyme conformation	98
3.3.7 Isothermal titration calorimetry (ITC).....	98
3.3.8 Differential scanning calorimetry (DSC)	99

	Page
3.4 Structural modeling of Y418 mutated CgAMs	99
3.5 Expression and purification of H461 mutated CgAMs	111
3.6 Effect of H461 mutation on enzyme characteristics	115
3.6.1 Various amylomaltase activities	115
3.6.2 Optimum conditions and stability	115
3.6.2.1 Effect of temperature on CgAM activity	115
3.6.2.2 Effect of pH on CgAM activity	115
3.6.2.3 Effect of temperature on CgAM stability	119
3.6.2.4 Effect of pH on CgAM stability	119
3.6.3 Substrate specificity	119
3.6.4 Determination of kinetic parameters	120
3.6.5 Analysis of LR-CD products	120
3.6.6 Enzyme conformation	120
3.7 Structural modeling of H461 mutated CgAM	121
3.8 Expression and purification of N287 mutated CgAMs	130
3.9 Effect of N287 mutation on enzyme characteristics	130
3.9.1 Various amylomaltase activities	130
3.9.2 Optimum conditions and stability	131
3.9.2.1 Effect of temperature on CgAM activity	131
3.9.2.2 Effect of pH on CgAM activity	131
3.9.2.3 <i>Effect of temperature on CgAM stability</i>	138
3.9.2.4 Effect of pH on CgAM stability	138
3.9.3 Substrate specificity	138
3.9.4 Determination of kinetic parameters	139
3.9.4.1 Kinetic study of disproportionation reaction	139
3.9.4.2 Kinetic study of cyclization reaction	139
3.9.5 Analysis of LR - CD products	139
3.9.5.1 Effect of incubation time	140
3.9.5.2 Effect of unit enzyme	140

	Page
3.9.6 Enzyme conformation	149
3.10 Structural modeling of N287 mutated <i>CgAM</i>	149
CHAPTER IV DISCUSSION.....	152
4.1 Construction of mutated amyloamylase genes from <i>C. glutamicum</i>	153
4.1.1 Selection of target amino acid residues of <i>CgAM</i>	153
4.1.2 Mutation of <i>CgAM</i> gene using site-directed mutagenesis.....	154
4.2 Expression and purification of the recombinant WT and mutated <i>CgAMs</i>	155
4.3 Characterization of mutated <i>CgAMs</i>	156
4.3.1 Various activities of amyloamylase	156
4.3.2 Substrate specificity and kinetic values.....	158
4.3.3 LR-CD products profile.....	163
4.3.4 Secondary structure	164
4.3.5 Isothermal titration calorimetry (ITC) and Differential scanning calorimetry (DSC)	164
4.4 The proposed model structures of mutated <i>CgAMs</i>	167
CHAPTER V CONCLUSIONS	172
REFERENCES	174
APPENDICES	187
APPENDIX 1: Preparation of polyacrylamide gel electrophoresis.....	188
APPENDIX 2: Preparation of agarose electrophoresis	191
APPENDIX 3: Preparation for buffers solutions.....	191
APPENDIX 4: Preparation of solution for cell preparation and enzyme purification	193
APPENDIX 5: Preparation of Iodine solution.....	194
APPENDIX 6: Preparation of Bradford solution	195
APPENDIX 7: Preparation for Bicinchoninic acid (BCA) assay.....	195
APPENDIX 8: Preparation for DNS reagent.....	196
APPENDIX 9: Bacterial media culture	197

	Page
APPENDIX 10: Ampicillin antibiotic	197
APPENDIX 11: Standard curve for protein determination by Bradford's method	198
APPENDIX 12: Standard curve for glucose determination by glucose oxidase assay	198
APPENDIX 13: Standard curve for starch degrading activity assay.....	199
APPENDIX 14: Standard curve for glucose determination by Bicinchoninic acid assay.....	199
APPENDIX 15: Restriction map of pET-19b vector	200
APPENDIX 16: Structure of amino acids commonly found in protein	201
APPENDIX 17: Abbreviation of amino acid residues	202
APPENDIX 18: Amino acid sequences alignment of amyloamaltases	203
APPENDIX 19: HPAEC profile of standard 0.8 mg/ml LR-CD	206
APPENDIX 20: Isothermal titration calorimetry (ITC)	207
APPENDIX 21: Differential scanning calorimetry (DSC).....	209
APPENDIX 22: Heat production of amyloamaltase from disproportionation reaction detected by ITC technique	211
VITA	212

LIST OF TABLES

	Page
Table 1.1 Enzymes belonging to the α -amylase family.	8
Table 1.2 Physicochemical properties of native small-ring CDs and LR-CDs.....	12
Table 1.3 Studies of inclusion complex formation between purified LR-CD or mixture of LR-CDs and guest molecules.....	13
Table 2.1 Y418 mutated <i>CgAM</i> gene primers.....	35
Table 2.2 H461 mutated <i>CgAM</i> gene primers.....	36
Table 2.3 N287 mutated <i>CgAM</i> gene primers.....	37
Table 3.1 Purification of WT and Y418 mutated <i>CgAMs</i> assayed by starch transglucosylation activity.....	80
Table 3.2 Purification of WT and Y418 mutated <i>CgAMs</i> assayed by disproportionation activity.....	81
Table 3.3 Activities of WT and Y418 mutated <i>CgAMs</i>	87
Table 3.4 Kinetic parameters of WT and Y418 mutated <i>CgAMs</i> from disproportionation reaction using maltotriose substrate.....	93
Table 3.5 Kinetic parameters of WT and Y418 mutated <i>CgAMs</i> from cyclization activity.....	94
Table 3.6 Kinetic parameters of WT, Y418A and Y418W <i>CgAMs</i> from disproportionation activity determined by ITC.....	103
Table 3.7 Peak temperature of WT, Y418A and Y418W <i>CgAMs</i> at different scan rate of DSC measurements.....	106
Table 3.8 Distance between amino acids at position 418 and F534 of WT and Y418 mutated <i>CgAMs</i>	110

Page

Table 3.9 Purification of WT and H461 mutated <i>Cg</i> AMs assayed by starch transglucosylation activity	113
Table 3.10 Purification of WT and H461 mutated <i>Cg</i> AMs assayed by disproportionation activity	114
Table 3.11 All activities of H461 mutated <i>Cg</i> AMs	116
Table 3.12 Kinetic parameters of WT and H461 mutated <i>Cg</i> AMs from the disproportionation reaction	125
Table 3.13 Purification of WT and N287 mutated <i>Cg</i> AMs assayed by starch transglucosylation activity	133
Table 3.14 Purification of WT and N287 mutated <i>Cg</i> AMs assayed by disproportionation activity	134
Table 3.15 All activities of N287 mutated <i>Cg</i> AMs	135
Table 3.16 Kinetic parameters of WT and N287 mutated <i>Cg</i> AMs from the disproportionation reaction	144
Table 3.17 Kinetic parameters of WT and N287 mutated <i>Cg</i> AMs from cyclization reaction.....	145

LIST OF FIGURES

	Page
Figure 1.1 The different enzymes involved in the degradation of starch.	8
Figure 1.2 Model of action of amyломaltase on linear and cyclic α -1,4 glucans. ...	9
Figure 1.3 Schematic presentation of α -CD.....	10
Figure 1.4 Solid state structure of LR-CDs (CD26).. ..	11
Figure 1.5 A pathway of maltose and glycogen degradation in <i>E. coli</i>	15
Figure 1.6 The amino acid sequence alignment of amyломaltases.....	22
Figure 1.7 The domain identification of <i>CgAM</i>	23
Figure 1.8 Comparison of N-domains of amyломaltases.	24
Figure 1.9 Active site of <i>CgAM</i>	25
Figure 1.10 Structure of amyломaltase from <i>C. glutamicum</i> (<i>CgAM</i>).....	26
Figure 1.11 Ribbon representation (stereo view) of the fold of amyломaltase <i>T. aquaticus</i> (<i>TaAM</i>) with acarbose.. ..	27
Figure 1.12 Proposed binding of maltoheptaose (G7) in the active site of amylo maltase from <i>Thermus thermophilus</i> (<i>TtAM</i>).....	28
Figure 1.13 Scheme of the interactions of acarbose bound to the secondary glucan binding site of amyломaltase from <i>T. aquaticus</i> (<i>TaAM</i>)	28
Figure 3.1 Amino acid sequence alignment of <i>TaAM</i> and <i>CgAM</i>	56
Figure 3.2 The superimposed structures of <i>CgAM</i> on <i>TaAM</i>	57
Figure 3.3 Overall structures of WT <i>CgAM</i>	58
Figure 3.4 Agarose gel electrophoresis of recombinant plasmid pET-19b- <i>CgAM</i>	59

Page

Figure 3.5 Agarose gel electrophoresis of amplified DNA containing <i>CgAM</i> gene with a single point mutation at Y418.....	60
Figure 3.6 Agarose gel electrophoresis of PCR product from pET-19b vector harboring <i>CgAM</i> gene with a single point mutation at Y418 after digested with <i>Nde</i> I and <i>Xho</i> I.....	61
Figure 3.7 Agarose gel electrophoresis of amplified DNA containing <i>CgAM</i> gene with a single point mutation at H461	62
Figure 3.8 Agarose gel electrophoresis of PCR product from pET-19b vector harboring <i>CgAM</i> gene with a single point mutation at H461 after digested with <i>Nde</i> I and <i>Xho</i> I.....	63
Figure 3.9 Agarose gel electrophoresis of amplified DNA containing <i>CgAM</i> gene with a single point mutation at N287.....	64
Figure 3.10 Agarose gel electrophoresis of PCR product from pET-19b vector harboring <i>CgAM</i> gene with a single point mutation at N287 after digested with <i>Nde</i> I and <i>Xho</i> I.....	65
Figure 3.11 Nucleotide sequences of six Y418 mutated <i>CgAMs</i> compared with that of WT.....	66
Figure 3.12 The deduced amino acid sequences of six Y418 mutated <i>CgAMs</i> compared with that of WT.....	72
Figure 3.13 Nucleotide sequences of five H461 mutated <i>CgAMs</i> compared with that of WT.....	74
Figure 3.14 The deduced amino acid sequences of five H461 mutated <i>CgAMs</i> compared with that of WT.....	75
Figure 3.15 Nucleotide sequences of five N287 mutated <i>CgAMs</i> compared with that of WT.....	76

	Page
Figure 3.16 The deduced amino acid sequences of five N287 mutated <i>CgAMs</i> compared with that of WT	77
Figure 3.17 SDS-PAGE of crude and purified enzyme expressed from cells harboring the series of Y418 mutated <i>CgAMs</i>	79
Figure 3.18 Effect of temperature (A) and pH (B) for WT and Y418 mutated <i>CgAMs</i> on disproportionation activity	88
Figure 3.19 Effect of temperature (A) and pH (B) for WT and Y418 mutated <i>CgAMs</i> on cyclization activity	89
Figure 3.20 Effect of temperature <i>CgAM</i> stability of WT and Y418 mutated <i>CgAMs</i>	90
Figure 3.21 Effect of pH on <i>CgAM</i> stability of WT and Y418 mutated <i>CgAMs</i>	91
Figure 3.22 Substrate specificity of WT and Y418 mutated <i>CgAMs</i> in disproportionation reaction	92
Figure 3.23 Lineweaver-Burk plot of WT and Y418 mutated <i>CgAMs</i> -catalyzed disproportionation reaction.....	93
Figure 3.24 Lineweaver-Burk plot of WT and Y418 mutated <i>CgAMs</i> -catalyzed cyclization reaction	94
Figure 3.25 HPAEC-PAD analysis of LR-CD products synthesized at different incubation time by WT and Y418 mutated <i>CgAMs</i>	95
Figure 3.26 HPAEC-PAD analysis of LR-CD products synthesized for 6 h at different enzyme unit by WT and Y418 mutated <i>CgAMs</i>	97

Page

Figure 3.27 Circular dichroism spectra and the predicted secondary structural compositions of WT and Y418 mutated CgAMs	101
Figure 3.28 Disproportionation activity of amyloamylase as measured from an enthalpy change when substrate binds to enzyme detected by ITC.....	102
Figure 3.29 Disproportionation activity of amyloamylase as measured from glucose product released by glucose oxidase assay	104
Figure 3.30 Product inhibition of WT (A), Y418A (B) and Y418W (C) CgAMs in disproportionation reaction as determined by ITC.	105
Figure 3.31 Differential scanning calorimetry (DSC) analysis of CgAMs	106
Figure 3.32 Structures of WT and Y418 mutated CgAMs.....	107
Figure 3.33 SDS-PAGE of crude and purified enzyme expressed from cells harboring the series of H461 mutated CgAMs	112
Figure 3.34 Effect of temperature (A) and pH (B) of WT and H461 mutated CgAMs on starch transglucosylation activity	117
Figure 3.35 Effect of temperature (A) and pH (B) of WT and H461 mutated CgAMs on disproportionation activity	118
Figure 3.36 Effect of temperature on CgAM stability of WT and H461 mutated CgAMs.....	122
Figure 3.37 Effect of pH on CgAM stability of WT and H461 mutated CgAMs.....	123
Figure 3.38 Substrate specificity of WT and H461 mutated CgAMs in disproportionation reaction	124
Figure 3.39 Lineweaver-Burk plot of WT and H461 mutated CgAMs - catalyzed disproportionation reaction.....	125

	Page
Figure 3.40 HPAEC-PAD analysis of the LR-CD products synthesized by WT and H461 mutated <i>CgAMs</i>	126
Figure 3.41 Circular dichroism spectra and the predicted secondary structural compositions of WT and H461 mutated <i>CgAMs</i>	128
Figure 3.42 Structures of WT and H461 mutated <i>CgAMs</i> with acarbose	129
Figure 3.43 SDS-PAGE of crude and purified enzyme expressed from cells harboring the series of N287 mutated <i>CgAMs</i>	132
Figure 3.44 Effect of temperature (A) and pH (B) for WT and N287 mutated <i>CgAMs</i> on disproportionation activity	136
Figure 3.45 Effect of temperature (A) and pH (B) for WT and N287 mutated <i>CgAMs</i> on cyclization activity	137
Figure 3.46 Effect of temperature on <i>CgAM</i> stability of WT and N287 mutated <i>CgAMs</i>	141
Figure 3.47 Effect of pH on <i>CgAM</i> stability of WT and N287 mutated <i>CgAMs</i>	142
Figure 3.48 Substrate specificity of WT and N287 mutated <i>CgAMs</i> in disproportionation reaction	143
Figure 3.49 Lineweaver-Burk plot of WT and N287 mutated <i>CgAMs</i> - catalyzed disproportionation reaction.....	144
Figure 3.50 Lineweaver-Burk plot of WT and N287 mutated <i>CgAMs</i> -catalyzed cyclization reaction	145
Figure 3.51 HPAEC-PAD analysis of LR-CD products synthesized at different incubation time of WT and N287 mutated <i>CgAMs</i>	146

Page

Figure 3.52 HPAEC-PAD analysis of LR-CD products synthesized for 6 h by WT and N287 mutated <i>CgAMs</i>	148
Figure 3.53 Circular dichroism spectra and the predicted secondary structural compositions of WT and N287 mutated <i>CgAMs</i>	150
Figure 3.54 Structures of WT and N287 mutated <i>CgAMs</i> with acarbose.....	151
Figure 4.1 Proposed binding of maltoheptaose (G7) in the active site of amylo maltase from <i>Thermus thermophilus</i> (<i>TtAM</i>).	161
Figure 4.2 Scheme of the interactions of acarbose bound to the secondary binding site of amylo maltase from <i>Thermus aquaticus</i> (<i>TaAM</i>).	162



LIST OF ABBREVIATIONS

A	absorbance
AM	amylomaltase
BSA	bovine serum albumin
° C	degree celcius
CDs	cyclodextrins
LR-CDs	large-ring cyclodextrins
Da	Dalton
D-enzyme	Disproportionation enzyme
DP	Degree of Polymerization
g	gram
4 α GTase	4- α -glucanotransferase
GH	glycoside hydrolase family
h	hour
l	litre
μ g	microgram
μ l	microliter
M	molar
mA	milliampere
min	minute
mg	milligram
ml	milliliter

mM	millimolar
MW	molecular weight
ND	not detectable
PAGE	polyacrylamide gel electrophoresis
rpm	revolution per minute
SDS	sodium dodecyl sulfate
U	unit



CHAPTER I

INTRODUCTION

1.1 Starch converting enzymes

A variety of different enzymes involving in the synthesis and degrading of starch have been studied (Van der Maarel *et al.*, 2002). Most of them belong to α -amylase family based on the amino acid sequence homology; (Table 1.1). They are basically classified into 4 groups (Figure 1.1); (i) endoamylase such as α -amylase with four highly conserved regions in their primary sequences (Van der Maarel *et al.*, 2002) and an $(\alpha/\beta)_8$ or TIM barrel in their structures (Banner *et al.*, 1975), the enzyme hydrolyzes α -1,4-glycosidic bond from inner chain of amylose or amylopectin, producing linear or branched oligosaccharides. α -amylase is a well-known endoamylase found in a wide variety of organisms. (ii) exoamylase which catalyzes the hydrolysis of α -1,4 and α -1,6-glycosidic linkages from non reducing end of amylose and amylopectin results in short chain products (Robyt and Ackerman, 1971); (iii) debranching enzyme such as isoamylase and pullulanase type I which hydrolyze α -1,6-glycosidic bond resulting in long chain oligosaccharides as products (Bender *et al.*, 1959); (iv) transferase or 4- α -glucanotranferase which hydrolyzes α -1,4-glycosidic linkages of donor and transfer to glycosidic acceptor so a new glycosidic bond is formed such as cyclodextrin glycosyltransferase (CGTase) and amyломaltase (AM) (MacGregor *et al.*, 2001).

1.2 The 4- α glucanotransferase

4 - α glucanotransferase is a specific type of transferase consisting of amyloamylase, CGTase and glycogen debranching enzyme (Takaha and Smith, 1999). 4- α glucanotransferase catalyzes inter- and intra-molecular transglucosylation reactions consisting of 4 different reactions (Figure 1.2). The first reaction is disproportionation reaction which is an intermolecular transglucosylation reaction. The enzyme transfers the glucosyl units from short chain oligosaccharides resulting in oligosaccharides of various lengths as in the following equation:



The second is cyclization reaction, an intramolecular transglucosylation. The enzyme converts a single linear glucan to a cyclic glucan which is called cyclodextrins (CDs) as shown:



The third reaction is coupling, a reverse reaction of cyclization. In this reaction, CD ring is opened and act as a donor, the enzyme transfers glucosyl units from CD to short chain oligosaccharides producing longer oligosaccharides as product. Finally, hydrolysis reaction, the enzyme catalyzes and transfers glucosyl residues to water which acts as acceptor. Among these reactions, amyloamylase has high activity in disproportionation and cyclization reactions, but low activity in coupling and hydrolysis reactions (Van der Maarel *et al.*, 2000). All of these reactions can be catalyzed by both amyloamylase and CGTase, but there is a different in the size of products from cyclization reaction. CGTase produces small ring cyclodextrins (SR-CDs) while amyloamylase produces large-ring cyclodextrins (LR-CDs). SR-CDs are

cyclic oligosaccharides consisting of 6, 7 and 8 glucose units linked by α -1,4-glycosidic bond which is called α , β and γ -CDs, respectively (Takaha and Smith, 1999) while LR-CDs comprise of glucose residues linked by α -1,4-glycosidic bond with degree of polymerization (DP) from 9 onwards (Van der Maarel *et al.*, 2000). Cyclization specificity is one of the most important properties of amyloamylase to catalyze the formation of cyclic glucans with degree of polymerization (DP) larger than 16 while DP9 - DP15 are produced from CGTase at short reaction period (Takaha and Smith, 1999).

1.3 Amyloamylase (AM)

Amyloamylases or AM (EC 2.4.1.25) is an intracellular $4\text{-}\alpha$ GTase catalyzed transglucosylation reactions to yield linear oligosaccharides and LR-CD products as described in section 1.2. (Takaha and Smith, 1999). The enzymes have been classified into glycoside hydrolase family 77 (GH77) (Coutinho *et al.*, 2003), which forms the α -amylase superfamily together with GH13 and GH70, sharing a similar fold and the active site residues (MacGregor *et al.*, 2001). Amyloamylases have been found in microorganisms as well as in plants, where they are known as disproportionating enzyme or D-enzyme (Tantanarat *et al.*, 2014). Amyloamylase was firstly found in *Escherichia coli* as maltose inducible enzyme which involved in maltose metabolism (Boos and Shuman, 1998). In plants, D-enzyme is involved in starch metabolism, a role has been implicated in nocturnal maltose metabolism in the cytoplasm (Smith *et al.*, 2004).

Amylomaltase gene was reported in many bacterial strains such as *Streptococcus pneumoniae* (STASsI *et al.*, 1981), *Clostridium butyricum* NCIMB7423 (Goda *et al.*, 1997), thermophilic bacteria *Thermus aquaticus* (Terada *et al.*, 1999), *Aquifex aeolicus* (Bhuiyan *et al.*, 2003) and some archaea such as hyperthermophilic *Thermococcus litoralis* (Jeon *et al.*, 1997) and hyperthermophilic *Pyrobaculum aerophilum* IM2 (Kaper *et al.*, 2005). D - enzyme in plant was found in potato tubers (Peat *et al.*, 1956), carrot roots (Manners and Rowe, 1969), spinach leaves (Okita *et al.*, 1979), arabidopsis (Tantanarat *et al.*, 2014), pea leaves (Kakefuda and Duke, 1989) and cassava *Manihot esculenta* Crantz tuber (Tantanarat *et al.*, 2014). The three dimensional structures of amylomaltases from *T. aquaticus* (Przylas *et al.*, 2000b), *Thermotoga maritime* (Roujeinikova *et al.*, 2002), *Thermus thermophilus* (Barends *et al.*, 2007), *Thermus brockianus* (Jung *et al.*, 2011), *A. aeolicus* (Barends, 2005), *E. coli* (Weiss *et al.*, 2015), *Corynebacterium glutamicum* (Joo *et al.*, 2016) Recently, the X-ray structure from *T. aquaticus* in complex with cycloamylose with a degree of polymerization of 34 (CA34) at resolution range 1.73-37 Å have been reported (Roth *et al.*, 2017).

1.4 Large-ring cyclodextrins (LR-CDs)

Cyclodextrins (CDs) or cycloamylose (CAs) is composed of glucose units joining to form a cyclic structure with 1,4 - glycosidic linkages (Figure 1.3). These molecules have unique structure with a hydrophilic rim, formed by hydroxyl groups, at both side of the cone (Van der Maarel *et al.*, 2002). The central hydrophobic cavity of CDs can trap hydrophobic guest molecules (Del Valle, 2004). The inclusion

complexes formed can change the solubility, reactivity and stability of the guest substances and have found many applications in the food, chemical and pharmaceutical industries (Takaha and Smith, 1999). LR-CDs apparently experience steric strain which results in a distortion of the previously annular molecule to form various structures due to possibility of different H-bonding. In CD10, the macrocyclic rings are deformed elliptical shape while cavity of CD14 is a narrow groove with a boat and butterfly-shaped. (Figure 1.3). CD9 has an intermediate structure between CD10 and CD14, it displays a distorted elliptical macrocyclic ring without a band flip (Endo, 2011). The largest cycloamylose that could be characterized by X-ray crystallography is CA26 (Gessler *et al.*, 1999). CA-26 folds into two short left handed V-amylose helices in an anti-parallel arrangement with a hydrophobic channel of 5.0-5.5 Å in diameter (Figure 1.4). This channel may form complexes with a large variety of guest molecules, in particular with long extended molecules. The physicochemical properties of CD26 to CD39 are shown in Table 1.2. The aqueous solubilities of LR-CDs, except for CD9, CD10, CD14 and CD26 are higher than those of α -, β - and γ -CD. This may be a consequence of high structural flexibility, on the basis of the formation of intramolecular and intermolecular hydrogen bonds. There are no marked differences in specific rotation among various sizes of LR-CDs (CD10 to CD39).

1.5 Applications of LR-CDs and amylomaltase

Due to the hydrophilic surface, LR-CDs can dissolve in water and form inclusion complexes with guest molecules such as fatty acid, alcohol (Zheng *et al.*, 2002), surfactant (Mun *et al.*, 2009) and benzene (Harata, 1981) by trapping guest

molecules into their hydrophobic cavity to improve solubility, stability or biological properties of guest molecules (Kim *et al.*, 2011). LR-CDs have been used in various applications: in food, pharmaceutical, cosmetic and paper industries (Takaha and Smith, 1999). In pharmaceutical application, LR-CDs form inclusion complexes with flubiprofen and ibuprofen resulted in 14 - and 2 - folds increase in drug solubility, respectively (Baek *et al.*, 2011). LR-CDs are also used as an artificial chaperone for protein refolding (Machida *et al.*, 2000). Table 1.3 summarizes studies on the inclusion complex formation between LR-CDs or mixture of LR-CDs and guest compounds (Endo, 2011).

Amylomaltase is used to modify starch to produce thermoreversible gel. The enzyme hydrolyzes α -1,4-glycosidic linkage of amylose chain and transfers the glucosyl units to amylopectin chain, resulting in a change in side chain distribution and thermoreversible properties (Kaper *et al.*, 2005). The modified starch is used in foods to replace gelatin from animal to make food edible for vegetarian and muslim. Moreover, the modified starch is used to replace fat or cream in dairy products to improve creaminess in low-fat yogurt (Alting *et al.*, 2009). Amylomaltase is also used to produce glucoside products through intermolecular transglucosylation such as isomalto-oligosaccharides (IMOs) with DP2-DP6 (Rudeekulthamrong *et al.*, 2013). IMOs are non digestible saccharides of glucose-based consisting of α -1,6-glycosidic linkage, they act as prebiotics that activate the growth of normal flora in digestive system which benefit human health. Amylomaltase was also reported to be used in the synthesis of maltosylsucrose with anticariogenic property (Saehu *et al.*, 2013).

1.6 *Corynebacterium glutamicum*

Corynebacterium glutamicum (*C. glutamicum*) is a mesophilic gram positive bacteria which has attracted biotechnology industry (Joo *et al.*, 2016). It is employed in large-scale fermentation due to its remarkable ability to produce amino acids, nucleotides and vitamins (Vertès *et al.*, 2005). *C. glutamicum* cells grow in a medium containing sugar accumulate glycogen and degrade that polymer when sugar becomes a limiting factor (Seibold *et al.*, 2007). Unlike other gram positive bacteria, *C. glutamicum* has a glycogen degradation pathway similar to that in *E. coli* (Seibold *et al.*, 2009). During the degradation of glycogen which is intertwined with maltose metabolism, it forms maltodextrins. Enzymes such as glycogen phosphorylase, glycogen debranching enzyme, glucokinase, α -phosphoglucomutase, maltodextrin glucosidase, maltodextrin phosphorylase and 4- α -glucanotransferase participate in maltose/maltodextrin metabolism and glycogen degradation in *E. coli* (Boos and Shuman, 1998; Seibold *et al.*, 2009) as shown in Figure 1.5. In *C. glutamicum*, maltose/maltodextrins serve as substrates in synthesis of trehalose. This disaccharide is involved in the response to osmotic stress and also in the biosynthesis of mycolic acids, which are an important component of bacteria cell wall (Wolf *et al.*, 2003).

Table 1. 1 Enzymes belonging to the α -amylase family with four highly conserved regions and the corresponding β -sheets found in their amino acid sequences. The five invariable catalytic sites are those highlighted (Van der Maarel *et al.*, 2002).

	I β 2	II β 4	III β 5	IV β 7
Amylomaltase	EALGIRIIGDMPIFVAED	LFHLVRIIDHFRG	VPVLAEDLGVI	VVYTGTHDNDT
Amylosucrase	HEAGISAVVDFIFNHTSN	GVDILRMDAVAF	VFFKSEAIIVHP	VNYVRSHDDIG
CGTase	HAKNIKVIIDFAPNHTSP	GIDGIRMDAVKH	VFTFGSEWFLGV	VTFIDNHDMER
CMDase	HDNGIKVIFDAVFNHCGY	DIDGWRLDVANE	AIIVGSEVWHTA	FNLIGSHDTER
BE	HQAGIGVILDWVPGHFCK	HVDGFRVDAVAN	ILMIAEDSTDW	FILPFSDHEVV
Isoamylase	HNAGIKVYMDVVYNHTAE	GVDGFRFDLASV	LDLFAEPPWAIG	INFIDVHGMT
M. amylase	HQKAIRVMLDAVFNHSGY	DIDGWRLDVANE	AYILGEIWHDA	FNLLGSHDTPR
Pullulanase	HAHGVRVILDGVFNHTGR	GVDGWRLDVPNE	AYIVGSEIWEAA	MNLLTSHDTPR
Sucrose Pase	LGECSHLMFDFVCNHMSA	GAEYVRLDAVGF	TVIITSEINVPH	FNFLASHDGGIG
BLamylase	HERGMYLMVDVVANHMGY	SIDGLRIDTVKH	VYCIGSEVLDGD	GTFVENHDNPR

CMDase = Cyclo-maltodextrinase, BE = Branching enzyme, M. amylase = maltogenic α -amylase, Sucrose Pase = Sucrose phosphorylase, BLamylase = α -amylase from *Bacillus licheniformis*

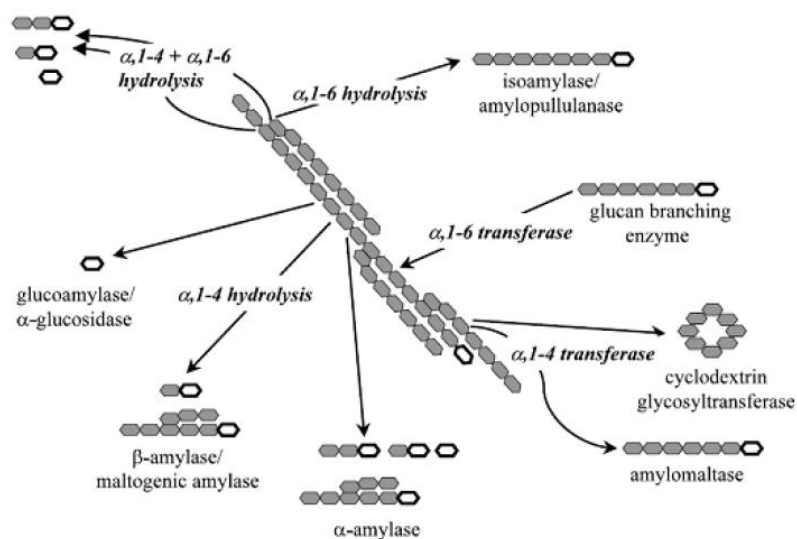


Figure 1. 1 The different enzymes involved in the degradation of starch. The open ring structure symbolizes the reducing end of a glucan molecule (Van der Maarel *et al.*, 2002).

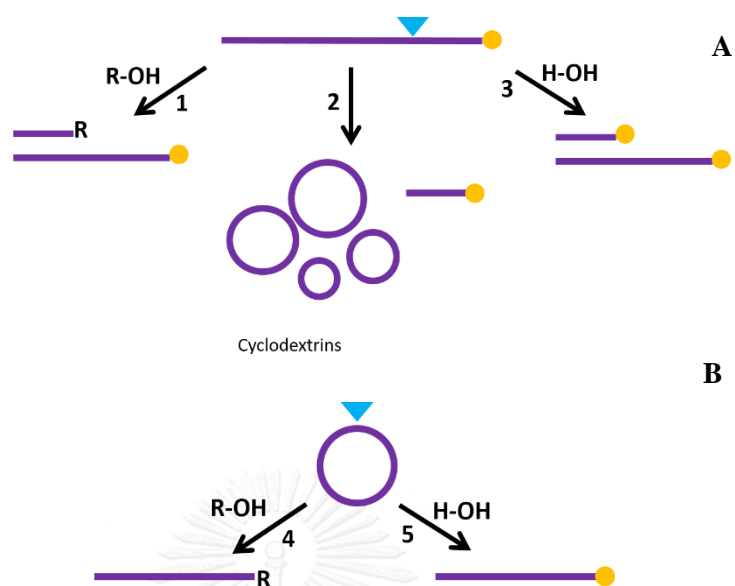


Figure 1. 2 Model of action of amyloamylase on linear and cyclic α -1,4 glucans. Reactions catalyzed by amyloamylase on amylose (A) and cyclodextrins (B). Lines and circles indicate linear and cyclic α -1,4 glucans chains, respectively. Blue closed triangles, attacked points by amyloamylase; yellow closed circles, glucosyl residues at reducing ends; R, α -1,4 glucans; 1, disproportionation reaction; 2, cyclization reaction; 3,5 hydrolysis reaction; 4, coupling reaction.

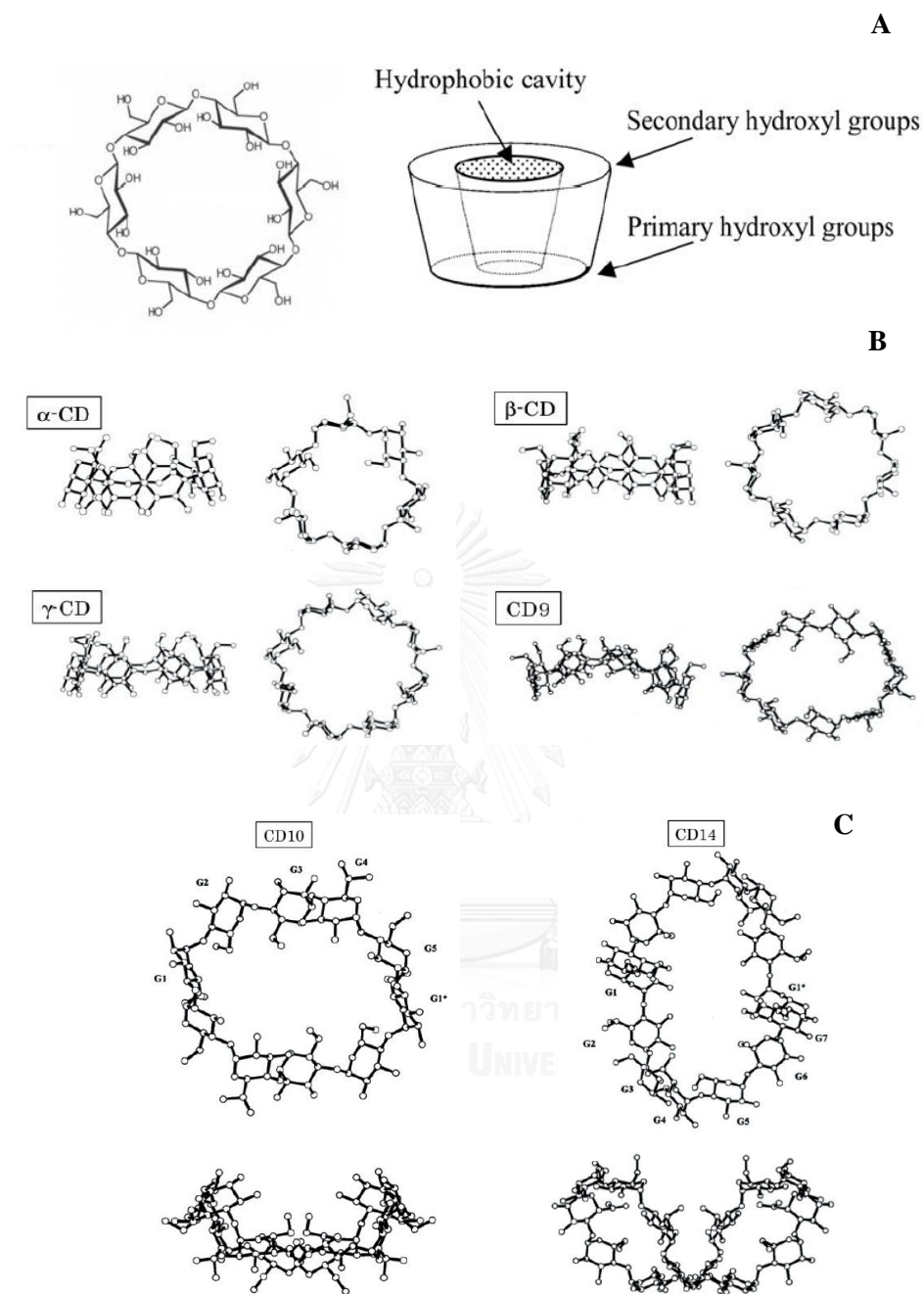


Figure 1. 3 Schematic presentation of α -CD (A) (Larsen, 2002). Molecular structures (side and top views) of α -CD, β -CD, γ -CD, CD9 (B) CD10 and CD14 (C) (Endo, 2011).

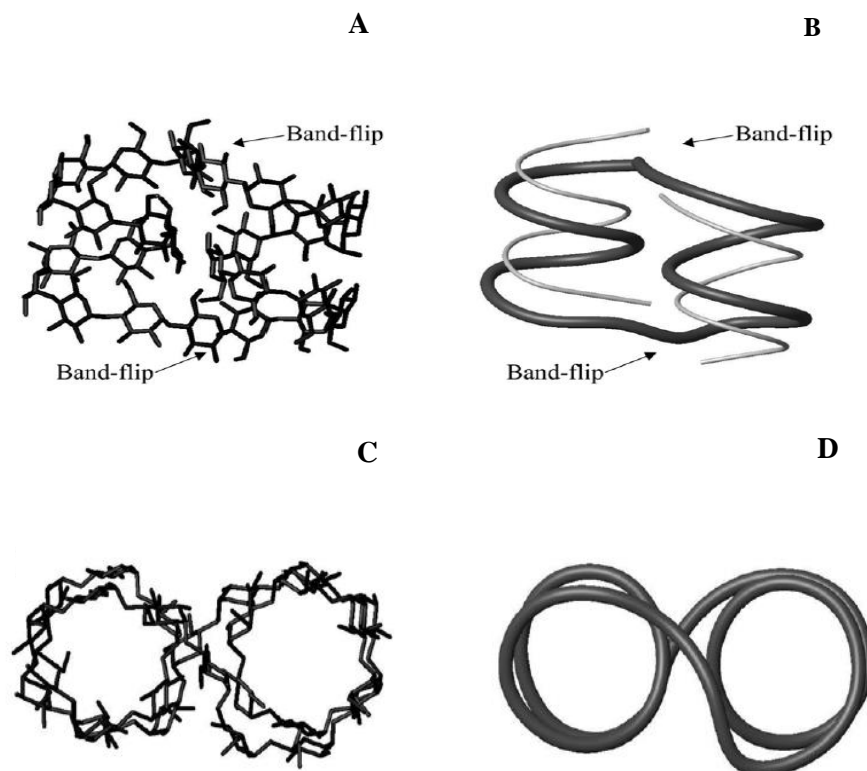


Figure 1. 4 Solid state structure of LR-CDs (CD26). Structure of CD26 indicating the positions of the band-flips and the V-amylose like segments (A). Same structure as A, the thick dark tube traces the position of C1, whereas the thin grey tube traces the position of C6. The band-flipped positions are clearly seen (B). CD26 viewed from the top (C). Same structure as C, the thick dark tube traces the position of C1 (D) (Larsen, 2002). A band flip was defined as a 180° inverted glycoside linkage (Taira *et al.*, 2006).

Table 1.2 Physicochemical properties of native small-ring CDs and LR-CDs (Endo, 2011).

	Theoretical ^{a)} molecular weight	Aqueous ^{b)} solubility (g/100 mL)	Surface ^{b)} tension (mN/m)	Specific rotation $[\alpha]_D^{25}$	Half-life of ^{c)} ring opening (h)		Theoretical ^{a)} molecular weight	Aqueous ^{b)} solubility (g/100 mL)	Surface ^{b)} tension (mN/m)	Specific rotation $[\alpha]_D^{25}$	Half-life of ^{c)} ring opening (h)
α -CD	972.8	14.5	72	+147.8	33	CD23	3729.2	>100	73	+196.6	2.7
β -CD	1135.0	1.85	73	+161.1	29	CD24	3891.4	>100	73	+196.0	2.6
γ -CD	1297.1	23.2	73	+175.9	15	CD25	4053.5	>100	73	+190.8	2.8
CD9	1459.3	8.19	72	+187.5	4.2	CD26	4215.7	22.4	73	+201.4	2.9
CD10	1621.4	2.82	72	+204.9	3.2	CD27	4377.8	>125	72	+189.4	2.8
CD11	1783.5	>150	72	+200.8	3.4	CD28	4539.9	>125	72	+191.2	2.6
CD12	1945.7	>150	72	+197.3	3.7	CD29	4702.1	>125	72	+190.2	2.5
CD13	2107.8	>150	72	+198.1	3.7	CD30	4864.2	>125	72	+189.1	2.3
CD14	2270.0	2.30	73	+199.7	3.6	CD31	5026.4	>125	71	+189.0	2.4
CD15	2432.1	>120	73	+203.9	2.9	CD32	5188.5	>125	71	+192.7	2.4
CD16	2594.2	>120	73	+204.2	2.5	CD33	5350.6	>125	71	+192.1	2.2
CD17	2756.4	>120	72	+201.0	2.5	CD34	5512.8	>125	72	+189.6	2.2
CD18	2918.5	>100	73	+204.0	3.0	CD35	5674.9	>125	71	+193.7	2.1
CD19	3080.7	>100	73	+201.0	3.4	CD36	5837.1	>100	71	+190.6	1.9
CD20	3242.8	>100	73	+199.7	3.4	CD37	5999.2	>100	71	+189.9	1.8
CD21	3405.0	>100	73	+205.3	3.2	CD38	6161.3	>100	71	+190.1	1.9
CD22	3567.1	>100	73	+197.7	2.6	CD39	6323.5	>100	70	+188.1	1.8

a) Calculated as $162.1406 * n$, where n is the number of glucopyranose unit.

b) Observed at 25 °C.

c) In 1 mol/L HCl at 50 °C.



Table 1.3 Studies of inclusion complex formation between purified LR-CD or mixture of LR-CDs and guest molecules (Endo, 2011).

CD	(Ref. No.)	Indicator or Method	Compound
(Pure LR-CD)			
CD9	(10)	Enhancement of solubility (UV/VIS absorption)	Anthracene Amphotericin B Ajmalicine Ajmaline Carbamazepine Digitoxin Spironolactone 9,10-Dibromoanthracene Perylene-3,4,9,10-tetracarboxylic dianhydride Spironolactone
		Solubility method	
CD9	(51, 53) (50, 52)	Enhancement of solubility (Spectrophotometry)	Fullerene C ₆₀ Fullerene C ₇₀
CD9	(45)	Enhancement of solubility (Spectrophotometry)	Reserpine [2,2]-Paracyclophane Perylene Triphenylene 1,8-Naphthalic anhydride Naphthalene-1,4,5,8-tetracarboxylic dianhydride Digitoxin Gitoxin Digoxin Methyl digoxin Lanatoside C G-Strophanthin Proscillaridin A Digitoxin
		Solubility method and NMR	
CD9	(87)	Simple precipitation	1,5-Cyclooctadiene Cyclononane Cyclodecanone Cycloundecanone Cyclododecanone Cyclotridecanone Cyclopentadecanone Cycloundecanone Cyclododecanone
		Powder X-ray diffraction DSC	
CD9 - CD13	(46-48)	Capillary electrophoresis	Benzoate 2-Methyl benzoate 3-Methyl benzoate 4-Methyl benzoate 2,4-Dimethyl benzoate 2,5-Dimethyl benzoate 3,5-Dimethyl benzoate 3,5-Dimethoxy benzoate Salicylate 3-Phenyl propionate 4- <i>tert</i> -Butyl benzoate Ibuprofen anion 1-Adamantane carboxylate

Table 1.3 (continue) Studies of inclusion complex formation between purified LR-CD or mixture of LR-CDs and guest molecules (Endo, 2011).

CD	(Ref. No.)	Indicator or Method	Compound
(Pure LR-CD)			
CD14 - CD17	(49)	Capillary electrophoresis	Salicylate 4-tert-Butyl benzoate Ibuprofen anion
CD21 - CD32	(56)	Isothermal titration calorimetry (ITC)	Iodine
CD9	(55)	X-ray crystallography	Cycloundecanone
CD12	(54)	NMR	Single wall carbon nanotube (SWNT)
CD26	(57, 88)	X-ray crystallography	NH ₄ I ₃ Ba(I ₃) ₂ Undecanoic acid Dodecanol
(Mixture of LR-CDs)			
CA(S) [*] and CA(L) ^{**}	(89)	Spectrofluorometry	8-Anilino-1-naphthalene sulfonic acid
CA(S) [*] and CA(L) ^{**}	(25, 89)	Simple precipitation	1-Octanol 1-Butanol Oleic acid
CA (with oligomerization degree of 22 to around 60)	(64)	Enhancement of solubility (Spectrophotometry)	Fullerene C ₆₀
CD21 - CD40	(90)	ITC	Sodium dodecyl sulfate Sodium myristoyl sulfate
CA	(91)	Simple precipitation	SB3-14 ^{***} SB3-16 ^{****}

* CA(S) : Mixture of LR-CDs with oligomerization degree around 20 to 55, mainly oligomerization degree of 25 to 50.

** CA(L) : Mixture of LR-CDs with average oligomerization degree of ca. 150, except CDs with smaller than oligomerization degree of 50.

*** SB3-14 : 3-(*N,N*-dimenylmyristylammonio)propansulfonate

**** SB3-16 : 3-(*N,N*-dimenylpalmitylammonio)propansulfonate

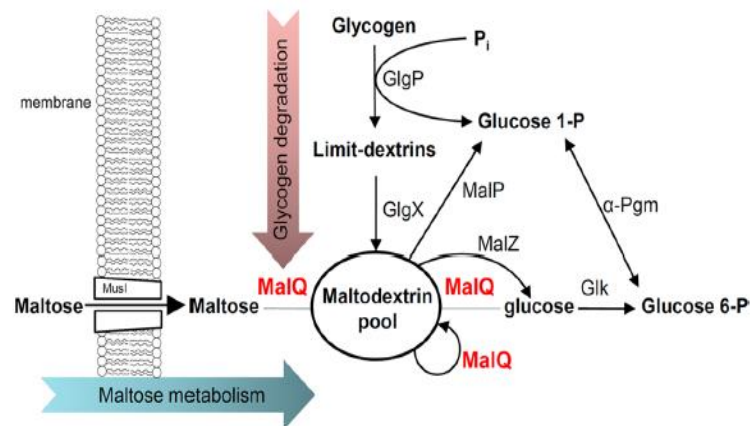


Figure 1. 5 A pathway of maltose/maltodextrin and glycogen degradation in *E. coli* (Seibold and Eikmanns, 2007). The compounds with bold black font are the key metabolites of the pathway. Proteins and enzymes encoded by genes shown are GlgP, glycogen phosphorylase; GlgX, glycogen debranching enzyme; MusI, a maltose transporter; Glk, glucose kinase; α -Pgm, α -phosphoglucomutase; MalZ, maltodextrin glucosidase; MalP, maltodextrin phosphorylase; MalQ, 4- α -glucanotransferase (Joo *et al.*, 2016).

1.7 Structure of Amylomaltase from *C. glutamicum*

A novel amylomaltase from a mesophilic bacteria *C. glutamicum* ATCC 13032 (*CgAM*) was characterized, analyzed, engineered and crystallized by our group to investigate functional roles of amino acid residues for the understanding of catalytic mechanism and enzyme improvement (Nimpiboon *et al.*, 2016a; Srisimarat *et al.*, 2012; Srisimarat *et al.*, 2013). *CgAM* is different from amylomaltase *T. aquaticus* (*TaAM*) in amino acid sequence and protein size with a different LR-CD product profile, having CD19 as the smallest product (Srisimarat *et al.*, 2011). We reported crystallization of *CgAM* at 1.7 Å resolution but not yet submitted the structure to the Protein Data Bank.

In 2016, the Korean group reported crystallization of *CgAM* complexed with bis-tris molecule at 1.70 Å resolution, and deposited the structure in Protein Data Bank (PDB code 5b68) (Joo *et al.*, 2016). However, the first three residues of the protein were invisible in the electron density map, 703 amino acids (Agr4-Asp703) out of 706 was obtained from their crystal structure. The amino acid sequence alignment of *CgAM*, *E. coli* (*EcAM*), *A. aeolicus* (*AaAM*), *T. thermophilus* (*TtAM*) and disproportionating enzyme DPE1 from *A. thaliana* (*AtDPE1*) was compared Figure 1.6. Interestingly, *CgAM* showed an overall folding similar to *EcAM* Figure 1.6. The *CgAM* structure consists of two distinctive domains: the N-terminal domain (N-domain; Met1-Arg165) and the C-terminal domain (C-domain; Leu166-Asp706) as shown in Figure 1.7A. The N-terminal domain is divided into two subdomains: Subdomain I (N1-subdomain, Met1-Pro72) which consists of three α -helices and one

double strand antiparallel β -sheet. The three α -helices form a helix bundle like shape and the β -sheet attached to the C-domain. Subdomain II (N2-subdomain, Leu73-Arg165) composed of two four-stranded β -sheets that form a β -sandwich. The N1 subdomain interacts directly with the C-domain whereas the N2-subdomain is loosely attached to the C-domain by forming independent folds.

The C-domain consists of four subdomains; one core subdomain and three auxiliary subdomains (Figure 1.7B). The core subdomain (CC-subdomain) is located at the center of C-domain and forms a $(\beta/\alpha)_8$ -barrel (TIM barrel) fold with eight helices (α_5 , α_9 , α_{12-14} , η_9 , α_8 and α_{20}) covering the eight stranded β -barrels (β_{12-14} , β_{17} , and β_{20-23}). The CC-subdomain forms a catalytic site and also contributes to the substrate binding site. Auxiliary subdomain I (CA1-subdomain; Met221-Try358) comprises of three 3_{10} -helices and three α -helices and is located at the edge of $(\beta/\alpha)_8^1$ and $(\beta/\alpha)_8^2$. Auxiliary subdomain II (CA2-subdomain; Val391-Gly439 and His461-Phe485) comprises of two 3_{10} -helices and a three-stranded twisted β -sheets, and attached to the $(\beta/\alpha)_8^3$ and $(\beta/\alpha)_8^4$ of the CC-subdomain. The CA2-subdomain connects to the N-domain by interacting with N1-subdomain. Auxiliary subdomain III (CA3-subdomain: Thr558-Gly625 and Leu650-Asn693) comprises of 3_{10} -helices and four α -helices, covering the edge of $(\beta/\alpha)_8^7$ and $(\beta/\alpha)_8^8$ and also contacts the CA1-subdomain. The auxiliary subdomains are heavily involved in the substrate-binding pocket by which CA2-subdomain is a main contributor.

1.7.1 Structural comparison of *CgAM* with other amylomaltases

Overall structure

The *CgAM* structure is homologous to amylomaltases from *E.coli* (*EcMalQ* or *EcAM*, PDB code 4S3P), *T. aquaticus* (*TaAM*, PDB code 1CWY), *T. thermophilus* (*TtAM*, PDB code 2OWX) and disproportionating enzyme (DPEs) from *A. thaliana* (*AtDPE1*, PDB code 5CPQ) (Holm and Sander, 1998). Both amylomaltase and DPE1 from plant belong to 4- α -glucanotransferase type. However, the superimposed structures of *CgAM*, *EcAM*, *TtAM* and *AtDPE1* revealed the striking difference of N-terminal domains whereas C-domains are closely matched and the N-domain interacting regions are similar (Figure 1.8A-B). In *CgAM* and *EcAM*, the extended domain from the N-terminal is found which is completely absent in the thermostable *TaAM* or *TtAM*. However, *AtDPE1* has a long N-terminal arm region that stretches toward the neighboring subunit to form a dimer of enzyme (Joo *et al.*, 2016; O'Neill *et al.*, 2015). The function of N-terminal extension domain of *CgAM* remains unclear.

Active site

In the active site cleft of *CgAM* structure (PDB Code 5B68), one bis-tris methane molecule and one sulfate ion were bound (Figure 1.9). The catalytic mechanism of *CgAM* was proposed from structural and biochemical studies on *EcAM* (Weiss *et al.*, 2015) and *TtAM* (Barends *et al.*, 2007) with the three catalytic conserved residues, two aspartates (D) and one glutamate (E). In *EcAM*, D448 acts as a base (the catalytic nucleophile), E496, a proton donor (acid/base catalysis) and D548, a transition state stabilizer (Weiss *et al.*, 2015). In *CgAM*, the catalytic residues D460, E508 and D561 are located at CC subdomain at the corresponding positions with D448, E496 and

D548 of *EcAM*, which suggested that *CgAM* catalyzes enzyme reaction by the mechanism similar to *EcMalQ* (Figure 1.9). In addition, the model for substrate (maltoheptaose; G7) binding of *TtAM* showed seven subsites (-4 to +3) in the active site of enzyme (Figure 1.12) (Kaper *et al.*, 2007). Three catalytic residues of *CgAM* are corresponded to catalytic residues of *TtAM* on the basis of the conserved residues at the active site of amylomaltase (Figure 1.6).

Unique loop

In *CgAM* structure, the 410s loop (residues 414-422) is the flexible lid connecting the helices $\alpha 15$ and $\alpha 16$ in CA2-subdomain (Figure 1.6). It is located on top of the active site cleft covering subsite +1 to +3 of the substrate-binding groove (Joo *et al.*, 2016) (Figure 1.10). The amino acid sequence around this loop is highly conserved compared to the 250s loop in *TaAM* and 400s loop in *EcAM* indicating that *CgAM* also contains the flexible lid which undergoes conformation change during substrate binding as observed in *TaAM* and *EcAM* (Figure 1.6). In *TaAM*, two solvent exposed hydrophobic residues at the tip of the loop: F251 and F366 residues, showed some disorder (flexibility) in the unliganded enzyme structure as well as in the complex with acarbose (Przylas *et al.*, 2000a). Since this loop is highly conserved in amylomaltases, these findings suggested that this loop is involved in the substrate binding (Jung *et al.*, 2011; Strater *et al.*, 2002). Possibly the loop changes conformation or becomes less flexible when larger substrate binds closely to the loop.

Second glucan binding site

In order to study substrate binding to the enzyme, crystals of *TaAM* were soaked with high concentration (100 mM) of acarbose, the potent inhibitor of many enzymes

in the α -amylase family (Przylas *et al.*, 2000a). It was found that beside the acarbose bound at the active site, a second acarbose molecule was located in a groove (near Y54 and Y101) close to the active site center of *TaAM* (Figure 1.11). The distance between the reducing end of acarbose and nonreducing end of the substrate analog bound to the active site is about 14 Å. Moreover, hydrophobic contacts of Y54 with glucose unit B and Y101 with unit C of the inhibitor are probably the most important interactions that determine the conformation and binding of the inhibitor to this site. Y101 of *TaAM* is involved in a hydrophobic stacking interaction with glucose unit C (Figure 1.13). The second acarbose has significantly fewer interactions with the protein compared to the acarbose bound to the active site (Przylas *et al.*, 2000a). Surprisingly, no second glucan binding site was reported in other amylomaltases with the X-ray crystal structures studied e.g. in thermophilic *TtAM* and *TbAM*, or the mesophilic *EcAM* and *CgAM* (Barends *et al.*, 2007; Joo *et al.*, 2016; Jung *et al.*, 2011; Srisimarat *et al.*, 2013; Weiss *et al.*, 2015). From the superimposed structures, Y23 and N287 or Y290 of *CgAM* are corresponding to Y54 and Y101 in the second glucan binding site of *TaAM*, respectively (Joo *et al.*, 2016; Przylas *et al.*, 2000a; Srisimarat *et al.*, 2013). It is observed that the residues around the second acarbose binding site are not strictly conserved compared to the acarbose binding to the active site (Strater *et al.*, 2002).

1.8 Objectives

For a better understanding of enzyme mechanism and a way to improve enzyme performance, we are interested in investigation of a structure-function relationship of CgAM. Our previous works on site-directed mutagenesis of residues in CgAM are summarized in Discussion section. In the present work, we aim to focus on the three different regions of CgAM; 410s loop, the active site, and the second glucan binding areas. Important residues will be selected to study and explore their functions involving in transglucosylation activity and LR-CD products profile. So, the work aims

1. To select the residues in the three regions and construct the mutated amyloamylase genes from *C. glutamicum* ATCC 13032 by site directed mutagenesis.
2. To express mutated CgAM genes in *E. coli*.
3. To purify and characterize recombinant mutated CgAMs.
4. To construct the model structures of mutated CgAMs by homology modeling program.
5. To compare structures and properties of mutated CgAMs with the wild-type enzyme and identify important residues related to functions of the enzyme.

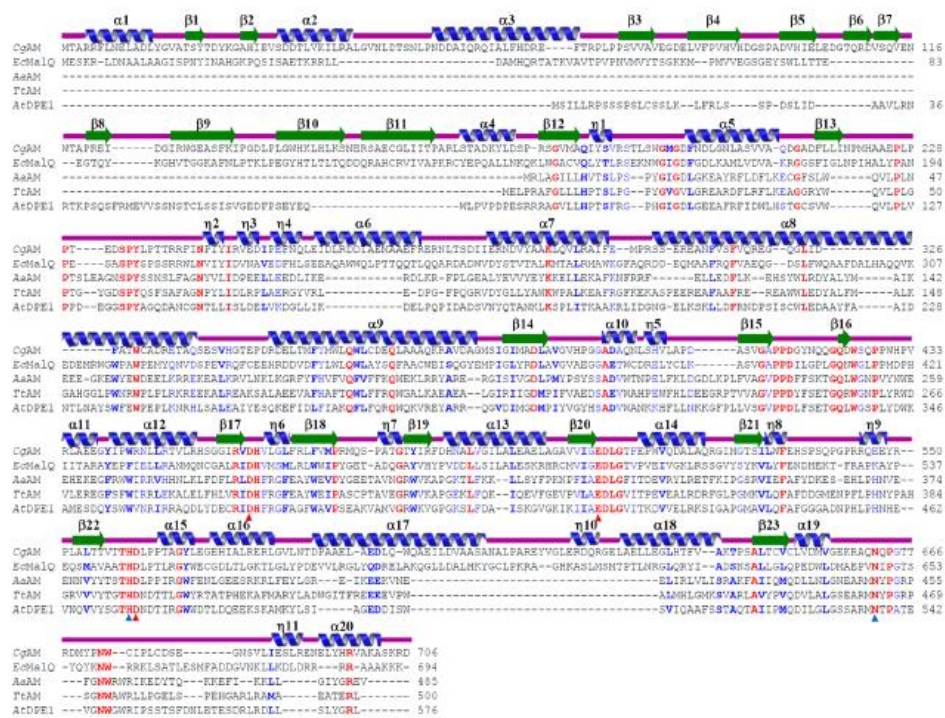


Figure 1. 6 The amino acid sequence alignment of amylomaltaes from *C. glutamicum* (CgAM), *E. coli* (EcAM), *A. aeolicus* (AaAM), *T. thermophilus* (TtAM) and disproportionating enzyme DPE1 from *A. thaliana* (AtDPE1). The secondary structure elements are marked on top of the alignment based on the CgAM structure: α -helices and 3_{10} -helices by a helix and β -strands by an arrow. The η symbol refers to a 3_{10} -helix. Conserved residues are boxed in white on a red background; similar residues are boxed in red with white background. Residues involved in enzyme catalysis and maltose binding are indicated with triangles colored with red and blue, respectively (Joo *et al.*, 2016).

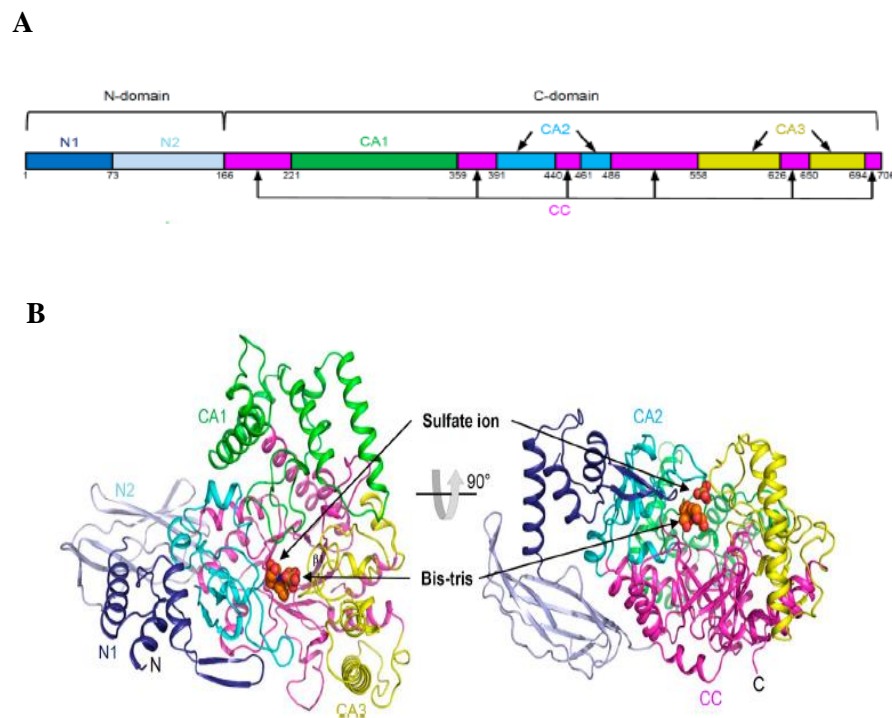


Figure 1.7 The Domain identification of *CgAM*. N1 and N2 represent N1- and N2-subdomains of N domain, CC is core subdomain of C-domain, and CA1, CA2 and CA3 are auxiliary subdomains I, II and III of C-domain, respectively (A). Overall structure of *CgAM* complexed with bis-tris and sulfate ion (B), the structure of *CgAM* is represented as a secondary structure diagram. The right side figure is rotated 90 degree in horizontal direction. A bis-tris molecule and sulfate ion bound in *CgAM* are shown as sphere models and labeled. The subdomains of *CgAMs* are distinguished with color scheme as in panel A (Joo *et al.*, 2016).

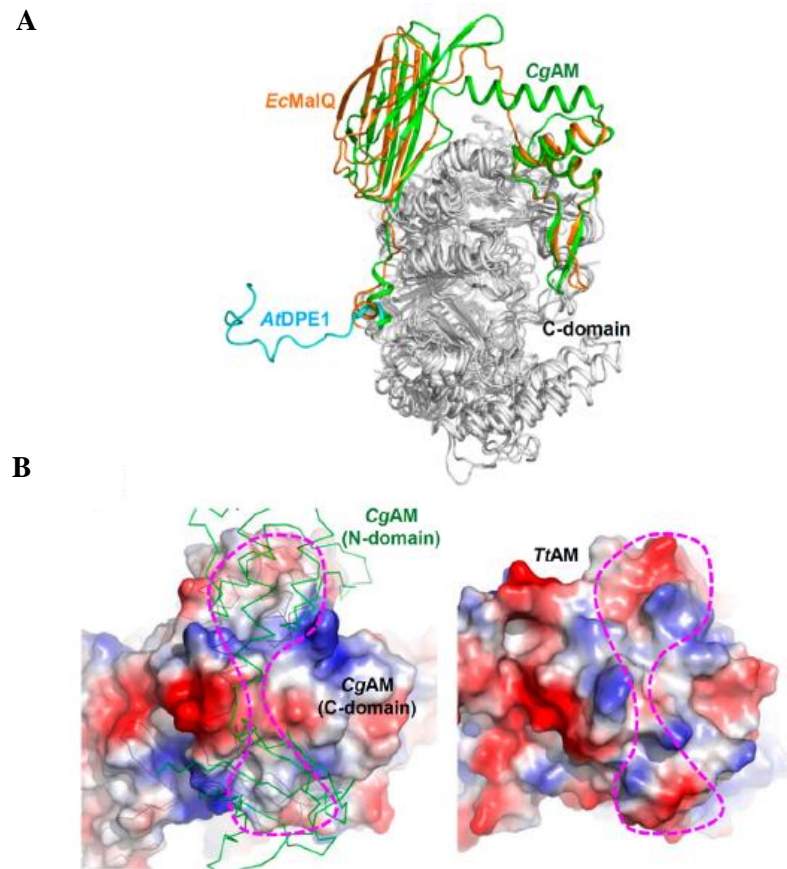


Figure 1. 8 Comparison of N-domains of amyloamylases. Structures of *CgAM*, *EcAM*, *TtAM* and *AtDPE1* are superimposed. C-domains of four enzymes are shown in grey while N-domains of *CgAM* and *EcAM* in green and orange, respectively, and N-terminal arm region of *AtDPE1* is shown in cyan (A). Charge distribution on the surfaces of C-domains of *CgAM* and *TtAM*. The N-domain and C-domain of *CgAM* are shown as ribbon and electrostatic potential surface mode (left), and *TtAM* as an electrostatic potential surface mode (right). N-domain interacting region on the C-domain is indicated as a magenta-colored dotted line (left), and the corresponding region of *TtAM* is indicated as in *CgAM* (B) (Joo *et al.*, 2016).

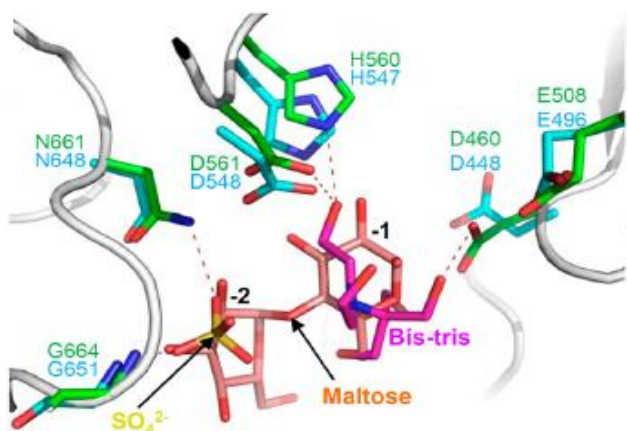


Figure 1. 9 Active site of *CgAM*. The superimposed amyloamylase structures of *CgAM* and *EcAM* with bis-tris methane and maltose complex, respectively. The bis-tris and sulfate molecule bound in *CgAM* are shown in pink and yellow, respectively. The maltose molecule bound in *EcAM* is shown as salmon-colored stick. Catalytic residues in *CgAM* (D460, E508 and D561) and *EcAM* (D448, E496 and D548) are shown in green and cyan-colored stick, respectively (Joo *et al.*, 2016).

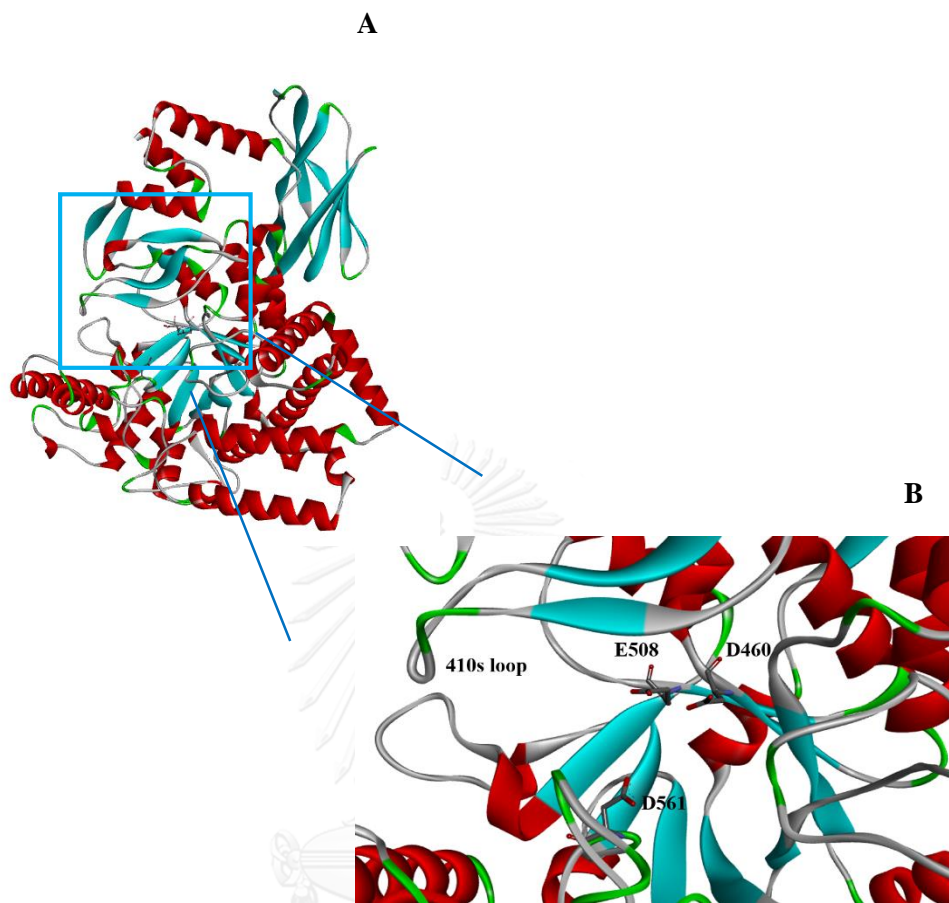


Figure 1. 10 Structure of amyloamylase from *C. glutamicum* (CgAM) (PDB code 5B68). α -helix, β -sheet and loop are red, cyan and green, respectively. The expanded structures in the box in (A) are the three catalytic residues (D460, E508 and D561) and 410s loop (B) (Joo *et al.*, 2016).

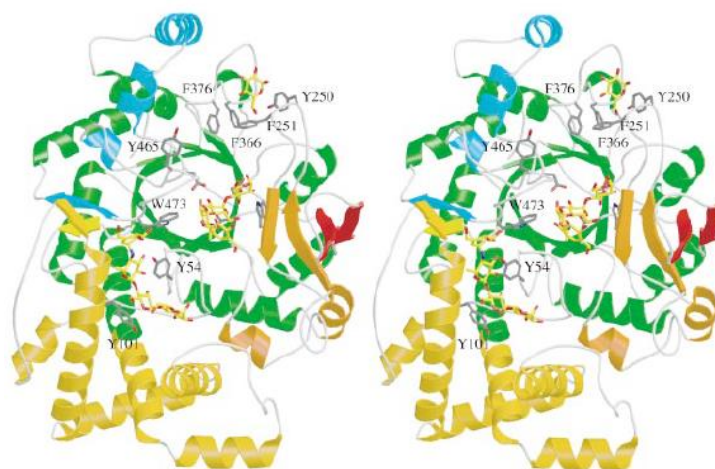


Figure 1.11 Ribbon representation (stereo view) of the fold of amyloamylase *T. aquaticus* (TaAM) with acarbose. In addition to the two acarbose molecules (yellow carbon atoms), selected protein side chains (dark gray carbon atoms) are shown. The acarbose molecule bound to the active site is on the upper right side, close to W473. The catalytic side chains (D293, E340 and D395) and W258 which are partially hidden by acarbose or protein residues are not labelled. The $(\beta/\alpha)_8$ barrel core structure (subdomain A) is colored in green, insertions between the first and fifth strand of the barrel (subdomains B2 and B1) are painted in a gradient going from yellow to red. Additional small insertions are shown in blue (subdomain B3) (Przylas *et al.*, 2000a).

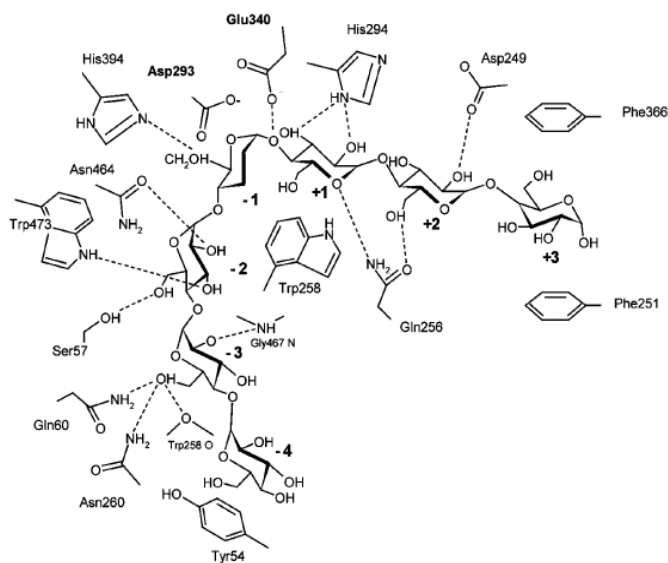


Figure 1. 12 Proposed binding of maltoheptaose (G7) in the active site of amyloamylase from *Thermus thermophilus* (*TtAM*). Catalytic residues are shown in boldface (D293 and E340) (Kaper *et al.*, 2007).

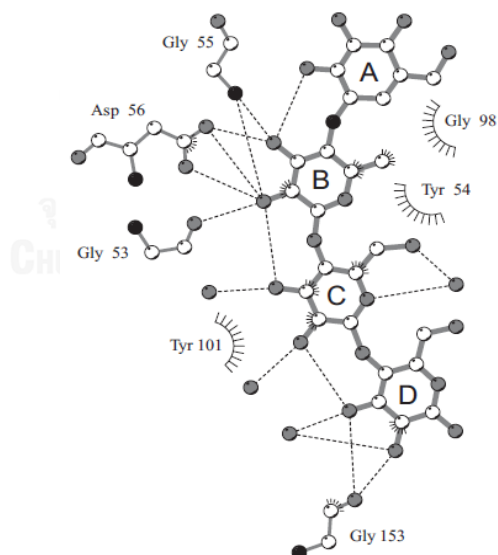


Figure 1. 13 Scheme of the interactions of acarbose bound to the secondary glucan binding site of amyloamylase from *T. aquaticus* (*TaAM*) (Przylas *et al.*, 2000a)

CHAPTER II

MATERIALS AND METHODS

2.1 Equipments

Autoclave: Model H-88LL, Kokusan Ensinki Co., Ltd., Japan

Autopipette: Pipetman, Gilson, France

Centrifuge, refrigerated centrifuge: Model Avanti™ J30-1I, Beckman Instrument Inc., USA

Electrophoresis unit:

- Mini protein, Bio-Rad, USA
- Agarose gel electrophoresis, Bio-Rad, USA

Differential scanning calorimeter, Microcal, LLC, Nothampton, USA

Gel Document: SYNGEND, England

Gel support film for polyacrylamide, Bio-Rad, USA

HPAEC DX-600: Dionex Corp., Sunnydale, USA)

- Column: Carbopac PA-100™ 4 x 250 mm
- Pulsed amperometric detector: DIONEX ED40
- Autosampler: DIONEX AS40
- Column oven DIONEX ICS-3000 SP

Incubator, waterbath:

- Model M20S, Lauda, Germany and BioChiller 2000, FOTODYNE Inc., USA
- ISOTEMP 210, Fisher Scientific, USA

Incubator shaker: Innova™ 4080, New Brunswick Scientific Co., Ltd., England

Isothermal titration calorimeter, Microcal, LLC, Nothampton, USA

Laminar flow: HT123, ISSCO, USA

Magnetic stirrer: Model Fisherbrand, Fisher Scientific, USA

Membrane filter: polyethersulfone (PES), pore size 0.45 µm, Whatman, England

Microcentrifuge: Eppendorf, Germany

pH meter: Model PHM95, Radiometer Copenhagen, Denmark

Power supply: Model POWER PAC 300, Bio-Rad, USA

Shaking waterbath: Model G-76, New Brunswick Scientific Co., Inc., USA

Sonicator: Bendelin, Germany

Spectrophotometer: DU Series 650, Beckman, USA

Thermal cycler: Mastercycler, Eppendorf, Germany

UV detector: Monitor UV-1, GE Healthcare Bio-Sciences AB, Sweden

Vortex: Model K-550-GE, Scientific Industries, Inc, USA

2.2 Chemicals

Acrylamide: Merck, Germany

Agar: Merck, Germany

Agarose: FMC Bioproducts, USA

Ammonium persulphate: Sigma, USA

Ammonium sulphate: Carlo Erba Reagenti, Italy

Ampicillin: Sigma, USA

Bovine serum albumin (BSA): Sigma, USA

Boric acid: Merck, Germany

Coomassie brilliant blue R-250: Sigma, USA

Copper sulfate: Carlo Erba Reagenti, Italy

4,4-Dicarboxy-2,2-biquinoline: Sigma, USA

Dimethyl sulfoxide (DMSO): Merck, Germany

di-Potassium hydrogen phosphate anhydrous: Carlo Earba Reagenti, Italy

di-Sodium ethylene diamine tetra acetic acid: M&B, England

1 kb DNA ladderTM: New England BioLabs Inc., USA and Fermentas, Canada

DNA extraction kit: Geneaid Biotech Ltd., Taiwan

dNTP: Stratagene, USA

Ethidium bromide: Sigma, USA

Ethyl alcohol absolute: Carlo Erba Reagenti, Italy

Ethylene diamine tetra acetic acid (EDTA): Merck, Germany

Gel extraction kit: Geneaids Biotech Ltd., Taiwan

Glacial acetic acid: Carlo Erba Reagenti, Italy

Glucose: BDH, England

Glucose liquicolor (Glucose oxidase kit): HUMAN, Germany

Glycerol: Merck, Germany

Glycine: Sigma, USA

Hydrochloric acid: Carlo Erba Reagenti, Italy

Iodine: Baker chemical, USA

Isopropylthio- β -D-galactoside (IPTG): Sigma, USA

Maltoheptaose (G7), Maltohexaose (G6), Maltopentaose (G5), Maltotetraose (G4),
and Maltotriose (G3): Wako Pure Chemical Industries, LTD., Japan

Maltose: BDH, England

β -Mercaptoethanol: Fluka, Switzerland

N, N'-Methylene-bis-acrylamide: Sigma, USA

N, N, N, N'-Tetramethyl-1, 2-diaminoethane (TEMED): Carlo Erba Reagenti, Italy

Pea starch: Emsland-Stärke GmbH, Germany

Peptone: Scharlau Microbiology, Spain

Phenol: Fisher Scientific, England

Phenylmethylsulfonyl fluoride (PMSF): Sigma, USA

Potassium iodide: Mallinckrodt, USA

Potassium phosphate monobasic: Carlo Erba Reagenti, Italy

Sodium acetate: Merck, Germany

Sodium carbonate anhydrous: Carlo Earba Reagenti, Italy

Sodium chloride: Carlo Earba Reagenti, Italy

Sodium citrate: Carlo Earba Reagenti, Italy

Sodium dodecyl sulfate: Sigma, USA

Sodium hydroxide: Merck, Germany

Soluble starch (potato): Scharlau Microbiology, Spain

Standard Large-ring cyclodextrin (LR-CD): Ezaki Glico Co., Ltd., Japan

Standard protein marker: Amersham Pharmacia Biotech Inc., USA

Tris (hydroxymethyl)-aminomethane: Carlo Earba Reagenti, Italy

Tryptone: Scharlau Microbiology, Spain

Yeast extract: Scharlau Microbiology, Spain

2.3 Enzymes, Restriction enzymes and Bacterial strains

Corynebacterium glutamicum ATCC 13032, Thailand Institute of Scientific and Technological Research, Thailand

E. coli BL21 (DE3): Novagen, Germany

Glucoamylase from *Aspergillus niger*: Fluka, Switzerland

Pfu Turbo[®] DNA polymerase: Promega, USA

Plasmid pET-19b: Novagen, Germany

Restriction enzymes

- *Dpn* I: New England BioLabs Inc. USA
- *Nde* I: Fermentas, Canada.
- *Xho* I: Fermentas, Canada.

2.4 Construction of mutated amyloamylase gene from *C. glutamicum*

2.4.1 Selection of target amino acid residues

Target amino acid residues of *CgAM* were selected by using the amino acid multiple sequence alignment and superimposed of X-ray structures between *CgAM* (Joo *et al.*, 2016; Srisimarath *et al.*, 2013) and well-known characterized amyloamylase from *Thermus* sp. (*TaAM*) (Przytylska *et al.*, 2000b). Three amino acid residues were chosen as followed;

1. Y418 residue at the tip of 410s loop which lies over the active site (corresponded to F251 in 250s loop in *Thermus* sp.)

2. H461 residue near the catalytic site of amyloamylase corresponded to H294 in *Thermus sp.*

3. N287 residue near the second binding site of amyloamylase corresponded to Y101 in *Thermus sp.*

2.4.2 Site-directed mutagenesis of *CgAM* gene

Site directed mutagenesis of *CgAM* gene was performed by amino acid substitution using mutated primers. A plasmid (pET-19b) carrying wild type (WT) *CgAM* gene was used as template to design mutated primers. Mutated *CgAM* genes were constructed by PCR mediated site-directed mutagenesis using Quick-Change kit (Stratagene, USA) and mutated primers which contained a mutation site at three residues (Y418, H461 and N287). Changes to alanine (A), aspartic acid (D), serine (S), arginine (R) and tryptophan (W) were performed. For Y418, substitution by phenylalanine (F) was also performed. The mutated primers were shown in Table 2.1, 2.2 and 2.3.

PCR conditions were pre-denaturation for 2 min at 95 °C, denaturation for 1 min at 95 °C, annealing for 30 sec at 68 °C, extension for 16 min at 72 °C and post-extension for 10 min at 72 °C. PCR product was digested with *Dpn* I endonuclease (target sequence: 5'-GA_{CH₃}[^]TC-3') which is specific for methylated as well as hemimethylated DNA. The enzyme was used to digest parental DNA template to select the mutation-containing DNA synthesized for 1 h. DNA isolated from almost all *E. coli* strain is dam-methylated which is susceptible to *Dpn* I. The nicked plasmid of *Dpn* I treated was then transformed into *E. coli* BL21 (DE3) electrocompetent cells.

2.4.3 Preparation of competent cells for electroporation (Sambrook and Russell, 2006)

A fresh overnight culture of *E. coli* BL21 (DE3) was inoculated into 100 ml of LB medium with 1% inoculum size. The cell culture was cultivated with shaking at 250 rpm until OD₆₀₀ reached 0.3 to 0.4. The culture was chilled on ice for 15 min at 4 °C. The cells were washed by cold sterilize water, centrifuged at 5,000 x g for 3 times at 4 °C. After centrifugation, the cells were resuspended in approximately 15-20 ml of 10% glycerol in distilled water and centrifuged at 5,000 x g for 10 min at 4 °C. Finally, the cells were resuspended again in 10 ml of 10% glycerol in distilled water and then 20-30 µl of cell suspension was aliquoted into each eppendorf tube and stored at -80 °C until use.

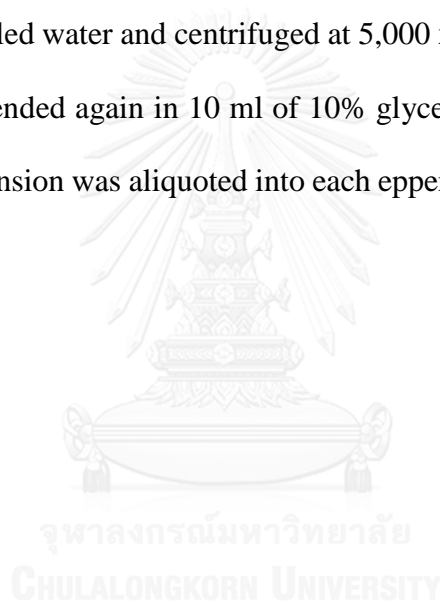


Table 2. 1 Y418 mutated *CgAM* gene primers for PCR mediated site - directed mutagenesis. The mutation positions were underlined.

Y418A_FWD	[5'- CGCCCCACCAGTTGGAG <u>CCA</u> ACCAGCAGGGCCAAG -3']
Y418A_REV	[5'- CTTGGCCCTGCTGGTTGG <u>CT</u> CCATCTGGTGGGGCG -3']
Y418S_FWD	[5'- CACCAGATGGAT <u>CCA</u> ACCAGCAGGG -3']
Y418S_REV	[5'- CCCTGCTGGTTGG <u>A</u> TCCATCTGGTG -3']
Y418D_FWD	[5'- CCACCAGATGGAG <u>ACA</u> ACCAGCAGG -3']
Y418D_REV	[5'- CCTGCTGGTTGTCTCCAT <u>C</u> TGGTGG - 3']
Y418R_FWD	[5'- CCACCAGATGGAG <u>CG</u> CAACCAGCAGGGC -3']
Y418R_REV	[5'- GCCCTGCTGGTTG <u>CG</u> TCCATCTGGTGG -3']
Y418W_FWD	[5'- CACCAGATGGAT <u>GGA</u> ACCAGCAGGGCCAAGACTGG -3']
Y418W_REV	[5'- CCAGTCTTGGCCCTGCTGGTT <u>CC</u> ATCCATCTGGTG -3']
Y418F_FWD	[5'- CCCACCAGATGGAT <u>TTA</u> ACCAGCAGGGCC -3']
Y418F_REV	[5' - GGCCCTGCTGGTTA <u>AA</u> TCCATCTGGTGGG -3']

Table 2. 2 H461 mutated *CgAM* gene primers for PCR mediated site - directed mutagenesis. The mutation positions were underlined.

H461A_FWD	[5'- GCGGAATCCGCGTGGAC <u>G</u> CGTTCTTGGTTTGTTTCAG- 3']
H461A_REV	[5'- CTGAACAAACCAAGAAC <u>G</u> CGGTCCACGCGGATTCCGC- 3']
H461S_FWD	[5'- CGGCGGAATCCGCGTGGAC <u>A</u> GCGTTCTTGGTTTGTTTCAGG- 3']
H461S_REV	[5'- CCTGAACAAACCAAGAACGCTG <u>T</u> CCACGCGGATTCCGCCG- 3']
H461D_FWD	[5'- GCGGAATCCGCGTGGACGACGTTCTTGGTTTGTTTC- 3']
H461D_REV	[5'- GAACAAACCAAGAAC <u>G</u> TCGTCCACGCGGATTCCGC- 3']
H461R_FWD	[5'- CGGAATCCGCGTGGAC <u>C</u> GCGTTCTTGGTTTGTTTC- 3']
H461R_REV	[5'- GAACAAACCAAGAACG <u>C</u> GGTCCACGCGGATTCCG- 3']
H461W_FWD	[5'- GCGGAATCCGCGTGGAC <u>T</u> GGGTTCTTGGTTTGTTTCAGG- 3']
H461W_REV	[5'- CCTGAACAAACCAAGA <u>A</u> CCAGTCCACGCGGATTCCGC- 3']

Table 2. 3 N287 mutated *CgAM* gene primers for PCR mediated site - directed mutagenesis. The mutation positions were underlined.

N287A_FWD	[5'- GACATCATTGAGCG <u>CG</u> CTGACGTCTACGCTGC -3']
N287A_REV	[5'- GCAGCGTAACGTCAGCG <u>CG</u> CTCAATGATGTC -3']
N287S_FWD	[5'- GACATCATTGAGCG <u>CT</u> CTGACGTCTACGCTGC -3']
N287S_REV	[5'- GCAGCGTAGACGTC <u>AG</u> AGCGCTCAATGATGTC -3']
N287D_FWD	[5'- CATCATTGAGCG <u>G</u> ATGACGTCTACGC -3']
N287D_REV	[5'- GCGTAGACGTCAT <u>C</u> GCGCTCAATGATG -3']
N287R_FWD	[5'- CCTCAGACATCATTGAG <u>CGCC</u> GCGACGTCTACGCTGCAAAGC -3']
N287R_REV	[5'- GCTTTGCAGCGTAGACGTC <u>CGCG</u> GCGCTCAATGATGTCTGAGG -3']
N287W_FWD	[5'- GACATCATTGAGCG <u>CTGGG</u> GACGTCTACGCTGC -3']
N287W_REV	[5'- GCAGCGTAGACG <u>TCCC</u> AGCGCTCAATGATG TC -3']

2.4.4 Plasmid transformation

The recombinant plasmids containing mutated *CgAM* gene from section 2.4.2 were introduced into *E. coli* BL21 (DE3) competent cells by electroporation technique. In the electroporation step, 0.2 cm cuvettes and sliding cuvette holder were chilled on ice before use. The Gene Pulser[®] apparatus was set to the 25 μ F capacitor, 2.5 kV, and the pulser controller unit was set to 200. The competent cells which were prepared as described in 2.4.3 were gently thawed on ice. One to five microliter of recombinant plasmid was mixed with 30 μ l of the electrocompetent cells and then placed on ice for 3 min. This mixture was transferred into a chilled cuvette. The cuvette was applied one pulse at the above settings. Subsequently, one milliliter of LB medium (1% tryptone, 0.5% yeast extract, and 0.5% NaCl) was added immediately to the cuvette. The cells were quickly resuspended, then the cell suspension was transferred to new sterilize tube and incubated at 37 °C for 45 min with 150 rpm shaking. Finally, the cell suspension was spread onto the LB agar plate containing 100 μ g/ml ampicillin. After incubation at 37 °C for 16 h, the colonies were picked.

2.4.5 Selection of mutated transformant clones

Transformation colonies were cultured in LB medium containing 100 μ g/ml ampicillin for 12 h. The recombinant mutated plasmids were extracted, and size check was performed by agarose gel electrophoresis. The point mutation was confirmed by nucleotide sequencing.

2.4.6 Nucleotide sequencing

About 50-100 ng of the recombinant mutated plasmids from section 2.4.5 were subjected to automated DNA sequencing (Wardmedic, Thailand). The sequencing was performed using T7 promoter and T7 terminator for DNA sequence 5' terminus and 3'

terminus of the inserted *CgAM* gene, respectively. The obtained DNA sequence was used to design internal primers of f2CgAM and r2CgAM for determining the residual sequence which was localized in the middle of the gene. The internal primers were used as shown below;

F2CgAM_FWD: [5'- TCTACTCTGTGCGTTCCACGTTG -3']

R2CgAM_REV: [5'- CCTGCGAGTTCTGCTTATAGG - 3']

The mutated gene was compared with WT- *CgAM* gene to determine point mutation by Clastal O program (1.2.4).

2.5 Expression and purification of recombinant amyloamylase

2.5.1 Expression of amyloamylase in *E. coli*

E. coli BL21(DE3) cells harboring WT or mutated *CgAM* genes were grown in LB medium (1% tryptone, 0.5% yeast extract and 0.5% NaCl) containing 100 µg/ml ampicillin at 37 °C, expression was triggered by 0.4 mM of isopropylthio-β-D-galactoside (IPTG) as described (Srisimarat *et al.*, 2011). Cells were cultured at 16 °C, 150 rpm for 20 h and harvested by centrifugation at 5000 x g for 15 min at 4 °C then washed by 0.85% NaCl and extraction buffer, respectively as described (Srisimarat *et al.*, 2011). Bacterial cells were resuspended in extraction buffer then disrupted by 15 cycles sonication (30% pulse for 1 min and stopped for 3 min for each cycle). Bacterial cells debris was removed by centrifugation at 12,000 x g, 4 °C for 45 min. The supernatant carrying crude enzyme was collected and dialyzed against 20 mM phosphate buffer pH 7.4.

2.5.2 Purification of amyloamylases

The crude amyloamylase (containing His-tag fragment) from section 2.5.1 was purified by Hisrap FF™ affinity at 4 °C. The column was equilibrated with 20 mM phosphate buffer pH 7.4 containing 20 mM imidazole and 0.5 M NaCl at the flow rate of 1ml/min. The crude enzyme solution was applied to Hisrap FF™ column (1 ml, two columns consecutively) and washed with the same buffer until A₂₈₀ of eluent decreased to baseline. The purified enzyme was eluted by the same buffer supplemented with 500 mM imidazole (Srisimarath *et al.*, 2011). Fractions were collected and the enzyme activity was determined. The active fractions were pooled and dialyzed against 20 mM phosphate buffer pH 7.4 and protein bands, protein concentration and enzyme activity were determined as described in section 2.6, 2.7 and 2.8 respectively.

2.6 Polyacrylamide gel electrophoresis (PAGE)

2.6.1 SDS-Polyacrylamide gel electrophoresis (SDS-PAGE)

Sodium dodecyl sulphate polyacrylamide gel electrophoresis (SDS-PAGE) was performed by using protein gel apparatus (Bio-rad Laboratory, USA). Before loading the sample on the gel, the samples were mixed with loading buffer which contained 60 mM Tris-HCl pH 6.8; 25% (v/v) glycerol; 2% (w/v) SDS; 14.4 mM 2-mercaptoethanol; 1% (w/v) bromophenol blue and boiled for 5 min. 7.5% Stacking gel and 5% separating gel were performed. Pre-stained Protein Ladder (Thermo Scientific Page Ruler), a mixture of proteins of various sizes (10 to 180 kDa), was used as protein marker. Protein bands were observed by Coomassie blue staining.

2.6.2 Detection of protein bands by Coomassie blue staining

The gel was stained by agitating with Coomassie staining solution (1%, w/v Coomassie blue R-250, 45%, v/v methanol and 10%, v/v glacial acetic acid) for 1-2 h. Then, destained by destaining solution (10%, v/v methanol and 10%, v/v glacial acetic acid) for several times until gel background was cleared.

2.7 Protein determination

Protein concentration was determined by coomassie blue according to Bradford method, using bovine serum albumin as standard (Bollag *et al.*, 1996). One hundred microliter of sample was mixed with 1 ml of Bradford working solution containing Coomassie blue G-250 for 10 min and the absorbance was measured at 595 nm.

2.8 Enzyme assay

All assays were performed for wild- type (WT) and mutated CgAMs. Amylomaltase activity was determined by six assays as described below.

2.8.1 Starch transglucosylation activity

The starch transglucosylation activity was measured by iodine method. The enzyme activity was determined by the ability to transfer glucosyl group from starch donor to maltose acceptor. The remained starch was detected by adding iodine solution (Park *et al.*, 2007). The reaction mixture containing 250 μ l of 0.2% soluble potato starch, 50 μ l of 1% (w/v) maltose, 100 μ l of enzyme and 600 μ l of 50 mM phosphate buffer, pH 6.0. The reaction was incubated at 30 °C for 10 min and stopped by boiling for 10 min. Then, 100 μ l of reaction mixture was aliquoted and mixed with 1 ml of

iodine solution (0.02% (w/v)) I₂ in 0.2% (w/v) KI) and the absorbance at 600 nm was measured.

One unit is defined as the amount of enzyme required to degrade 1 mg starch/ml per min under the described condition.

2.8.2 Disproportionation activity

This activity was measured by following glucose produced from glucosyl transfer between short oligosaccharides using glucose oxidase method (Miwa *et al.*, 1972). The 50 µl of reaction mixture, containing 5% (w/v) maltotriose (G3) and enzyme in 50 mM phosphate buffer, pH 6.0 was incubated at 40 °C for 10 min, the reaction was stopped by boiling for 10 min. An aliquot of 10 µl was mixed with glucose oxidase reagent kit and incubated at 30 °C for 10 min. The absorbance at 505 nm was measured.

One unit defined as the amount of enzyme required for the production of 1 µmole of glucose per min under the described condition.

2.8.3 Starch degrading activity

This activity was determined by measuring the degraded starch in the reaction by iodine method (Srisimarat *et al.*, 2011). The 250 µl of reaction mixture, containing 100 µl of 0.75% (w/v) potato soluble starch, 50 µl of the enzyme and 50 mM phosphate buffer pH 6.0. The reaction was incubated at 30 °C for 10 min, stopped by adding 500 µl of 1 N HCl. Then, 100 µl of reaction mixture was aliquoted and mixed with 900 µl of iodine solution (0.005% (w/v)) I₂ in 0.05% (w/v) KI) and the absorbance at 660 nm was measured.

One unit is defined as the amount of enzyme required to degrade 1 mg starch/ml per min under the described condition.

2.8.4 Cyclization activity

This activity was determined by measuring LR-CD product using high-performance anion exchange chromatography with pulse amperometric detection (HPAEC-PAD) (Srisimarat *et al.*, 2011). The reaction mixture contained 150 μ l of 2% (w/v) pea starch and 50 μ l of enzyme in 50 mM phosphate buffer pH 6.0 in a total volume of 1.5 ml. The reaction was incubated at 37 °C for 1.5 h, then stopped by boiling for 10 min. After cooling, 8 U of glucoamylase was added and further incubated at 40 °C for 18 h. The reaction was inactivated by boiling for 10 min, then the reaction was cooled down and analyzed by (HPAEC-PAD) (model ICS-5000 single pump, Dionex, USA), using Carbopac PA-100 (4x250 mm). Elution was by six continuous steps linear gradient of sodium nitrate in sodium hydroxide as previously described (Srisimarat *et al.*, 2011). The size of LR-CD products was compared with standard LR-CDs (CD22-CD50).

One unit is defined as the amount of enzyme required for the production of 1 nC of CD31 per min under the described condition.

2.8.5 Coupling activity

This activity is a reverse of cyclization activity, measured by DNS method (Zhu *et al.*, 2005). The 500 μ l of reaction mixture, containing 100 μ l of 3 mg/ml of LR-CDs, 100 μ l of 1 mg/ml (w/v) of glucose and 100 μ l of the enzyme in 50 mM phosphate buffer pH 6.0. The reaction was incubated at 30 °C for 10 min, then stopped by boiling. 8 U of glucoamylase was added to reaction, incubated at 40 °C for 30 min and inactivated by boiling. DNS reagent (3,5-dinitrosalicylic acid, 500 μ l was added and boiled for 5 min, cooled down the reaction at room temperature and added 4 ml of distilled water. The absorbance at 540 nm was measured.

One unit is defined as the amount of enzyme required for the production of 1 μ mole of reduced glucose per min under described condition.

2.8.6 Hydrolytic activity

This activity was determined by measuring glucose produced from hydrolysis of LR-CDs by bicinchoninic acid (BCA) assay (Srisimararat *et al.*, 2011). The 50 μ l of reaction mixture, containing 30 μ l of 0.5 mg/ml of LR-CDs and 10 μ l of the enzyme in the total volume of 50 μ l of 50 mM phosphate buffer pH 6.0. The reaction was incubated at 30 °C for 10 min, then stopped by adding 30 μ l of 1 N HCl. Bicinchoninic acid reagent was added to make the final volume of 1 ml, incubated at 80 °C for 25 min, inactivated the reaction on ice for 5 min. The absorbance at 562 nm was measured.

One unit is defined as the amount of enzyme required for the production of 1 μ mole of reduced glucose per min under the described condition.

2.9 Characterization of amyloamylase

2.9.1 Effect of temperature on amyloamylase activity

The effect of temperature on starch transglucosylation, disproportionation and cyclization activities of WT and mutated CgAMs were determined at optimum pH of 6.0 using 50 mM phosphate buffer. The temperature was varied in the range of 25-70 °C. The activity was determined as described in section 2.8.1, 2.8.2 and 2.8.4. The maximum activity observed for each enzyme was set as 100%.

2.9.2 Effect of pH on amyloamylase activity

The effect of pH on enzyme activity for starch transglucosylation, disproportionation and cyclization activities were determined as described in section 2.8.1, 2.8.2 and 2.8.4, respectively. WT and mutated CgAMs were incubated in various buffers: acetate buffer (pH 4.0-6.0), phosphate buffer (pH 6.0-8.0) and tris-HCl buffer (pH 8.0-9.0) at each optimum temperature before determination of enzyme activity. The results were shown as percentage of relative activity. The highest activity was defined as 100%.

2.9.3 Effect of temperature on amyloamylase stability

The effect of temperature on enzyme stability for disproportionation reaction was determined. WT and mutated CgAMs were incubated at various temperatures (30-40 °C) for 0-180 min and then enzyme activity was measured under the standard condition as described in section 2.8.2. The results were shown as percentage of relative activity. The highest activity was defined as 100%.

2.9.4 Effect of pH on amyloamylase stability

The effect of pH on enzyme stability for disproportionation reaction was determined as described in section 2.8.2. WT and mutated CgAMs were incubated at 30 °C in phosphate buffer pH 7.0 and tris-HCl buffer pH 8.0 for 0-120 min before determination of enzyme activity. The results were shown as percentage of relative activity. The highest activity was defined as 100%.

2.9.5 Substrate specificity

Substrate specificity was determined by measuring disproportionation activity using maltose (G2) to maltoheptaose (G7) as substrates. 0.2 U starch transglucosylation activity of CgAMs were incubated with 50 mM substrate in phosphate buffer pH 6.0 and the amount of glucose product was determined by glucose oxidase method as described in 2.8.2. The relative activities were calculated by using WT activity with G3 substrate as the control.

2.9.6 Determination of kinetic parameters

2.9.6.1 Disproportionation reaction

Kinetic study of disproportionation reaction was performed by incubating various concentrations of G3 substrate (0-40 mM) with CgAMs at 30 °C for 5 min. The kinetic parameters K_m and V_{max} were determined from Lineweaver-Burk plot, k_{cat} and k_{cat}/K_m values were calculated. The activities of mutated enzymes were determined by glucose oxidase method as described in section 2.8.2.

2.9.6.2 Cyclization reaction

0.05 U starch degrading activity of CgAMs was incubated with various concentrations of pea starch substrate (0-0.5%) in 50 mM phosphate buffer, pH 6.0 at 30 °C for 90 min then reaction was stopped by boiling for 10 min. 8 U of glucoamylase was added and incubated at 40 °C for 18 h. LR-CD products were analyzed by HPAEC-PAD as described in 2.8.4. The kinetic parameters of CgAMs on cyclization activity, K_m and V_{max} were determined from Lineweaver-Burk plot, k_{cat} and k_{cat}/K_m values were calculated.

2.9.7 Analysis of pattern of LR-CD products

LR-CD products were determined by HPAEC-PAD as described in 2.8.4.

2.9.7.1 Effect of incubation time on LR-CD profile

The reaction mixtures contained 0.2% (w/v) pea starch and 0.10 U starch degrading activity of CgAMs in 50 mM phosphate buffer, pH 6.0. The reaction was incubated at 30 °C for 1.5, 6, 12 and 24 h and then stopped by boiling. 8 U of glucoamylase was added and further incubated at 40 °C for 18 h and inactivated by boiling. The reaction products of CgAMs were analyzed by HPAEC-PAD.

2.9.7.2 Effect of the amount of enzyme on LR-CD profile

The reaction mixtures contained 0.2% (w/v) pea starch with various amounts of 0.5, 0.10 and 0.20 U starch degrading activity of CgAMs in 50 mM phosphate buffer, pH 6.0. The reaction was incubated at 30 °C for 6 h and then stopped by boiling. 8 U of glucoamylase was added, then incubated at 40 °C overnight and inactivated by boiling. The reaction products of CgAMs were analyzed by HPAEC-PAD.

2.9.8 Circular dichroism spectra

The spectra were obtained using a J-815 CD spectrometer (Jasco, Japan). A protein concentration of 0.2 mg/ml was used in the wavelength scanning range of 190-250 nm at 25 °C. Each CD spectrum was monitored in three scans at 20 nm/min with constant time at 2 sec and 2 nm bandwidth.

For the CD spectra, the Mean Residue Weight (MRW) for estimating the quantity of the peptide bond in protein as shown in equation (1) was calculated (Kelly *et al.*, 2005).

$$\text{MRW} = \frac{M}{(N-1)} \quad (1)$$

Where M is the molecular weight of the polypeptide chain (Da), N stands for the number of amino acid residues in the chain and N-1 is the number of peptide bonds. The mean residue ellipticity (MRE) at each of wavelength λ ($[\theta]_{\text{mrw}, \lambda}$) is given by equation (2)

$$[\theta]_{\text{mrw}, \lambda} = \frac{\text{MRW} \times \theta_{\lambda}}{10 \times d} \quad (2)$$

Where θ_{λ} = the observed ellipticity (degrees) at each wavelength

d = pathlength of cuvette (cm)

c = the protein concentration (g/ml)

If the molar concentration (m) of solute was known, the molar ellipticity at wavelength λ ($[\theta]_{\text{molar}, \lambda}$) is given by equation (3)

$$[\theta]_{\text{molar}, \lambda} = \frac{100 \times \theta_{\lambda}}{m \times d} \quad (3)$$

The unit of MRE and molar ellipticity is $\text{deg.cm}^2.\text{dmol}^{-1}$ (Kelly *et al.*, 2005). The percentages of protein secondary structures were calculated using the Dichroweb server program.

2.10 Biophysical characterization of amyломaltase

2.10.1 Isothermal titration calorimetry (ITC)

The enthalpy associated with CgAM activity interacted with G3 substrate in disproportionation reaction was determined by a Microcal VP-ITC isothermal titration calorimeter (Microcal, LLC, Nothampton, USA). Buffer and sample solutions were degassed immediately by centrifugation at $10,000 \times g$ 4°C for 45 min prior to conducting the assay. The reference cell, sample cell and titration syringe were filled with degassed milliQ water, 10 mM G3 in 20 mM phosphate buffer, pH 6.0 and 20 μM of each enzyme in 20 mM phosphate buffer pH 6.0, respectively. The system was equilibrated at 30°C which is the optimum condition of CgAMs with stirring at 329 rpm prior to titration of enzyme. Titration was performed by single injecting 20 μl of 20 μM purified WT and Y418A/W mutated CgAMs in 20 mM phosphate buffer containing 100 mM NaCl pH 6.0 into a stirred (329 rpm) cell of 1.3187 ml which contained 10 mM G3 in the same buffer, with reference power of 34.5 $\mu\text{cal/sec}$, initial delay of 100 sec for 4500 sec spacing time. For each titration experiment, buffer was titrated as a control instead of using enzyme. Titrations of both WT and Y418A/W mutated CgAMs were carried out similarly and continued until no significant signal response was observed on enzyme activity. The mean values of activities were calculated from three independent experiments.

To confirm the amyloamylase activity from ITC, disproportionation activity by glucose oxidase method was performed using the same condition of ITC experiment. The reaction mixtures containing various concentrations of substrate G3 (10 - 30 mM) were incubated with 20 μ M of CgAMs for 0, 1, 3, 5, 10, 20, 40 and 75 min. Then the enzyme activity was measured by glucose oxidase method as previously described in 2.8.2.

2.10.2 Kinetic measurements by ITC

All reactions were carried out at 30 °C in 20 mM phosphate buffer containing 100 mM NaCl pH 6.0. The cells were filled with similar solutions as described in 2.11.1 except that three sets of sample cells were filled with G3 at 10, 20 and 30 mM. Titration parameters of WT and Y418A/W mutated CgAMs were as described in 2.10.1. Origin software program was used to analyze the data.

2.10.3 Differential scanning calorimetry (DSC)

DSC analysis was performed using VP-DSC calorimeter (MicroCal, Northampton, MA, USA) with the cell volume of 0.52061 ml at every scan rate of 0.75, 1.0 and 1.5 °C/min in the temperature range of 10 - 90 °C. WT and mutated CgAMs were dissolved in 50 mM phosphate buffer containing 100 mM NaCl pH 6.0. All samples were determined for protein concentration by measuring absorbance at 280 nm using the Thermo Scientific Nanodrop 2000C spectrophotometer and also degassed by centrifugation at 3,000 x g, 4 °C for 30 min. Protein concentration of all CgAMs used was around 80 μ M. Base-line scan collected with buffer in the sample cells while degassed water was filled in the reference cell. The reversibility of enzyme thermal transition was evaluated by checking the reproducibility of scan rate on immediate cooling and rescanning. Origin program software with DSC add-on module was used

for data analysis, T_m (unfolding temperature, defined as the temperature of maximum apparent heat capacity) and T_p (peak temperature) were obtained. Thermal transition curves were obtained from the plot of heat capacity against temperature.

2.11 Structural Modeling

The X-ray structure of *CgAM* was previously reported (Joo *et al.*, 2016). In this study, the model structures of all mutated *CgAMs* were constructed by the Discovery Studio 3.5 Client program (Chikan *et al.*, 2013) using WT *CgAM* X-ray structure (PDB code 5B68) (Joo *et al.*, 2016) as template. The acarbose molecule bound at the active site of the X-ray structure of *TaAM* (PDB 1esw) (Przylas *et al.*, 2000a) was used to superimpose with WT and *CgAM* model structures.

The distances between the two residues Y418 and F534 at the loop entrance of WT and Y418 mutated *CgAMs* were determined. The interactions within enzyme molecule and between enzyme and acarbose at the active site through H-bond were examined and compared to WT enzyme..

CHAPTER III

RESULTS

The present work is to investigate the structure-function relationship of CgAM, particularly focuses on the structure important for controlling activity and LR-CD product formation of the enzyme. Site-directed mutagenesis was performed by substitution of amino acid residues of interest and their effects on enzyme structure and activities were monitored.

3.1 Construction of mutated amyломaltase gene from *C. glutamicum*

3.1.1 Selection of target amino acid residues of CgAM

Three amino acid residues from three regions of thermophilic amyломaltase (F251; H294 and Y101 in 250s unique loop, active site and 2nd binding glucan, respectively) (Jung *et al.*, 2011; Kaper *et al.*, 2007; Przylas *et al.*, 2000a) were selected as template residues in this study (see detail in Discussion section 4.1.1). By comparison of the amino acid sequence of TaAM with CgAM, our target residues for point mutation: F251, H294 and Y101 of TaAM are corresponded to Y418, H461 and Y290 of CgAM Figure 3.1. However, the result from superimposed structures of TaAM PDB code 1CWY (Przylas *et al.*, 2000b) with CgAM (Unpublished data), (Srisimarath *et al.*, 2013), which is more convincing than sequence comparison showed that F251, H294 and Y101 of TaAM are corresponded to Y418, H461 and N287, not Y290 of CgAM (Figure3.2).

The first residue of interest was Y418 which was at the tip of 410s loop in CgAM (corresponded to F251 in 250s loop of AM from *Thermus* sp. (Jung *et al.*, 2011). The second target was H461 which was near the catalytic site of amyloamylase corresponded to H294 in *Thermus* sp. (Kaper *et al.*, 2007). The third target was N287 which is near the second glucan binding site corresponded to Y101 in AM from *Thermus* sp. (Przylas *et al.*, 2000a). To investigate the effect of these positions (Figure 3.3) on the structure and function relationship of CgAM, site-directed mutagenesis of CgAM gene was performed as described in 2.4.2.

3.1.2 Extraction of recombinant plasmid pET - 19b - CgAM

The recombinant plasmid pET-19b containing CgAM gene (Srisimararat *et al.*, 2011) was extracted from *E. coli* DH5 α and DNA fragments were checked by agarose gel electrophoresis (Figure 3.4 Lane 1). After double digestion with *Nde* I and *Xho* I, it was found that the sizes of pET-19b vector and CgAM gene were around 5.7 kb and 2.1 k, respectively (Figure 3.4 Lane 2). The measured ratio of A260/A280 was 1.8 indicated the sufficient purity of this extracted recombinant plasmid for use as a template for PCR amplification.

3.1.3 Site-directed mutagenesis of CgAM gene

Through site-directed mutagenesis of CgAM gene, all mutants were constructed by a single point mutation at three positions: Y418, H461 and N287. All target residues were substituted by alanine, A (non polar aliphatic), tryptophan, W (aromatic), serine, S (polar uncharge), aspartic acid, D (negative charge) and arginine, R (positive charge). In addition, Y418 was also substituted by phenylalanine, F to mimic its corresponding residue of *Thermus* sp. amyloamylase.

The recombinant plasmid pET-19b containing *CgAM* gene was used a template for site-directed mutagenesis. The product from PCR amplification was found as a single band on agarose gel electrophoresis as shown in Figure 3.5, 3.7 and 3.9 for Y418-, H461- and N287-mutated *CgAM* genes, respectively. The size of PCR product was 7.8 kb as expected for *CgAM* gene and pET-19b.

3.1.4 Transformation

The PCR products after digestion with *Dpn* I were purified and transformed into the competent cells of *E. coli* BL21 (DE3) by electroporation. Two hundred microliters of transformants were spread on LB agar plate containing 100 µg/ml ampicillin and incubated overnight at 37 °C. The *E. coli* BL21 (DE3) containing pET-19b vector harboring each mutated *CgAM* gene was grown on the plate. To confirm the insertion of mutated *CgAM* genes into the pET-19b, the transformant clones were picked for plasmid extraction and digested with *Nde* I and *Xho* I. The agarose gel pattern of recombinant plasmid containing mutated *CgAM* genes was shown in Figure 3.6, 3.8 and 3.10 for Y418-, H461- and N287-mutated *CgAM* genes, respectively.

3.1.5 Nucleotide sequencing

To investigate the result of mutation on *CgAM* gene, the recombinant plasmids were subjected to DNA sequencing. T7 promoter and T7 terminator primers were used to sequence the 5' terminus and 3' terminus, respectively. The residual sequence of *CgAM* gene was extended by two primer pairs of f2*CgAM* and r2*CgAM* (sequence shown in section 2.4.6). The nucleotide sequences of Y418-, H461- and N287- mutated *CgAM* genes were aligned with WT-*CgAM* gene by Clustal O (1.2.4) program (Figure 3.11, 3.13 and 3.15), respectively. It was found that the nucleotide sequences of Y418, H461 and N287 mutated *CgAMs* contained 2,121 bp which could be deduced to 706

amino acids similar to WT gene. The deduced amino acid sequences of mutated *CgAM* genes were then compared to the WT sequencing using Clustal O program. Y418 was changed to Ala (A), Glu (D), Ser (S), Trp (W), Arg (R) and Phe (F) as shown in Figure 3.12 while H461 and N287 were changed to Ala (A), Glu (D), Ser (S), Trp (W) and Arg (R), respectively (Figure 3.14 and 3.16). These results confirmed that single point mutations at Y418, H461 and N287 on *CgAM* gene were successfully performed.



<i>TaAM</i>	-----	0
<i>CgAM</i>	MTARRFLNELADLYGVATSYPDYKGAHIEVSDDTLVKILRALGVNLDTSNLPNDDAIQRQ	60
<i>TaAM</i>	-----	0
<i>CgAM</i>	IALFHDFREFTRPLPPSVVAVEGDELVPVHVHDGSPADVHIELEDGTQRDVSQVENWTAP	120
<i>TaAM</i>	-----MELPRAFGLLLHPTSLPG-----	18
<i>CgAM</i>	REIDGIRWGEASFKIPGDLPLGWHLHLKSNERSAECGLIITPARLSTADKYLDSPRSGV	180
	* **: : * : *	
<i>TaAM</i>	-----PYGVVGLGLEARDFLRFLKAGGRFWQVLPFGPT----GYGDSPLYQAFS	63
<i>CgAM</i>	MAQIYSVRSTLSWGMGDFND-LGNLASVVAQDGADFLINPMHAAEPLPPTEDSPYLPTT	239
	: * : * : . : : : . : : * . * : * : : : : * * * * : :	
<i>TaAM</i>	AFAGNPYLIDLRPLAEKGYLV-----LKDPGFPQGRVDYGWLYAWKWPAKKA	110
<i>CgAM</i>	RRFINPIYIRVEDIPEFNQLEIDLRDDIAEMAAEFRERNLTSDIERNVYAAKLQVLRRA	299
	** * : . : * . * : : : . : . : . : : * * * * . * : *	
<i>TaAM</i>	AYQGFLEKAPRKEREDFPFQEQEASWLKDYALFMALKAQHGGLPWNRWPLPRLRREEKA	170
<i>CgAM</i>	IFEM---PRSSERANFVSVFVQR-----EGQGLIDFATWCADRETAQSES	341
	: : : . . : * : * : : : : * : : : * . : : : :	
<i>TaAM</i>	MKEAEEAALAEVAFHAWTQWLFFFEAWKALKEEAEALG--IQIIGDMPIFVAEDSAEVDWAH	228
<i>CgAM</i>	VHGTEPDRDELTMFYMWLQWLCDEQLAAAQKRAVDAGMSIGIMADLAVGVHPGGAD----	397
	: : : * * . * : * * * * * * : : : * * * * : : * : * : * : * : * : *	
<i>TaAM</i>	PEWFHLDEEGRPLVVAGVPPDYFSETGQRWGNPLYRWDVLEREGFSFWIARLAKALELFH	288
<i>CgAM</i>	--AQNLSHVLAPDASVGAAPPDGNQQGQDWSQPPWHPVRLAEEGYIPWRNLLRTVLRHSG	455
	: * . . * . . * * * * : : * * * : * : : * . * * : * * * . * . *	
<i>TaAM</i>	LVRVHFRGFEEAYWEIPASCPTAVEGRWVKASGEKLFDR--IQEVFGEVPILA ^Y DLGVIT	346
<i>CgAM</i>	GIRVTHVVLGLFRLFVMPRMQSP-ATGTYIRFDHNALVGI ^H LALAEELAGAVVIG ^D DLGTFE	514
	: * * * * * * : : : * : : . * : : : . : * . : : : . : : * * * * : :	
<i>TaAM</i>	PEVEFLDRDRYGLPGMKVLQFAFDHGMENPFLPHNYPAHGRVVVYTGTH ^D NDTTLGWYRTA	406
<i>CgAM</i>	PWVQDALAQRGIMGTSILWFEHSPSQPPRRQEEYRPLAL--TTVTTH ^D LPPTAGYLEGE	572
	* * : : : * : * : * . : * . . . * : : * . . . * * * * * * : .	
<i>TaAM</i>	SPHERAFLERYLADWGISFRQEEVFPWALMGLCLKSVARLAIYPVQDVLA-----	456
<i>CgAM</i>	HIALRERLGVLNTD--PAAELAEDLQWQAEILDV--AASANALPAREYVGLERDQRGELA	628
	* * : * : . * : : * * : . * * : : : .	
<i>TaAM</i>	-----LGSEARMNYPGRPSG---NWAWRLLPGQLTQEHA-	487
<i>CgAM</i>	ELLEGLHTFVAKTPSALTCVCLVDMVGEKRAQNQPGTTRDMYPNWCIPLCDSEGNSVLIE	688
	: * : : * * * . * * . * : : .	
<i>TaAM</i>	----ARL-LAMAEATGRT 500	
<i>CgAM</i>	SLRENELYHRVAKASKRD 706	
	. * : * : * : *	

Figure 3. 1 Amino acid sequence alignment of *TaAM* and *CgAM* using Clustal O (1.2.14). Three conserved catalytic residues (D293, E340 and D395 in *TaAM*; D460, E508 and D561 in *CgAM*) of amyloamylases were shown in red highlight. Y418, H461 and Y290 residues of *CgAM* were shown in green, blue and yellow, respectively. (*), (.) and (:.) represented amino acid identity, semi-conserved substitution and conserved substitution, respectively.

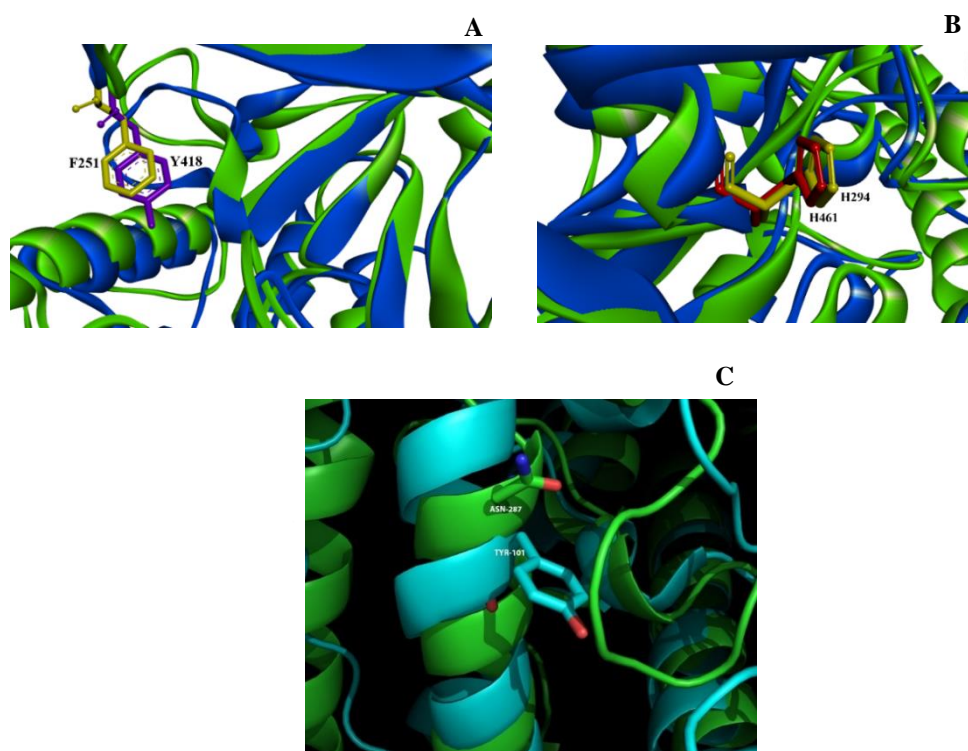


Figure 3. 2 The superimposed structures of CgAM (green) PDB 5B68 (Joo *et al.*, 2016; Srisimarath *et al.*, 2013) on TaAM (blue) PDB 1CWY (Przylas *et al.*, 2000b). The enzyme structures are displayed as secondary structures generated by Discovery Studio Client program 3.5. Corresponding residues are displayed as stick and colored by atom name: Y418-CgAM and F251-TaAM are shown in purple and yellow (A), H461-CgAM and H294-TaAM are shown in red and yellow (B), while N287-CgAM and Y101-TaAM are shown in green and cyan (C).

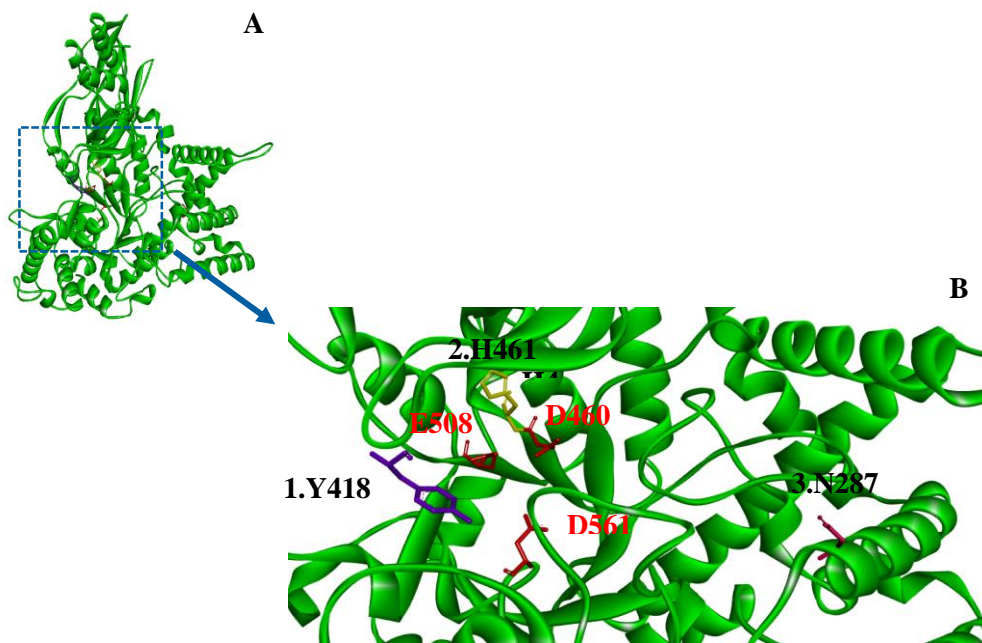


Figure 3. 3 Overall structures of WT CgAM (PDB code 5B68) (Joo *et al.*, 2016) (A). The expanded structure of that in the box in (A) are displayed (B). The three catalytic residues represented in red (D460, E508, D561) while Y418, H461 and N287 are shown in purple, yellow and pink, respectively.

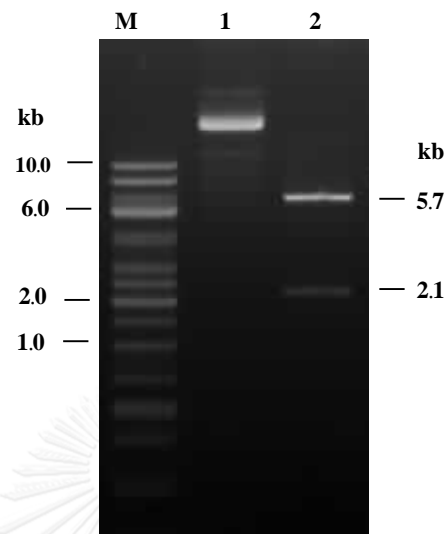


Figure 3. 4 Agarose gel electrophoresis of recombinant plasmid pET-19b-*CgAM*. The DNA samples were separated on 0.75% agarose gel and visualized by ethidium bromide staining.

Lane M = GeneRuler™ 1 kb DNA ladder (Fermentas, Canada)

Lane 1 = Recombinant plasmid containing *CgAM*

Lane 2 = Recombinant plasmid containing *CgAM* after double digestion with *Nde* I and

Xho I

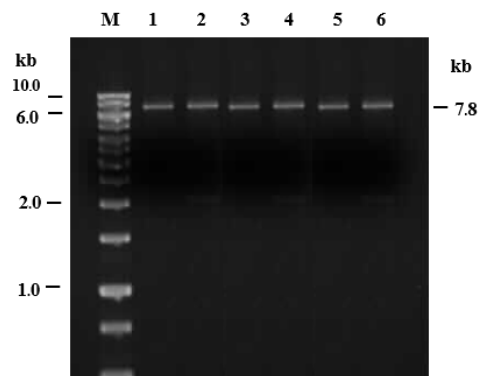


Figure 3. 5 Agarose gel electrophoresis of amplified DNA containing *CgAM* gene with a single point mutation at Y418. The DNA samples were separated on 0.75% agarose gel and visualized by ethidium bromide staining.

Lane M = GeneRuler™ 1 kb DNA ladder (Fermentas, Canada)

Lane 1, 2, 3, 4, 5 and 6 = PCR product from mutated Y418A-, Y418S-, Y418D-, Y418R-, Y418W- and Y418F-*CgAM*, respectively.

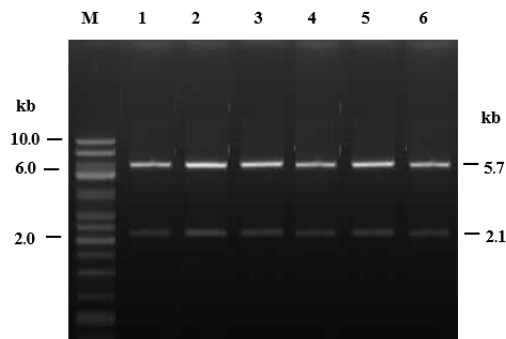


Figure 3. 6 Agarose gel electrophoresis of PCR product from pET-19b vector harboring *CgAM* gene with a single point mutation at Y418 after digested with *Nde* I and *Xho* I. The DNA samples were separated on 0.75% agarose gel and visualized by ethidium bromide staining.

Lane M = GeneRuler™ 1 kb DNA ladder (Fermentas, Canada)

Lane 1, 2, 3, 4, 5 and 6 = PCR product from pET19-b vector harboring mutated *CgAM* gene: Y418A, Y418S, Y418D, Y418R, Y418W and Y418F, respectively.

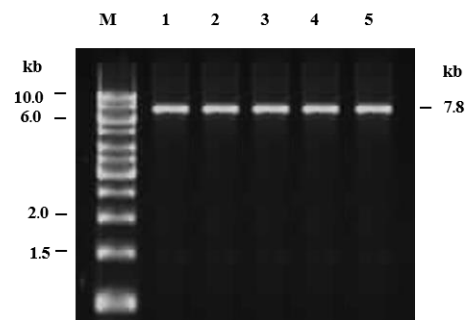


Figure 3. 7 Agarose gel electrophoresis of amplified DNA containing *CgAM* gene with a single point mutation at H461. The DNA samples were separated on 0.75% agarose gel and visualized by ethidium bromide staining.

Lane M = GeneRuler™ 1 kb DNA ladder (Fermentas, Canada)

Lane 1, 2, 3, 4 and 5 = PCR product from mutated H461A-, H461S-, H461D-, H461R- and H461W-*CgAM*, respectively.

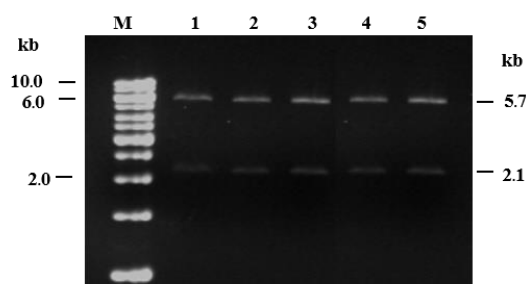


Figure 3. 8 Agarose gel electrophoresis of PCR product from pET-19b vector harboring CgAM gene with a single point mutation at H461 after digested with *Nde* I and *Xho* I. The DNA samples were separated on 0.75% agarose gel and visualized by ethidium bromide staining.

Lane M = GeneRuler™ 1 kb DNA ladder (Fermentas, Canada)

Lane 1, 2, 3, 4, 5 and 6 = PCR product from pET19-b vector harboring mutated CgAM gene: H461A, H461S, H461D, H461R and H461W, respectively.

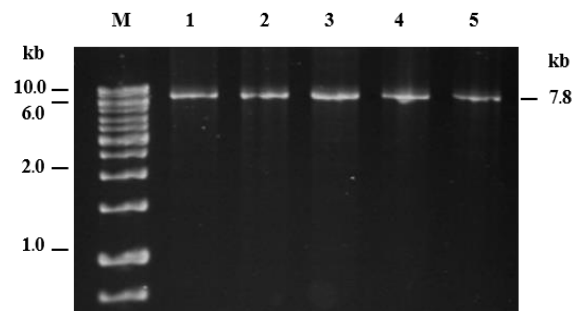


Figure 3. 9 Agarose gel electrophoresis of amplified DNA containing *CgAM* gene with a single point mutation at N287. The DNA samples were separated on 0.75% agarose gel and visualized by ethidium bromide staining.

Lane M = GeneRuler™ 1 kb DNA ladder (Fermentas, Canada)

Lane 1, 2, 3, 4 and 5 = PCR product from mutated N287A-, N287S-, N287D-, N287R- and N287W-*CgAM*, respectively.

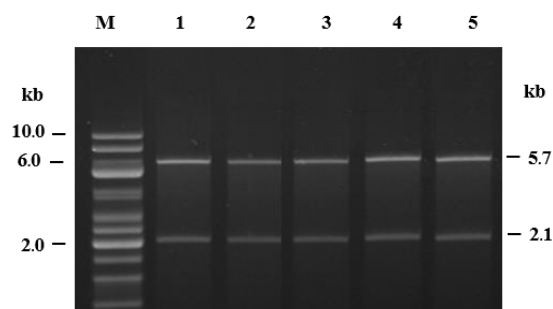


Figure 3. 10 Agarose gel electrophoresis of PCR product from pET-19b vector harboring *CgAM* gene with a single point mutation at N287 after digested with *Nde* I and *Xho* I. The DNA samples were separated on 0.75% agarose gel and visualized by ethidium bromide staining.

Lane M = GeneRuler™ 1 kb DNA ladder (Fermentas, Canada)

Lane 1, 2, 3, 4, 5 and 6 = PCR product from pET19-b vector harboring mutated *CgAM* gene: N287A, N287S, N287D, N287R and N287W, respectively.

Y418F_CgAM	ATGACTGCTCGCAGATTTTGAATGAACTCGCCGATCTCTACGGCGTAGCAACTTCTTAC	60
Y418W_CgAM	ATGACTGCTCGCAGATTTTGAATGAACTCGCCGATCTCTACGGCGTAGCAACTTCTTAC	60
Y418R_CgAM	ATGACTGCTCGCAGATTTTGAATGAACTCGCCGATCTCTACGGCGTAGCAACTTCTTAC	60
WT_CgAM	ATGACTGCTCGCAGATTTTGAATGAACTCGCCGATCTCTACGGCGTAGCAACTTCTTAC	60
Y418D_CgAM	ATGACTGCTCGCAGATTTTGAATGAACTCGCCGATCTCTACGGCGTAGCAACTTCTTAC	60
Y418A_CgAM	ATGACTGCTCGCAGATTTTGAATGAACTCGCCGATCTCTACGGCGTAGCAACTTCTTAC	60
Y418S_CgAM	ATGACTGCTCGCAGATTTTGAATGAACTCGCCGATCTCTACGGCGTAGCAACTTCTTAC	60

Y418F_CgAM	ACTGATTACAAAGGTGCCCATATTGAGGTCAGCGATGACACATTAGTGAAAACTCTGCGT	120
Y418W_CgAM	ACTGATTACAAAGGTGCCCATATTGAGGTCAGCGATGACACATTAGTGAAAACTCTGCGT	120
Y418R_CgAM	ACTGATTACAAAGGTGCCCATATTGAGGTCAGCGATGACACATTAGTGAAAACTCTGCGT	120
WT_CgAM	ACTGATTACAAAGGTGCCCATATTGAGGTCAGCGATGACACATTAGTGAAAACTCTGCGT	120
Y418D_CgAM	ACTGATTACAAAGGTGCCCATATTGAGGTCAGCGATGACACATTAGTGAAAACTCTGCGT	120
Y418A_CgAM	ACTGATTACAAAGGTGCCCATATTGAGGTCAGCGATGACACATTAGTGAAAACTCTGCGT	120
Y418S_CgAM	ACTGATTACAAAGGTGCCCATATTGAGGTCAGCGATGACACATTAGTGAAAACTCTGCGT	120

Y418F_CgAM	GCTCTGGGTGTGAATTTAGATACAAGCAACCTCCCCAACGATGACGCTATCCAACGCCAA	180
Y418W_CgAM	GCTCTGGGTGTGAATTTAGATACAAGCAACCTCCCCAACGATGACGCTATCCAACGCCAA	180
Y418R_CgAM	GCTCTGGGTGTGAATTTAGATACAAGCAACCTCCCCAACGATGACGCTATCCAACGCCAA	180
WT_CgAM	GCTCTGGGTGTGAATTTAGATACAAGCAACCTCCCCAACGATGACGCTATCCAACGCCAA	180
Y418D_CgAM	GCTCTGGGTGTGAATTTAGATACAAGCAACCTCCCCAACGATGACGCTATCCAACGCCAA	180
Y418A_CgAM	GCTCTGGGTGTGAATTTAGATACAAGCAACCTCCCCAACGATGACGCTATCCAACGCCAA	180
Y418S_CgAM	GCTCTGGGTGTGAATTTAGATACAAGCAACCTCCCCAACGATGACGCTATCCAACGCCAA	180

Y418F_CgAM	ATTGCCCTCTTCCATGATCGAGAGTTCACCTCGCCCACTGCCTCCATCGGTGGTTGCAGTT	240
Y418W_CgAM	ATTGCCCTCTTCCATGATCGAGAGTTCACCTCGCCCACTGCCTCCATCGGTGGTTGCAGTT	240
Y418R_CgAM	ATTGCCCTCTTCCATGATCGAGAGTTCACCTCGCCCACTGCCTCCATCGGTGGTTGCAGTT	240
WT_CgAM	ATTGCCCTCTTCCATGATCGAGAGTTCACCTCGCCCACTGCCTCCATCGGTGGTTGCAGTT	240
Y418D_CgAM	ATTGCCCTCTTCCATGATCGAGAGTTCACCTCGCCCACTGCCTCCATCGGTGGTTGCAGTT	240
Y418A_CgAM	ATTGCCCTCTTCCATGATCGAGAGTTCACCTCGCCCACTGCCTCCATCGGTGGTTGCAGTT	240
Y418S_CgAM	ATTGCCCTCTTCCATGATCGAGAGTTCACCTCGCCCACTGCCTCCATCGGTGGTTGCAGTT	240

Y418F_CgAM	GAAGGTGATGAAGTAGTTTTCCCGGTGCATGTGCACGACGCTTCCCCTGCAGATGTCCAC	300
Y418W_CgAM	GAAGGTGATGAAGTAGTTTTCCCGGTGCATGTGCACGACGCTTCCCCTGCAGATGTCCAC	300
Y418R_CgAM	GAAGGTGATGAAGTAGTTTTCCCGGTGCATGTGCACGACGCTTCCCCTGCAGATGTCCAC	300
WT_CgAM	GAAGGTGATGAAGTAGTTTTCCCGGTGCATGTGCACGACGCTTCCCCTGCAGATGTCCAC	300
Y418D_CgAM	GAAGGTGATGAAGTAGTTTTCCCGGTGCATGTGCACGACGCTTCCCCTGCAGATGTCCAC	300
Y418A_CgAM	GAAGGTGATGAAGTAGTTTTCCCGGTGCATGTGCACGACGCTTCCCCTGCAGATGTCCAC	300
Y418S_CgAM	GAAGGTGATGAAGTAGTTTTCCCGGTGCATGTGCACGACGCTTCCCCTGCAGATGTCCAC	300

Y418F_CgAM	ATCGAATTGGAAGACGGCACGCAGCGGGATGTTTCTCAGGTGAAAACTGGACAGCGCCA	360
Y418W_CgAM	ATCGAATTGGAAGACGGCACGCAGCGGGATGTTTCTCAGGTGAAAACTGGACAGCGCCA	360
Y418R_CgAM	ATCGAATTGGAAGACGGCACGCAGCGGGATGTTTCTCAGGTGAAAACTGGACAGCGCCA	360
WT_CgAM	ATCGAATTGGAAGACGGCACGCAGCGGGATGTTTCTCAGGTGAAAACTGGACAGCGCCA	360
Y418D_CgAM	ATCGAATTGGAAGACGGCACGCAGCGGGATGTTTCTCAGGTGAAAACTGGACAGCGCCA	360
Y418A_CgAM	ATCGAATTGGAAGACGGCACGCAGCGGGATGTTTCTCAGGTGAAAACTGGACAGCGCCA	360
Y418S_CgAM	ATCGAATTGGAAGACGGCACGCAGCGGGATGTTTCTCAGGTGAAAACTGGACAGCGCCA	360

Figure 3. 11 Nucleotide sequences of six Y418 mutated *CgAMs* compared with that of WT using Clustal O (1.2.4) multiple sequence alignment. Mutated codons are shaded.

Y418F_CgAM	CGGGAAATTGATGGGATTAGGTGGGGCGAGGCATCGTTAAGATTCCCTGGTGATCTCCCC	420
Y418W_CgAM	CGGGAAATTGATGGGATTAGGTGGGGCGAGGCATCGTTAAGATTCCCTGGTGATCTCCCC	420
Y418R_CgAM	CGGGAAATTGATGGGATTAGGTGGGGCGAGGCATCGTTAAGATTCCCTGGTGATCTCCCC	420
WT_CgAM	CGGGAAATTGATGGGATTAGGTGGGGCGAGGCATCGTTAAGATTCCCTGGTGATCTCCCC	420
Y418D_CgAM	CGGGAAATTGATGGGATTAGGTGGGGCGAGGCATCGTTAAGATTCCCTGGTGATCTCCCC	420
Y418A_CgAM	CGGGAAATTGATGGGATTAGGTGGGGCGAGGCATCGTTAAGATTCCCTGGTGATCTCCCC	420
Y418S_CgAM	CGGGAAATTGATGGGATTAGGTGGGGCGAGGCATCGTTAAGATTCCCTGGTGATCTCCCC	420

Y418F_CgAM	TTGGGTTGGCACAAGCTTCACCTTAAATCCAATGAACGCTCAGCTGAGTGCGGTTTGATC	480
Y418W_CgAM	TTGGGTTGGCACAAGCTTCACCTTAAATCCAATGAACGCTCAGCTGAGTGCGGTTTGATC	480
Y418R_CgAM	TTGGGTTGGCACAAGCTTCACCTTAAATCCAATGAACGCTCAGCTGAGTGCGGTTTGATC	480
WT_CgAM	TTGGGTTGGCACAAGCTTCACCTTAAATCCAATGAACGCTCAGCTGAGTGCGGTTTGATC	480
Y418D_CgAM	TTGGGTTGGCACAAGCTTCACCTTAAATCCAATGAACGCTCAGCTGAGTGCGGTTTGATC	480
Y418A_CgAM	TTGGGTTGGCACAAGCTTCACCTTAAATCCAATGAACGCTCAGCTGAGTGCGGTTTGATC	480
Y418S_CgAM	TTGGGTTGGCACAAGCTTCACCTTAAATCCAATGAACGCTCAGCTGAGTGCGGTTTGATC	480

Y418F_CgAM	ATCACCCCGGCTCGTCTGTCTACTGTGCTGATAAGTATCTTGATTCCCCTCGCAGTGGTGTC	540
Y418W_CgAM	ATCACCCCGGCTCGTCTGTCTACTGTGCTGATAAGTATCTTGATTCCCCTCGCAGTGGTGTC	540
Y418R_CgAM	ATCACCCCGGCTCGTCTGTCTACTGTGCTGATAAGTATCTTGATTCCCCTCGCAGTGGTGTC	540
WT_CgAM	ATCACCCCGGCTCGTCTGTCTACTGTGCTGATAAGTATCTTGATTCCCCTCGCAGTGGTGTC	540
Y418D_CgAM	ATCACCCCGGCTCGTCTGTCTACTGTGCTGATAAGTATCTTGATTCCCCTCGCAGTGGTGTC	540
Y418A_CgAM	ATCACCCCGGCTCGTCTGTCTACTGTGCTGATAAGTATCTTGATTCCCCTCGCAGTGGTGTC	540
Y418S_CgAM	ATCACCCCGGCTCGTCTGTCTACTGTGCTGATAAGTATCTTGATTCCCCTCGCAGTGGTGTC	540

Y418F_CgAM	ATGGCGCAGATCTACTCTGTGCGTTCCACGTTGTCGTGGGGCATGGGTGATTTCAATGAT	600
Y418W_CgAM	ATGGCGCAGATCTACTCTGTGCGTTCCACGTTGTCGTGGGGCATGGGTGATTTCAATGAT	600
Y418R_CgAM	ATGGCGCAGATCTACTCTGTGCGTTCCACGTTGTCGTGGGGCATGGGTGATTTCAATGAT	600
WT_CgAM	ATGGCGCAGATCTACTCTGTGCGTTCCACGTTGTCGTGGGGCATGGGTGATTTCAATGAT	600
Y418D_CgAM	ATGGCGCAGATCTACTCTGTGCGTTCCACGTTGTCGTGGGGCATGGGTGATTTCAATGAT	600
Y418A_CgAM	ATGGCGCAGATCTACTCTGTGCGTTCCACGTTGTCGTGGGGCATGGGTGATTTCAATGAT	600
Y418S_CgAM	ATGGCGCAGATCTACTCTGTGCGTTCCACGTTGTCGTGGGGCATGGGTGATTTCAATGAT	600

Y418F_CgAM	TTAGGAAACTTGGCAAGTGTGGTTGCCAGGATGGAGCAGACTTCCTGCTCATCAACCCC	660
Y418W_CgAM	TTAGGAAACTTGGCAAGTGTGGTTGCCAGGATGGAGCAGACTTCCTGCTCATCAACCCC	660
Y418R_CgAM	TTAGGAAACTTGGCAAGTGTGGTTGCCAGGATGGAGCAGACTTCCTGCTCATCAACCCC	660
WT_CgAM	TTAGGAAACTTGGCAAGTGTGGTTGCCAGGATGGAGCAGACTTCCTGCTCATCAACCCC	660
Y418D_CgAM	TTAGGAAACTTGGCAAGTGTGGTTGCCAGGATGGAGCAGACTTCCTGCTCATCAACCCC	660
Y418A_CgAM	TTAGGAAACTTGGCAAGTGTGGTTGCCAGGATGGAGCAGACTTCCTGCTCATCAACCCC	660
Y418S_CgAM	TTAGGAAACTTGGCAAGTGTGGTTGCCAGGATGGAGCAGACTTCCTGCTCATCAACCCC	660

Y418F_CgAM	ATGCACGCTGCAGAGCCGCTGCCTCCTACTGAGGACTCTCCTTATCTGCCACAACCAGG	720
Y418W_CgAM	ATGCACGCTGCAGAGCCGCTGCCTCCTACTGAGGACTCTCCTTATCTGCCACAACCAGG	720
Y418R_CgAM	ATGCACGCTGCAGAGCCGCTGCCTCCTACTGAGGACTCTCCTTATCTGCCACAACCAGG	720
WT_CgAM	ATGCACGCTGCAGAGCCGCTGCCTCCTACTGAGGACTCTCCTTATCTGCCACAACCAGG	720
Y418D_CgAM	ATGCACGCTGCAGAGCCGCTGCCTCCTACTGAGGACTCTCCTTATCTGCCACAACCAGG	720
Y418A_CgAM	ATGCACGCTGCAGAGCCGCTGCCTCCTACTGAGGACTCTCCTTATCTGCCACAACCAGG	720
Y418S_CgAM	ATGCACGCTGCAGAGCCGCTGCCTCCTACTGAGGACTCTCCTTATCTGCCACAACCAGG	720

Figure 3.11 (continue) Nucleotide sequences of six Y418 mutated *CgAMs* compared with that of WT using Clustal O (1.2.4) multiple sequence alignment. Mutated codons are shaded.

Y418F_CgAM	CGCTTTATCAACCCGATCTACATTCCGGGTAGAAGATATCCGGAGTTAATCAGCTTGAG	780
Y418W_CgAM	CGCTTTATCAACCCGATCTACATTCCGGGTAGAAGATATCCGGAGTTAATCAGCTTGAG	780
Y418R_CgAM	CGCTTTATCAACCCGATCTACATTCCGGGTAGAAGATATCCGGAGTTAATCAGCTTGAG	780
WT_CgAM	CGCTTTATCAACCCGATCTACATTCCGGGTAGAAGATATCCGGAGTTAATCAGCTTGAG	780
Y418D_CgAM	CGCTTTATCAACCCGATCTACATTCCGGGTAGAAGATATCCGGAGTTAATCAGCTTGAG	780
Y418A_CgAM	CGCTTTATCAACCCGATCTACATTCCGGGTAGAAGATATCCGGAGTTAATCAGCTTGAG	780
Y418S_CgAM	CGCTTTATCAACCCGATCTACATTCCGGGTAGAAGATATCCGGAGTTAATCAGCTTGAG	780

Y418F_CgAM	ATTGATCTACGCGATGATATCGCAGAGATGGCTGCGGAATCCCGCAACGCAATCTGACC	840
Y418W_CgAM	ATTGATCTACGCGATGATATCGCAGAGATGGCTGCGGAATCCCGCAACGCAATCTGACC	840
Y418R_CgAM	ATTGATCTACGCGATGATATCGCAGAGATGGCTGCGGAATCCCGCAACGCAATCTGACC	840
WT_CgAM	ATTGATCTACGCGATGATATCGCAGAGATGGCTGCGGAATCCCGCAACGCAATCTGACC	840
Y418D_CgAM	ATTGATCTACGCGATGATATCGCAGAGATGGCTGCGGAATCCCGCAACGCAATCTGACC	840
Y418A_CgAM	ATTGATCTACGCGATGATATCGCAGAGATGGCTGCGGAATCCCGCAACGCAATCTGACC	840
Y418S_CgAM	ATTGATCTACGCGATGATATCGCAGAGATGGCTGCGGAATCCCGCAACGCAATCTGACC	840

Y418F_CgAM	TCAGACATCATTGAGCGCAATGACGCTACGCTGCAAAGCTTCAAGTGTGCGCGCCATT	900
Y418W_CgAM	TCAGACATCATTGAGCGCAATGACGCTACGCTGCAAAGCTTCAAGTGTGCGCGCCATT	900
Y418R_CgAM	TCAGACATCATTGAGCGCAATGACGCTACGCTGCAAAGCTTCAAGTGTGCGCGCCATT	900
WT_CgAM	TCAGACATCATTGAGCGCAATGACGCTACGCTGCAAAGCTTCAAGTGTGCGCGCCATT	900
Y418D_CgAM	TCAGACATCATTGAGCGCAATGACGCTACGCTGCAAAGCTTCAAGTGTGCGCGCCATT	900
Y418A_CgAM	TCAGACATCATTGAGCGCAATGACGCTACGCTGCAAAGCTTCAAGTGTGCGCGCCATT	900
Y418S_CgAM	TCAGACATCATTGAGCGCAATGACGCTACGCTGCAAAGCTTCAAGTGTGCGCGCCATT	900

Y418F_CgAM	TTTGAATGCCTCGTTCCAGCGAACGTGAAGCCAACCTTGTCTCCTTCGTGCAACGGGAA	960
Y418W_CgAM	TTTGAATGCCTCGTTCCAGCGAACGTGAAGCCAACCTTGTCTCCTTCGTGCAACGGGAA	960
Y418R_CgAM	TTTGAATGCCTCGTTCCAGCGAACGTGAAGCCAACCTTGTCTCCTTCGTGCAACGGGAA	960
WT_CgAM	TTTGAATGCCTCGTTCCAGCGAACGTGAAGCCAACCTTGTCTCCTTCGTGCAACGGGAA	960
Y418D_CgAM	TTTGAATGCCTCGTTCCAGCGAACGTGAAGCCAACCTTGTCTCCTTCGTGCAACGGGAA	960
Y418A_CgAM	TTTGAATGCCTCGTTCCAGCGAACGTGAAGCCAACCTTGTCTCCTTCGTGCAACGGGAA	960
Y418S_CgAM	TTTGAATGCCTCGTTCCAGCGAACGTGAAGCCAACCTTGTCTCCTTCGTGCAACGGGAA	960

Y418F_CgAM	GGCCAAGGTCTTATTGATTTCCGCCACCTGGTGC GCGGACCGCGAAACTGCACAGTCTGAA	1020
Y418W_CgAM	GGCCAAGGTCTTATTGATTTCCGCCACCTGGTGC GCGGACCGCGAAACTGCACAGTCTGAA	1020
Y418R_CgAM	GGCCAAGGTCTTATTGATTTCCGCCACCTGGTGC GCGGACCGCGAAACTGCACAGTCTGAA	1020
WT_CgAM	GGCCAAGGTCTTATTGATTTCCGCCACCTGGTGC GCGGACCGCGAAACTGCACAGTCTGAA	1020
Y418D_CgAM	GGCCAAGGTCTTATTGATTTCCGCCACCTGGTGC GCGGACCGCGAAACTGCACAGTCTGAA	1020
Y418A_CgAM	GGCCAAGGTCTTATTGATTTCCGCCACCTGGTGC GCGGACCGCGAAACTGCACAGTCTGAA	1020
Y418S_CgAM	GGCCAAGGTCTTATTGATTTCCGCCACCTGGTGC GCGGACCGCGAAACTGCACAGTCTGAA	1020

Y418F_CgAM	TCTGTCCACGGAAGTGCAGCCAGACCGCGATGAGCTGACCATGTTCTACATGTGGTTGCAG	1080
Y418W_CgAM	TCTGTCCACGGAAGTGCAGCCAGACCGCGATGAGCTGACCATGTTCTACATGTGGTTGCAG	1080
Y418R_CgAM	TCTGTCCACGGAAGTGCAGCCAGACCGCGATGAGCTGACCATGTTCTACATGTGGTTGCAG	1080
WT_CgAM	TCTGTCCACGGAAGTGCAGCCAGACCGCGATGAGCTGACCATGTTCTACATGTGGTTGCAG	1080
Y418D_CgAM	TCTGTCCACGGAAGTGCAGCCAGACCGCGATGAGCTGACCATGTTCTACATGTGGTTGCAG	1080
Y418A_CgAM	TCTGTCCACGGAAGTGCAGCCAGACCGCGATGAGCTGACCATGTTCTACATGTGGTTGCAG	1080
Y418S_CgAM	TCTGTCCACGGAAGTGCAGCCAGACCGCGATGAGCTGACCATGTTCTACATGTGGTTGCAG	1080

Figure 3.11 (continue) Nucleotide sequences of six Y418 mutated *CgAMs* compared with that of WT using Clustal O (1.2.4) multiple sequence alignment. Mutated codons are shaded.

Y418F_CgAM	TGGCTATGTGATGAGCAGCTGGCGGCAGCTCAAAGCGCGCTGTCGATGCCGGAATGTTCG	1140
Y418W_CgAM	TGGCTATGTGATGAGCAGCTGGCGGCAGCTCAAAGCGCGCTGTCGATGCCGGAATGTTCG	1140
Y418R_CgAM	TGGCTATGTGATGAGCAGCTGGCGGCAGCTCAAAGCGCGCTGTCGATGCCGGAATGTTCG	1140
WT_CgAM	TGGCTATGTGATGAGCAGCTGGCGGCAGCTCAAAGCGCGCTGTCGATGCCGGAATGTTCG	1140
Y418D_CgAM	TGGCTATGTGATGAGCAGCTGGCGGCAGCTCAAAGCGCGCTGTCGATGCCGGAATGTTCG	1140
Y418A_CgAM	TGGCTATGTGATGAGCAGCTGGCGGCAGCTCAAAGCGCGCTGTCGATGCCGGAATGTTCG	1140
Y418S_CgAM	TGGCTATGTGATGAGCAGCTGGCGGCAGCTCAAAGCGCGCTGTCGATGCCGGAATGTTCG *****	1140
Y418F_CgAM	ATCGGCATCATGGCAGACCTGGCAGTTGGTGTGCATCCAGTGGTGTGATGCCCAGAAC	1200
Y418W_CgAM	ATCGGCATCATGGCAGACCTGGCAGTTGGTGTGCATCCAGTGGTGTGATGCCCAGAAC	1200
Y418R_CgAM	ATCGGCATCATGGCAGACCTGGCAGTTGGTGTGCATCCAGTGGTGTGATGCCCAGAAC	1200
WT_CgAM	ATCGGCATCATGGCAGACCTGGCAGTTGGTGTGCATCCAGTGGTGTGATGCCCAGAAC	1200
Y418D_CgAM	ATCGGCATCATGGCAGACCTGGCAGTTGGTGTGCATCCAGTGGTGTGATGCCCAGAAC	1200
Y418A_CgAM	ATCGGCATCATGGCAGACCTGGCAGTTGGTGTGCATCCAGTGGTGTGATGCCCAGAAC	1200
Y418S_CgAM	ATCGGCATCATGGCAGACCTGGCAGTTGGTGTGCATCCAGTGGTGTGATGCCCAGAAC *****	1200
Y418F_CgAM	CTCAGCCACGTACTTGTCTCCGGATGCGTCAGTGGGCGCCCCACCAGATGGATTTAACCAG	1260
Y418W_CgAM	CTCAGCCACGTACTTGTCTCCGGATGCGTCAGTGGGCGCCCCACCAGATGGATGGAACCAG	1260
Y418R_CgAM	CTCAGCCACGTACTTGTCTCCGGATGCGTCAGTGGGCGCCCCACCAGATGGACGCAACCAG	1260
WT_CgAM	CTCAGCCACGTACTTGTCTCCGGATGCGTCAGTGGGCGCCCCACCAGATGGATACAACCAG	1260
Y418D_CgAM	CTCAGCCACGTACTTGTCTCCGGATGCGTCAGTGGGCGCCCCACCAGATGGAGACAACCAG	1260
Y418A_CgAM	CTCAGCCACGTACTTGTCTCCGGATGCGTCAGTGGGCGCCCCACCAGATGGAGCAACCAG	1260
Y418S_CgAM	CTCAGCCACGTACTTGTCTCCGGATGCGTCAGTGGGCGCCCCACCAGATGGATCCAACCAG *****	1260
Y418F_CgAM	CAGGGCCAAGACTGGTCCCAGCCACCATGGCATCCAGTGCCTTGCAGAGGAAGGCTAC	1320
Y418W_CgAM	CAGGGCCAAGACTGGTCCCAGCCACCATGGCATCCAGTGCCTTGCAGAGGAAGGCTAC	1320
Y418R_CgAM	CAGGGCCAAGACTGGTCCCAGCCACCATGGCATCCAGTGCCTTGCAGAGGAAGGCTAC	1320
WT_CgAM	CAGGGCCAAGACTGGTCCCAGCCACCATGGCATCCAGTGCCTTGCAGAGGAAGGCTAC	1320
Y418D_CgAM	CAGGGCCAAGACTGGTCCCAGCCACCATGGCATCCAGTGCCTTGCAGAGGAAGGCTAC	1320
Y418A_CgAM	CAGGGCCAAGACTGGTCCCAGCCACCATGGCATCCAGTGCCTTGCAGAGGAAGGCTAC	1320
Y418S_CgAM	CAGGGCCAAGACTGGTCCCAGCCACCATGGCATCCAGTGCCTTGCAGAGGAAGGCTAC *****	1320
Y418F_CgAM	ATTCCGTGGCGTAATCTGCTGCGCACTGTGCTGCGTCACTCCGGCGGAATCCGCGTGGAC	1380
Y418W_CgAM	ATTCCGTGGCGTAATCTGCTGCGCACTGTGCTGCGTCACTCCGGCGGAATCCGCGTGGAC	1380
Y418R_CgAM	ATTCCGTGGCGTAATCTGCTGCGCACTGTGCTGCGTCACTCCGGCGGAATCCGCGTGGAC	1380
WT_CgAM	ATTCCGTGGCGTAATCTGCTGCGCACTGTGCTGCGTCACTCCGGCGGAATCCGCGTGGAC	1380
Y418D_CgAM	ATTCCGTGGCGTAATCTGCTGCGCACTGTGCTGCGTCACTCCGGCGGAATCCGCGTGGAC	1380
Y418A_CgAM	ATTCCGTGGCGTAATCTGCTGCGCACTGTGCTGCGTCACTCCGGCGGAATCCGCGTGGAC	1380
Y418S_CgAM	ATTCCGTGGCGTAATCTGCTGCGCACTGTGCTGCGTCACTCCGGCGGAATCCGCGTGGAC *****	1380
Y418F_CgAM	CACGTTCTTGGTTTGTTCAGGCTCTTTGTGCATGCCACGCATGCAATCCCCTGCTACGGGC	1440
Y418W_CgAM	CACGTTCTTGGTTTGTTCAGGCTCTTTGTGCATGCCACGCATGCAATCCCCTGCTACGGGC	1440
Y418R_CgAM	CACGTTCTTGGTTTGTTCAGGCTCTTTGTGCATGCCACGCATGCAATCCCCTGCTACGGGC	1440
WT_CgAM	CACGTTCTTGGTTTGTTCAGGCTCTTTGTGCATGCCACGCATGCAATCCCCTGCTACGGGC	1440
Y418D_CgAM	CACGTTCTTGGTTTGTTCAGGCTCTTTGTGCATGCCACGCATGCAATCCCCTGCTACGGGC	1440
Y418A_CgAM	CACGTTCTTGGTTTGTTCAGGCTCTTTGTGCATGCCACGCATGCAATCCCCTGCTACGGGC	1440
Y418S_CgAM	CACGTTCTTGGTTTGTTCAGGCTCTTTGTGCATGCCACGCATGCAATCCCCTGCTACGGGC *****	1440

Figure 3.11 (continue) Nucleotide sequences of six Y418 mutated *CgAMs* compared with that of WT using Clustal O (1.2.4) multiple sequence alignment. Mutated codons are shaded.

Y418F_CgAM	ACCTATATCCGCTTCGACCATAATGCGTTGGTAGGCATTCAGCCCTAGAAGCAGAATC	1500
Y418W_CgAM	ACCTATATCCGCTTCGACCATAATGCGTTGGTAGGCATTCAGCCCTAGAAGCAGAATC	1500
Y418R_CgAM	ACCTATATCCGCTTCGACCATAATGCGTTGGTAGGCATTCAGCCCTAGAAGCAGAATC	1500
WT_CgAM	ACCTATATCCGCTTCGACCATAATGCGTTGGTAGGCATTCAGCCCTAGAAGCAGAATC	1500
Y418D_CgAM	ACCTATATCCGCTTCGACCATAATGCGTTGGTAGGCATTCAGCCCTAGAAGCAGAATC	1500
Y418A_CgAM	ACCTATATCCGCTTCGACCATAATGCGTTGGTAGGCATTCAGCCCTAGAAGCAGAATC	1500
Y418S_CgAM	ACCTATATCCGCTTCGACCATAATGCGTTGGTAGGCATTCAGCCCTAGAAGCAGAATC	1500

Y418F_CgAM	GCAGGCGCCGTTGTCATTGGTGAAGATCTGGGAACGTTTGAGCCTTGGGTACAAGATGCA	1560
Y418W_CgAM	GCAGGCGCCGTTGTCATTGGTGAAGATCTGGGAACGTTTGAGCCTTGGGTACAAGATGCA	1560
Y418R_CgAM	GCAGGCGCCGTTGTCATTGGTGAAGATCTGGGAACGTTTGAGCCTTGGGTACAAGATGCA	1560
WT_CgAM	GCAGGCGCCGTTGTCATTGGTGAAGATCTGGGAACGTTTGAGCCTTGGGTACAAGATGCA	1560
Y418D_CgAM	GCAGGCGCCGTTGTCATTGGTGAAGATCTGGGAACGTTTGAGCCTTGGGTACAAGATGCA	1560
Y418A_CgAM	GCAGGCGCCGTTGTCATTGGTGAAGATCTGGGAACGTTTGAGCCTTGGGTACAAGATGCA	1560
Y418S_CgAM	GCAGGCGCCGTTGTCATTGGTGAAGATCTGGGAACGTTTGAGCCTTGGGTACAAGATGCA	1560

Y418F_CgAM	TTGGCTCAGCGTGGCATCATGGGCACCTCGATCCTATGGTTCGAGCATTCGCCAAGCCAG	1620
Y418W_CgAM	TTGGCTCAGCGTGGCATCATGGGCACCTCGATCCTATGGTTCGAGCATTCGCCAAGCCAG	1620
Y418R_CgAM	TTGGCTCAGCGTGGCATCATGGGCACCTCGATCCTATGGTTCGAGCATTCGCCAAGCCAG	1620
WT_CgAM	TTGGCTCAGCGTGGCATCATGGGCACCTCGATCCTATGGTTCGAGCATTCGCCAAGCCAG	1620
Y418D_CgAM	TTGGCTCAGCGTGGCATCATGGGCACCTCGATCCTATGGTTCGAGCATTCGCCAAGCCAG	1620
Y418A_CgAM	TTGGCTCAGCGTGGCATCATGGGCACCTCGATCCTATGGTTCGAGCATTCGCCAAGCCAG	1620
Y418S_CgAM	TTGGCTCAGCGTGGCATCATGGGCACCTCGATCCTATGGTTCGAGCATTCGCCAAGCCAG	1620

Y418F_CgAM	CCGGGTCTCGCCGCCAGGAAGAGTATCGTCCGCTGGCCTTGACCACCTGTGACCACTCAT	1680
Y418W_CgAM	CCGGGTCTCGCCGCCAGGAAGAGTATCGTCCGCTGGCCTTGACCACCTGTGACCACTCAT	1680
Y418R_CgAM	CCGGGTCTCGCCGCCAGGAAGAGTATCGTCCGCTGGCCTTGACCACCTGTGACCACTCAT	1680
WT_CgAM	CCGGGTCTCGCCGCCAGGAAGAGTATCGTCCGCTGGCCTTGACCACCTGTGACCACTCAT	1680
Y418D_CgAM	CCGGGTCTCGCCGCCAGGAAGAGTATCGTCCGCTGGCCTTGACCACCTGTGACCACTCAT	1680
Y418A_CgAM	CCGGGTCTCGCCGCCAGGAAGAGTATCGTCCGCTGGCCTTGACCACCTGTGACCACTCAT	1680
Y418S_CgAM	CCGGGTCTCGCCGCCAGGAAGAGTATCGTCCGCTGGCCTTGACCACCTGTGACCACTCAT	1680

Y418F_CgAM	GATCTCCCTCCGACTGCTGGTTATTTGGAGGGCGAGCACATTGCTCTTCGTGAGCGATTG	1740
Y418W_CgAM	GATCTCCCTCCGACTGCTGGTTATTTGGAGGGCGAGCACATTGCTCTTCGTGAGCGATTG	1740
Y418R_CgAM	GATCTCCCTCCGACTGCTGGTTATTTGGAGGGCGAGCACATTGCTCTTCGTGAGCGATTG	1740
WT_CgAM	GATCTCCCTCCGACTGCTGGTTATTTGGAGGGCGAGCACATTGCTCTTCGTGAGCGATTG	1740
Y418D_CgAM	GATCTCCCTCCGACTGCTGGTTATTTGGAGGGCGAGCACATTGCTCTTCGTGAGCGATTG	1740
Y418A_CgAM	GATCTCCCTCCGACTGCTGGTTATTTGGAGGGCGAGCACATTGCTCTTCGTGAGCGATTG	1740
Y418S_CgAM	GATCTCCCTCCGACTGCTGGTTATTTGGAGGGCGAGCACATTGCTCTTCGTGAGCGATTG	1740

Y418F_CgAM	GGGGTGCTCAAACTGATCCTGCTGCAGAACTCGCTGAGGATCTGCAGTGGCAAGCGGAG	1800
Y418W_CgAM	GGGGTGCTCAAACTGATCCTGCTGCAGAACTCGCTGAGGATCTGCAGTGGCAAGCGGAG	1800
Y418R_CgAM	GGGGTGCTCAAACTGATCCTGCTGCAGAACTCGCTGAGGATCTGCAGTGGCAAGCGGAG	1800
WT_CgAM	GGGGTGCTCAAACTGATCCTGCTGCAGAACTCGCTGAGGATCTGCAGTGGCAAGCGGAG	1800
Y418D_CgAM	GGGGTGCTCAAACTGATCCTGCTGCAGAACTCGCTGAGGATCTGCAGTGGCAAGCGGAG	1800
Y418A_CgAM	GGGGTGCTCAAACTGATCCTGCTGCAGAACTCGCTGAGGATCTGCAGTGGCAAGCGGAG	1800
Y418S_CgAM	GGGGTGCTCAAACTGATCCTGCTGCAGAACTCGCTGAGGATCTGCAGTGGCAAGCGGAG	1800

Figure 3.11 (continue) Nucleotide sequences of six Y418 mutated *CgAMs* compared with that of WT using Clustal O (1.2.4) multiple sequence alignment. Mutated codons are shaded.

Y418F_CgAM	ATCCTTGATGTCGCAGCATCTGCCAACGCATTGCCAGCCCAGGGAATACGTGGGACTCGAA	1860
Y418W_CgAM	ATCCTTGATGTCGCAGCATCTGCCAACGCATTGCCAGCCCAGGGAATACGTGGGACTCGAA	1860
Y418R_CgAM	ATCCTTGATGTCGCAGCATCTGCCAACGCATTGCCAGCCCAGGGAATACGTGGGACTCGAA	1860
WT_CgAM	ATCCTTGATGTCGCAGCATCTGCCAACGCATTGCCAGCCCAGGGAATACGTGGGACTCGAA	1860
Y418D_CgAM	ATCCTTGATGTCGCAGCATCTGCCAACGCATTGCCAGCCCAGGGAATACGTGGGACTCGAA	1860
Y418A_CgAM	ATCCTTGATGTCGCAGCATCTGCCAACGCATTGCCAGCCCAGGGAATACGTGGGACTCGAA	1860
Y418S_CgAM	ATCCTTGATGTCGCAGCATCTGCCAACGCATTGCCAGCCCAGGGAATACGTGGGACTCGAA	1860

Y418F_CgAM	CGCGATCAGCGCGGTGAGTTGGCTGAGCTGTTGGAAGGCCGTCACACATTTTCGTTGCGAAA	1920
Y418W_CgAM	CGCGATCAGCGCGGTGAGTTGGCTGAGCTGTTGGAAGGCCGTCACACATTTTCGTTGCGAAA	1920
Y418R_CgAM	CGCGATCAGCGCGGTGAGTTGGCTGAGCTGTTGGAAGGCCGTCACACATTTTCGTTGCGAAA	1920
WT_CgAM	CGCGATCAGCGCGGTGAGTTGGCTGAGCTGTTGGAAGGCCGTCACACATTTTCGTTGCGAAA	1920
Y418D_CgAM	CGCGATCAGCGCGGTGAGTTGGCTGAGCTGTTGGAAGGCCGTCACACATTTTCGTTGCGAAA	1920
Y418A_CgAM	CGCGATCAGCGCGGTGAGTTGGCTGAGCTGTTGGAAGGCCGTCACACATTTTCGTTGCGAAA	1920
Y418S_CgAM	CGCGATCAGCGCGGTGAGTTGGCTGAGCTGTTGGAAGGCCGTCACACATTTTCGTTGCGAAA	1920

Y418F_CgAM	ACCCCTTCAGCACTGACCTGTGTCTGCTTGGTAGACATGGTCGGTGAAAAGCGGGCACAG	1980
Y418W_CgAM	ACCCCTTCAGCACTGACCTGTGTCTGCTTGGTAGACATGGTCGGTGAAAAGCGGGCACAG	1980
Y418R_CgAM	ACCCCTTCAGCACTGACCTGTGTCTGCTTGGTAGACATGGTCGGTGAAAAGCGGGCACAG	1980
WT_CgAM	ACCCCTTCAGCACTGACCTGTGTCTGCTTGGTAGACATGGTCGGTGAAAAGCGGGCACAG	1980
Y418D_CgAM	ACCCCTTCAGCACTGACCTGTGTCTGCTTGGTAGACATGGTCGGTGAAAAGCGGGCACAG	1980
Y418A_CgAM	ACCCCTTCAGCACTGACCTGTGTCTGCTTGGTAGACATGGTCGGTGAAAAGCGGGCACAG	1980
Y418S_CgAM	ACCCCTTCAGCACTGACCTGTGTCTGCTTGGTAGACATGGTCGGTGAAAAGCGGGCACAG	1980

Y418F_CgAM	AATCAGCCGGGCACAACGAGGGATATGTATCCCAACTGGTGTATCCCACTGTGTGACAGC	2040
Y418W_CgAM	AATCAGCCGGGCACAACGAGGGATATGTATCCCAACTGGTGTATCCCACTGTGTGACAGC	2040
Y418R_CgAM	AATCAGCCGGGCACAACGAGGGATATGTATCCCAACTGGTGTATCCCACTGTGTGACAGC	2040
WT_CgAM	AATCAGCCGGGCACAACGAGGGATATGTATCCCAACTGGTGTATCCCACTGTGTGACAGC	2040
Y418D_CgAM	AATCAGCCGGGCACAACGAGGGATATGTATCCCAACTGGTGTATCCCACTGTGTGACAGC	2040
Y418A_CgAM	AATCAGCCGGGCACAACGAGGGATATGTATCCCAACTGGTGTATCCCACTGTGTGACAGC	2040
Y418S_CgAM	AATCAGCCGGGCACAACGAGGGATATGTATCCCAACTGGTGTATCCCACTGTGTGACAGC	2040

Y418F_CgAM	GAAGGCAACTCCGTGCTCATTGAATCGCTGCGTGAAAATGAGCTGTATCACCGTGTGGCA	2100
Y418W_CgAM	GAAGGCAACTCCGTGCTCATTGAATCGCTGCGTGAAAATGAGCTGTATCACCGTGTGGCA	2100
Y418R_CgAM	GAAGGCAACTCCGTGCTCATTGAATCGCTGCGTGAAAATGAGCTGTATCACCGTGTGGCA	2100
WT_CgAM	GAAGGCAACTCCGTGCTCATTGAATCGCTGCGTGAAAATGAGCTGTATCACCGTGTGGCA	2100
Y418D_CgAM	GAAGGCAACTCCGTGCTCATTGAATCGCTGCGTGAAAATGAGCTGTATCACCGTGTGGCA	2100
Y418A_CgAM	GAAGGCAACTCCGTGCTCATTGAATCGCTGCGTGAAAATGAGCTGTATCACCGTGTGGCA	2100
Y418S_CgAM	GAAGGCAACTCCGTGCTCATTGAATCGCTGCGTGAAAATGAGCTGTATCACCGTGTGGCA	2100

Y418F_CgAM	AAGGCAAGCAAGCGAGATTAG	2121
Y418W_CgAM	AAGGCAAGCAAGCGAGATTAG	2121
Y418R_CgAM	AAGGCAAGCAAGCGAGATTAG	2121
WT_CgAM	AAGGCAAGCAAGCGAGATTAG	2121
Y418D_CgAM	AAGGCAAGCAAGCGAGATTAG	2121
Y418A_CgAM	AAGGCAAGCAAGCGAGATTAG	2121
Y418S_CgAM	AAGGCAAGCAAGCGAGATTAG	2121

Figure 3.11 (continue) Nucleotide sequences of six Y418 mutated *CgAMs* compared with that of WT using Clustal O (1.2.4) multiple sequence alignment. Mutated codons are shaded.

WT_CgAM	MTARRFLNELADLYGVATSYTDYKGAHIEVSDDTLVKILRALGVNLDTSNLPNDDAIQRQ	60
Y418A_CgAM	MTARRFLNELADLYGVATSYTDYKGAHIEVSDDTLVKILRALGVNLDTSNLPNDDAIQRQ	60
Y418S_CgAM	MTARRFLNELADLYGVATSYTDYKGAHIEVSDDTLVKILRALGVNLDTSNLPNDDAIQRQ	60
Y418D_CgAM	MTARRFLNELADLYGVATSYTDYKGAHIEVSDDTLVKILRALGVNLDTSNLPNDDAIQRQ	60
Y418R_CgAM	MTARRFLNELADLYGVATSYTDYKGAHIEVSDDTLVKILRALGVNLDTSNLPNDDAIQRQ	60
Y418W_CgAM	MTARRFLNELADLYGVATSYTDYKGAHIEVSDDTLVKILRALGVNLDTSNLPNDDAIQRQ	60
Y418F_CgAM	MTARRFLNELADLYGVATSYTDYKGAHIEVSDDTLVKILRALGVNLDTSNLPNDDAIQRQ	60

WT_CgAM	IALFHDREFTRPLPPSVVAVEGDELVFPVHVHDGSPADVHIELEDGTQRDVSQVENWTAP	120
Y418A_CgAM	IALFHDREFTRPLPPSVVAVEGDELVFPVHVHDGSPADVHIELEDGTQRDVSQVENWTAP	120
Y418S_CgAM	IALFHDREFTRPLPPSVVAVEGDELVFPVHVHDGSPADVHIELEDGTQRDVSQVENWTAP	120
Y418D_CgAM	IALFHDREFTRPLPPSVVAVEGDELVFPVHVHDGSPADVHIELEDGTQRDVSQVENWTAP	120
Y418R_CgAM	IALFHDREFTRPLPPSVVAVEGDELVFPVHVHDGSPADVHIELEDGTQRDVSQVENWTAP	120
Y418W_CgAM	IALFHDREFTRPLPPSVVAVEGDELVFPVHVHDGSPADVHIELEDGTQRDVSQVENWTAP	120
Y418F_CgAM	IALFHDREFTRPLPPSVVAVEGDELVFPVHVHDGSPADVHIELEDGTQRDVSQVENWTAP	120

WT_CgAM	REIDGIRWGEASFKIPGDLPLGWHKHLHLSNERSAECGLIITPARLSTADKYLDSPRSGV	180
Y418A_CgAM	REIDGIRWGEASFKIPGDLPLGWHKHLHLSNERSAECGLIITPARLSTADKYLDSPRSGV	180
Y418S_CgAM	REIDGIRWGEASFKIPGDLPLGWHKHLHLSNERSAECGLIITPARLSTADKYLDSPRSGV	180
Y418D_CgAM	REIDGIRWGEASFKIPGDLPLGWHKHLHLSNERSAECGLIITPARLSTADKYLDSPRSGV	180
Y418R_CgAM	REIDGIRWGEASFKIPGDLPLGWHKHLHLSNERSAECGLIITPARLSTADKYLDSPRSGV	180
Y418W_CgAM	REIDGIRWGEASFKIPGDLPLGWHKHLHLSNERSAECGLIITPARLSTADKYLDSPRSGV	180
Y418F_CgAM	REIDGIRWGEASFKIPGDLPLGWHKHLHLSNERSAECGLIITPARLSTADKYLDSPRSGV	180

WT_CgAM	MAQIYSVRSTLSWGMGDFNDLGNLASVVAQDGADFLINPMHAAEPLPPTEDSPYLPTR	240
Y418A_CgAM	MAQIYSVRSTLSWGMGDFNDLGNLASVVAQDGADFLINPMHAAEPLPPTEDSPYLPTR	240
Y418S_CgAM	MAQIYSVRSTLSWGMGDFNDLGNLASVVAQDGADFLINPMHAAEPLPPTEDSPYLPTR	240
Y418D_CgAM	MAQIYSVRSTLSWGMGDFNDLGNLASVVAQDGADFLINPMHAAEPLPPTEDSPYLPTR	240
Y418R_CgAM	MAQIYSVRSTLSWGMGDFNDLGNLASVVAQDGADFLINPMHAAEPLPPTEDSPYLPTR	240
Y418W_CgAM	MAQIYSVRSTLSWGMGDFNDLGNLASVVAQDGADFLINPMHAAEPLPPTEDSPYLPTR	240
Y418F_CgAM	MAQIYSVRSTLSWGMGDFNDLGNLASVVAQDGADFLINPMHAAEPLPPTEDSPYLPTR	240

WT_CgAM	RFINPIYIRVEDIPEFNQLEIDLRRDDIAEMAAEFRRNLTSDIERNDVYAAKLQVLRAI	300
Y418A_CgAM	RFINPIYIRVEDIPEFNQLEIDLRRDDIAEMAAEFRRNLTSDIERNDVYAAKLQVLRAI	300
Y418S_CgAM	RFINPIYIRVEDIPEFNQLEIDLRRDDIAEMAAEFRRNLTSDIERNDVYAAKLQVLRAI	300
Y418D_CgAM	RFINPIYIRVEDIPEFNQLEIDLRRDDIAEMAAEFRRNLTSDIERNDVYAAKLQVLRAI	300
Y418R_CgAM	RFINPIYIRVEDIPEFNQLEIDLRRDDIAEMAAEFRRNLTSDIERNDVYAAKLQVLRAI	300
Y418W_CgAM	RFINPIYIRVEDIPEFNQLEIDLRRDDIAEMAAEFRRNLTSDIERNDVYAAKLQVLRAI	300
Y418F_CgAM	RFINPIYIRVEDIPEFNQLEIDLRRDDIAEMAAEFRRNLTSDIERNDVYAAKLQVLRAI	300

WT_CgAM	FEMPRSSEREANFVSFVQREGQLIDFATWCADRETAQSESVHGTPEPDRDELTMFYMWLQ	360
Y418A_CgAM	FEMPRSSEREANFVSFVQREGQLIDFATWCADRETAQSESVHGTPEPDRDELTMFYMWLQ	360
Y418S_CgAM	FEMPRSSEREANFVSFVQREGQLIDFATWCADRETAQSESVHGTPEPDRDELTMFYMWLQ	360
Y418D_CgAM	FEMPRSSEREANFVSFVQREGQLIDFATWCADRETAQSESVHGTPEPDRDELTMFYMWLQ	360
Y418R_CgAM	FEMPRSSEREANFVSFVQREGQLIDFATWCADRETAQSESVHGTPEPDRDELTMFYMWLQ	360
Y418W_CgAM	FEMPRSSEREANFVSFVQREGQLIDFATWCADRETAQSESVHGTPEPDRDELTMFYMWLQ	360
Y418F_CgAM	FEMPRSSEREANFVSFVQREGQLIDFATWCADRETAQSESVHGTPEPDRDELTMFYMWLQ	360

WT_CgAM	WLCDEQLAAAQKRAVDAGMSIGIMADLAVGVHPGGADAQNLSHVLAPDASVGAPPDGNQ	420
Y418A_CgAM	WLCDEQLAAAQKRAVDAGMSIGIMADLAVGVHPGGADAQNLSHVLAPDASVGAPPDGNQ	420
Y418S_CgAM	WLCDEQLAAAQKRAVDAGMSIGIMADLAVGVHPGGADAQNLSHVLAPDASVGAPPDGNQ	420
Y418D_CgAM	WLCDEQLAAAQKRAVDAGMSIGIMADLAVGVHPGGADAQNLSHVLAPDASVGAPPDGNQ	420
Y418R_CgAM	WLCDEQLAAAQKRAVDAGMSIGIMADLAVGVHPGGADAQNLSHVLAPDASVGAPPDGNQ	420
Y418W_CgAM	WLCDEQLAAAQKRAVDAGMSIGIMADLAVGVHPGGADAQNLSHVLAPDASVGAPPDGNQ	420
Y418F_CgAM	WLCDEQLAAAQKRAVDAGMSIGIMADLAVGVHPGGADAQNLSHVLAPDASVGAPPDGNQ	420
	***** **	

Figure 3. 12 The deduced amino acid sequences of six Y418 mutated CgAMs compared with that of WT using Clustal O (1.2.4) multiple sequence alignment. Mutated amino acids are shaded.

WT_CgAM	QQQDWSQPPWHPVRLAEEGYIPWRNLLRTVLRHSGGIRVDHVLGLFRLFVMPRMQSPATG	480
Y418A_CgAM	QQQDWSQPPWHPVRLAEEGYIPWRNLLRTVLRHSGGIRVDHVLGLFRLFVMPRMQSPATG	480
Y418S_CgAM	QQQDWSQPPWHPVRLAEEGYIPWRNLLRTVLRHSGGIRVDHVLGLFRLFVMPRMQSPATG	480
Y418D_CgAM	QQQDWSQPPWHPVRLAEEGYIPWRNLLRTVLRHSGGIRVDHVLGLFRLFVMPRMQSPATG	480
Y418R_CgAM	QQQDWSQPPWHPVRLAEEGYIPWRNLLRTVLRHSGGIRVDHVLGLFRLFVMPRMQSPATG	480
Y418W_CgAM	QQQDWSQPPWHPVRLAEEGYIPWRNLLRTVLRHSGGIRVDHVLGLFRLFVMPRMQSPATG	480
Y418F_CgAM	QQQDWSQPPWHPVRLAEEGYIPWRNLLRTVLRHSGGIRVDHVLGLFRLFVMPRMQSPATG	480

WT_CgAM	TYIRFDHNALVGI LALEAELAGAVVIGEDLGTFFEPWVQDALAQRGIMGTSILWFEHSPSQ	540
Y418A_CgAM	TYIRFDHNALVGI LALEAELAGAVVIGEDLGTFFEPWVQDALAQRGIMGTSILWFEHSPSQ	540
Y418S_CgAM	TYIRFDHNALVGI LALEAELAGAVVIGEDLGTFFEPWVQDALAQRGIMGTSILWFEHSPSQ	540
Y418D_CgAM	TYIRFDHNALVGI LALEAELAGAVVIGEDLGTFFEPWVQDALAQRGIMGTSILWFEHSPSQ	540
Y418R_CgAM	TYIRFDHNALVGI LALEAELAGAVVIGEDLGTFFEPWVQDALAQRGIMGTSILWFEHSPSQ	540
Y418W_CgAM	TYIRFDHNALVGI LALEAELAGAVVIGEDLGTFFEPWVQDALAQRGIMGTSILWFEHSPSQ	540
Y418F_CgAM	TYIRFDHNALVGI LALEAELAGAVVIGEDLGTFFEPWVQDALAQRGIMGTSILWFEHSPSQ	540

WT_CgAM	PGPRRQEEYRPLALTTVTTTHDLPPTAGYLEGEHIALRERLGVLNTDPAELAEDLQWQAE	600
Y418A_CgAM	PGPRRQEEYRPLALTTVTTTHDLPPTAGYLEGEHIALRERLGVLNTDPAELAEDLQWQAE	600
Y418S_CgAM	PGPRRQEEYRPLALTTVTTTHDLPPTAGYLEGEHIALRERLGVLNTDPAELAEDLQWQAE	600
Y418D_CgAM	PGPRRQEEYRPLALTTVTTTHDLPPTAGYLEGEHIALRERLGVLNTDPAELAEDLQWQAE	600
Y418R_CgAM	PGPRRQEEYRPLALTTVTTTHDLPPTAGYLEGEHIALRERLGVLNTDPAELAEDLQWQAE	600
Y418W_CgAM	PGPRRQEEYRPLALTTVTTTHDLPPTAGYLEGEHIALRERLGVLNTDPAELAEDLQWQAE	600
Y418F_CgAM	PGPRRQEEYRPLALTTVTTTHDLPPTAGYLEGEHIALRERLGVLNTDPAELAEDLQWQAE	600

WT_CgAM	ILDVAASANALPAREYVGLERDQRGELAELEGLHTFVAKTPSALTCVCLVDMVGEKRAQ	660
Y418A_CgAM	ILDVAASANALPAREYVGLERDQRGELAELEGLHTFVAKTPSALTCVCLVDMVGEKRAQ	660
Y418S_CgAM	ILDVAASANALPAREYVGLERDQRGELAELEGLHTFVAKTPSALTCVCLVDMVGEKRAQ	660
Y418D_CgAM	ILDVAASANALPAREYVGLERDQRGELAELEGLHTFVAKTPSALTCVCLVDMVGEKRAQ	660
Y418R_CgAM	ILDVAASANALPAREYVGLERDQRGELAELEGLHTFVAKTPSALTCVCLVDMVGEKRAQ	660
Y418W_CgAM	ILDVAASANALPAREYVGLERDQRGELAELEGLHTFVAKTPSALTCVCLVDMVGEKRAQ	660
Y418F_CgAM	ILDVAASANALPAREYVGLERDQRGELAELEGLHTFVAKTPSALTCVCLVDMVGEKRAQ	660

WT_CgAM	NQPGTTRDMYPNWCIPLCDSEGNVSVLIESLRENELYHRVAKASKRD	706
Y418A_CgAM	NQPGTTRDMYPNWCIPLCDSEGNVSVLIESLRENELYHRVAKASKRD	706
Y418S_CgAM	NQPGTTRDMYPNWCIPLCDSEGNVSVLIESLRENELYHRVAKASKRD	706
Y418D_CgAM	NQPGTTRDMYPNWCIPLCDSEGNVSVLIESLRENELYHRVAKASKRD	706
Y418R_CgAM	NQPGTTRDMYPNWCIPLCDSEGNVSVLIESLRENELYHRVAKASKRD	706
Y418W_CgAM	NQPGTTRDMYPNWCIPLCDSEGNVSVLIESLRENELYHRVAKASKRD	706
Y418F_CgAM	NQPGTTRDMYPNWCIPLCDSEGNVSVLIESLRENELYHRVAKASKRD	706



จุฬาลงกรณ์มหาวิทยาลัย

Figure 3.12 (continue) The deduced amino acid sequences of six Y418 mutated CgAM compared with that of WT using Clustal O (1.2.4) multiple sequence alignment. Mutated amino acids are shaded.

H461S_CgAM	TGGCTATGTGATGAGCAGCTGGCGGCAGCTCAAAGCGCGCTGTCGATGCCGGAATGTCG	1140
H461R_CgAM	TGGCTATGTGATGAGCAGCTGGCGGCAGCTCAAAGCGCGCTGTCGATGCCGGAATGTCG	1140
WT_CgAM	TGGCTATGTGATGAGCAGCTGGCGGCAGCTCAAAGCGCGCTGTCGATGCCGGAATGTCG	1140
H461A_CgAM	TGGCTATGTGATGAGCAGCTGGCGGCAGCTCAAAGCGCGCTGTCGATGCCGGAATGTCG	1140
H461D_CgAM	TGGCTATGTGATGAGCAGCTGGCGGCAGCTCAAAGCGCGCTGTCGATGCCGGAATGTCG	1140
H461W_CgAM	TGGCTATGTGATGAGCAGCTGGCGGCAGCTCAAAGCGCGCTGTCGATGCCGGAATGTCG	1140

H461S_CgAM	ATCGGCATCATGGCAGACCTGGCAGTTGGTGTGCATCCAGTGGTGTGATGCCCAGAAC	1200
H461R_CgAM	ATCGGCATCATGGCAGACCTGGCAGTTGGTGTGCATCCAGTGGTGTGATGCCCAGAAC	1200
WT_CgAM	ATCGGCATCATGGCAGACCTGGCAGTTGGTGTGCATCCAGTGGTGTGATGCCCAGAAC	1200
H461A_CgAM	ATCGGCATCATGGCAGACCTGGCAGTTGGTGTGCATCCAGTGGTGTGATGCCCAGAAC	1200
H461D_CgAM	ATCGGCATCATGGCAGACCTGGCAGTTGGTGTGCATCCAGTGGTGTGATGCCCAGAAC	1200
H461W_CgAM	ATCGGCATCATGGCAGACCTGGCAGTTGGTGTGCATCCAGTGGTGTGATGCCCAGAAC	1200

H461S_CgAM	CTCAGCCACGTACTTGCTCCGGATGCGTCAGTGGGCGCCCCACCAGATGGATACAACCAG	1260
H461R_CgAM	CTCAGCCACGTACTTGCTCCGGATGCGTCAGTGGGCGCCCCACCAGATGGATACAACCAG	1260
WT_CgAM	CTCAGCCACGTACTTGCTCCGGATGCGTCAGTGGGCGCCCCACCAGATGGATACAACCAG	1260
H461A_CgAM	CTCAGCCACGTACTTGCTCCGGATGCGTCAGTGGGCGCCCCACCAGATGGATACAACCAG	1260
H461D_CgAM	CTCAGCCACGTACTTGCTCCGGATGCGTCAGTGGGCGCCCCACCAGATGGATACAACCAG	1260
H461W_CgAM	CTCAGCCACGTACTTGCTCCGGATGCGTCAGTGGGCGCCCCACCAGATGGATACAACCAG	1260

H461S_CgAM	CAGGGCCAAGACTGGTCCCAGCCACCATGGCATCCAGTGCCTTGCAGAGGAAGGCTAC	1320
H461R_CgAM	CAGGGCCAAGACTGGTCCCAGCCACCATGGCATCCAGTGCCTTGCAGAGGAAGGCTAC	1320
WT_CgAM	CAGGGCCAAGACTGGTCCCAGCCACCATGGCATCCAGTGCCTTGCAGAGGAAGGCTAC	1320
H461A_CgAM	CAGGGCCAAGACTGGTCCCAGCCACCATGGCATCCAGTGCCTTGCAGAGGAAGGCTAC	1320
H461D_CgAM	CAGGGCCAAGACTGGTCCCAGCCACCATGGCATCCAGTGCCTTGCAGAGGAAGGCTAC	1320
H461W_CgAM	CAGGGCCAAGACTGGTCCCAGCCACCATGGCATCCAGTGCCTTGCAGAGGAAGGCTAC	1320

H461S_CgAM	ATTCCGTGGCGTAATCTGCTGCGCACTGTGCTGCGTCACTCCGGCGGAATCCGCGTGGAC	1380
H461R_CgAM	ATTCCGTGGCGTAATCTGCTGCGCACTGTGCTGCGTCACTCCGGCGGAATCCGCGTGGAC	1380
WT_CgAM	ATTCCGTGGCGTAATCTGCTGCGCACTGTGCTGCGTCACTCCGGCGGAATCCGCGTGGAC	1380
H461A_CgAM	ATTCCGTGGCGTAATCTGCTGCGCACTGTGCTGCGTCACTCCGGCGGAATCCGCGTGGAC	1380
H461D_CgAM	ATTCCGTGGCGTAATCTGCTGCGCACTGTGCTGCGTCACTCCGGCGGAATCCGCGTGGAC	1380
H461W_CgAM	ATTCCGTGGCGTAATCTGCTGCGCACTGTGCTGCGTCACTCCGGCGGAATCCGCGTGGAC	1380

H461S_CgAM	AGCGTTCCTGGTTTGTTCAGGCTCTTTGTCATGCCACGCATGCAATCCCCTGCTACGGGC	1440
H461R_CgAM	AGCGTTCCTGGTTTGTTCAGGCTCTTTGTCATGCCACGCATGCAATCCCCTGCTACGGGC	1440
WT_CgAM	AGCGTTCCTGGTTTGTTCAGGCTCTTTGTCATGCCACGCATGCAATCCCCTGCTACGGGC	1440
H461A_CgAM	AGCGTTCCTGGTTTGTTCAGGCTCTTTGTCATGCCACGCATGCAATCCCCTGCTACGGGC	1440
H461D_CgAM	AGCGTTCCTGGTTTGTTCAGGCTCTTTGTCATGCCACGCATGCAATCCCCTGCTACGGGC	1440
H461W_CgAM	AGCGTTCCTGGTTTGTTCAGGCTCTTTGTCATGCCACGCATGCAATCCCCTGCTACGGGC	1440

Figure 3. 13 Nucleotide sequences of five H461 mutated *CgAMs* compared with that of WT using Clustal O (1.2.4) multiple sequence alignment. Mutated codons are shaded. (Only the sequences from NT 1081-1440 are shown here, the sequences from NT1-NT1080 and NT1441-NT2121 which are the same in all *CgAMs* are not shown.)

WT_CgAM	QQQDWSQPPWHPVRLAEEGYIPWRNLLRTVLRHSGGIRVDHVLGLFRLFVMPRMQSPATG	480
H461A_CgAM	QQQDWSQPPWHPVRLAEEGYIPWRNLLRTVLRHSGGIRVDHVLGLFRLFVMPRMQSPATG	480
H461S_CgAM	QQQDWSQPPWHPVRLAEEGYIPWRNLLRTVLRHSGGIRVDSVVLGLFRLFVMPRMQSPATG	480
H461D_CgAM	QQQDWSQPPWHPVRLAEEGYIPWRNLLRTVLRHSGGIRVDHVLGLFRLFVMPRMQSPATG	480
H461R_CgAM	QQQDWSQPPWHPVRLAEEGYIPWRNLLRTVLRHSGGIRVDHVLGLFRLFVMPRMQSPATG	480
H461W_CgAM	QQQDWSQPPWHPVRLAEEGYIPWRNLLRTVLRHSGGIRVDHVLGLFRLFVMPRMQSPATG	480

WT_CgAM	TYIRFDHNALVGLALEAELAGAVVIGEDLGTFFEPWVQDALAQRGIMGTSILWFEHSPSQ	540
H461A_CgAM	TYIRFDHNALVGLALEAELAGAVVIGEDLGTFFEPWVQDALAQRGIMGTSILWFEHSPSQ	540
H461S_CgAM	TYIRFDHNALVGLALEAELAGAVVIGEDLGTFFEPWVQDALAQRGIMGTSILWFEHSPSQ	540
H461D_CgAM	TYIRFDHNALVGLALEAELAGAVVIGEDLGTFFEPWVQDALAQRGIMGTSILWFEHSPSQ	540
H461R_CgAM	TYIRFDHNALVGLALEAELAGAVVIGEDLGTFFEPWVQDALAQRGIMGTSILWFEHSPSQ	540
H461W_CgAM	TYIRFDHNALVGLALEAELAGAVVIGEDLGTFFEPWVQDALAQRGIMGTSILWFEHSPSQ	540

WT_CgAM	PGRRQEEYRPLALTTVTTTHDLPPTAGYLEGEHIALRERLGVNLTPAAELAEDLQWQAE	600
H461A_CgAM	PGRRQEEYRPLALTTVTTTHDLPPTAGYLEGEHIALRERLGVNLTPAAELAEDLQWQAE	600
H461S_CgAM	PGRRQEEYRPLALTTVTTTHDLPPTAGYLEGEHIALRERLGVNLTPAAELAEDLQWQAE	600
H461D_CgAM	PGRRQEEYRPLALTTVTTTHDLPPTAGYLEGEHIALRERLGVNLTPAAELAEDLQWQAE	600
H461R_CgAM	PGRRQEEYRPLALTTVTTTHDLPPTAGYLEGEHIALRERLGVNLTPAAELAEDLQWQAE	600
H461W_CgAM	PGRRQEEYRPLALTTVTTTHDLPPTAGYLEGEHIALRERLGVNLTPAAELAEDLQWQAE	600

WT_CgAM	ILDVAASANALPAREYVGLERDQRGELAELEGLHTFVAKTPSALTCVCLVDMVGEKRAQ	660
H461A_CgAM	ILDVAASANALPAREYVGLERDQRGELAELEGLHTFVAKTPSALTCVCLVDMVGEKRAQ	660
H461S_CgAM	ILDVAASANALPAREYVGLERDQRGELAELEGLHTFVAKTPSALTCVCLVDMVGEKRAQ	660
H461D_CgAM	ILDVAASANALPAREYVGLERDQRGELAELEGLHTFVAKTPSALTCVCLVDMVGEKRAQ	660
H461R_CgAM	ILDVAASANALPAREYVGLERDQRGELAELEGLHTFVAKTPSALTCVCLVDMVGEKRAQ	660
H461W_CgAM	ILDVAASANALPAREYVGLERDQRGELAELEGLHTFVAKTPSALTCVCLVDMVGEKRAQ	660

WT_CgAM	NQPGTTRDMYPNWCIPLCDSEGNVLIESLRENELYHRVAKASKRD	706
H461A_CgAM	NQPGTTRDMYPNWCIPLCDSEGNVLIESLRENELYHRVAKASKRD	706
H461S_CgAM	NQPGTTRDMYPNWCIPLCDSEGNVLIESLRENELYHRVAKASKRD	706
H461D_CgAM	NQPGTTRDMYPNWCIPLCDSEGNVLIESLRENELYHRVAKASKRD	706
H461R_CgAM	NQPGTTRDMYPNWCIPLCDSEGNVLIESLRENELYHRVAKASKRD	706
H461W_CgAM	NQPGTTRDMYPNWCIPLCDSEGNVLIESLRENELYHRVAKASKRD	706

Figure 3. 14 The deduced amino acid sequences of five H461 mutated CgAMs compared with that of WT using Clustal O (1.2.4) multiple sequence alignment. Mutated amino acids are shaded. (Only the sequences from AA421-AA706 are shown here, the sequences from AA1-AA420 which are the same in all CgAMs are not shown.)

N287R_CgAM	CGCTTTATCAACCCGATCTACATTCCGGGTAGAAGATATCCGGAGTTTAATCAGCTTGAG	780
N287W_CgAM	CGCTTTATCAACCCGATCTACATTCCGGGTAGAAGATATCCGGAGTTTAATCAGCTTGAG	780
WT_CgAM	CGCTTTATCAACCCGATCTACATTCCGGGTAGAAGATATCCGGAGTTTAATCAGCTTGAG	780
N287D_CgAM	CGCTTTATCAACCCGATCTACATTCCGGGTAGAAGATATCCGGAGTTTAATCAGCTTGAG	780
N287A_CgAM	CGCTTTATCAACCCGATCTACATTCCGGGTAGAAGATATCCGGAGTTTAATCAGCTTGAG	780
N287S_CgAM	CGCTTTATCAACCCGATCTACATTCCGGGTAGAAGATATCCGGAGTTTAATCAGCTTGAG	780

N287R_CgAM	ATTGATCTACGCGATGATATCGCAGAGATGGCTGCGGAATCCCGCAACGCAATCTGACC	840
N287W_CgAM	ATTGATCTACGCGATGATATCGCAGAGATGGCTGCGGAATCCCGCAACGCAATCTGACC	840
WT_CgAM	ATTGATCTACGCGATGATATCGCAGAGATGGCTGCGGAATCCCGCAACGCAATCTGACC	840
N287D_CgAM	ATTGATCTACGCGATGATATCGCAGAGATGGCTGCGGAATCCCGCAACGCAATCTGACC	840
N287A_CgAM	ATTGATCTACGCGATGATATCGCAGAGATGGCTGCGGAATCCCGCAACGCAATCTGACC	840
N287S_CgAM	ATTGATCTACGCGATGATATCGCAGAGATGGCTGCGGAATCCCGCAACGCAATCTGACC	840

N287R_CgAM	TCAGACATCATTGAGCGCGGACGCTACGCTGCAAAGCTTCAAGTGTGCGCGCCATT	900
N287W_CgAM	TCAGACATCATTGAGCGCTGGGACGCTACGCTGCAAAGCTTCAAGTGTGCGCGCCATT	900
WT_CgAM	TCAGACATCATTGAGCGCAATGACGCTACGCTGCAAAGCTTCAAGTGTGCGCGCCATT	900
N287D_CgAM	TCAGACATCATTGAGCGCGATGACGCTACGCTGCAAAGCTTCAAGTGTGCGCGCCATT	900
N287A_CgAM	TCAGACATCATTGAGCGCGCTGACGCTACGCTGCAAAGCTTCAAGTGTGCGCGCCATT	900
N287S_CgAM	TCAGACATCATTGAGCGCTCTGACGCTACGCTGCAAAGCTTCAAGTGTGCGCGCCATT	900

N287R_CgAM	TTTGAATGCCTCGTTCAGCGAACGTTGAAGCCAACCTTGTCTCCTTCGTGCAACGGGAA	960
N287W_CgAM	TTTGAATGCCTCGTTCAGCGAACGTTGAAGCCAACCTTGTCTCCTTCGTGCAACGGGAA	960
WT_CgAM	TTTGAATGCCTCGTTCAGCGAACGTTGAAGCCAACCTTGTCTCCTTCGTGCAACGGGAA	960
N287D_CgAM	TTTGAATGCCTCGTTCAGCGAACGTTGAAGCCAACCTTGTCTCCTTCGTGCAACGGGAA	960
N287A_CgAM	TTTGAATGCCTCGTTCAGCGAACGTTGAAGCCAACCTTGTCTCCTTCGTGCAACGGGAA	960
N287S_CgAM	TTTGAATGCCTCGTTCAGCGAACGTTGAAGCCAACCTTGTCTCCTTCGTGCAACGGGAA	960

N287R_CgAM	GGCCAAGGTCTTATTGATTCGCCACCTGGTGCGCGGACCGCGAAACTGCACAGTCTGAA	1020
N287W_CgAM	GGCCAAGGTCTTATTGATTCGCCACCTGGTGCGCGGACCGCGAAACTGCACAGTCTGAA	1020
WT_CgAM	GGCCAAGGTCTTATTGATTCGCCACCTGGTGCGCGGACCGCGAAACTGCACAGTCTGAA	1020
N287D_CgAM	GGCCAAGGTCTTATTGATTCGCCACCTGGTGCGCGGACCGCGAAACTGCACAGTCTGAA	1020
N287A_CgAM	GGCCAAGGTCTTATTGATTCGCCACCTGGTGCGCGGACCGCGAAACTGCACAGTCTGAA	1020
N287S_CgAM	GGCCAAGGTCTTATTGATTCGCCACCTGGTGCGCGGACCGCGAAACTGCACAGTCTGAA	1020

N287R_CgAM	TCTGTCCACGGAAGTACGAGCCAGACCGGATGAGCTGACCATGTTCTACATGTGGTTGCAG	1080
N287W_CgAM	TCTGTCCACGGAAGTACGAGCCAGACCGGATGAGCTGACCATGTTCTACATGTGGTTGCAG	1080
WT_CgAM	TCTGTCCACGGAAGTACGAGCCAGACCGGATGAGCTGACCATGTTCTACATGTGGTTGCAG	1080
N287D_CgAM	TCTGTCCACGGAAGTACGAGCCAGACCGGATGAGCTGACCATGTTCTACATGTGGTTGCAG	1080
N287A_CgAM	TCTGTCCACGGAAGTACGAGCCAGACCGGATGAGCTGACCATGTTCTACATGTGGTTGCAG	1080
N287S_CgAM	TCTGTCCACGGAAGTACGAGCCAGACCGGATGAGCTGACCATGTTCTACATGTGGTTGCAG	1080

Figure 3. 15 Nucleotide sequences of five N287 mutated *CgAMs* compared with that of WT using Clustal O (1.2.4) multiple sequence alignment. Mutated codons are shaded. (Only the sequences from NT 721-1080 are shown here, the sequences from NT1-NT720 and NT1081-NT2121 which are the same in all *CgAMs* are not shown.)

WT_CgAM	MTARRFLNELADLYGVATSYTDYKGAHIEVSDDTLVKILRALGVNLDTSNLPNDDAIQRQ	60
N287A_CgAM	MTARRFLNELADLYGVATSYTDYKGAHIEVSDDTLVKILRALGVNLDTSNLPNDDAIQRQ	60
N287S_CgAM	MTARRFLNELADLYGVATSYTDYKGAHIEVSDDTLVKILRALGVNLDTSNLPNDDAIQRQ	60
N287D_CgAM	MTARRFLNELADLYGVATSYTDYKGAHIEVSDDTLVKILRALGVNLDTSNLPNDDAIQRQ	60
N287R_CgAM	MTARRFLNELADLYGVATSYTDYKGAHIEVSDDTLVKILRALGVNLDTSNLPNDDAIQRQ	60
N287W_CgAM	MTARRFLNELADLYGVATSYTDYKGAHIEVSDDTLVKILRALGVNLDTSNLPNDDAIQRQ	60

WT_CgAM	IALFHDFREFTRPLPPSVVAVEGDELVFPVHVHDGSPADVHIELEDGTQRDVSQVENWTAP	120
N287A_CgAM	IALFHDFREFTRPLPPSVVAVEGDELVFPVHVHDGSPADVHIELEDGTQRDVSQVENWTAP	120
N287S_CgAM	IALFHDFREFTRPLPPSVVAVEGDELVFPVHVHDGSPADVHIELEDGTQRDVSQVENWTAP	120
N287D_CgAM	IALFHDFREFTRPLPPSVVAVEGDELVFPVHVHDGSPADVHIELEDGTQRDVSQVENWTAP	120
N287R_CgAM	IALFHDFREFTRPLPPSVVAVEGDELVFPVHVHDGSPADVHIELEDGTQRDVSQVENWTAP	120
N287W_CgAM	IALFHDFREFTRPLPPSVVAVEGDELVFPVHVHDGSPADVHIELEDGTQRDVSQVENWTAP	120

WT_CgAM	REIDGIRWGEASFKIPGDLPLGWHKHLHLSNERSAECGLIITPARLSTADKYLDSPRSGV	180
N287A_CgAM	REIDGIRWGEASFKIPGDLPLGWHKHLHLSNERSAECGLIITPARLSTADKYLDSPRSGV	180
N287S_CgAM	REIDGIRWGEASFKIPGDLPLGWHKHLHLSNERSAECGLIITPARLSTADKYLDSPRSGV	180
N287D_CgAM	REIDGIRWGEASFKIPGDLPLGWHKHLHLSNERSAECGLIITPARLSTADKYLDSPRSGV	180
N287R_CgAM	REIDGIRWGEASFKIPGDLPLGWHKHLHLSNERSAECGLIITPARLSTADKYLDSPRSGV	180
N287W_CgAM	REIDGIRWGEASFKIPGDLPLGWHKHLHLSNERSAECGLIITPARLSTADKYLDSPRSGV	180

WT_CgAM	MAQIYSVRSTLSWGMGDFNDLGNLASVVAQDGADFLINPMHAAEPLPPTEDSPYLPTR	240
N287A_CgAM	MAQIYSVRSTLSWGMGDFNDLGNLASVVAQDGADFLINPMHAAEPLPPTEDSPYLPTR	240
N287S_CgAM	MAQIYSVRSTLSWGMGDFNDLGNLASVVAQDGADFLINPMHAAEPLPPTEDSPYLPTR	240
N287D_CgAM	MAQIYSVRSTLSWGMGDFNDLGNLASVVAQDGADFLINPMHAAEPLPPTEDSPYLPTR	240
N287R_CgAM	MAQIYSVRSTLSWGMGDFNDLGNLASVVAQDGADFLINPMHAAEPLPPTEDSPYLPTR	240
N287W_CgAM	MAQIYSVRSTLSWGMGDFNDLGNLASVVAQDGADFLINPMHAAEPLPPTEDSPYLPTR	240

WT_CgAM	RFINPIYIRVEDIPEFNQLEIDLRRDDIAEMAAEFRRNLTSDIIERNDVYAAKLQVLRAI	300
N287A_CgAM	RFINPIYIRVEDIPEFNQLEIDLRRDDIAEMAAEFRRNLTSDIIERNDVYAAKLQVLRAI	300
N287S_CgAM	RFINPIYIRVEDIPEFNQLEIDLRRDDIAEMAAEFRRNLTSDIIERNDVYAAKLQVLRAI	300
N287D_CgAM	RFINPIYIRVEDIPEFNQLEIDLRRDDIAEMAAEFRRNLTSDIIERNDVYAAKLQVLRAI	300
N287R_CgAM	RFINPIYIRVEDIPEFNQLEIDLRRDDIAEMAAEFRRNLTSDIIERNDVYAAKLQVLRAI	300
N287W_CgAM	RFINPIYIRVEDIPEFNQLEIDLRRDDIAEMAAEFRRNLTSDIIERNDVYAAKLQVLRAI	300

WT_CgAM	FEMPRSSEREANFVSFVQREGQLIDFATWCADRETAQSESVHGTPEPDRDELTMFYMWLQ	360
N287A_CgAM	FEMPRSSEREANFVSFVQREGQLIDFATWCADRETAQSESVHGTPEPDRDELTMFYMWLQ	360
N287S_CgAM	FEMPRSSEREANFVSFVQREGQLIDFATWCADRETAQSESVHGTPEPDRDELTMFYMWLQ	360
N287D_CgAM	FEMPRSSEREANFVSFVQREGQLIDFATWCADRETAQSESVHGTPEPDRDELTMFYMWLQ	360
N287R_CgAM	FEMPRSSEREANFVSFVQREGQLIDFATWCADRETAQSESVHGTPEPDRDELTMFYMWLQ	360
N287W_CgAM	FEMPRSSEREANFVSFVQREGQLIDFATWCADRETAQSESVHGTPEPDRDELTMFYMWLQ	360

WT_CgAM	WLCDEQLAAAQKRAVDAGMSIGIMADLAVGVHPGGADAQNLSHVLAPDASVGAPPDGYNQ	420
N287A_CgAM	WLCDEQLAAAQKRAVDAGMSIGIMADLAVGVHPGGADAQNLSHVLAPDASVGAPPDGYNQ	420
N287S_CgAM	WLCDEQLAAAQKRAVDAGMSIGIMADLAVGVHPGGADAQNLSHVLAPDASVGAPPDGYNQ	420
N287D_CgAM	WLCDEQLAAAQKRAVDAGMSIGIMADLAVGVHPGGADAQNLSHVLAPDASVGAPPDGYNQ	420
N287R_CgAM	WLCDEQLAAAQKRAVDAGMSIGIMADLAVGVHPGGADAQNLSHVLAPDASVGAPPDGYNQ	420
N287W_CgAM	WLCDEQLAAAQKRAVDAGMSIGIMADLAVGVHPGGADAQNLSHVLAPDASVGAPPDGYNQ	420

Figure 3. 16 The deduced amino acid sequences of five N287 mutated CgAMs compared with that of WT using Clustal O (1.2.4) multiple sequence alignment. Mutated amino acids are shaded. (Only the sequences from AA1-AA420 are shown here, the sequences from AA421-AA706 which are the same in all CgAMs are not shown.)

Expression, Purification and Characterization of Y418 mutated amyloamylases

3.2 Expression and purification of Y418 mutated amyloamylases

After *CgAMs* were successfully expressed by induction with 0.4 mM IPTG, cell pellets were disrupted by sonication, and the supernatant carrying crude enzyme was purified by affinity column. The crude and purified enzymes were subjected to electrophoresis on 7.5% separating SDS-polyacrylamide gel. SDS-PAGE of crude and purified preparations of six Y418 mutated *CgAMs* were shown in Figure 3.17. All mutated *CgAMs* showed an overexpression of the enzyme with the major protein band approximately at 84 kDa similar to WT *CgAM*. This suggested that mutated *CgAMs* were successfully purified by His-trap column chromatography. The fraction that showed high enzyme activity were pooled and dialyzed against 20 mM phosphate buffer, pH 7.4 at 4 °C. The specific starch transglucosylation and disproportionation activities of the purified Y418 mutated *CgAMs* were 1.2-3.0 fold and 1.3-3.0 fold lower than that of the WT, respectively (Table 3.1). For both activities, the specific activities of WT and Y418F mutant were closed (25.0 and 21.0 U/mg protein for starch transglucosylation activity, respectively) while those of Y418A/D/S/W mutants were 1.3-2.3 -fold lower than WT. Interestingly, Y418R mutant was most affected with the lowest specific activity of 8.36 U/mg (Table 3.1). In addition, percent yields of WT and all mutated *CgAMs* were similar. It is noticeable that the yields of all enzymes assayed by disproportionation activity were 4.0-fold lower than assayed by starch transglucosylation activity (Table 3.1 and 3.2).

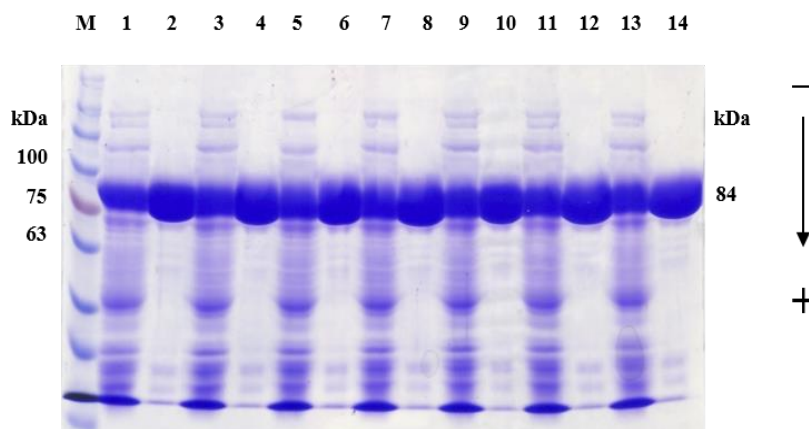


Figure 3. 17 SDS-PAGE of crude and purified enzyme expressed from cells harboring the series of Y418 mutated CgAMs.

Lane M = Protein markers

Lane 1, 3, 5, 7, 9, 11 and 13 = 20 μ g of crude WT-, Y418A-, Y418S-, Y418D-, Y418R-, Y418W- and Y418F-CgAMs, respectively

Lane 2, 4, 6, 8, 10, 12 and 14 = 10 μ g of purified WT-, Y418A-, Y418S-, Y418D-, Y418R-, Y418W- and Y418F-CgAMs, respectively

Table 3. 1 Purification of WT and Y418 mutated CgAMs assayed by starch transglucosylation activity.

CgAM	Total protein (mg)	Total activity (U)	Specific activity (U/mg)	Purification (fold)	Yield (%)
WT					
Crude	284	425	1.50	1	100
Purified	7.15	179	25.0	16.7	42.1
Y418A					
Crude	242	254	1.05	1	100
Purified	5.61	94.1	16.8	16.0	37.0
Y418S					
Crude	264	304	1.15	1	100
Purified	8.05	146	11.8	10.2	48.0
Y418D					
Crude	235	305	1.30	1	100
Purified	6.84	130	19.0	14.6	42.6
Y418R					
Crude	252	278	1.10	1	100
Purified	7.42	62	8.36	7.57	22.3
Y418W					
Crude	265	204	0.77	1	100
Purified	6.65	72	10.8	14.1	35.3
Y418F					
Crude	300	415	1.38	1	100
Purified	8.12	170	20.9	15.1	41.0

Table 3.2 Purification of WT and Y418 mutated CgAMs assayed by disproportionation activity.

<i>CgAM</i>	Total protein (mg)	Total activity (U)	Specific activity (U/mg)	Purification (fold)	Yield (%)
WT					
Crude	284	1785	6.29	1	100
Purified	7.15	196	27.4	4.36	11.0
Y418A					
Crude	242	975	4.03	1	100
Purified	5.61	98.7	17.6	4.37	10.1
Y418S					
Crude	264	964	3.65	1	100
Purified	8.05	112	13.9	3.81	11.6
Y418D					
Crude	235	954	4.06	1	100
Purified	6.84	130	19.0	4.68	13.6
Y418R					
Crude	252	578	2.29	1	100
Purified	7.42	69.4	9.35	4.08	12.0
Y418W					
Crude	265	613	2.31	1	100
Purified	6.65	78.5	11.8	5.10	12.8
Y418F					
Crude	300	1643	5.48	1	100
Purified	8.12	178	21.9	4.00	10.8

3.3 Effect of Y418 mutation on enzyme characteristics

To determine the effect of Y418 mutation on enzyme, various biochemical and biophysical properties together with the product formation of the series of Y418 mutated CgAMs (Y418A/S/D/R/W/F) were measured and compared to the WT.

Biochemical properties of CgAMs

3.3.1 Various amyloamylase activities

The effect of single point mutation at Y418 residue on various activities of CgAM was examined as described in 2.8 and the result was shown in Table 3.3. Mutation at Y418 caused an obvious change in enzyme activities; both the inter- and intra-molecular transglucosylation reactions were affected. A significant decrease in the three main activities of AM: starch transglucosylation (1.2-3.0 folds), disproportionation (1.2-2.6 folds) and especially cyclization (1.3-7.3 folds) was observed (Table 3.3). Y418F, Y418A/S/D and Y418W/R mutants showed a slight, moderate and dramatic reduction in those activities, respectively when compared to WT. However, the hydrolysis and coupling activities were mostly not changed except for coupling of R mutant which showed half reduction. From these results, it could be summarized that all Y418 mutated CgAMs showed lower activity of the three main transglucosylation activities than those of WT CgAM.

3.3.2 Optimum conditions and stability

In this experiment, the optimum conditions for two main activities, disproportionation and cyclization of CgAMs were determined.

3.3.2.1 Effect of temperature on CgAM activity

Optimum temperatures of disproportionation and cyclization activities of CgAMs were determined as described in section 2.9.1. For disproportionation activity,

the optimum temperature of Y418 mutated CgAMs was 40 °C similar to WT enzyme (Figure 3.18A). At 55 °C, all CgAMs showed half of the maximum disproportionation activity. The cyclization activity of CgAMs was also investigated, the optimum temperature of WT and Y418 mutated CgAMs was 30 °C (Figure 3.19A). All enzymes had less than 50% residual cyclization activity at temperature higher than 45 °C, especially the D, R and W mutants which had less than 10% activity. The cyclization activity of Y418A/S/D/R/W at 50 °C could not be detected while that of the WT and Y418F had 10-20% residual activity.

3.3.2.2 Effect of pH on CgAM activity

The effect of pH on enzyme activity was examined by disproportionation and cyclization activities as described in section 2.9.2. The optimum pH for disproportionation activity of WT and all Y418 mutated CgAMs was pH 6.0 (Figure 3.18B). At pH 9.0, both WT and mutated CgAMs showed similar activity, 60-70% relative activity still remained. While only 10% activity was observed at pH 4.0 and higher than 80% CgAM activity remained in the pH range of 6.0-8.0. In addition, the optimum pH for cyclization activity of WT and Y418 mutated CgAMs was also investigated (Figure 3.19B), the results showed that all CgAMs had optimum pH at pH 6.0. Interestingly, 50-70% of activity of all CgAMs still remained at pH 9.0.

3.3.2.3 Effect of temperature stability of CgAM

Temperature stability of CgAM was determined by following disproportionation activity as a function of time. CgAMs were pre-incubated at different temperature, ranging from 30 °C, 35 °C and 40 °C for 0-180 min as described in 2.9.3. It was observed that WT-CgAM was more stable than all Y418 mutated enzymes at all temperatures tested. All CgAMs well maintained its activity when

incubated at 30 °C for 180 min, about 70% activity was still observed (Figure 3.20A). The loss of 50% activity was found after 180 min at 35 °C especially for Y418R and Y418W mutated CgAMs (Figure 3.20B). At 40 °C, all enzymes showed nearly 100% activity at short incubation time of 10 min but their activities were dramatically decreased to 10% at 90 min incubation time, and lost all activities after 90 min (Figure 3.20C).

3.3.2.4 Effect of pH stability of CgAM

The pH stability of disproportionation activity of CgAM was followed at 30 °C as described in 2.9.4. The result was shown in Figure 3.21. At pH 7.0, nearly 90% of WT and Y418F activities were remained at 120 min incubation time while other mutated enzymes had 70-80% activity. At pH 8.0 and the same incubation time of 120 min, the residual activities of WT-, Y418F- and Y418A- CgAMs were about 50-60% while other mutated CgAMs showed 40% remaining activity (Figure 3.21B).

3.3.3 Substrate specificity

The ability of mutated CgAMs to catalyze different substrates (G2-G7) of disproportionation reaction was determined and compared to that of the WT as described in 2.9.5 (Fig. 3.22). G3 was the best while G7 was the worst substrate for both WT and mutated CgAMs. For most of mutated enzymes, specificity for G3 was close to that of G4 while the WT significantly used G3 better than G4. It is noticeable here that Y418F showed an increase in preference for G5 to G7 (Figure. 3.22).

3.3.4 Determination of kinetic parameters

3.3.4.1 Kinetic study of disproportionation reaction

The kinetic analysis of CgAMs was performed using G3, the most favorable substrate of disproportionation reaction as described in section 2.9.6.1. Figure 3.23

represented the Lineweaver-Burk plot of CgAMs. All mutated CgAMs except the F mutant had a lower k_{cat} and k_{cat}/K_m values, the W and R mutants showed the lowest k_{cat}/K_m with 8- and 12-fold lower than the WT's value (Table 3.3). The mutation affected more on the k_{cat} , 1.4 to 10.8-fold lower than that of the WT while the K_m values were not much changed with the values around 16-20 mM.

3.3.4.2 Kinetic study of cyclization reaction

Y418A and Y418W were selected for the study of the kinetics of cyclization reaction compared to WT enzyme as described in section 2.9.6.2. Figure 3. 24 represented the Lineweaver- Burk plot of CgAMs. All kinetic parameters were calculated and shown in Table 3.4. The K_m values of Y418A and Y418W CgAMs were about 1.5-fold higher than that of WT, indicating lower affinity towards pea starch substrate. The k_{cat}/K_m of Y418A and Y418W CgAMs were approximately 3.0 -7.8 fold lower than the WT's value.

3.3.5 Analysis of pattern of LR-CDs products

Production of LR-CDs was performed, CgAMs were incubated with 2% (w/v) pea starch at 30 °C, pH 6.0 which was their optimum condition. LR-CD mixtures in the reaction were analyzed by HPAEC-PAD described in section 2.9.7

3.3.5.1 Effect of incubation time

Effect of incubation time on LR-CDs production was carried out as described in section 2.9.7.1. To compare the LR-CDs production patterns of WT and Y418 mutated CgAMs, the enzymes with 0.10 U starch degradation activity were incubated at various times (1.5, 6, 12 and 24 h). It was clearly observed that the LR-CD yields of all CgAMs were significantly increased at longer incubation time (Figure 3.25). Interestingly, WT and Y418F mutated CgAMs gave CD29-CD33 as main CD product

while Y418A/D/S mutants yielded CD38-CD40 as principle product at 6 and 12 h. In addition, Y418W and Y418R mutants showed broad size of LR-CDs at every incubation time.

3.3.5.2 Effect of unit enzyme

To observe the influence of enzyme concentration on LR-CDs formation, 0.05 U, 0.1 U and 0.2 U starch degradation activities of enzymes were used as described in section 2.9.7.2. The result showed that the increase in enzyme concentration resulted in a shift of the principle CD products to smaller size as shown in Figure 3.26.



Table 3. 3 Activities of WT and Y418 mutated CgAMs

	Specific activity (U/mg)				
	Starch transglucosylation	Disprop.	Cyclization	Coupling	Hydrolysis
WT	26.0 ± 1.50	24.4 ± 0.93	0.44 ± 0.08	0.16 ± 0.01	0.03 ± 0.00
Y418A	17.0 ± 0.26	19.4 ± 0.76	0.19 ± 0.04	0.19 ± 0.01	0.04 ± 0.01
Y418S	12.5 ± 1.65	18.8 ± 1.00	0.17 ± 0.06	0.14 ± 0.01	0.03 ± 0.00
Y418D	16.0 ± 1.56	19.0 ± 1.08	0.25 ± 0.07	0.14 ± 0.02	0.02 ± 0.01
Y418R	8.93 ± 1.64	9.56 ± 0.98	0.06 ± 0.02	0.08 ± 0.03	0.03 ± 0.02
Y418W	12.1 ± 0.33	11.4 ± 0.51	0.08 ± 0.03	0.13 ± 0.01	0.03 ± 0.01
Y418F	20.9 ± 1.59	20.8 ± 1.28	0.33 ± 0.03	0.13 ± 0.01	0.03 ± 0.01

Data are shown as the mean ± standard deviation and are derived from three independent experiments.

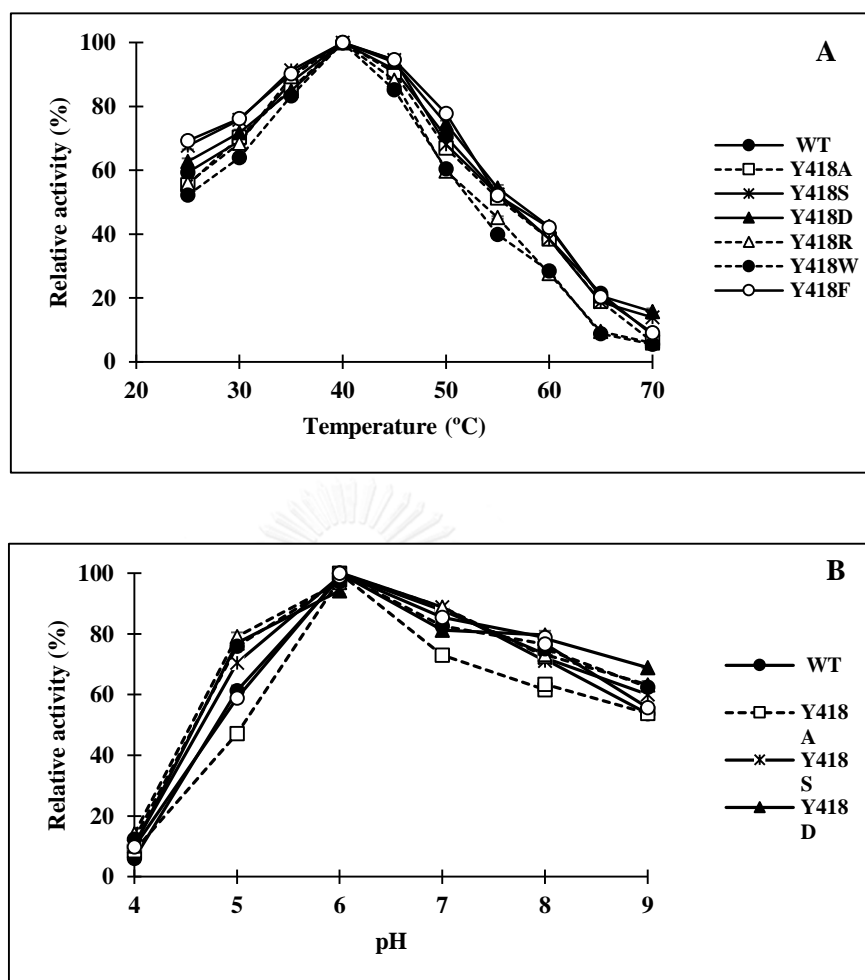


Figure 3. 18 Effect of temperature (A) and pH (B) for WT and Y418 mutated CgAMs on disproportionation activity. The enzymes were fixed at pH 6.0 in (A) and 30°C (B). Buffer used were: acetate buffer (pH 4.0-6.0), phosphate buffer (pH 6.0-8.0) and tris-HCl buffer (pH 8.0 -9.0). The experiments were performed as described in section 2.9.1 and 2.9.2. Data are shown as the mean \pm SD and are derived from three independent repeats.

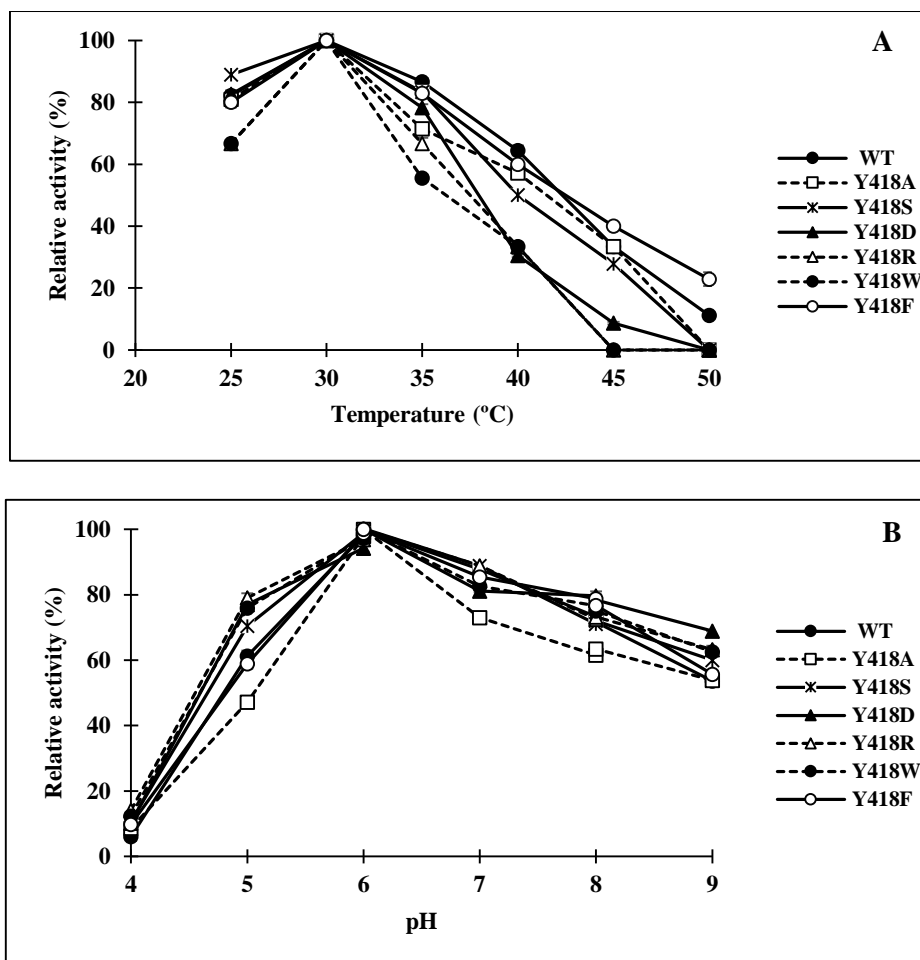


Figure 3. 19 Effect of temperature (A) and pH (B) for WT and Y418 mutated CgAMs on cyclization activity. The enzymes were fixed at pH 6.0 in (A) and 30°C (B). Buffer used were: acetate buffer (pH 4.0-6.0), phosphate buffer (pH 6.0-8.0) and tris-HCl buffer (pH 8.0-9.0). The experiments were performed as described in section 2.9.1 and 2.9.2. WT and Y418 mutated CgAMs were incubated with 2% (w/v) of pea starch for 90 min at various temperature and pH. LR-CD products were analyzed by HPAEC-PAD. Data are shown as the mean \pm SD and are derived from three independent repeats.

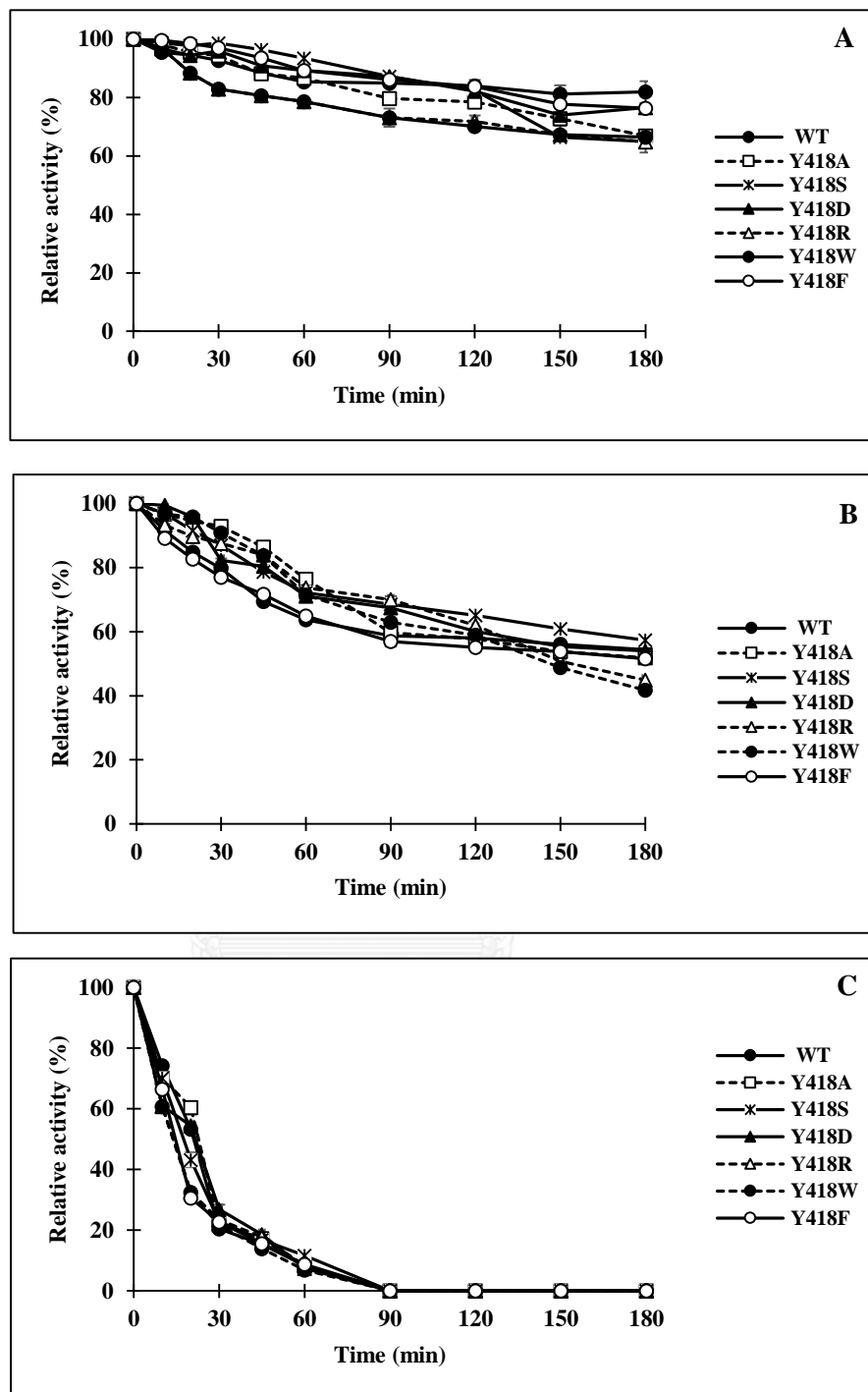


Figure 3. 20 Effect of temperature *CgAM* stability. WT and Y418 mutated *CgAMs* were incubated in phosphate buffer pH 6.0 at 30 °C (A), 35 °C (B), 40 °C (C) for 0 to 180 min. The activity was assayed by disproportionation activity assay as described in 2.9.3

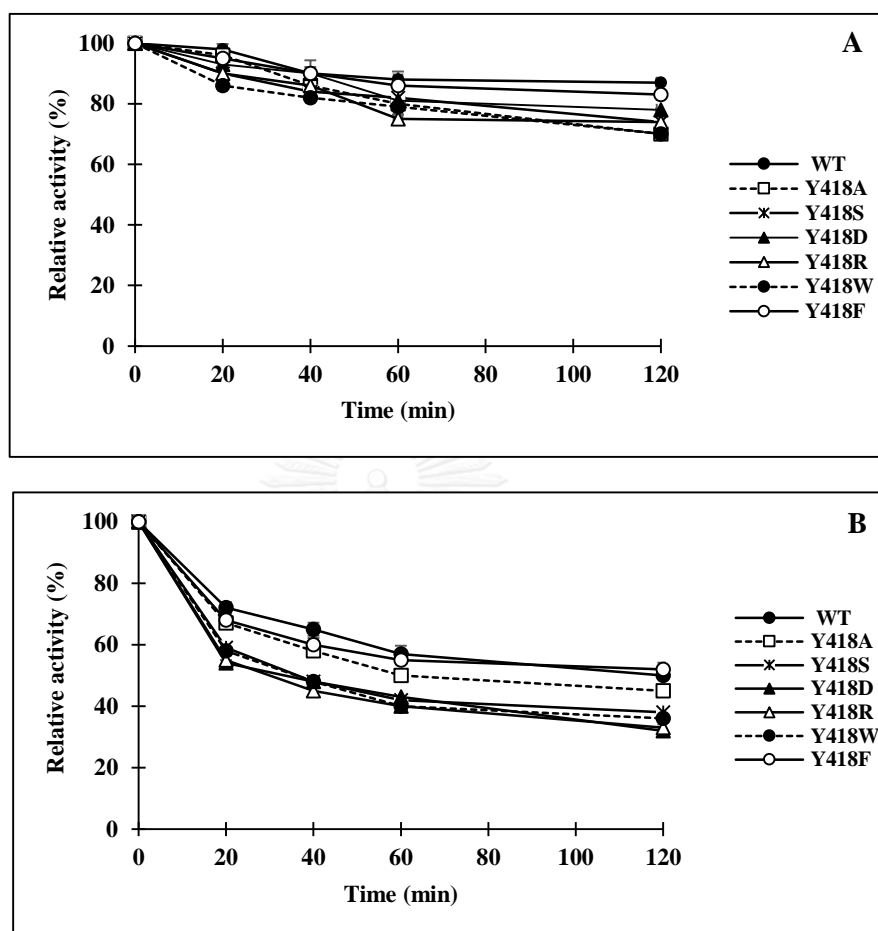


Figure 3. 21 Effect of pH on CgAM stability. WT and Y418 mutated CgAMs were incubated at 30 °C in phosphate buffer pH 7.0 (A) and tris-HCl buffer pH 8.0 (B) for 0-120 min. The activity was assayed by disproportionation activity as described in 2.9.4.

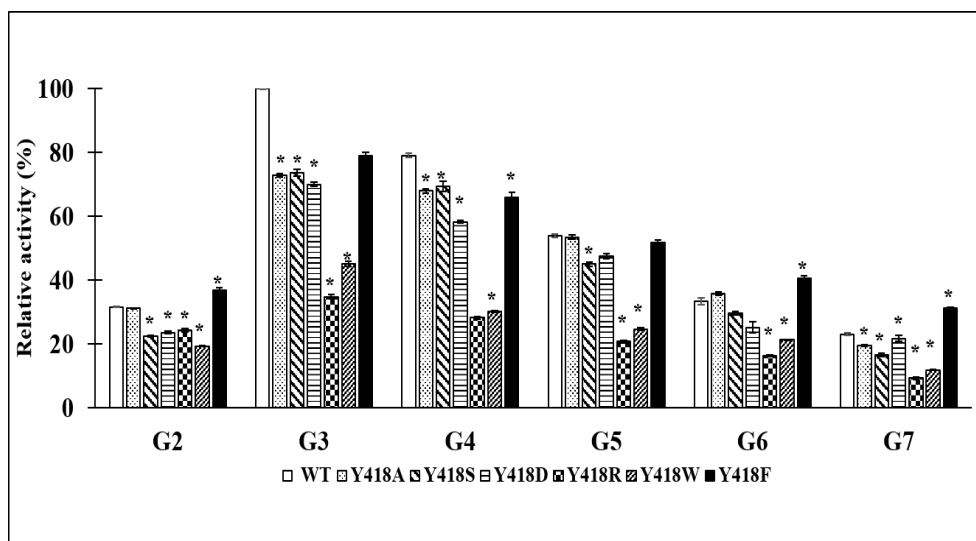


Figure 3.22 Substrate specificity of WT and Y418 mutated *CgAMs* in disproportionation reaction using malto-oligosaccharides (maltose, G2 to maltoheptaose, G7) as substrate. The activity of WT - *CgAM* on G3 substrate was set as 100%. * $P < 0.05$ (Student's t-Test) with respect to the disproportionation reaction of WT - *CgAM*. Data are presented as the mean \pm SD and are derived from three independent experiments.

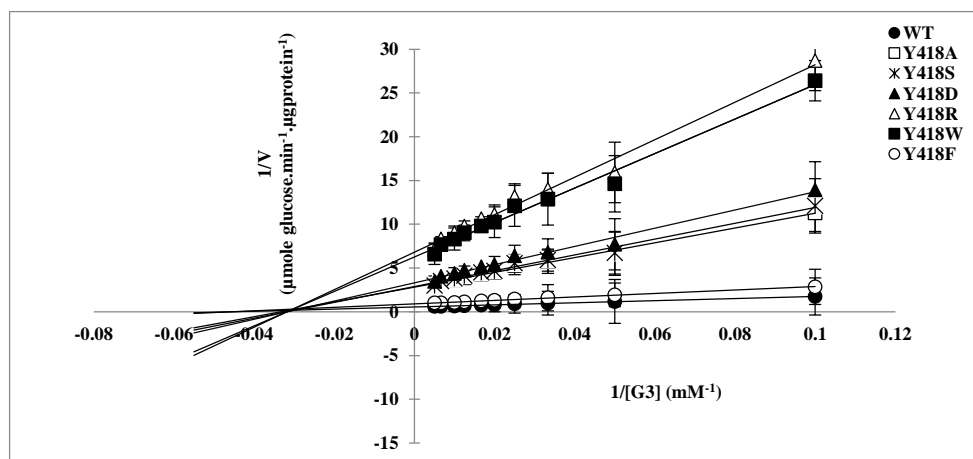


Figure 3. 23 Lineweaver- Burk plot of WT and Y418 mutated CgAMs-catalyzed disproportionation reaction. All CgAMs were incubated with various concentrations of maltotriose (G3) in 50 mM phosphate buffer, pH 6.0 at 40 °C for 5 min. Glucose oxidase method was used to determine the amount of free glucose produced during the reaction.

Table 3.4 Kinetic parameters of WT and Y418 mutated CgAMs from disproportionation reaction using maltotriose substrate.

CgAM	K_m (mM)	V_{max} ($\mu\text{mole glucose}\cdot\text{min}^{-1}\cdot\mu\text{gprotein}^{-1}$)	k_{cat} (min^{-1}) [10^3]	k_{cat}/K_m ($\text{mM}^{-1}\cdot\text{min}^{-1}$) [10^3]
WT	17.2 ± 1.67	2.21 ± 0.31	168 ± 3.30	9.80 ± 1.09
Y418A	15.7 ± 0.58	0.44 ± 0.21	118 ± 2.60	7.52 ± 0.41
Y418S	18.0 ± 0.68	0.43 ± 0.18	110 ± 3.56	6.11 ± 0.42
Y418D	16.3 ± 1.02	0.37 ± 0.11	112 ± 3.34	6.90 ± 0.64
Y418R	19.5 ± 0.82	0.19 ± 0.08	15.5 ± 1.70	0.80 ± 0.09
Y418W	20.4 ± 0.75	0.18 ± 0.05	24.2 ± 3.14	1.18 ± 0.13
Y418F	18.2 ± 0.95	1.88 ± 0.26	160 ± 6.49	8.80 ± 0.21

Data are shown as the mean \pm standard deviation and are derived from three independent experiments.

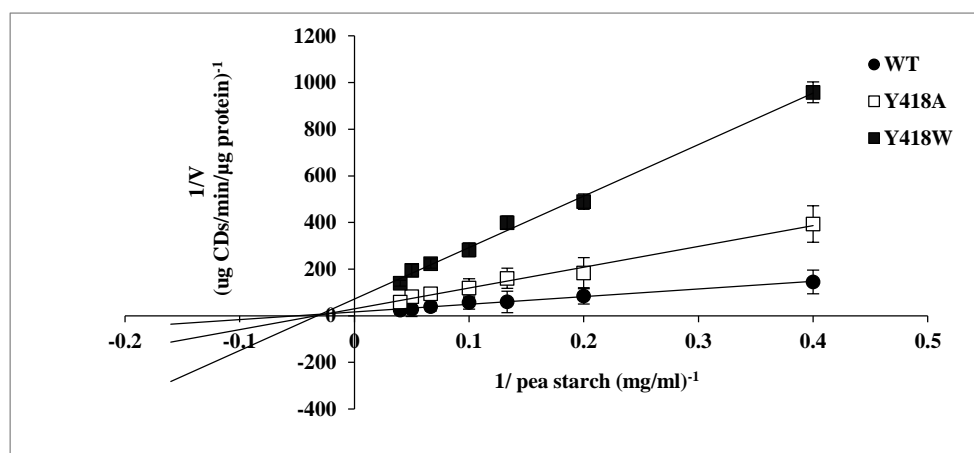


Figure 3. 24 Lineweaver- Burk plot of WT and Y418 mutated CgAMs-catalyzed cyclization reaction. CgAMs (0.05 U starch degrading activity) were incubated with varying concentrations of pea starch at 30 °C for 60 min. LR-CD products were analyzed by HPAEC -PAD.

Table 3. 5 Kinetic parameters of WT and Y418 mutated CgAMs from cyclization activity using pea starch as the substrate.

CgAM	K_m (mg/ml)	V_{max} ($\mu\text{g CD}\cdot\text{min}^{-1}\cdot$ $\mu\text{gprotein}^{-1}$)	k_{cat} (min^{-1}) [10^3]	k_{cat}/K_m ($\text{mg}\cdot\text{ml}^{-1}\cdot\text{min}^{-1}$) [10^3]
WT	19.9 ± 1.78	0.06 ± 0.13	6.12 ± 1.35	0.31 ± 0.06
Y418A	30.0 ± 2.16	0.03 ± 0.06	3.25 ± 1.20	0.11 ± 0.07
Y418W	31.7 ± 3.55	0.01 ± 0.02	1.13 ± 0.26	0.04 ± 0.03

Data are shown as the mean \pm standard deviation and are derived from three independent experiments.

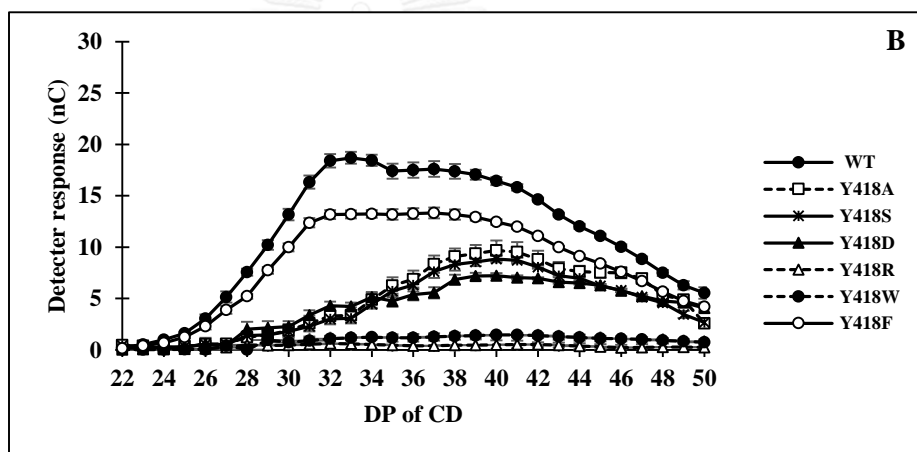
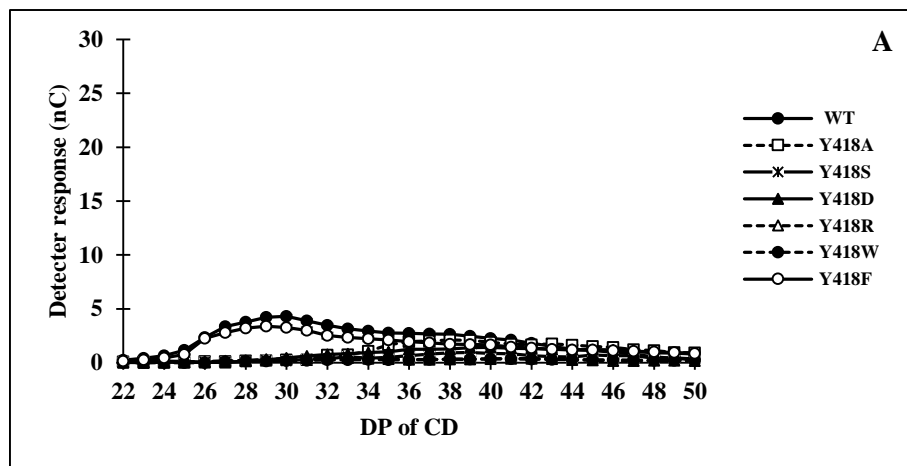


Figure 3. 25 HPAEC- PAD analysis of LR- CD products synthesized at different incubation time 1.5 h (A), 6 h (B), 12 h (C) and 24 h (D) by WT and Y418 mutated CgAMs (DP = Degree of Polymerization).

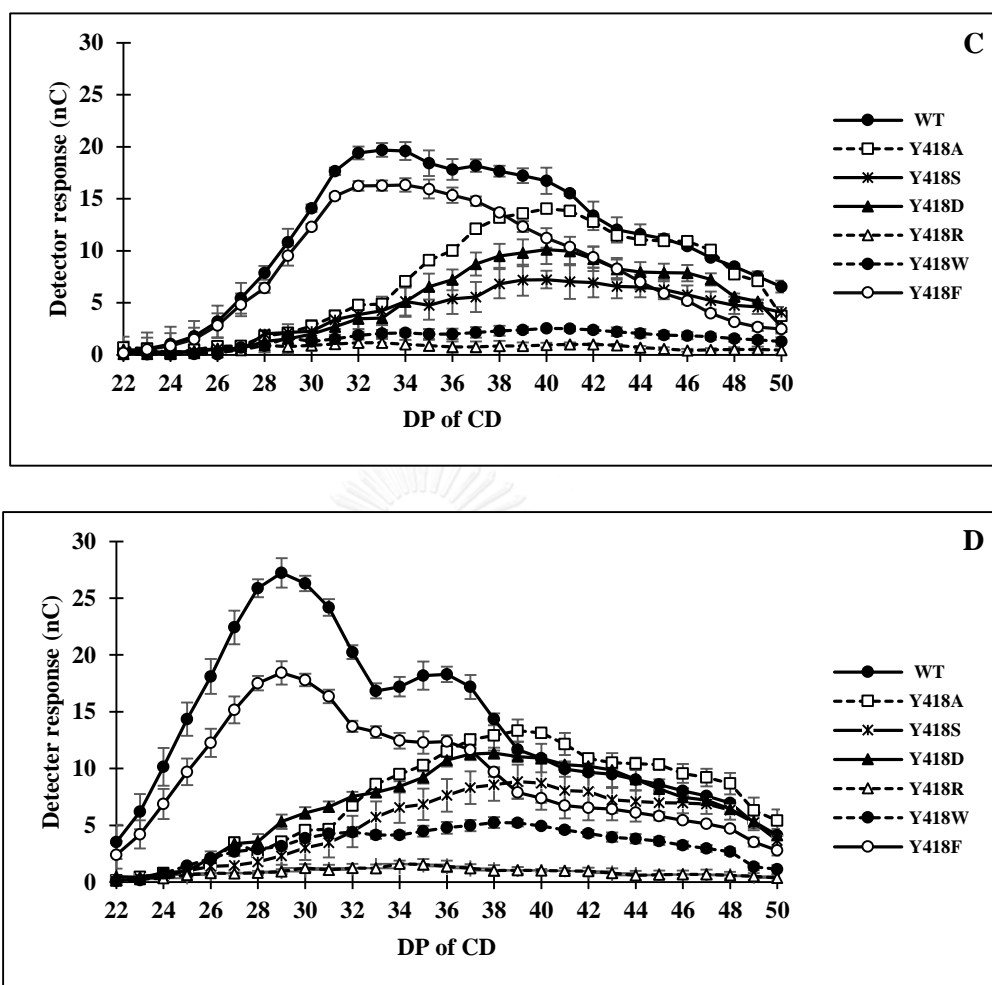


Figure 3.25 (continue) HPAEC-PAD analysis of LR-CD products synthesized at different incubation time 1.5 h (A), 6 h (B), 12 h (C) and 24 h (D) by WT and Y418 mutated *Cg*AMs (DP = Degree of Polymerization).

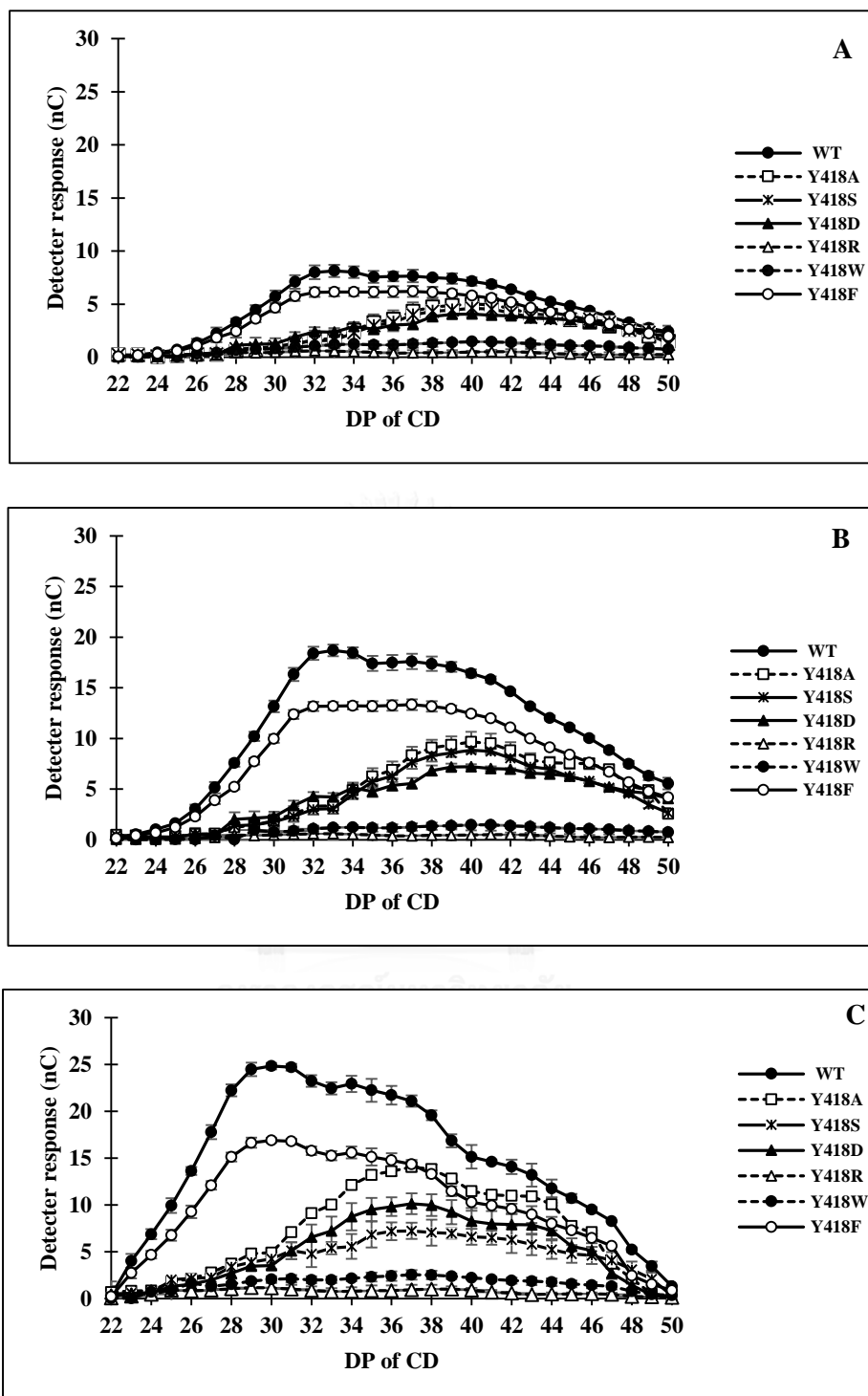


Figure 3.26 HPAEC-PAD analysis of LR-CD products synthesized for 6 h at different enzyme unit; 0.05 U (A), 0.10 U (B) and 0.20 U (C) by WT and Y418 mutated CgAMs (DP = Degree of Polymerization).

3.3.6 Enzyme conformation

In order to investigate the effect of Y418 mutation on secondary structure and folding property of CgAM, circular dichroism (CD) analysis was performed. Purified WT and Y418 mutated CgAMs at 0.2 mg/ml protein concentration were used in the wavelength scanning range from 190 to 250 nm. The CD spectra of Y418 mutated CgAMs were compared with WT as shown in Figure 3.27. The result showed that the CD spectra of the mutated CgAMs and WT were closely overlaid, a slight change was observed in CD spectra of the mutated enzymes. The contents of the secondary structures calculated as described in section 2.9.8 were: α -helix 26-27%, β -sheet 20-22% and random coil 51-52%.

Biophysical properties of CgAMs

3.3.7 Isothermal titration calorimetry (ITC)

In this work, ITC was performed to study the heat change during enzyme catalysis. Maltotriose (G3) was used as a substrate of disproportionation reaction to determine the heat of enzyme reaction between WT and Y418A/W mutated CgAMs as described in section 2.10.1. The thermal power level ($\mu\text{cal}/\text{sec}$) after titration of the enzyme into sample cell showed heat production of enzyme reaction. The average of three replicates gave a thermal power value of WT CgAM which was higher than those of Y418A (1.5 folds) and Y418W (2.5 folds) CgAMs (Figure 3.28). ITC results thus showed a different heat production of WT and Y418A/W enzymes which was corresponded to the activities of CgAMs measured by biochemical method as shown in (Figure 3.29).

To determine the kinetic parameters of CgAMs, the average thermal power prior to the subsequent titration was converted to the rate of G3 catalysis. Every experimental data was fit to the systematic curve fitting analysis (Global fitting program) and estimates of kinetic parameters, the V_{max}/K_m , were obtained. WT CgAM showed the highest value, V_{max}/K_m values of WT, Y418A and Y418W for 10 mM G3 were 1.75, 1.15 and 0.94 $\text{mM}^{-1}\text{s}^{-1}$, respectively. (Table 3.6). The graph plotted between V_{max}/K_m against concentration of G3 showed the product inhibition was occurred at high G3 concentration for WT, Y418A and Y418W mutated CgAMs (Figure 3.30).

3.3.8 Differential scanning calorimetry (DSC)

In this work, DSC was performed in the temperature range of 10 °C to 90 °C in an attempt to compare the thermal stability between WT and Y418A/W mutated CgAMs. The thermal transition curves from this temperature range of all scanning rate (0.75 °C/min, 1.0 °C/min and 1.5 °C/min) for WT and Y418A/W mutated CgAMs in phosphate buffer pH 6.0 were plotted (Figure 3.31). The results showed that, all CgAMs demonstrated the irreversible transition. The heat capacity profiles of WT CgAM at all scanning rate gave a closer peak temperature (T_p) to that of Y418A but a higher T_p than Y418W mutated CgAM. At 1.0 °C/min a shift of peak temperature of Y418W towards 4 °C lower than the value of WT was observed (Table 3.7).

3.4 Structural modeling of Y418 mutated CgAMs

The 3D - structure of CgAM was recently reported (Joo *et al.*, 2016). In this present study, the model structures of all Y418 mutated CgAMs were constructed by the Discovery Studio 3.5 Client program using WT CgAM X-ray structure (PDB code 5B68) (Joo *et al.*, 2016) as template. We found eight residues in the 410s loop including

D416, G417, N419, Q420, R577, V582, Q662 and P663 are within 5 Å away from Y418 position. In the WT and the Y418A/S/D/W/F mutants, no hydrogen bond was observed between residues 418 and these residues, but the R mutant had one H-bond forming with D416 (Fig. 3.32 1A-1G).

The distance between the residues position 418 and F534 which forms the substrate channels was also predicted using the same Discovery Studio Program (Table 3.8). Y418A and Y418W provided a distance of 1.0 Å longer and 5.6 Å shorter than that of the WT, respectively. The molecular surfaces of aromatic edge of CgAMs were determined to show the hydrophobic interaction between Y418 and F534 residues (Fig. 3.32 2A-2G). WT-CgAM showed the strongest hydrophobic interaction (gold color in Figure 3.32-1A) while moderate interaction was found in Y418F/W mutants probably due to the inward direction of F/W side chain. For the Y418A/S/D/R mutants, low or no interaction was observed (grey color in Fig 3.32 - 2B; 2C; 2D; 2E).

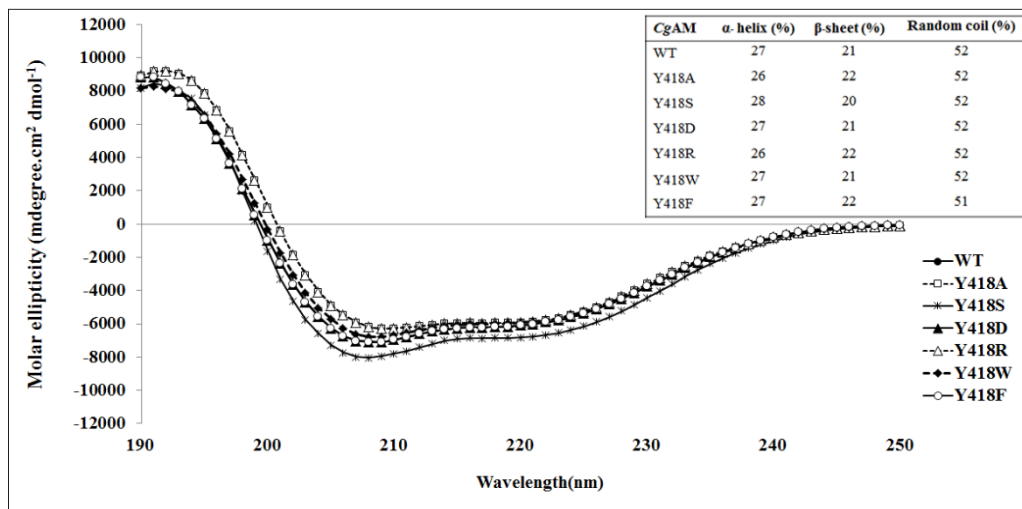


Figure 3. 27 Circular dichroism spectra and the predicted secondary structural compositions of WT and Y418 mutated CgAMs.

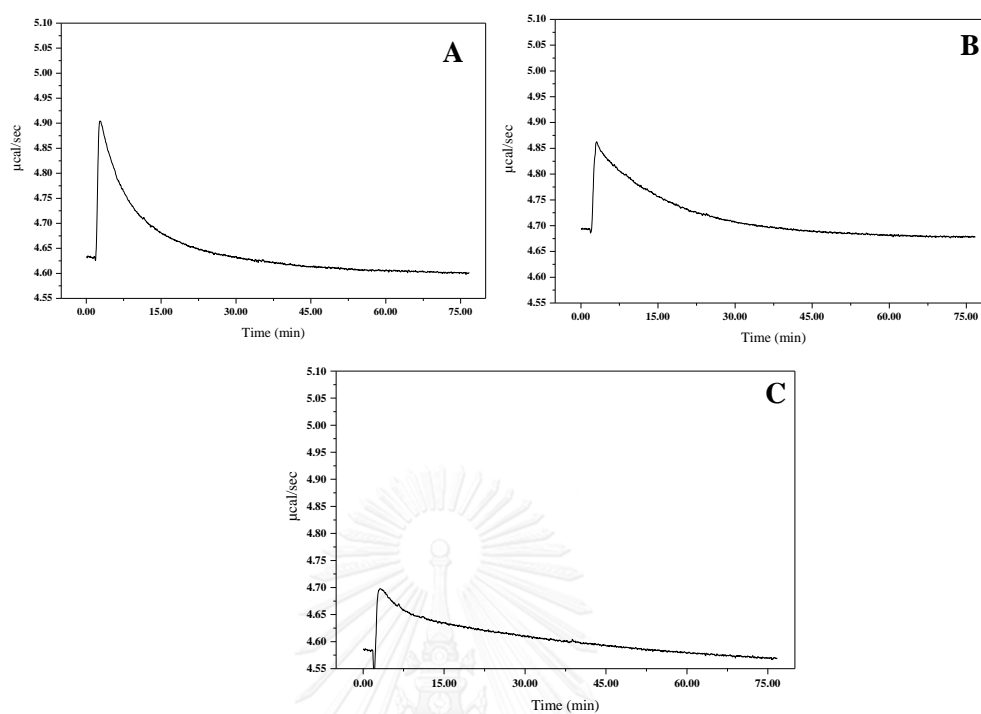


Figure 3. 28 Disproportionation activity of amyloamylase as measured from an enthalpy change when substrate binds to enzyme detected by ITC. Data heat rate as a function of time from a single injection of 20 μM enzymes into 1.4482 ml of 10 mM G3 in 20 mM phosphate buffer pH 6.0 containing 100 mM NaCl, WT (A), Y418A (B) and Y418W(C) CgAMs.

Table 3. 6 Kinetic parameters (V_{max}/K_m) of WT, Y418A and Y418W CgAMs from disproportionation activity determined by ITC.

G3(mM)	$V_{max}/K_m \text{ app} * 10^{-3} \text{ (s}^{-1}\text{)}$		
	WT	Y418A	Y418W
10	1.748 ± 0.024	1.149 ± 0.068	0.940 ± 0.046
20	1.236 ± 0.042	0.722 ± 0.030	0.685 ± 0.026
30	0.899 ± 0.032	0.687 ± 0.160	0.433 ± 0.120

Data are shown as the mean ± standard deviation and are derived from three independent experiments.

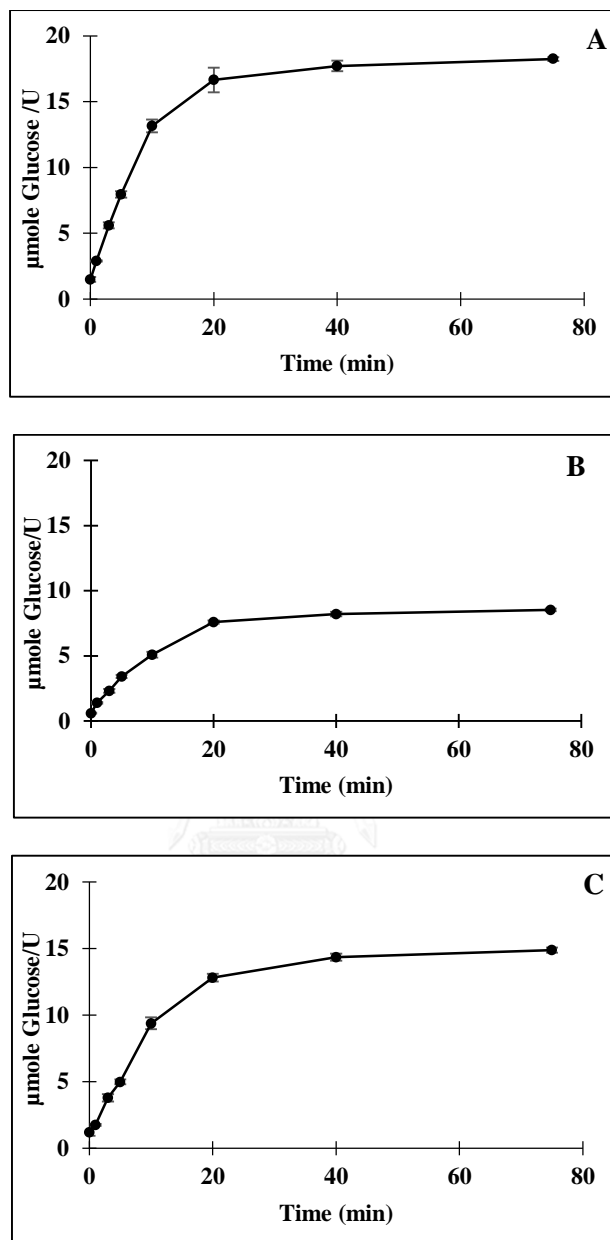


Figure 3. 29 Disproportionation activity of amyloamylase as measured from glucose product released by glucose oxidase assayed spectrophotometrically. G1 liberates as a function of time from incubation of various concentrations of 10 mM G3 with 20 μM WT (A), Y418A (B) and Y418W (C) *CgAMs*.

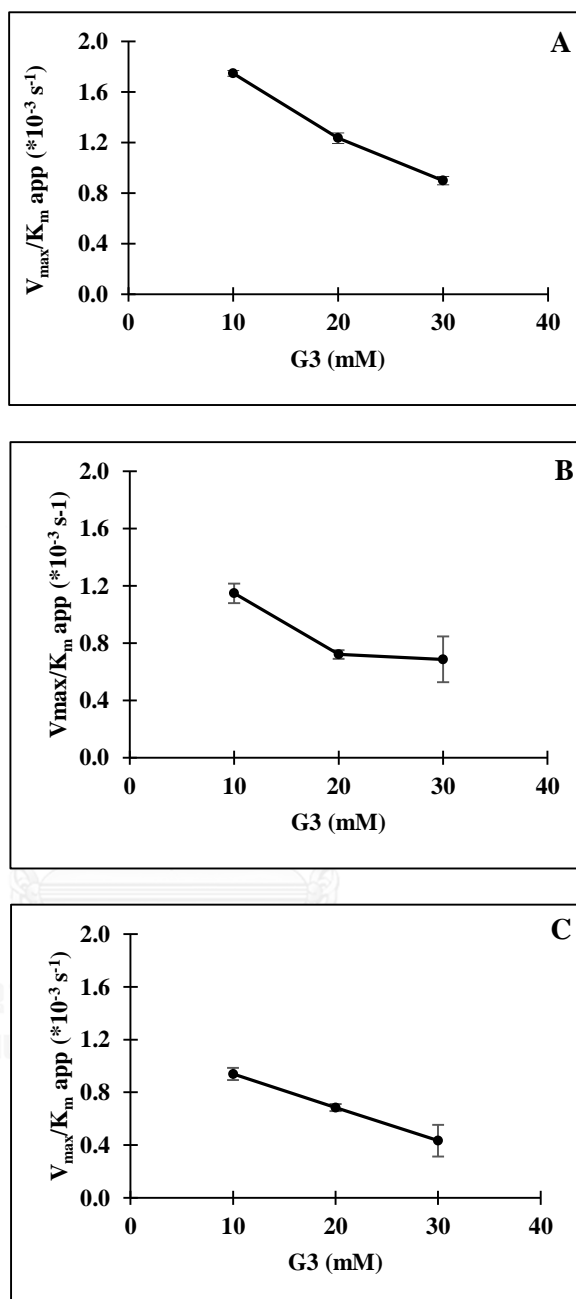


Figure 3. 30 Product inhibition of WT (A), Y418A (B) and Y418W (C) CgAMs in disproportionation reaction as determined by ITC. Error bars are derived from three independent experiments.

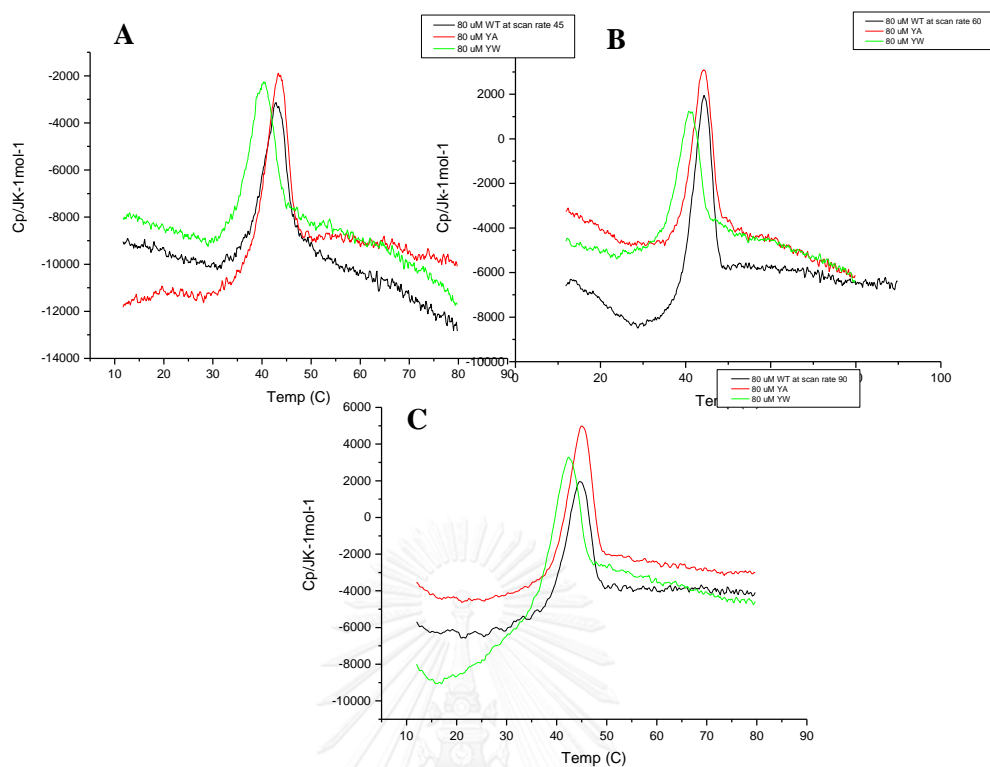


Figure 3. 31 Differential scanning calorimetry (DSC) analysis of CgAMs at a scan rate of 0.75 °C/min (A), 1.0 °C/min (B) and 1.5 °C/min (C). The black, red and green lines represent the thermograms of 80 μ M of WT, Y418A and Y418W CgAMs, respectively. Thermal profile of 50 mM phosphate buffer pH 6.0 containing 100 mM NaCl as reference was subtracted from sample profile.

Table 3. 7 Peak temperature of WT, Y418A and Y418W CgAMs at different scan rate of DSC measurements.

	<i>T_p</i> (°C)		
	Scan rate 0.75 °C/min	Scan rate 1.0 °C/min	Scan rate 1.50 °C/min
WT	42.89	44.26	44.45
Y418A	43.29	44.19	44.96
Y418W	40.45	40.57	42.29

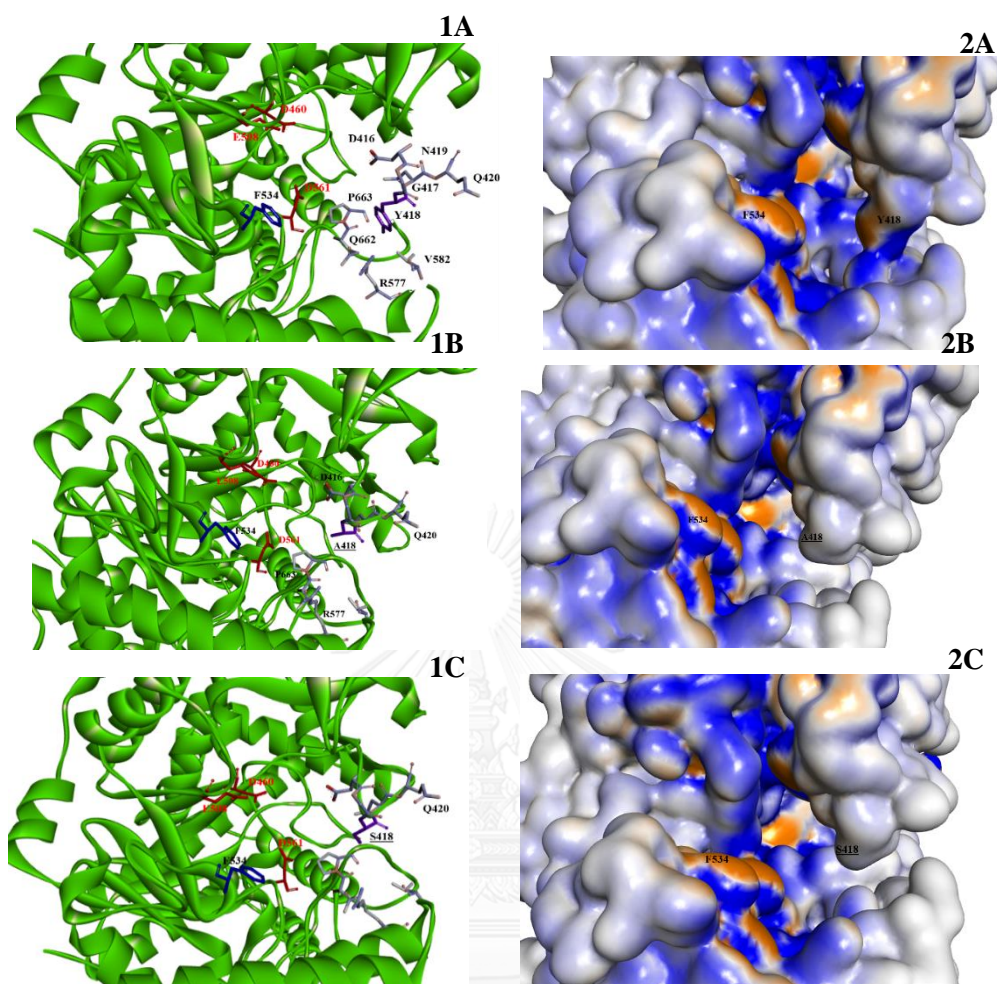


Figure 3.32 Structures of WT and Y418 mutated CgAMs. The X-ray structure of WT CgAM (PDB code 5B68) (Joo *et al.*, 2016) was used as template to prepare the model structures of Y418 mutated CgAMs. Proposed amino acid residues shown are those within 5 Å away from Y418 residues and the three catalytic residues represented in red (D460, E508, D561) of WT (1A), Y418A (1B), Y418S (1C), Y418D (1D), Y418R (1E), Y418W (1F), and Y418F (1G) CgAMs, respectively. Hydrogen bonds are shown as dashed red line. Aromatic surfaces of WT (2A), Y418A (2B), Y418S (2C), Y418D (2D), Y418R (2E), Y418W (2F), and Y418F (2G) CgAMs, respectively, are displayed with low or no hydrophobicity shown in grey, medium in blue and high in gold.

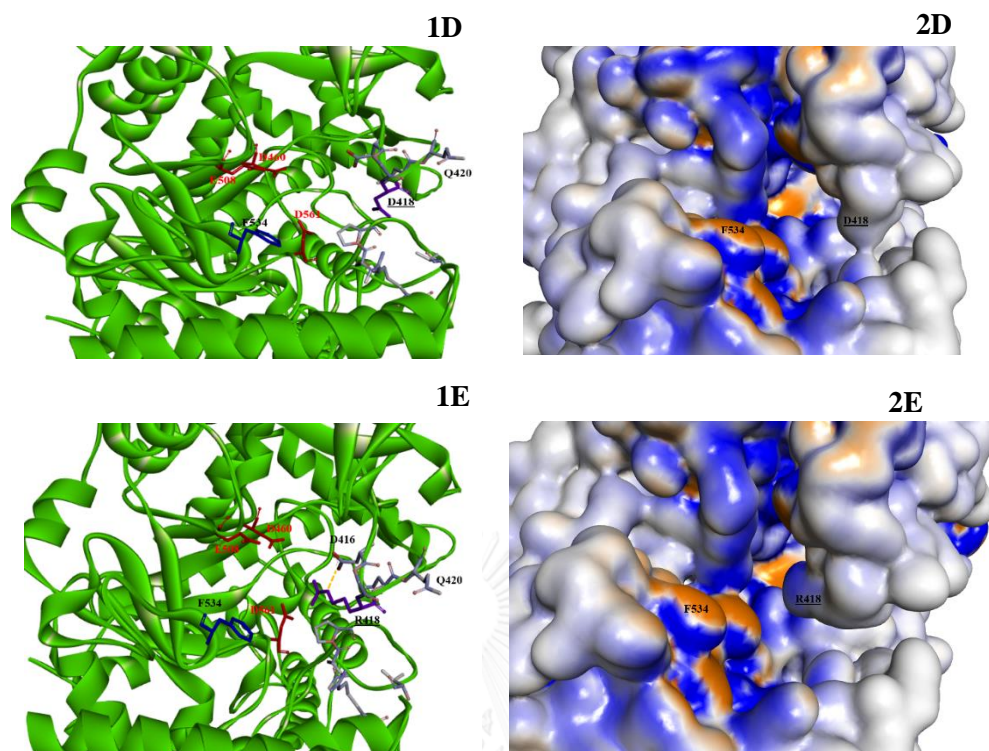


Figure 3.32 (continue) Structures of WT and Y418 mutated CgAMs. The X-ray structure of WT CgAM (PDB code 5B68) (Joo *et al.*, 2016) was used as template to prepare the model structures of Y418 mutated CgAMs. Proposed amino acid residues shown are those within 5 Å away from Y418 residues and the three catalytic residues represented in red (D460, E508, D561) of WT (1A), Y418A (1B), Y418S (1C), Y418D (1D), Y418R (1E), Y418W (1F), and Y418F (1G) CgAMs, respectively. Hydrogen bonds are shown as dashed red line. Aromatic surfaces of WT (2A), Y418A (2B), Y418S (2C), Y418D (2D), Y418R (2E), Y418W (2F), and Y418F (2G) CgAMs, respectively, are displayed with low or no hydrophobicity shown in grey, medium in blue and high in gold.

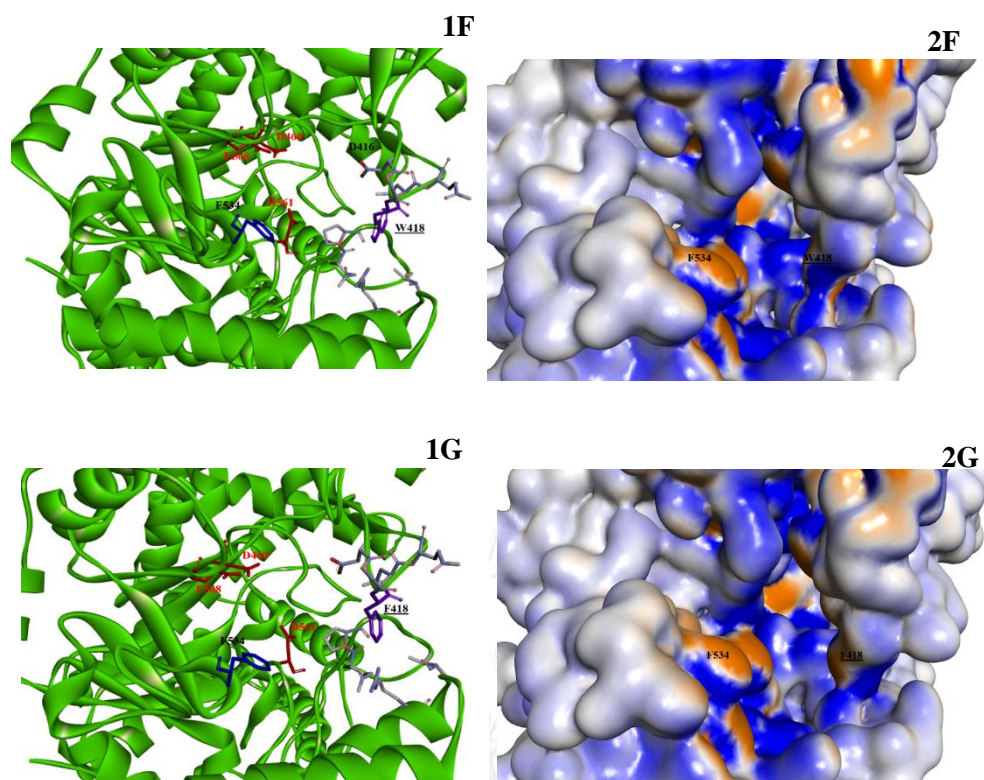


Figure 3.32 (continue) Structures of WT and Y418 mutated CgAMs. The X-ray structure of WT CgAM (PDB code 5B68) (Joo *et al.*, 2016) was used as template to prepare the model structures of Y418 mutated CgAMs. Proposed amino acid residues shown are those within 5 Å away from Y418 residues and the three catalytic residues represented in red (D460, E508, D561) of WT (1A), Y418A (1B), Y418S (1C), Y418D (1D), Y418R (1E), Y418W (1F), and Y418F (1G) CgAMs, respectively. Hydrogen bonds are shown as dashed red line. Aromatic surfaces of WT (2A), Y418A (2B), Y418S (2C), Y418D (2D), Y418R (2E), Y418W (2F), and Y418F (2G) CgAMs, respectively, are displayed with low or no hydrophobicity shown in grey, medium in blue and high in gold.

Table 3.8 Distance between amino acids at position 418 and F534 of WT and Y418 mutated CgAMs as measured by Discovery Studio 3.5 Client program.

	Distance (Å)
WT (Y418-F534)	11.2
Y418A - F534	12.2
Y418S - F534	9.7
Y418D - F534	8.4
Y418R - F534	6.7
Y418W - F534	5.6
Y418F - F534	10.8

Expression, Purification and Characterization of H461 mutated CgAMs

3.5 Expression and purification of H461 mutated CgAMs

Five H461 mutated CgAMs were expressed and purified as similar to the WT and Y418 mutated CgAMs. The protein patterns of crude and purified CgAMs on SDS-PAGE were shown in Figure 3.33. All H461 mutated CgAMs showed overexpression of the major protein band approximately at 84 kDa similar to WT enzyme, they were thus successfully purified by only one affinity His-trap column. The fractions that showed high enzyme activity were pooled and dialyzed against 20 mM phosphate buffer, pH 7.4 at 4 °C. The specific disproportionation activities of the purified H461S/D, H461R/W and H461A mutated CgAMs were significantly lower than that of the WT (for 3.4 - 6.0 and 8.0 folds, respectively) (Table 3.9). It is noticed that when compared to WT, the decrease in starch transglucosylation activity of H461 mutated CgAMs was greater than decrease in disproportionation activity. The specific starch transglucosylation activities of H461S/D, H461R/W and H461A mutated CgAMs were 5.0, 14 -23 and 44 - fold lower than that of the WT, respectively (Table 3.10).

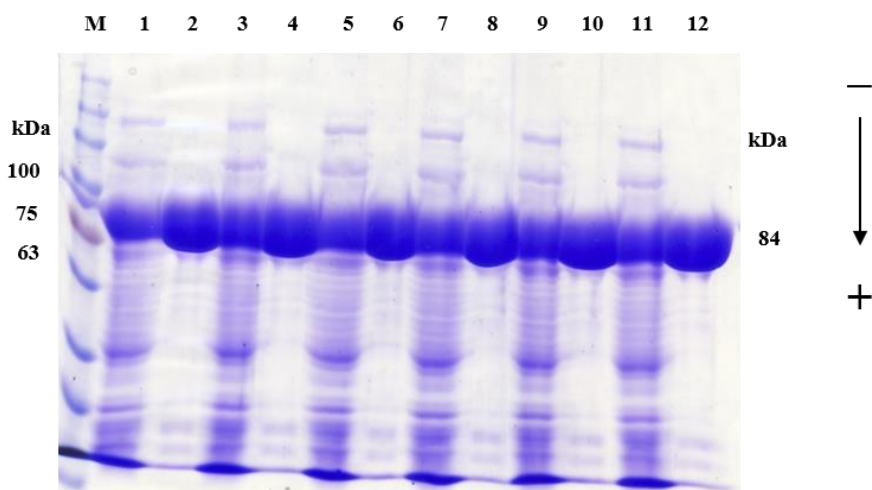


Figure 3. 33 SDS-PAGE of crude and purified enzyme expressed from cells harboring the series of H461 mutated *CgAMs*.

Lane M = Protein markers

Lane 1, 3, 5, 7, 9 and 11 = 20 μg of crude WT-, H461A-, H461S, H461D-, H461R- and H461W-*CgAMs*, respectively

Lane 2, 4, 6, 8, 10 and 12 = 10 μg of purified WT-, H461A-, H461S, H461D-, H461R- and H461W-*CgAMs*, respectively

Table 3. 9 Purification of WT and H461 mutated CgAMs assayed by starch transglucosylation activity.

CgAM	Total protein (mg)	Total activity (U)	Specific activity (U/mg)	Purification (fold)	Yield (%)
WT					
Crude	294	467	1.59	1	100
Purified	7.68	188	24.5	15.4	40.3
H461A					
Crude	257	114	0.44	1	100
Purified	7.00	3.92	0.56	1.26	3.40
H461S					
Crude	297	184	0.62	1	100
Purified	7.35	34.1	4.64	7.50	18.6
H461D					
Crude	221	227	1.03	1	100
Purified	6.65	31.3	4.66	4.53	13.7
H461R					
Crude	247	88.3	0.36	1	100
Purified	5.28	5.52	1.05	2.92	6.25
H461W					
Crude	283	121	0.43	1	100
Purified	6.30	11.4	1.81	4.22	9.41

Table 3. 10 Purification of WT and H461 mutated CgAMs assayed by disproportionation activity.

CgAM	Total protein (mg)	Total activity (U)	Specific activity (U/mg)	Purification (fold)	Yield (%)
WT					
Crude	294	1670	5.68	1	100
Purified	7.68	169	22.0	3.87	10.1
H461A					
Crude	257	231	0.90	1	100
Purified	7.00	19.5	2.80	3.10	8.44
H461S					
Crude	297	396	1.30	1	100
Purified	7.35	47.6	6.50	4.86	12.0
H461D					
Crude	221	572	2.60	1	100
Purified	6.65	43.4	6.50	2.51	7.59
H461R					
Crude	247	415	1.70	1	100
Purified	5.28	18.9	3.60	2.13	4.55
H461W					
Crude	283	455	1.60	1	100
Purified	6.30	26.2	4.20	2.59	5.76

3.6 Effect of H461 mutation on enzyme characteristics

3.6.1 Various amyloamylase activities

The effect of H461 mutation on various activities of CgAM was investigated as shown in Table 3.11. When compared to WT, transglucosylation activities of all mutated enzymes including starch transglucosylation and disproportionation activities were dramatically decreased especially for H461A (8.7 and 32 -fold lower) and H461R (9.1 and 22 -fold lower). In addition, cyclization activity of H461 mutated CgAMs could not be detected by HPAEC-PAD while hydrolysis and coupling activities were not different from that of WT CgAM.

3.6.2 Optimum conditions and stability

In this experiment, the optimum conditions for starch transglucosylation and disproportionation reactions were determined.

3.6.2.1 Effect of temperature on CgAM activity

The optimum temperatures of all H461 mutated CgAMs for starch transglucosylation and disproportionation reactions were 30 °C and 40 °C, respectively (Figure 3.34A and 3.35A). The values were the same as those of WT and Y418 mutated CgAMs. In addition, at temperature higher than 45 °C the activity of all H461 mutants was totally lost while WT-CgAM had 50% of relative activity.

3.6.2.2 Effect of pH on CgAM activity

The optimum pH of all H461 mutated CgAMs for starch transglucosylation and disproportionation reactions was the same, at pH 6.0 (Figure 3.34B and 3.35B). The value was the same as that for WT and Y418 mutated CgAMs. At pH 7.0, H461 mutants completely lost their activities while WT had maintained 90% of relative activity.

Table 3. 11 All activities of H461 mutated CgAMs

	Specific activity (U/mg)				
	Starch transglucosylation	Disprop.	Cyclization	Coupling	Hydrolysis
WT	25.9 ± 1.59	24.2 ± 1.02	0.44 ± 0.08	0.15 ± 0.01	0.03 ± 0.00
H461A	0.81 ± 0.51	2.79 ± 0.35	ND	0.02 ± 0.00	0.02 ± 0.00
H461S	5.58 ± 1.59	5.32 ± 0.49	ND	0.04 ± 0.01	0.03 ± 0.00
H461D	4.87 ± 0.46	6.55 ± 0.54	ND	0.03 ± 0.01	0.02 ± 0.00
H461R	1.18 ± 0.20	2.64 ± 0.53	ND	0.03 ± 0.01	0.02 ± 0.01
H461W	1.75 ± 0.19	3.67 ± 0.58	ND	0.03 ± 0.01	0.02 ± 0.01

Data are shown as the mean ± standard deviation and are derived from three independent experiments. ND = not detectable

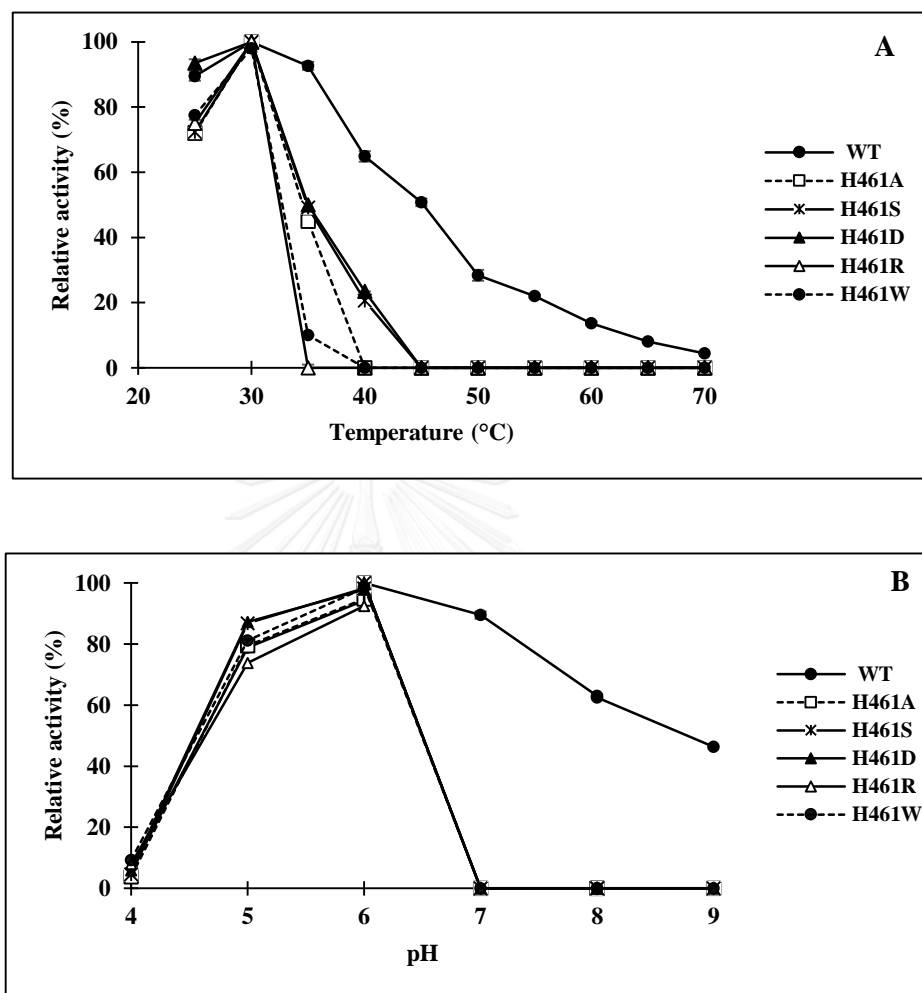


Figure 3. 34 Effect of temperature (A) and pH (B) for WT and H461 mutated CgAMs on starch transglucosylation activity. The enzymes were fixed at pH 6.0 in (A) and 30°C (B). Buffer used were: acetate buffer (pH 4.0-6.0), phosphate buffer (pH 6.0-8.0) and tris-HCl buffer (pH 8.0 -9.0). The experiments were performed as described in section 2.9.1 and 2.9.2. Data are shown as the mean \pm SD and are derived from three independent repeats.

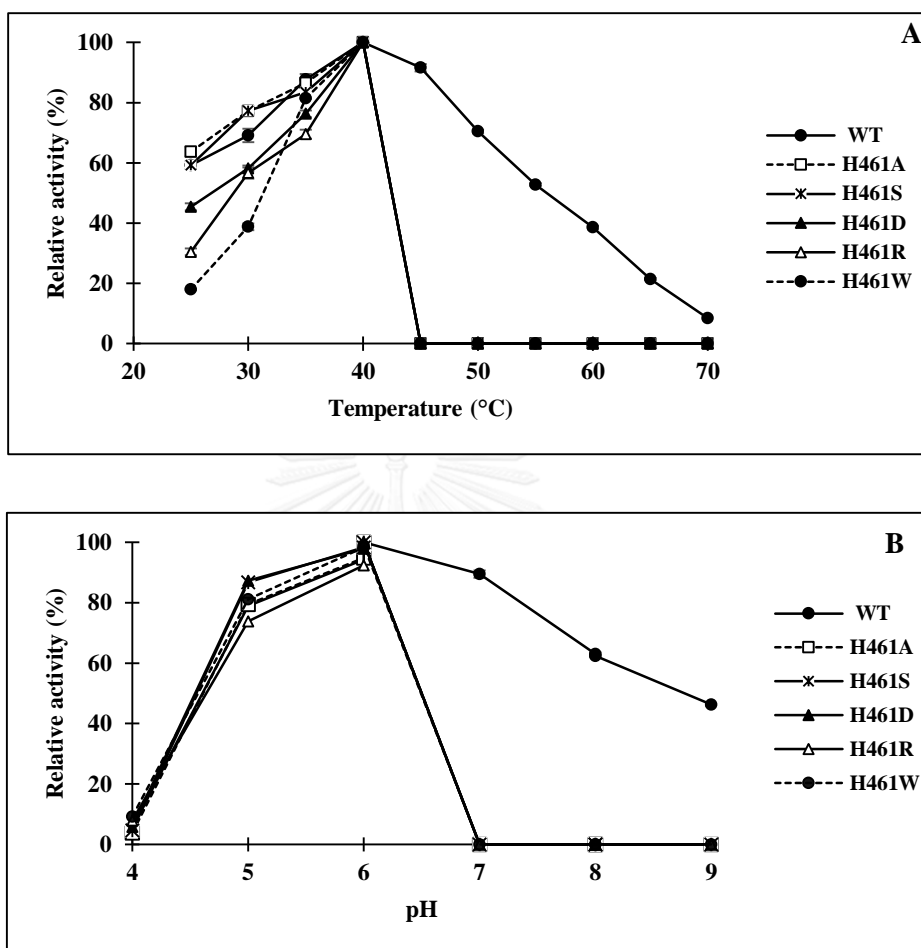


Figure 3.35 Effect of temperature (A) and pH (B) for WT and H461 mutated CgAMs on disproportionation activity. The enzymes were fixed at pH 6.0 in (A) and 40°C (B). Buffer used were: acetate buffer (pH 4.0-6.0), phosphate buffer (pH 6.0-8.0) and tris-HCl buffer (pH 8.0-9.0). The experiments were performed as described in section 2.9.1 and 2.9.2. Data are shown as the mean \pm SD and are derived from three independent repeats.

3.6.2.3 Effect of temperature on CgAM stability

The effect of H461 mutation on temperature stability was followed by determining disproportionation activity as described in 2.9.3 at different temperature (30 °C, 35 °C and 40 °C) (Figure 3.36). At 30 °C, WT enzyme maintained 90% of its activity while H461 mutants lost 50% of their activities after 45 min incubation. When the temperature stability was determined at 35 °C and 40 °C, H461 mutated CgAMs were totally lost their activities at 20 min and 10 min incubation time, respectively. At long incubation time of 180 min at 30 °C and 35 °C, 80% and 60% residual activity of WT, respectively, were observed. The results showed that all H461 mutated CgAMs were significantly less stable than WT enzyme.

3.6.2.4 Effect of pH on CgAM stability

The effect of H461 mutation on pH stability was followed by determining disproportionation activity as described in 2.9.4 at pH 7.0 and pH 8.0. The same results were found at both pHs, WT CgAM maintained 90% of its activity while all of H461 mutants totally lost their activities at 20 min incubation time (Figure 3.37). At long incubation time of 120 min at pH 7.0 and 8.0, the WT still showed 90% and 50% residual activity, respectively.

3.6.3 Substrate specificity

The substrate specificity for disproportionation reaction using malto-oligosaccharide substrate (maltose; G2 to maltoheptaose; G7) was determined. Maltotriose (G3) was the most efficient substrate while maltoheptaose (G7) was poor substrate for WT-CgAM. The substrate specific activity for WT was in order of G3>G4>G5>G6>G2>G7 (Figure 3.38). Interestingly, H461 mutants showed a different

order of G2>G3>G4>G5=G6>G7. It was shown that H461 mutants could use maltose as the best substrate.

3.6.4 Determination of kinetic parameters

Kinetic study of disproportionation reaction

The kinetic analysis of CgAMs was performed using G3, the most favorable substrate in disproportionation reaction of the WT. Figure 3.39 represented the Lineweaver-Burk plot of CgAMs. All H461 mutated CgAMs had a lower k_{cat} and k_{cat}/K_m values, the R mutant showed the lowest k_{cat}/K_m with 36-fold lower than the WT's value (Table 3.12). The mutations were severely affected on the k_{cat} , 14 to 18-fold lower than that of the WT while the K_m values were higher than the WT (18 mM) with the values around 30-37 mM.

3.6.5 Analysis of LR-CD products

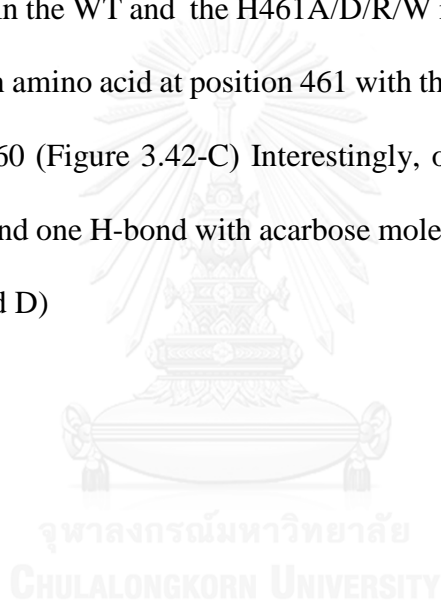
To compare the LR-CDs production profile of WT- and H461 mutated CgAMs, the enzymes were incubated with pea starch substrate as described in section 2.9.7 and LR-CD products were determined by HPAEC-PAD. It was found that all H461 mutants could not produce LR-CD products (Figure 3.40).

3.6.6 Enzyme conformation

To investigate the result of H461 mutation on enzyme conformational change, analysis of secondary structure was performed using circular dichroism (CD) spectrometer scanning from 190 to 250 nm. The CD-spectra of all mutated and the WT enzymes were compared at pH 6.0 (Figure 3.41). The result showed that the CD spectra of H461 mutated CgAMs and WT were closely overlaid, only a slight change was observed in the spectra of mutants. The contents of the secondary structure were: α -helix 26-27%, β -sheet 20-22% and random coil 51-52%.

3.7 Structural modeling of H461 mutated CgAM

The model structures of H461 mutated CgAMs were constructed by the Discovery Studio 3.5 Client program using WT CgAM X-ray structure (PDB code 5B68) (Joo *et al.*, 2016) as template (Figure 3.42). All CgAM structures were superimposed with acarbose ligand from the TaAM X-ray structure (PDB 1esw) (Przylas *et al.*, 2000a) In area of active site, twelve residues including Y23, G412, W425, D460, V462, L463, G464, L465, R467, L468 and E508 are within 5 Å away from H461 position. In the WT and the H461A/D/R/W mutants, no hydrogen bonding was observed between amino acid at position 461 with these residues, but S mutant had one H-bond with D460 (Figure 3.42-C) Interestingly, only WT and H461D mutated CgAMs formed two and one H-bond with acarbose molecule at subsite +1 of the active site (Figure 3.42A and D)



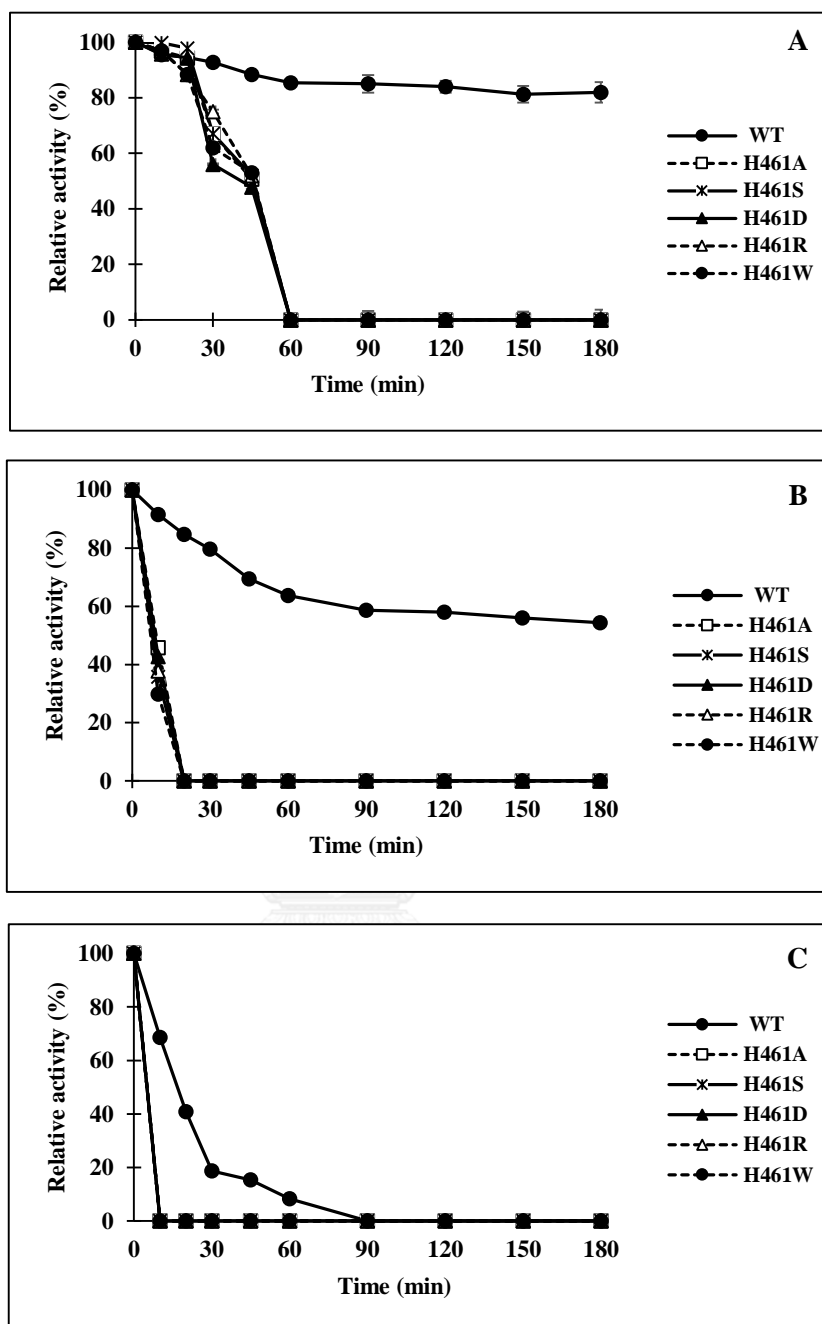


Figure 3.36 Effect of temperature on CgAM stability. WT and H461 mutated CgAMs were incubated in phosphate buffer pH 6.0 at 30 °C (A), 35 °C (B), 40 °C (C) for 0 to 180 min. Disproportionation activity was assayed as described in 2.9.3. Data are shown as the mean \pm SD and are derived from three independent experiments.

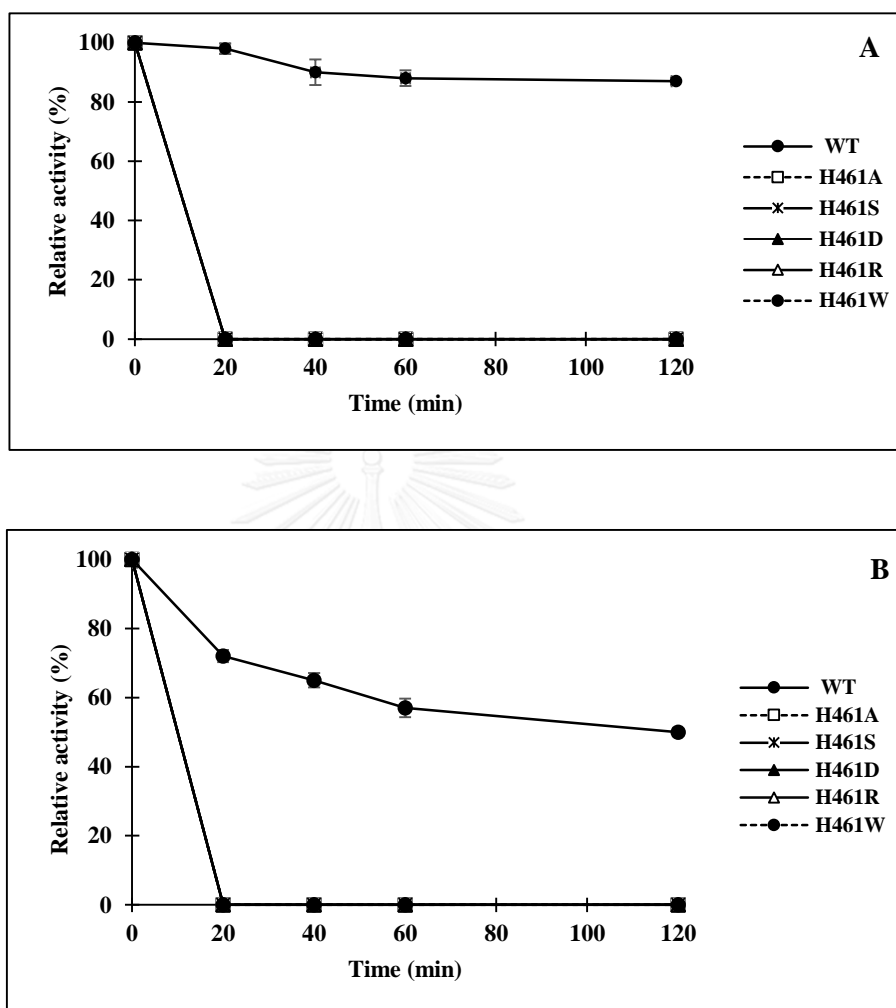


Figure 3.37 Effect of pH on CgAM stability. WT and H461 mutated CgAMs were incubated at 30°C in phosphate buffer pH 7.0 (A) and tris-HCl buffer pH 8.0 (B) for 0-120 min. Disproportionation activity was assayed as described in 2.9.4. Data are shown as the mean \pm SD and are derived from three independent experiments.

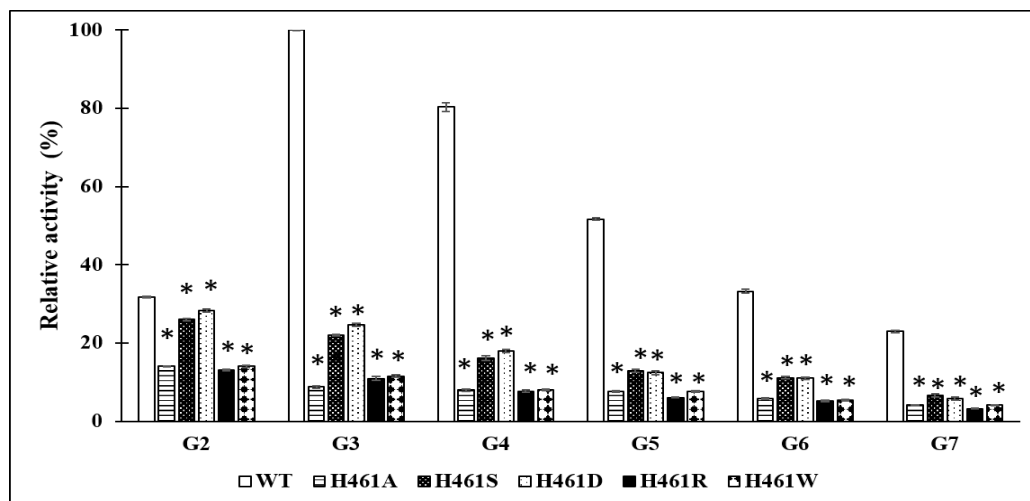


Figure 3. 38 Substrate specificity of WT and H461 mutated CgAMs in disproportionation reaction using malto-oligosaccharides (maltose, G2 to maltoheptaose, G7) as substrate. The activity of WT-CgAM on G3 substrate was set as 100%. *P < 0.05 (Student's t-Test) with respect to the disproportionation reaction of WT-CgAM. Data are presented as the mean \pm SD and are derived from three independent experiments.

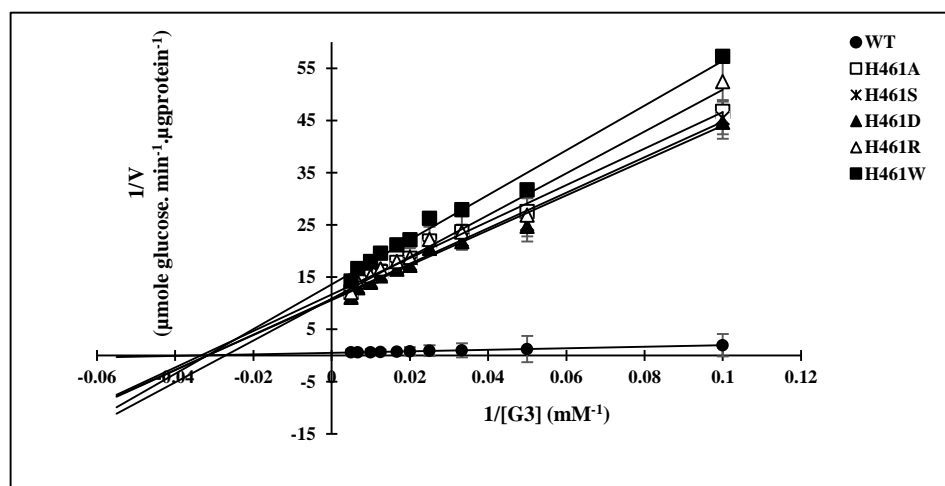


Figure 3. 39 Lineweaver-Burk plot of WT and H461 mutated *CgAMs* - catalyzed disproportionation reaction. All *CgAMs* were incubated with various concentrations of maltotriose (G3) in 50 mM phosphate buffer, pH 6.0 at 40 °C for 5 min. Glucose oxidase method was used to determine the amount of free glucose produced during the reaction.

Table 3. 12 Kinetic parameters of WT and H461 mutated *CgAMs* derived from the disproportionation reaction using maltotriose as the substrate.

<i>CgAM</i>	K_m (mM)	V_{max} ($\mu\text{mole glucose}\cdot\text{min}^{-1}\cdot\mu\text{gprotein}^{-1}$)	k_{cat} (min^{-1}) [10^3]	k_{cat}/K_m ($\text{mM}^{-1}\text{min}^{-1}$) [10^3]
WT	18.2 ± 1.34	1.98 ± 0.28	157 ± 4.56	8.63 ± 3.45
H461A	29.7 ± 2.45	0.08 ± 0.03	10.2 ± 1.05	0.34 ± 0.25
H461S	31.5 ± 3.26	0.09 ± 0.05	11.0 ± 2.11	0.35 ± 0.31
H461D	32.4 ± 4.55	0.09 ± 0.07	11.2 ± 2.04	0.35 ± 0.18
H461R	36.8 ± 3.27	0.08 ± 0.07	8.94 ± 1.86	0.24 ± 0.17
H461W	33.4 ± 1.28	0.09 ± 0.04	9.32 ± 1.21	0.28 ± 0.19

Data are shown as the mean \pm standard deviation and are derived from three independent experiments.

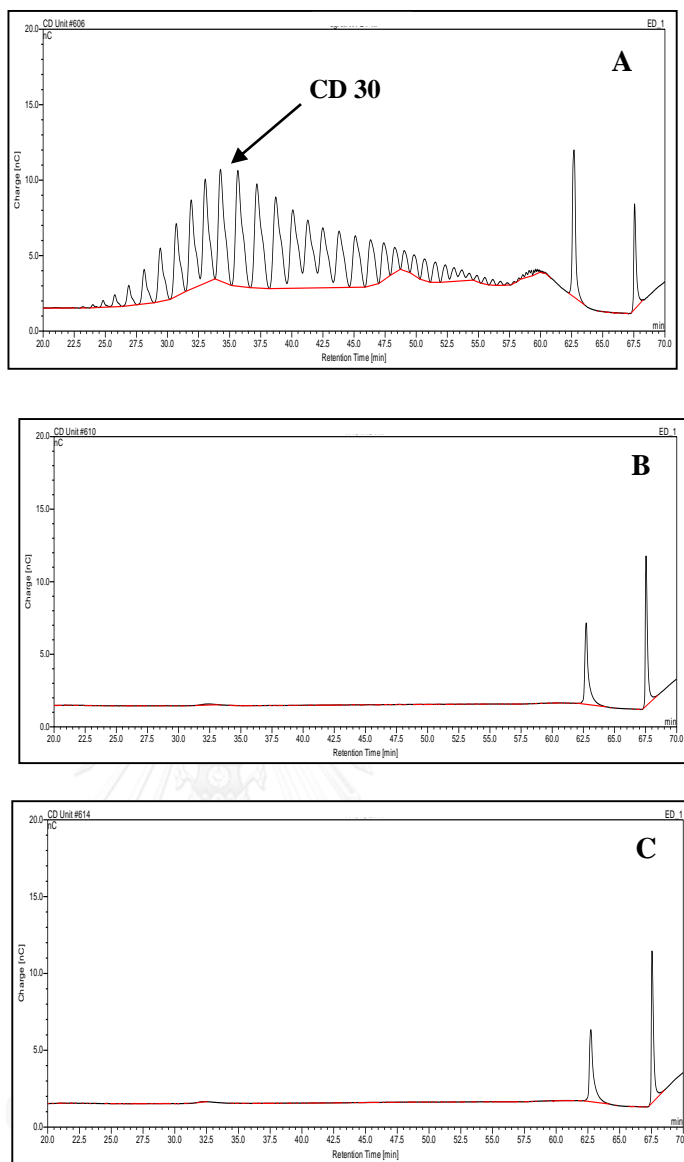


Figure 3. 40 HPAEC-PAD analysis of the LR-CD products synthesized by using 0.2% pea starch incubated with 0.4 mg protein of enzyme at 30 °C, phosphate buffer pH 6.0 for 90 min. The LR-CD products from WT (A), H461A (B), H461S (C), H461D (D), H461R (E) and H461W (F) mutated CgAMs, the arrow indicated LR-CD at DP 30.

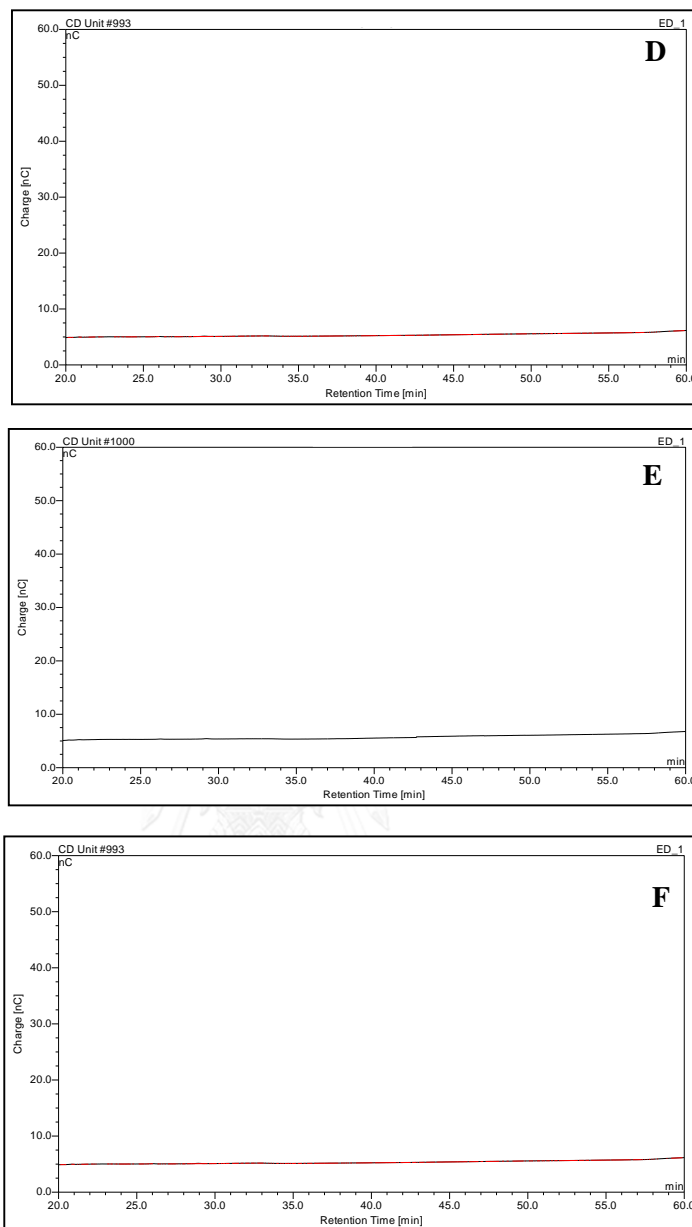


Figure 3.40 (continue) HPAEC-PAD analysis of the LR-CD products synthesized by using 0.2% pea starch incubated with 0.3 mg protein of enzyme at 30 °C, phosphate buffer pH 6.0 for 90 min. The LR-CD products from WT (A), H461A (B), H461S (C), H461D (D), H461R (E) and H461W (F) mutated CgAMs, the arrow indicated LR-CD at DP 30.

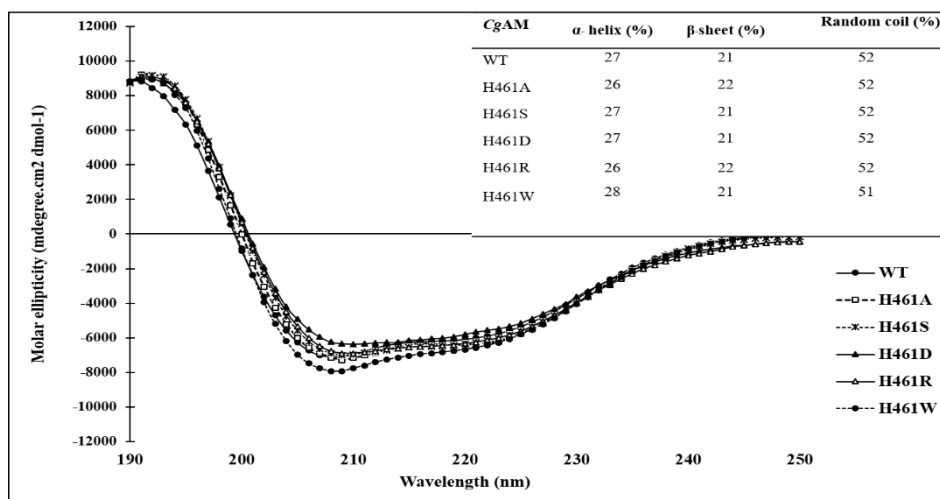


Figure 3. 41 Circular dichroism spectra and the predicted secondary structural compositions of WT and H461 mutated CgAMs.

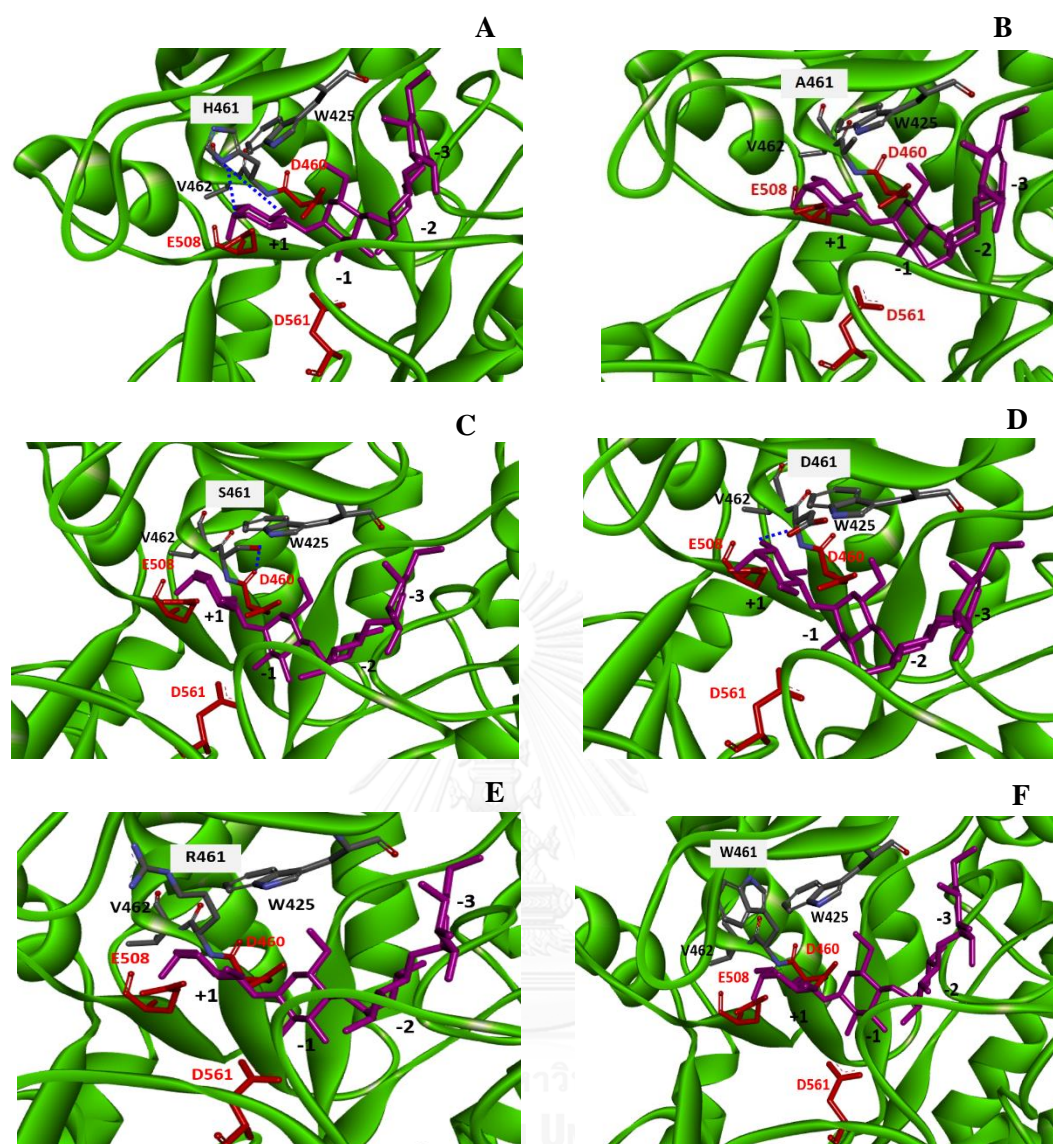


Figure 3.42 Structures of WT and H461 mutated *CgAMs* with acarbose (in purple). The X-ray structure of WT *CgAM* (PDB code 5B68) (Joo *et al.*, 2016) was used as template to prepare the model structures of H461 mutated *CgAMs*. All *CgAM* structures were superposed with acarbose ligand bound at active site of the X-ray structure of *T. aquaticus* amyloamylase (PDB 1esw) (Przylas *et al.*, 2000a) Proposed amino acid residues shown are those within 5 Å away from H461 residues of WT (A), H461A (B), H461S (C), H461D (D), H461R (E) and H461W (F) *CgAMs*, respectively. The three catalytic residues (D460, E508, D561) are represented in red. Hydrogen bonds are shown as dashed blue line.

Expression, Purification and Characterization of N287 mutated CgAMs

3.8 Expression and purification of N287 mutated CgAMs

Overexpression of the major protein band approximately at 84 kDa similar to WT was observed for all five N287 mutated CgAMs (Figure 3.43). The mutated enzymes were thus successfully purified by His-trap column chromatography. The fractions that showed high enzyme activity were pooled and dialyzed as described for Y418 and H461 mutated CgAMs. The specific starch transglucosylation activities of the purified N287S/D/W and N287A/R mutated CgAMs were 4.3-9.0 fold and 14-33 fold lower than that of WT, respectively (Table 3.13). In addition, specific disproportionation activity of all mutated CgAMs was less affected than starch transglucosylation activity, N287S/D/W and N287A/R mutants were 3.0-5.0 fold and 8.0-11 fold lower than WT, respectively (Table 3.14). Interestingly, N287W mutant showed highest specific activity in both reactions than other mutated CgAMs.

3.9 Effect of N287 mutation on enzyme characteristics

3.9.1 Various amyloamylase activities

The effect of N287 mutation on various activities of CgAM was determined, transglucosylation activities of the mutated enzymes including starch transglucosylation and disproportionation were significantly decreased compare to WT enzyme. N287A and R mutants had lowest specific activities of 0.81 and 1.47 U/mg protein for starch transglucosylation activity which was 33 and 19 - fold lower than WT, respectively (Table 3.15). In addition, cyclization activities of all N287 mutated CgAMs were 5.4 to 22 - fold lower than WT, the R mutant showed the lowest specific

activity. Coupling activity was also decreased while hydrolysis activity was not change (Table 3.15).

3.9.2 Optimum conditions and stability

The optimum conditions for disproportionation and cyclization reactions of CgAMs were determined.

3.9.2.1 Effect of temperature on CgAM activity

The optimum temperatures of all N287 mutated CgAMs for disproportionation and cyclization reactions were 40 °C and 30 °C, respectively (Figure 3.44A and 3.45A). The values were the same as those of WT, Y418 and H461 mutated CgAMs. In addition, at temperature higher than 45 °C, the activities of all N287 mutants were completely lost while WT-CgAM still showed 50% of relative activity.

3.9.2.2 Effect of pH on CgAM activity

The optimum pH of all N287 mutated CgAMs for disproportionation and cyclization reactions was the same, at pH 6.0 (Figure 3.44B and 3.45B). The values was the same as those results of WT, Y418 and H461 mutated CgAMs. At pH 7.0, N287R mutant completely lost its activity while N287A/D/S/W lost their activities at pH 8.0. Interestingly, the WT still maintained 40% of relative activity even at pH 9.0.

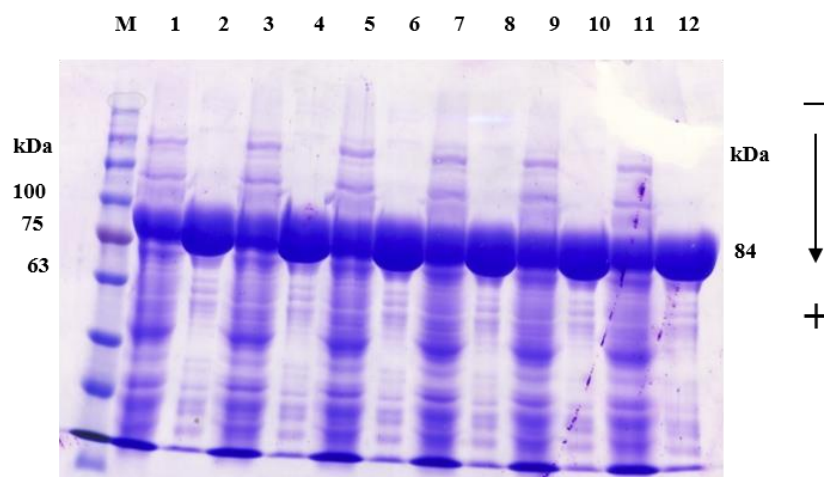


Figure 3. 43 SDS-PAGE of crude and purified enzyme expressed from cells harboring the series of N287 mutated CgAMs.

Lane M = Protein markers

Lane 1, 3, 5, 7, 9 and 11 = 20 μ g of crude WT-, N287A-, N287S, N287D-, N287R- and N287W-CgAMs, respectively

Lane 2, 4, 6, 8, 10 and 12 = 10 μ g of purified WT-, N287A-, N287S, N287D-, N287R- and N287W-CgAMs, respectively

Table 3. 13 Purification of WT and N287 mutated CgAMs assayed by starch transglucosylation activity.

CgAM	Total protein (mg)	Total activity (U)	Specific activity (U/mg)	Purification (fold)	Yield (%)
WT					
Crude	295	453	1.54	1	100
Purified	7.86	186	23.6	15.4	41.1
N287A					
Crude	245	123	0.50	1	100
Purified	6.88	4.98	0.72	1.44	4.05
N287S					
Crude	276	176	0.64	1	100
Purified	7.14	29.7	4.16	6.52	16.9
N287D					
Crude	258	217	0.84	1	100
Purified	7.23	18.9	2.61	3.11	8.70
N287R					
Crude	278	114	0.41	1	100
Purified	6.97	12.1	1.74	4.23	10.6
N287W					
Crude	281	185	0.66	1	100
Purified	7.12	36.7	5.15	7.83	19.8

Table 3. 14 Purification of WT and N287 mutated CgAMs assayed by disproportionation activity.

CgAM	Total protein (mg)	Total activity (U)	Specific activity (U/mg)	Purification (fold)	Yield (%)
WT					
Crude	295	1748	5.93	1	100
Purified	7.86	223	28.4	4.8	12.8
N287A					
Crude	245	248	1.01	1	100
Purified	6.88	25.8	3.75	3.70	10.4
N287S					
Crude	276	374	1.36	1	100
Purified	7.14	40.3	5.64	4.17	10.8
N287D					
Crude	258	621	2.41	1	100
Purified	7.23	68.4	9.46	3.93	11.0
N287R					
Crude	278	401	1.44	1	100
Purified	6.97	17.5	2.51	1.74	4.4
N287W					
Crude	281	672	2.39	1	100
Purified	7.12	70.3	9.87	4.13	10.5

Table 3. 15 All activities of N287 mutated CgAMs

	Specific activity (U/mg)				
	Starch transglucosylation	Disprop.	Cyclization	Coupling	Hydrolysis
WT	26.8 ± 1.52	26.1 ± 2.82	0.43 ± 0.09	0.10 ± 0.04	0.03 ± 0.00
N287A	0.81 ± 0.51	3.51 ± 0.63	0.07 ± 0.03	0.02 ± 0.01	0.02 ± 0.01
N287S	3.04 ± 0.44	5.66 ± 0.54	0.04 ± 0.02	0.04 ± 0.01	0.03 ± 0.00
N287D	2.7 ± 0.64	9.97 ± 1.27	0.10 ± 0.03	0.13 ± 0.01	0.03 ± 0.01
N287R	1.47 ± 0.16	2.92 ± 0.29	0.02 ± 0.03	0.03 ± 0.01	0.02 ± 0.01
N287W	4.87 ± 0.46	8.95 ± 0.2	0.09 ± 0.04	0.03 ± 0.01	0.02 ± 0.00

Data are shown as the mean ± standard deviation and are derived from three independent experiments.



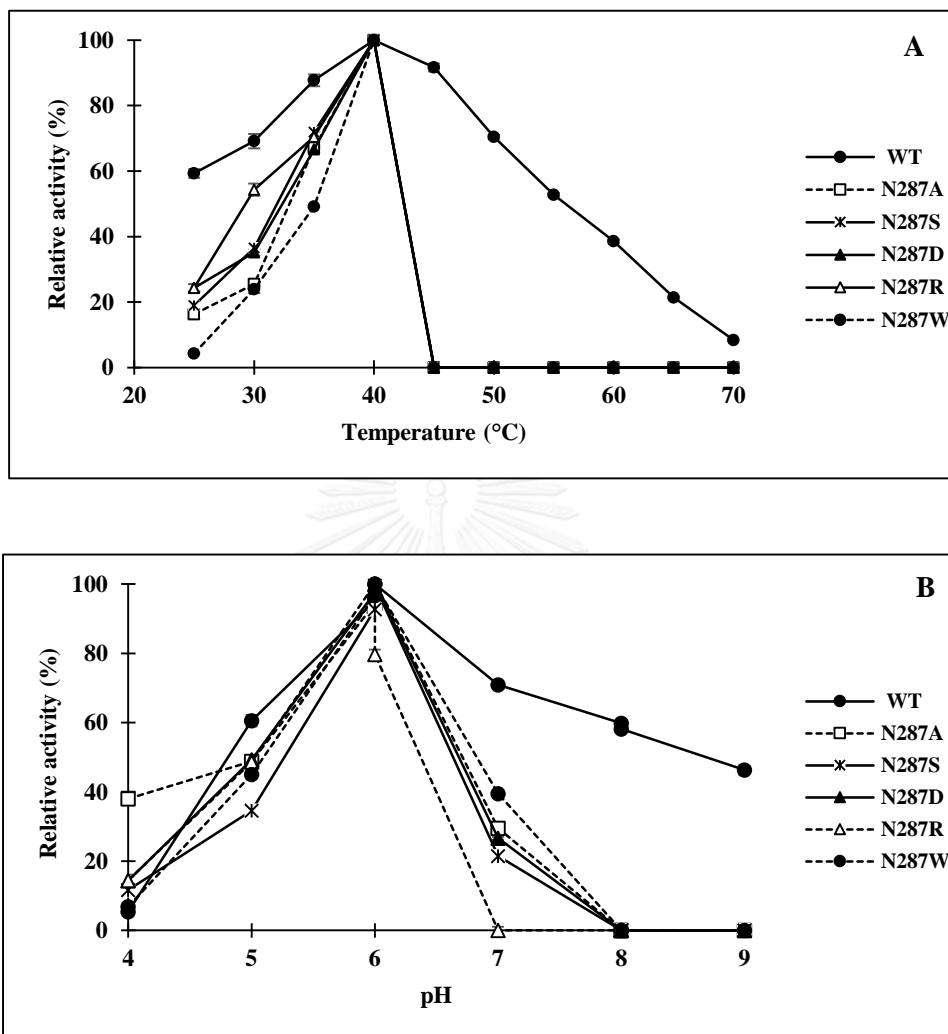


Figure 3.44 Effect of temperature (A) and pH (B) for WT and N287 mutated CgAMs on disproportionation activity. The enzymes were fixed at pH 6.0 in (A) and 30°C (B). Buffer used were: acetate buffer (pH 4.0-6.0), phosphate buffer (pH 6.0-8.0) and tris-HCl buffer (pH 8.0-9.0). The experiments were performed as described in section 2.9.1 and 2.9.2. Data are shown as the mean \pm SD and are derived from three independent repeats.

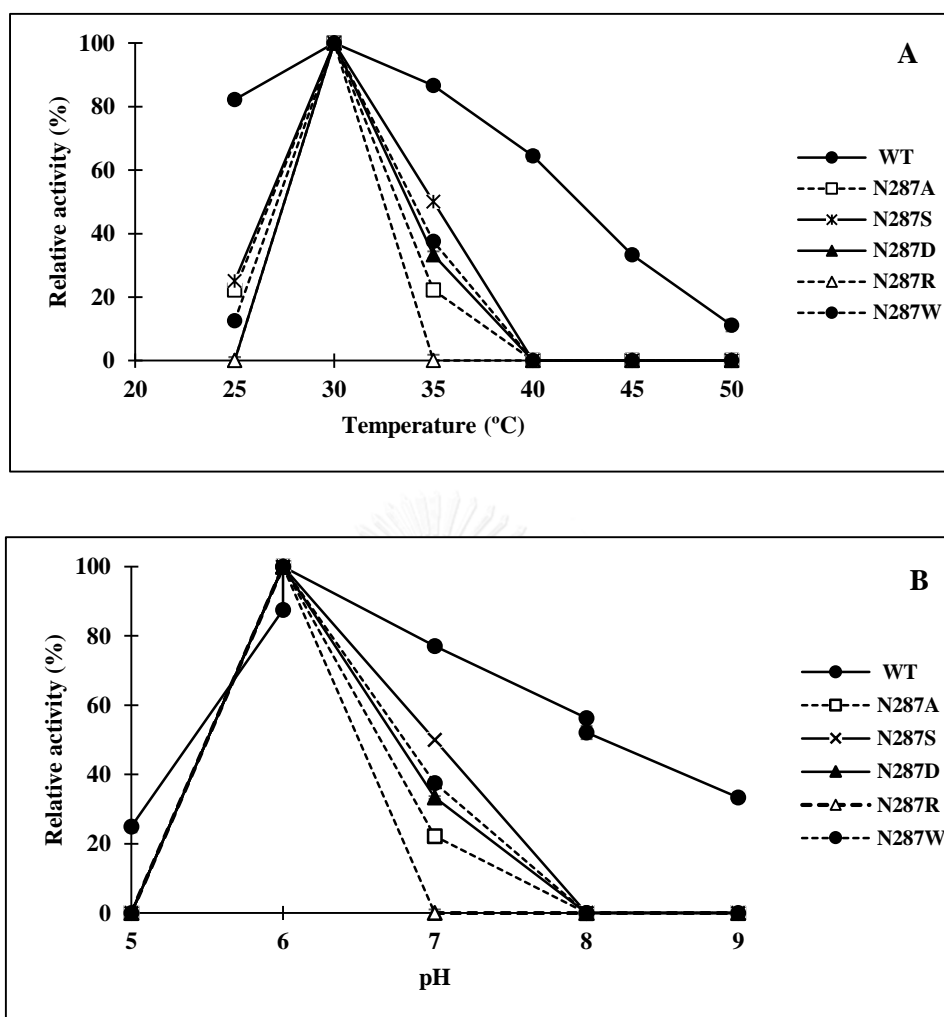


Figure 3.45 Effect of temperature (A) and pH (B) for WT and N287 mutated CgAMs on cyclization activity. The enzymes were fixed at pH 6.0 in (A) and 30°C (B). Buffer used were: acetate buffer (pH 4.0-6.0), phosphate buffer (pH 6.0-8.0) and tris-HCl buffer (pH 8.0-9.0). The experiments were performed as described in section 2.9.1 and 2.9.2. WT and N287 mutated CgAMs were incubated with 2% (w/v) of pea starch for 90 min at various temperatures and pHs. LR-CD products were analyzed by HPAEC-PAD. Data are shown as the mean \pm SD and are derived from three independent repeats.

3.9.2.3 Effect of temperature on CgAM stability

For the effect of N287 mutation on temperature stability, disproportionation activity was determined as described in 2.9.3 at different temperature (30 °C, 35 °C and 40 °C) (Figure 3.46). At 30 °C, WT enzyme maintained 90% of its activity while all N287mutants showed 50% of their activities at 45 min incubation. All mutated enzymes lost their activities at 90 min while 90% activity of WT still remained up to 180 min (Figure 3.46A). When the temperature stability was determined at 35 °C, WT enzyme maintained 60% of activity at 180 min while N287 mutants lost 50% of their activities at early incubation time of 20 min. At 40 °C, activities of WT and N287 mutated CgAMs were totally lost at 90 min and 10 min, respectively. The results showed that N287 mutated CgAMs were significantly less stable than WT enzyme.

3.9.2.4 Effect of pH on CgAM stability

The effect of N287 mutation on pH stability was followed by determining disproportionation activity as described in 2.9.4 at pH 7.0 and pH 8.0. Similar results were found at both pHs, at long incubation time of 120 min, WT CgAM maintained 80% and 50% of its activity at pH 7.0 and 8.0, respectively (Figure 3.47). N287W mutant was more stable than other mutants at 20 min, however, activities of all N287 mutants were totally lost at 40 min incubation time (Figure 3.47).

3.9.3 Substrate specificity

The substrate specificity for disproportionation reaction using malto-oligosaccharide substrate (maltose; G2 to maltoheptaose; G7) was determined (Figure 3.48). Maltotriose (G3) was the most efficient substrate while maltoheptaose (G7) was poor substrate for both WT and N287 mutated CgAMs. The substrate specific activities

of all enzymes were in the order of G3>G4>G5>G6>G2>G7. The result suggested that N287 residue is not involved in substrate specificity.

3.9.4 Determination of kinetic parameters

3.9.4.1 Kinetic study of disproportionation reaction

The kinetic analysis of CgAMs was performed using G3, the most favorable substrate in disproportionation reaction. Figure 3.49 represented the Lineweaver-Burk plot of CgAMs. All mutated N287 CgAMs had a lower k_{cat} and k_{cat}/K_m values, the R mutants showed the lowest k_{cat}/K_m with 19-fold lower than the WT's value (Table 3.16). The mutation affected more on the k_{cat} , 4.7 to 10 -fold lower than that of the WT while the K_m values were (30-37 mM) higher than WT's value (20 mM).

3.9.4.2 Kinetic study of cyclization reaction

Y418A and Y418W were selected for kinetic study of cyclization reaction compared to WT enzyme as described in section 2.9.6.1. Figure 3.50 represented the Lineweaver-Burk plot of CgAMs. All kinetic parameters were calculated and shown in Table 3.17. The K_m values of N287A and N287W CgAMs were 31.0 and 29.1 mg/ml which were higher than that of WT (19.9 mM), indicating lower affinity towards pea starch which is a substrate. The k_{cat}/K_m of N287A and N287W CgAMs were approximately 2.8-7.8 fold lower than WT's value. Interestingly, N287W showed 2.8 - fold higher catalytic efficiency than N287A.

3.9.5 Analysis of LR - CD products

CgAMs were incubated with 2% (w/v) pea starch at 30 °C and pH 6.0, the optimum condition of the enzyme. LR-CD mixtures in the reaction were analyzed by HPAEC-PAD as described in section 2.9.7

3.9.5.1 Effect of incubation time

Effect of incubation time on LR-CDs production was carried out as described in section 2.9.7.1. To compare the LR-CDs production patterns of WT and N287 mutated CgAMs, 0.10 U starch degradation activity of CgAM was used and incubation time was varied (1.5, 6, 12 and 24 h). It was clearly found that the LR-CD yields of WT and N287 mutated CgAMs were significantly increased at long incubation time (Figure 3.51). Interestingly, N287 mutated CgAMs showed CD28-CD33 as main CD products while CD32-CD34 were principle products of WT at 24 h. In addition, the amounts of LR-CDs produced by all N287 mutants were significant lower than that of the WT at every incubation time.

3.9.5.2 Effect of unit enzyme

To observe the influence of enzyme concentration on LR-CDs formation, 0.05 U, 0.1 U and 0.2 U starch degradation activities of enzymes were used. The result showed that the increase in enzyme units gave rise to the increase in LR-CD yields. At 6 h, N287 mutated CgAMs showed a shift of the principle CD products to smaller size (CD26-CD29). The yield of CD32 (the maximum product of WT) at 0.2 U enzyme was 2 to 3 - fold increased when compared with using 0.05 U of the same enzyme Figure 3.52.

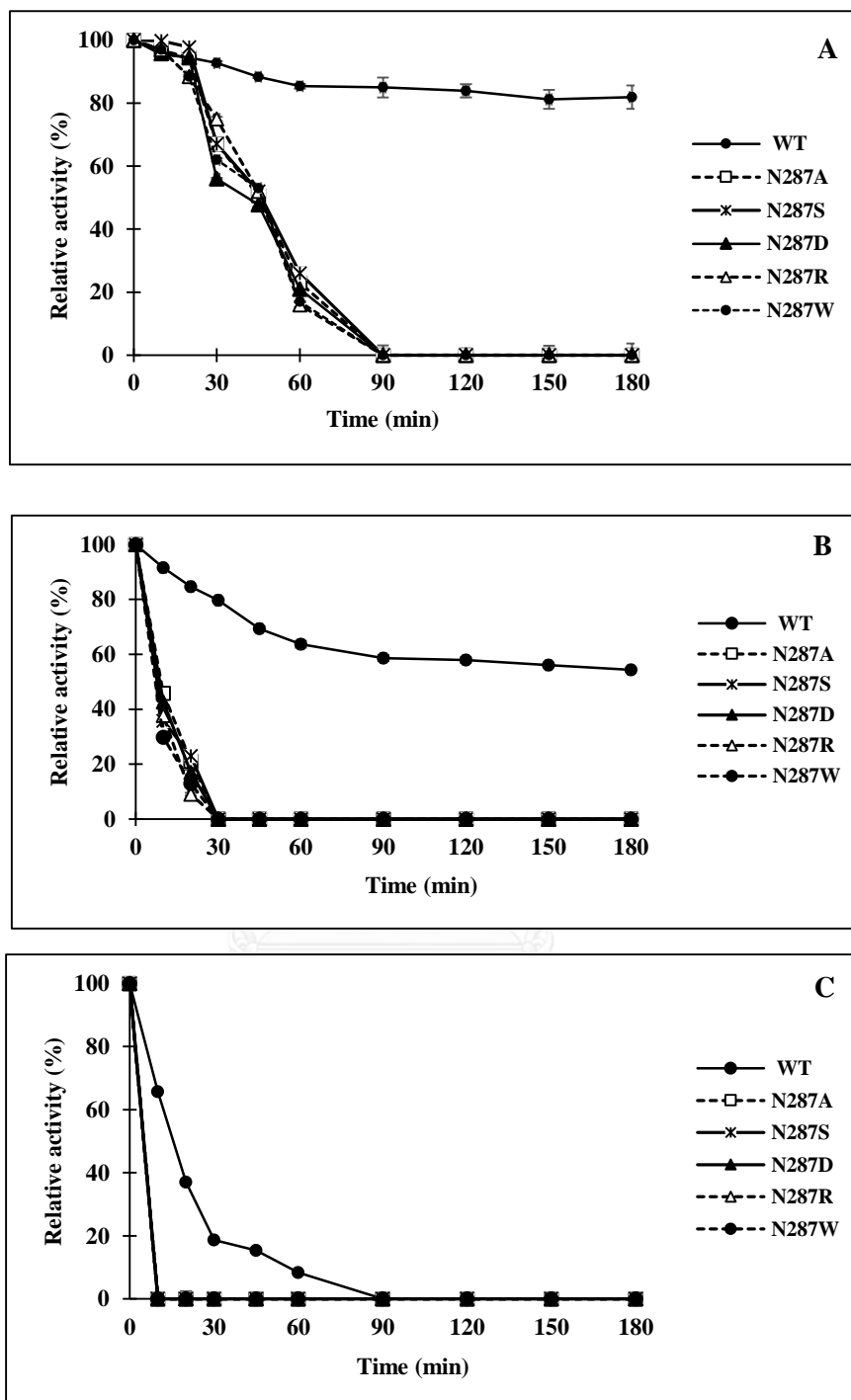


Figure 3.46 Effect of temperature on CgAM stability. WT and N287 mutated CgAMs were incubated in phosphate buffer pH 6.0 at 30 °C (A), 35 °C (B), 40 °C (C) for 0 to 180 min. Disproportionation activity was assayed as described in 2.9.3. Data are shown as the mean \pm SD and are derived from three independent experiments.

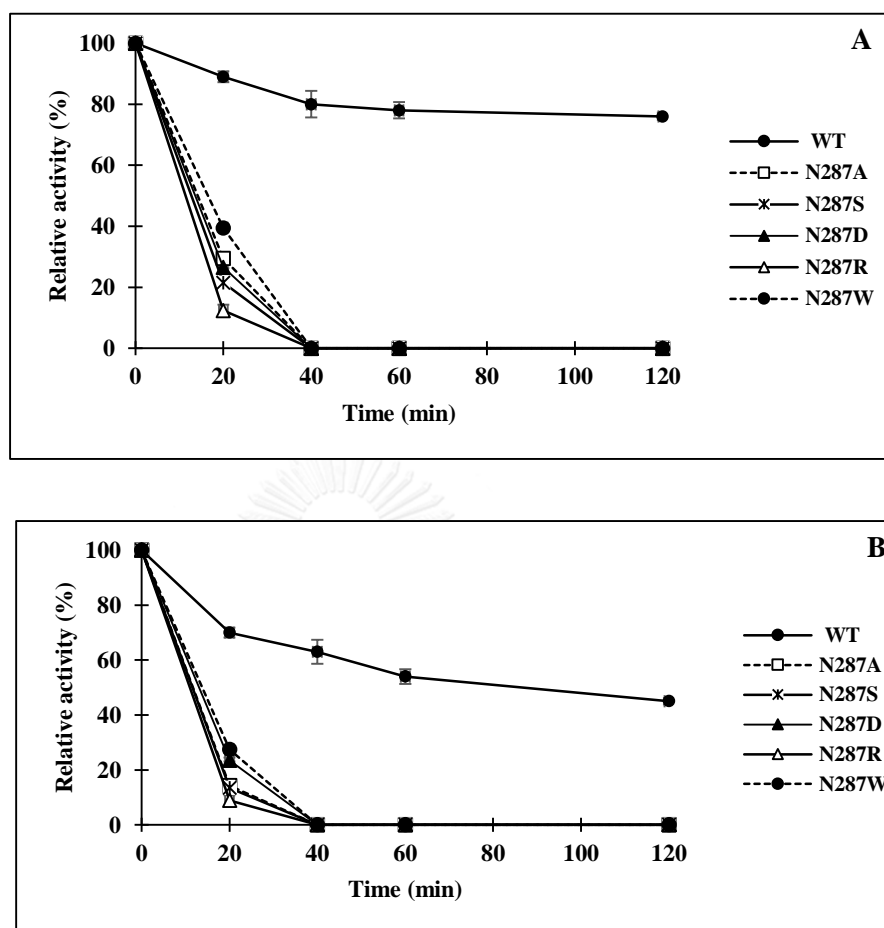


Figure 3. 47 Effect of pH on CgAM stability. WT and N287 mutated CgAMs were incubated at 30 °C in phosphate buffer pH 7.0 (A) and tris - HCl buffer pH 8.0 (B) for 0-120 min. Disproportionation activity was assayed as described in 2.9.4. Data are shown as the mean \pm SD and are derived from three independent experiments.

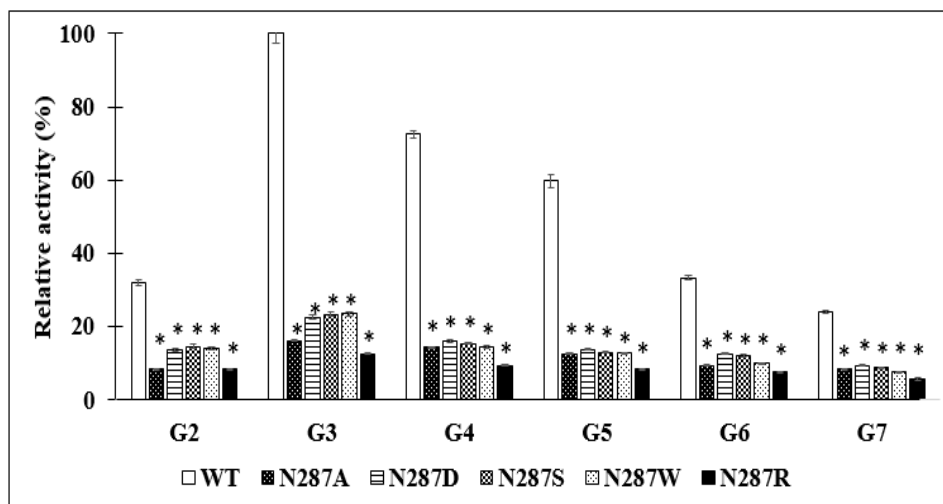


Figure 3. 48 Substrate specificity of WT and N287 mutated *CgAMs* in disproportionation reaction using malto-oligosaccharides (maltose, G2 to maltoheptaose, G7) as substrate. The activity of WT-*CgAM* on G3 substrate was set as 100%. * $P < 0.05$ (Student's *t*-Test) with respect to the disproportionation reaction of WT-*CgAM*. Data are presented as the mean \pm SD and are derived from three independent experiments.

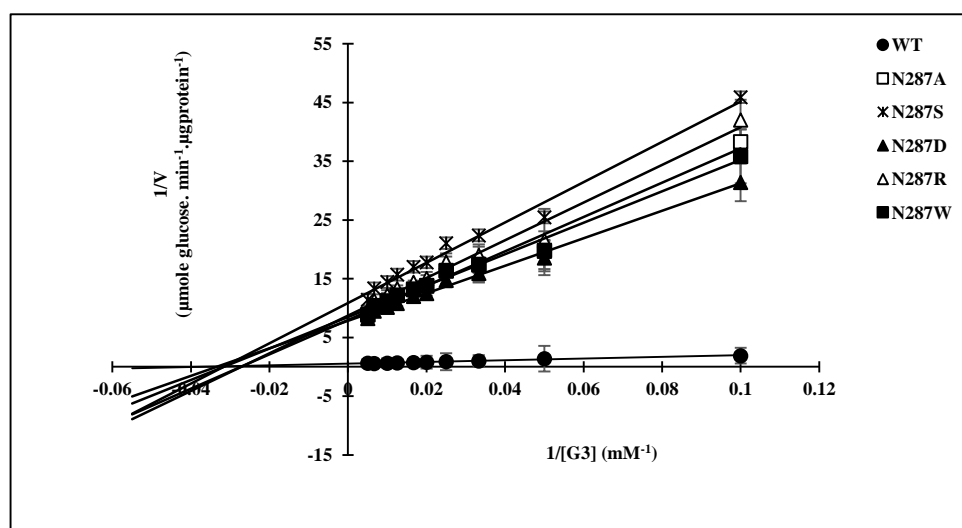


Figure 3. 49 Lineweaver-Burk plot of WT and N287 mutated *CgAMs* - catalyzed disproportionation reaction. All *CgAMs* were incubated with various concentrations of maltotriose (G3) in 50 mM phosphate buffer, pH 6.0 at 40 °C for 5 min. Glucose oxidase method was used to determine the amount of free glucose produced during the reaction.

Table 3. 16 Kinetic parameters of WT and N287 mutated *CgAMs* derived from the disproportionation reaction using maltotriose as the substrate.

<i>CgAM</i>	K_m (mM)	V_{max} ($\mu\text{mole glucose} \cdot \text{min}^{-1} \cdot \mu\text{gprotein}^{-1}$)	k_{cat} (min^{-1}) [10^3]	k_{cat}/K_m ($\text{mM}^{-1} \cdot \text{min}^{-1}$) [10^3]
WT	19.7 ± 1.52	2.05 ± 0.58	182 ± 5.38	9.23 ± 2.76
N287A	35.8 ± 3.21	0.06 ± 0.17	32.7 ± 2.44	0.91 ± 0.31
N287S	35.4 ± 3.52	0.09 ± 0.01	19.3 ± 3.16	0.54 ± 0.23
N287D	29.8 ± 5.21	0.13 ± 0.16	38.5 ± 4.18	1.29 ± 0.21
N287R	37.0 ± 5.77	0.06 ± 0.08	18.2 ± 2.75	0.49 ± 0.27
N287W	32.5 ± 4.27	0.12 ± 0.21	28.5 ± 2.13	0.88 ± 0.12

Data are shown as the mean \pm standard deviation and are derived from three independent experiments.

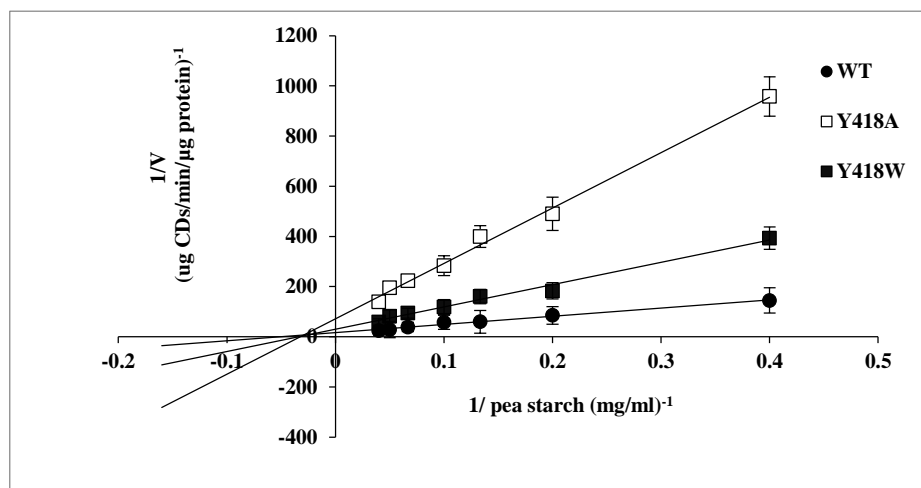


Figure 3. 50 Lineweaver- Burk plot of WT and N287 mutated *CgAMs*-catalyzed cyclization reaction. *CgAMs* (0.05 U starch degrading activity) were incubated with various concentrations of pea starch at 30 °C for 60 min. LR-CD products were analyzed by HPAEC-PAD.

Table 3. 17 Kinetic parameters of WT and N287 mutated *CgAMs* derived from cyclization reaction using pea starch as the substrate.

<i>CgAM</i>	K_m (mg/ml)	V_{max} ($\mu\text{g CD}\cdot\text{min}^{-1}\cdot\mu\text{g protein}^{-1}$)	k_{cat} (min^{-1}) [10^3]	k_{cat}/K_m ($\text{mg}\cdot\text{ml}^{-1}\cdot\text{min}^{-1}$) [10^3]
WT	19.9 ± 1.78	0.06 ± 0.13	6.12 ± 1.35	0.31 ± 0.06
N287A	31.0 ± 2.16	0.01 ± 0.06	1.13 ± 1.20	0.04 ± 0.07
N287W	29.1 ± 3.55	0.04 ± 0.02	3.25 ± 0.26	0.11 ± 0.03

Data are shown as the mean \pm standard deviation and are derived from three independent experiments.

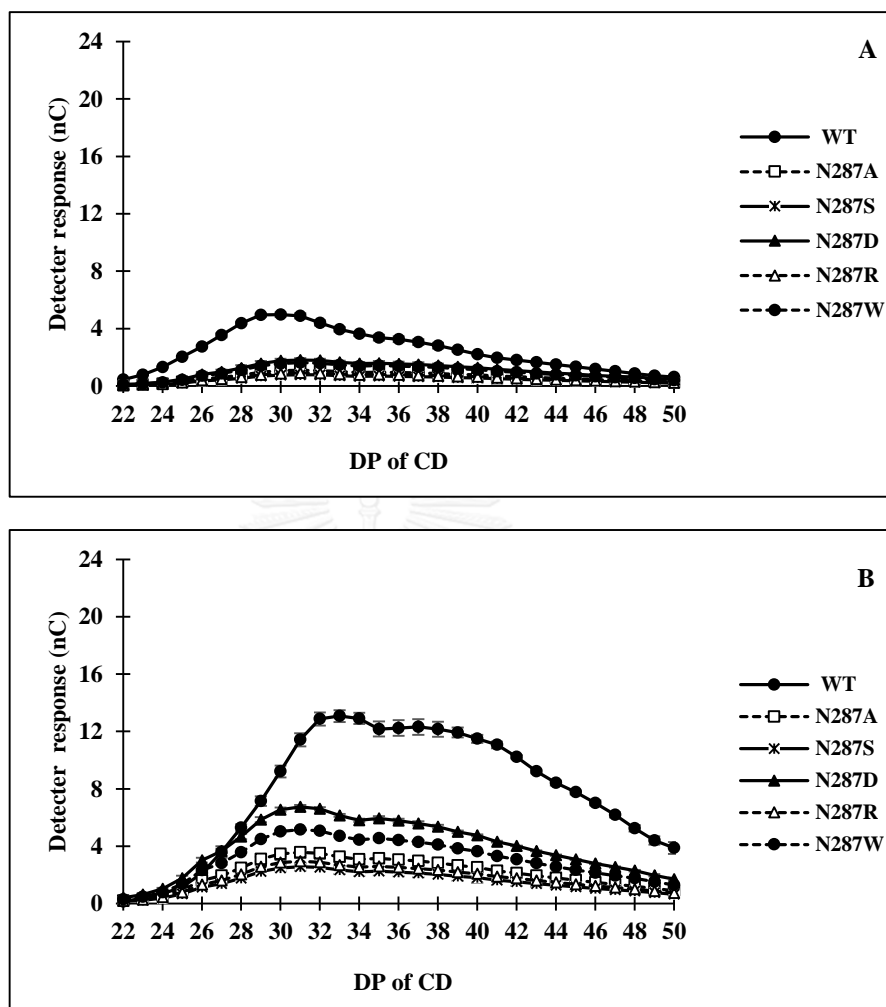


Figure 3. 51 HPAEC- PAD analysis of LR- CD products synthesized at different incubation time 1.5 h (A), 6 h (B), 12 h (C) and 24 h (D) by 0.10 unit of WT and N287 mutated *CgAMs*.(DP = Degree of polymerization).

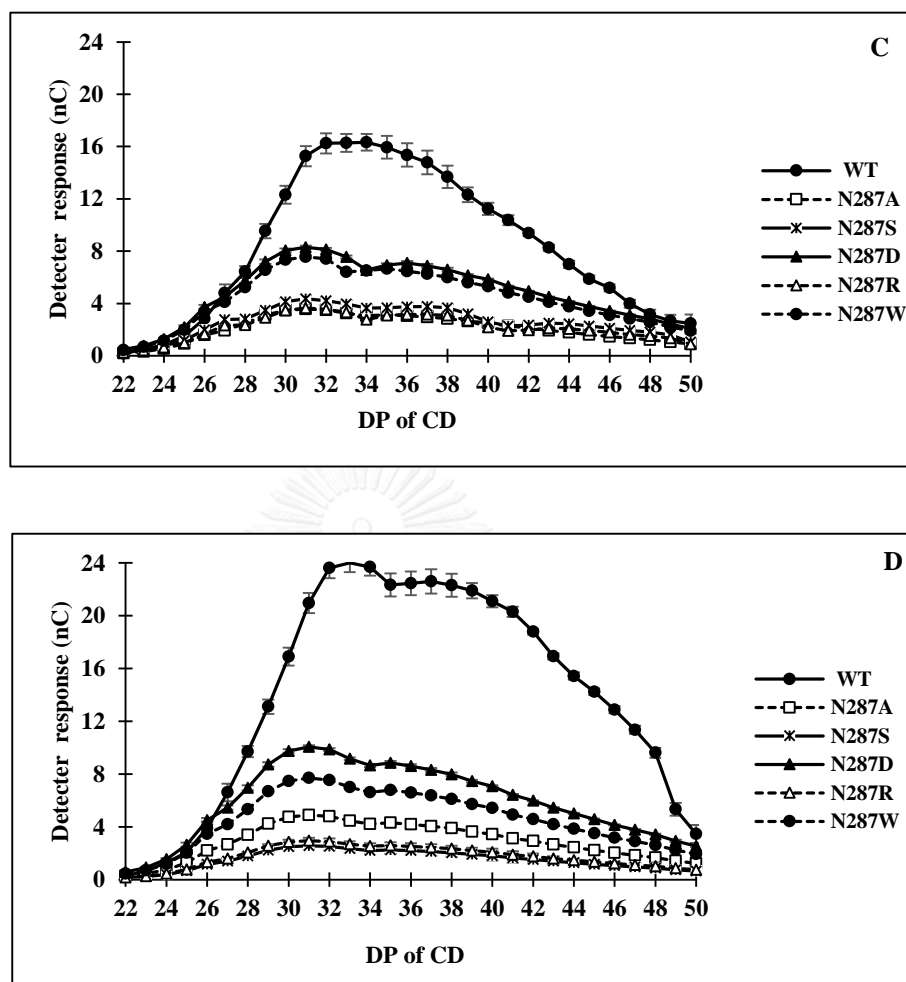


Figure 3.51 (continue) HPAEC-PAD analysis of LR-CD products synthesized at different incubation time 1.5 h (A), 6 h (B), 12 h (C) and 24 h (D) by 0.10 unit WT and N287 mutated CgAMs. (DP = Degree of polymerization).

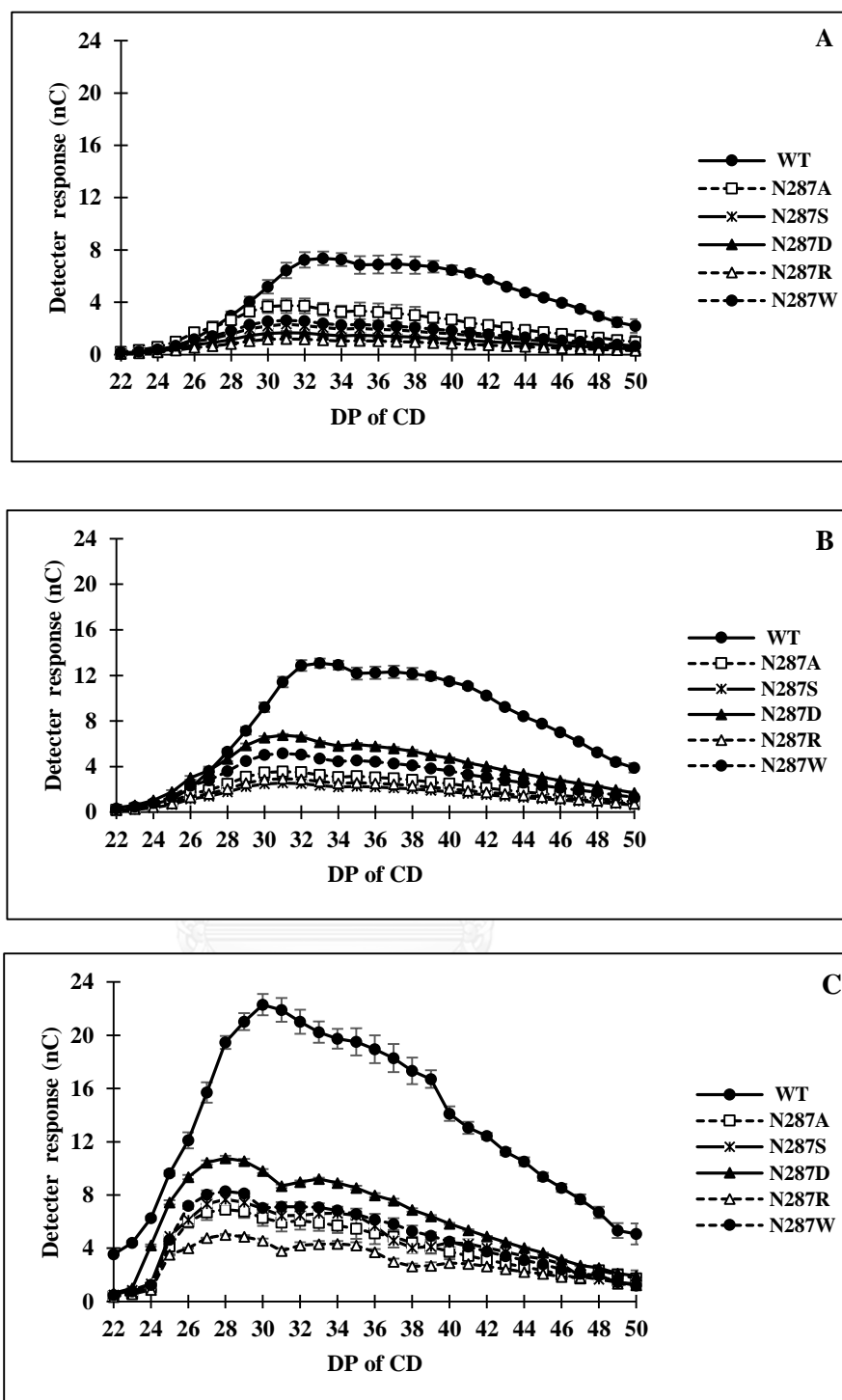


Figure 3.52 HPAEC-PAD analysis of LR-CD products synthesized for 6 h at different enzyme unit; 0.05 U (A), 0.10 U (B) and 0.20 U (C) by WT and N287 mutated CgAMs (DP = 22-50). (DP = Degree of polymerization).

3.9.6 Enzyme conformation

To investigate the effect of N287 mutation on enzyme conformational change, analysis of secondary structure was performed using circular dichroism (CD) as described before. The result showed that the CD spectra of N287 mutated and WT enzymes at pH 6.0 were closely overlaid (Figure 3.53). All mutated CgAMs showed a slight change in CD spectra as compared to the WT. The contents of the secondary structure were: α -helix 26-27%, β -sheet 20-22% and random coil 51-52%.

3.10 Structural modeling of N287 mutated CgAM

The model structures of N287 mutated CgAMs were constructed by the Discovery Studio 3.5 Client program using WT CgAM X-ray structure (PDB code 5B68) (Joo *et al.*, 2016) as template. The CgAM model structures were superimposed with acarbose ligand from the TaAM X-ray structure (PDB 1esw) (Przylas *et al.*, 2000a) in vicinity of N287 residue, ten residues including E225, P228, P229, T230, D285, R286, D288, V289, Y290 and A291 are within 5 Å away from this position (Figure 3.54). It was observed that amino acid at position 287 could form H-bond with three residues, T230, D285 and Y290 depending on its side chain. We found that all CgAMs had one hydrogen bond between amino acid position 287 with Y290 (Figure 3.54). While only N287D mutant had one hydrogen bond formed with unit C of acarbose (Figure 3.54 D).

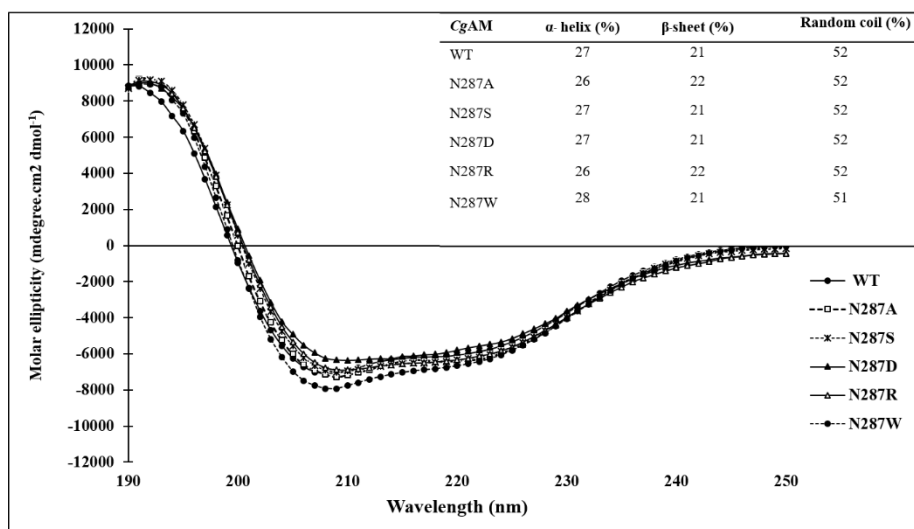


Figure 3. 53 Circular dichroism spectra and the predicted secondary structural compositions of WT and N287 mutated CgAMs.

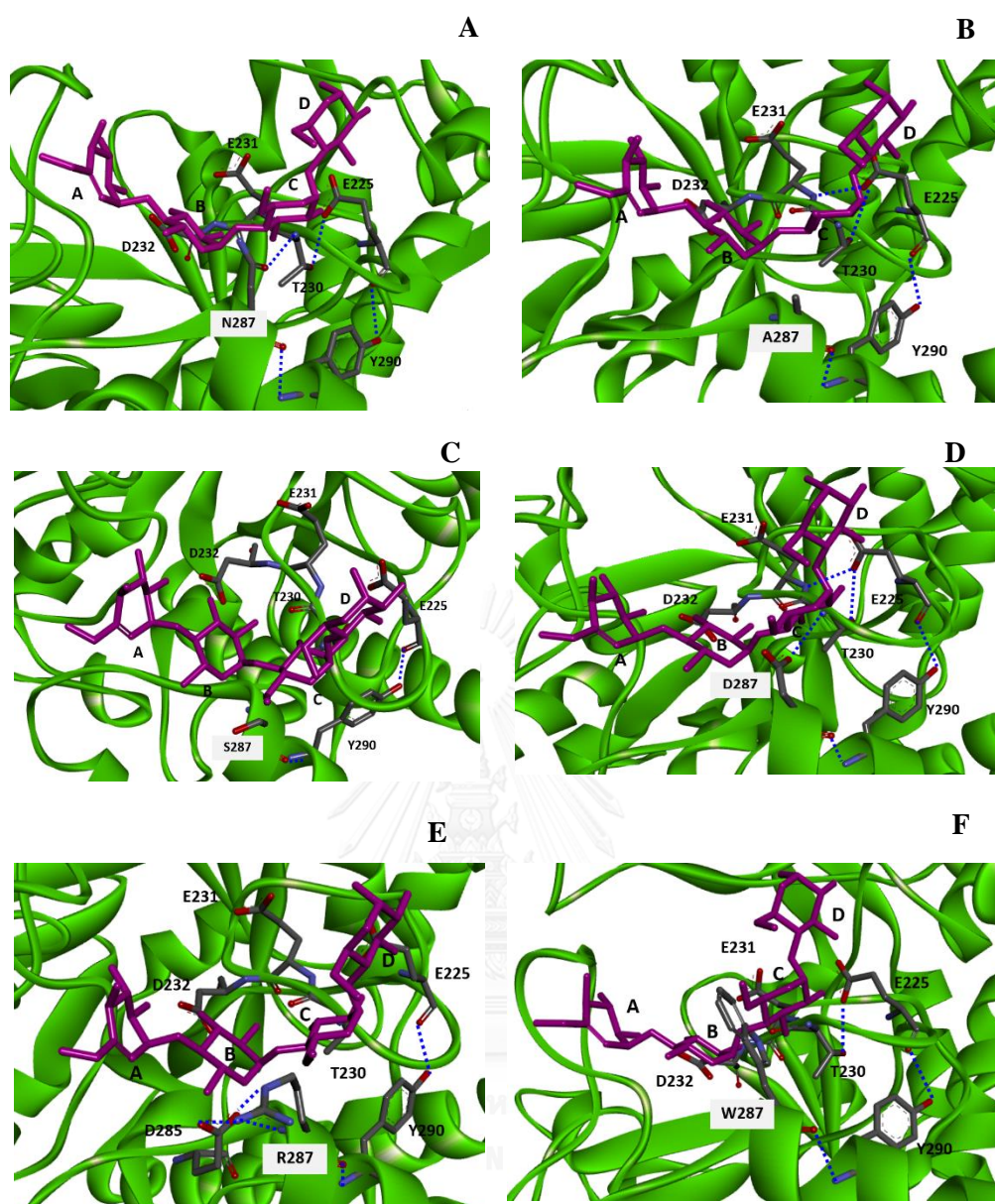


Figure 3.54 Structures of WT and N287 mutated CgAMs with acarbose (in purple).

The X-ray structure of WT CgAM (PDB code 5B68) (Joo *et al.*, 2016) was used as template to prepare the model structures of N287 mutated CgAMs. All CgAM structures were superposed with acarbose bound at active site of the X-ray structure of *T. aquaticus* amylomaltase (PDB 1esw) (Przylas *et al.*, 2000a). Proposed amino acid residues shown are those within 5 Å away from N287 residues of WT (A), N287A (B), N287S (C), N287D (D), N287R (E) and N287W (F) CgAMs, respectively. Hydrogen bonds are shown as dashed blue line.

CHAPTER IV

DISCUSSION

A novel amylomaltase from *C. glutamicum* (CgAM) was previously cloned with the open reading frame (ORF) of 2,121 bps which could be deduced to 706 amino acids, and expressed in *E. coli* BL21(DE3) by our research group (Srisimararat *et al.*, 2011). CgAM is larger in size and has a low amino acid sequence identity (about 26% identity) to those well characterized AMs from *Thermus* sp. The X-ray crystal structure of CgAM has been solved by our group but not yet published, then in 2016 the Korean group deposited the structure in Protein database as PDB code 5B68 (Joo *et al.*, 2016). CgAM has additional N-terminal domain which was not present in *Thermus* amylomaltases (Joo *et al.*, 2016; Przytylski *et al.*, 2000b).

In recent years, site-directed mutagenesis of CgAM has been previously studied by our group to investigate functional roles of different residues for the understanding of catalytic mechanism and enzyme improvement. We target residues involved with substrate binding. Y172 and N287 in the proposed second glucan binding site were shown to control transglucosylation activities and LR-CD product profile (Nimpiboon *et al.*, 2016b; Srisimararat *et al.*, 2012). N287Y showed an increase in thermostability as well as A406V/L (Nimpiboon *et al.*, 2016a; Nimpiboon *et al.*, 2016b). W425 at substrate-binding edge, next to 410s loop is proved to be essential for substrate binding, total loss of cyclization activity was observed in W425A suggesting the importance of hydrophobicity around here (Rachadech *et al.*, 2015). In the present study, three residues of CgAMs (Y418, H461 and N287) were our target for mutation to explore

their functions. We here described the construction of mutated *CgAMs* gene by site-directed mutagenesis, sequencing to identify the site of mutation, investigating the functions of target residues by enzyme characterization, comparing the properties of the mutated *CgAMs* to that of the WT enzyme and construction of the model structures of mutated *CgAMs* based on the WT structure in order to explain the *CgAM* function.

4.1 Construction of mutated amyломaltase genes from *C. glutamicum*

4.1.1 Selection of target amino acid residues of *CgAM*

In this work, amino acid sequence alignment and superimposed structure of *CgAM* (PDB code 5b68) with that of *TaAM* (PDB code 1CWY), a well-characterized AM, were compared. Three amino acid residues consisted of F251, H294 and Y101 of *TaAM* were selected as target residues for study. F251 which is in the 250s loop of *TaAM* and all *Thermus* AMs were previously reported as important residue for substrate recognition and transglucosylation activity from the result of site-directed mutagenesis study in AM from *T. brockianus* (*TbAM*) (Jung *et al.*, 2011). H294 has no evidence on its function but it was proposed to be important for binding with substrate in *T. thermophilus* amyломaltase (*TtAM*) (Kaper *et al.*, 2007). While Y101 which is in the second glucan binding site was reported to be involved in cyclization activity of amyломaltase as evidenced from site-directed mutagenesis study in *TaAM* (Fujii *et al.*, 2005; Fujii *et al.*, 2007).

From our amino acid sequence alignments, the results showed that F251, H294 and Y101 of *TaAM* are corresponded to Y418, H461 and Y290 of *CgAM*. The same results were found when the X-ray structures were superimposed except in the third residue (Y101). The multiple sequence alignment showed that Y101 is not conserved

in all species of AM, though in *CgAM*, this residue seems to be aligned with Y290 (Figure 3.1). By superimposing the X-ray structure of *CgAM* solved by our group (unpublished structures)(Srisimarath *et al.*, 2013) with that of *TaAM*, N287 rather than Y290 of *CgAM* has closed interaction with acarbose then was closer to Y101 of *TaAM* (Figure 3.2). We then decided to investigate the roles of Y418, H461 and N287 of *CgAM* in structure-function relationship of this enzyme.

4.1.2 Mutation of *CgAM* gene using site-directed mutagenesis

Site-directed mutagenesis is a common technique used for mutagenesis in the attempt to study the importance of amino acid residues on the structure and the function of protein or enzyme. The mutated primers were designed based on *E. coli* codon usage, to anneal with target site of gene then PCR amplification was performed. Substitutions at three residues (Y418, H461 and N287) by six residues representing different amino acid groups as indicated in Result section 3.1.3 were performed.

The series of Y418 (Y418A/S/D/R/W/F), H461 (H461A/S/D/R/W) and N287 (N287A/S/D/R/W) mutated *CgAM* genes were obtained and sequenced to confirm mutation sites (Figure 3.4-3.8). The involvement of Y418, H461 and N287 on *CgAM* characteristics was explored. From the previous study, we found only one mutation study at F251 (in 250s loop, the unique loop lies over the enzyme active site, see Figure 4.1) of *Thermus* AMs which is corresponding to Y418 (in 410s loop) of *CgAM*. Site-directed mutagenesis of loop tip residue F251 together with Q256 and W258 in *T. brockianus* AM (*TbAM*) was reported. The decrease in transglucosylation activity, the changes in substrate affinity and specificity were reported in F251G, Q256G and W258G mutated *TbAM* (Jung *et al.*, 2011). For H461 of *CgAM*, this residue is corresponded to H294 of *Thermus* AMs of which no previous report on mutagenesis

was found. From amino acid sequence alignment and superimposed structures of *CgAM* and *TaAM*, these histidine (H) residues were in the active site area, near the catalytic residues of the two enzymes (Figure 3.1). In the model structure of *TiAM*, H294 forms two hydrogen bonding with glucose residue (at subsite +1) of G7 substrate (Figure 4.1), thus the role in substrate binding was suggested.

For the third residue of interest which is corresponded to N287 of *CgAM*, Y101 located close to glucose unit C in the 2nd glucan binding site of *TaAM* (Figure 4.2) was reported to affect cyclization activity (Y101G caused higher cyclization activity) (Fujii *et al.*, 2007). Recent study by our group showed the increase in thermostability, the change in substrate specificity for disproportionation reaction, and a significant decrease in the three main activities of *CgAM*, (starch transglucosylation, disproportionation and cyclization) when substituted N287 of *CgAM* with Y (Nimpiboon *et al.*, 2016b).

4.2 Expression and purification of the recombinant WT and mutated *CgAM*s

E. coli has been commonly used as host cell for AMs expression, gene expression was induced by IPTG. All expressed AMs are intracellular enzyme as previously reported (Kaewpathomsri *et al.*, 2015; Kaper *et al.*, 2007; Srisimararat *et al.*, 2011). The recombinant WT, Y418, H461 and N287 mutated *CgAM* genes were expressed in *E. coli* BL21(DE3) using the expression vector pET-19b and 0.4 mM IPTG, cells were cultivated at 16 °C for 20 h. The results revealed that all *CgAM*s showed higher expression as soluble protein (Figure 3.17, 3.33 and 3.43). The recombinant WT and mutated *CgAM* genes in *E. coli* BL21 (DE3) containing pET-19b harboring *CgAM* genes were expressed as enzymes containing his-tag residues at the

N-terminus. All enzymes were successfully purified by HisTrap FFTM affinity. Specific activities and yields of all mutated CgAMs were decreased to a different extent (Table 3.1, 3.10 and 3.13) depending on mutated position and activity assay.

The molecular weight of the WT, and all mutated CgAMs containing his-tag residues was 84 kDa (Figure 3.17, 3.33 and 3.43) as similar to the previous study (Srisimarat *et al.*, 2011), thus the mutations did not affect the size of AM. When compared to other AMs, the size of CgAM was close to those of 4 α GTase from *Thermococcus litoralis* (79 kDa) (Xavier *et al.*, 1999) and AM from *E. coli*, EcAM (78.5 kDa) (Weiss *et al.*, 2015) but different from TaAM (57 kDa) (Terada *et al.*, 1999), *Synechocystis sp.* PCC6803 (57 kDa) (Lee *et al.*, 2009) and AM from *T. filiformis* JCM 11600 (55 kDa) (Kaewpathomsri *et al.*, 2015), as well as plant D-enzyme from Cassava and *Arabidopsis sp.* (59 kDa) (Tantanarat *et al.*, 2014). AMs from mesophilic bacteria (*E. coli* and *C. glutamicum*) is larger in size than AMs from thermophilic bacteria and plant D-enzymes.

4.3 Characterization of mutated CgAMs

4.3.1 Various activities of amyloamylase

The effect of Y418, H461 and N287 mutations on various activities of CgAM was investigated, all mutations caused a significant decrease in enzyme activities; both the inter- and intra-molecular transglucosylation reactions were affected. No change in optimum conditions of CgAM was observed upon these mutations. Optimum temperatures and pH of WT and all mutated CgAMs were: 40 °C, pH 6.0 for disproportionation reaction (Figure 3.18, 3.35, 3.44); and 30 °C, pH 6.0 for cyclization reaction (values for H461 could not be determined since no cyclization activity could

be detected) (Figure 3.19, 3.45). These values are in accordance with previous reports from the WT (Nimpiboon *et al.*, 2016b; Srisimarath *et al.*, 2011).

For Y418 mutated CgAMs, a significant decrease in the three main activities of AM: starch transglucosylation, disproportionation and especially cyclization was observed (Table 3.3). Our result agrees well with the mutation study of the corresponding residue F251 which showed the decrease in the three main activities when substituted by glycine (G) (Jung *et al.*, 2011) in *TbAM* or insertion of the two serines closed by (+SY²⁵⁰F²⁵¹+S) in *TaAM* (Roth *et al.*, 2017). The reduction in CgAM activities observed can be explained by the inability of the 410s loop to adopt the proper conformation of the enzyme during substrate binding. We propose that hydrophobic interaction is required here and Y418 contributes to suitable conformation flexibility of 410s loop to enable highest catalytic activity of CgAM. The hydrophobicity of 410s loop (with Y418) in CgAM is different from that of 250s loop (with F251) in *Thermus* AM (Joo *et al.*, 2016; Jung *et al.*, 2011). Interestingly, *EcAM* had L406 in 400s loop (Weiss *et al.*, 2015) as corresponding residue to Y418. Thus hydrophobic environment at this loop tip position of AMs is important, the residues may either be aromatic Y/F or aliphatic L depending on the enzyme. These differences covering the extended edge of substrate-binding site might make each AM differ in recognizing long polysaccharide substrate (Joo *et al.*, 2016).

H461 mutations resulted in nearly total loss of all transglucosylation activities. Cyclization activity of H461 mutated CgAMs could not be detected by HPAEC-PAD while hydrolysis activity was not affected (Table 3.11). From multiple sequence alignment, we found that histidine (H) residue in active site area is highly conserved among AMs. And from our proposed modeling structure of CgAM, H461 is very close

to the two catalytic residues (D460 and E508) inside the active pocket of the enzyme (Figure 3.42-A). *Kaper et al*, 2007 reported the model structure of substrate binding sites in the active site area of amylomaltase from *T. thermophilus* HB8, seven subsites forming H-bonds with maltoligosaccharide substrate were proposed. H294 of *TtAM* found close to catalytic residues (E340 and D249) showed two hydrogen bonding interactions at subsite +1 with maltoheptaose (G7) (Figure 4.1). Due to H461 of *CgAM* is corresponded to H294 of *Thermus sp.* amylomaltase, which is proposed to be important in substrate binding, we proposed here that H461 in *CgAM* is an essential residue for enzyme catalysis.

Mutation at the third residue of interest, N287, resulted in a dramatic decrease in all transglucosylation activities but not hydrolysis (Table 3.15). This result was similar to previous work from our group on N287Y mutated *CgAM* which reported that the transglucosylation activities (starch transglucosylation, disproportionation and cyclization) were diminished (Nimpiboon *et al.*, 2016b). N287 of *CgAM* is corresponded to Y101 of *TaAM* which locates in the secondary binding site of enzyme (Fujii *et al.*, 2007). Y101G mutated *TaAM* was also reported to affect cyclization and disproportionation activities of the enzyme (Fujii *et al.*, 2007; Roth *et al.*, 2017) Further explanation that relates how Y418/H461/N287 mutations affect structural change in vicinity of target residues leading to changes in *CgAM* activity is discussed in 4.4.

4.3.2 Substrate specificity and kinetic values

Specificity for malto-oligosaccharide substrates in disproportionation reaction of all mutated *CgAMs* was compared to WT (Figure 3.22, 3.38, 3.48). For WT, Y418 and N287 mutated *CgAMs*, G3 was the best while G7 was the worst substrate. Highest

specificity for G3 was reported in almost all WT AMs, including those from *Thermus* sp. (Srisimarath *et al.*, 2012; Terada *et al.*, 1999; Van der Maarel *et al.*, 2000). It is noticeable here that Y418F showed an increase in preference for G5 to G7 (Figure 3.22). For Y418 residues, our result was different from *TbAM* study in which substitution of a hydrophobic F251 by a small aliphatic G changed substrate specificity to longer oligosaccharides (G4 to G7) while the WT preferred G3 (Jung *et al.*, 2011). Also for N287, our N287A/S/D/R/W mutants preferred G3 as similar to WT, whereas previous study by our group showed that N287Y-*CgAM* preferred longer oligosaccharide maltopentaose (G5) (Nimpiboon *et al.*, 2016b). For H461 mutated *CgAMs*, these enzymes were different from WT in substrate specificity, they preferred G2 to G3. From these overall results, mutation at H461 caused the change in substrate specificity of disproportionation reaction while mutation at Y418 did not. For mutation at N287, change in substrate specificity was observed when substituted by Y (Nimpiboon *et al.*, 2016b) but not by A/S/D/R/W.

Kinetic parameters of disproportionation reaction of the WT with G3 substrate were in accordance with previous report (Nimpiboon *et al.*, 2016b). A lower k_{cat} and k_{cat}/K_m values were observed for all Y418 mutated *CgAMs* while value for the F mutant was similar to the WT. The W and R mutants showed the lowest k_{cat}/K_m (Table 3.4). The mutation affected more on the k_{cat} while the K_m values were not much changed (16-20 mM). Our result is contradicted to the report in F251G *TbAM* in which the K_m for maltotriose increased 3 folds with 9 folds decrease in k_{cat} (Jung *et al.*, 2011).

In this study, kinetics of cyclization reaction was also investigated with the two mutants, Y418A and Y418W, k_{cat} and k_{cat}/K_m were lower than that of WT (Table 3.5) while K_m values with pea starch substrate were higher (30 mM vs 19 mM of WT).

These results suggested that binding of short oligosaccharide (like G3) was not changed but binding of large substrate like pea starch was affected upon Y418 mutation while catalytic rates of both reactions with different substrate were decreased. The aromatic side chain at position 418 is thus required for high CgAM activity especially for long polysaccharide substrate. However, bulky side chain of tryptophan led to activity decrease.

For H461 mutated CgAMs, only kinetics of disproportionation reaction using maltose (G2) as substrate were determined since cyclization activity could not be detected. Mutation at H461 resulted in a significant decrease in k_{cat} and k_{cat}/K_m while the K_m values were larger than that of WT (30-37 mM vs 20 mM of WT) (Table 3.12). The mutation at this position thus affected affinity of substrate binding and enzyme catalytic rate.

For N287, kinetics of disproportionation (with G3 substrate) and cyclization (with pea starch) reactions were performed. For both reactions, mutation at N287 affected binding of small and large saccharide substrates (higher K_m for all mutants), also the reaction rate and catalytic efficiency (lower k_{cat} and k_{cat}/K_m) (Table 3.16 and 3.17). Our results on kinetic analysis of N287 mutated CgAMs were similar to the previous study in N287Y mutant (Nimpiboon *et al.*, 2016b).

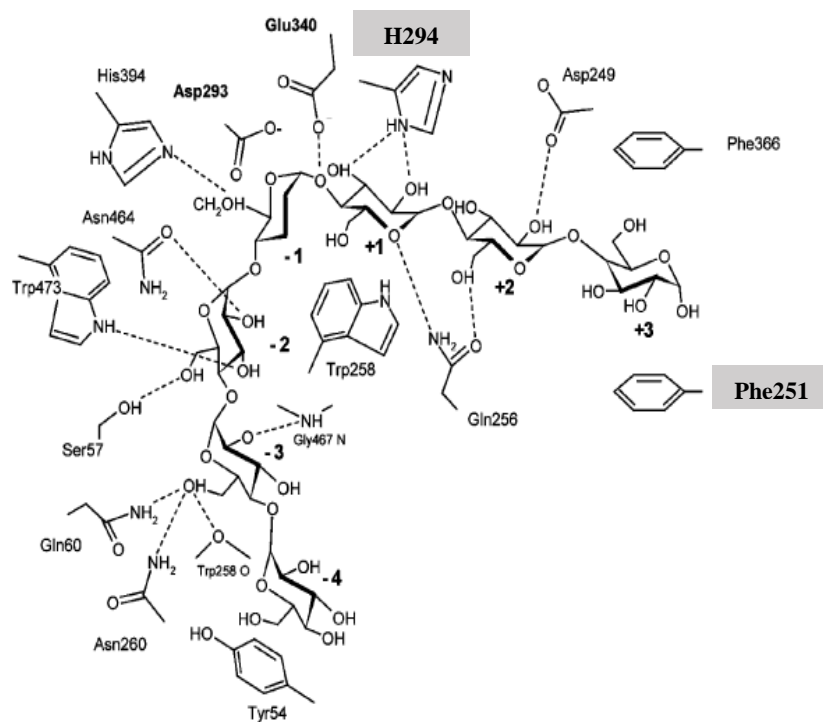


Figure 4. 1 Proposed binding of maltoheptaose (G7) in the active site of amylo maltase from *Thermus thermophilus* (TtAM). Catalytic residues are shown in boldface (D293 and E340). Histidine 294 (His294) and Phenylalanine 251 (Phe251) residues are shaded (Kaper *et al.*, 2007).

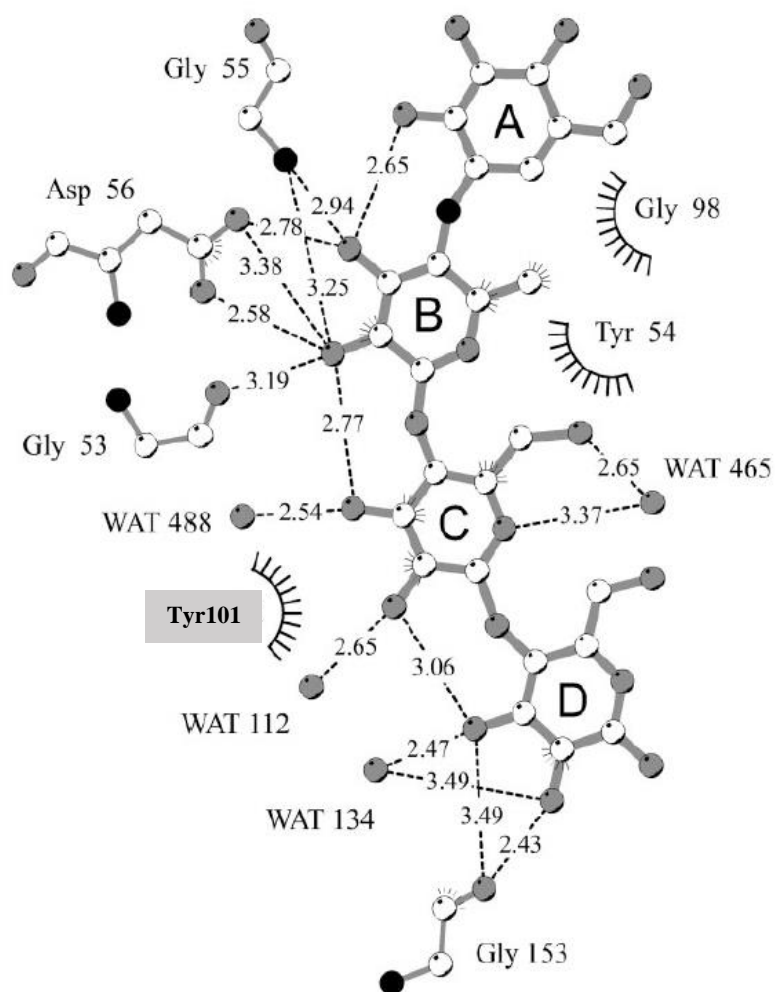


Figure 4. 2 Scheme of the interactions of acarbose bound to the secondary binding site of amyloamylase from *Thermus aquaticus* (TaAM). Tyrosine 101 (Tyr 101) residues are shaded (Przylas *et al.*, 2000a).

4.3.3 LR-CD products profile

LR-CD was analyzed by HPAEC-PAD (Srisimarat *et al.*, 2012), the total CD yields and product patterns of all CgAMs were depended on incubation time and enzyme concentration. Long incubation time and high enzyme concentration gave high yield and smaller size of LR-CDs. This is in accordance with previous report by our group (Srisimarat *et al.*, 2012).

The product patterns of all mutated CgAMs except for Y418F were different from that of the WT. The signal indicated yield from WT reached the highest at 28 nC followed by yields of Y418F, Y418A, Y418D, Y418S, Y418W and Y418R mutated CgAMs (Figure 3.25-D). Interestingly, the main products of the WT and Y418F were CD29-CD33 while Y418A/D/S/R/W - CgAMs showed a shift to the larger product size, CD36-CD40 (Figure 3.25 and 3.26). The amounts of LR-CDs formed from all mutated enzymes, especially from the W and R mutants, were less than that of the WT. Y418R gave the lowest amount of LR-CD. The product yields were corresponded to the cyclization activities observed (Table 3.3).

For N287 mutated CgAMs, the LR-CDs production profiles were different from WT and Y418 mutated CgAMs, the yield was lower and LR-CDs pattern shifted to the smaller CD size (CD26-CD29) (Figure 3.51 and 3.52). Our results are different from N287Y, the main product of N287Y was CD29-CD31 which may be due to increase in hydrophobic interaction (Nimpiboon *et al.*, 2016b).

From the results of our study, substitution of Y418 and N287 residues of CgAM thus affected not only the size but also the yield of LR-CD product. We propose that appropriate hydrophobicity with Y/F residues at the position 418 is required for high LR-CD production of CgAM whereby the products are of the relatively large CD size.

However, for the position 287, mutation to A/S/D/R/W caused the decrease in LR-CDs yield and a shift to smaller CD size. On the other hand, an increase in hydrophobicity as in N287Y resulted in larger size of LR-CDs and higher yield at 24 h incubation time due to enzyme thermostability (Nimpiboon *et al.*, 2016b).

4.3.4 Secondary structure

The enzyme secondary structure was analyzed by CD spectrophotometry and the content of the structure was determined. All mutated CgAMs showed a slight change in CD spectra as compared to the WT (Figure 3.27, 3.41, 3.53). The proportions of the secondary structure of all CgAMs were: α -helix 26-28%, β -sheet 20-22% and random coil 51-52%. Hence, mutations at Y418, H461 and N287 residues did not result in a massive conformational change of CgAM. The composition of the secondary structure of WT CgAM obtained is the same as that previously reported (Nimpiboon *et al.*, 2016a; Rachadech *et al.*, 2015). Changes in enzyme activities, kinetic parameters and LR-CDs profile were thus mainly due to a single amino acid substitution at Y418, H461 and N287 suggesting that these residues are required for maintaining such properties of CgAM.

4.3.5 Isothermal titration calorimetry (ITC) and Differential scanning calorimetry (DSC)

To compare biophysical properties of WT and mutated CgAMs, ITC and DSC were performed. This is the first work to use ITC for characterization of amylomaltase. We investigated the molar enthalpy change in disproportionation reaction of WT, Y418A and Y418W CgAMs. The enzyme catalyzed - disproportionation reaction was endothermic (heat was produced) thus producing a large positive deflection in thermal power (Figure 3.28). The return of thermal power to the level matching the initial base

line indicated complete catalysis of G3 in the sample cell. Heat production by WT was higher than those of Y418A and Y418W CgAMs (Figure 3.28), corresponded to the relative activities of the three CgAMs as measured by biochemical method (Figure 3.29). It was observed that Y418W had less molar enthalpy or heat production than the WT and Y418A even though tryptophan (W) is in the same aromatic amino acid group as similar to tyrosine (Y) of WT. Explanation can be given by comparing the model structures of these two mutants with the X-ray structure of WT CgAM (Joo *et al.*, 2016) as illustrated in Figure 3.32 and further discussed in 4.4. Y418A had a low hydrophobic interaction with F534, the residue that supposed to be involved in the loop entrance area of the enzyme. While Y418W though aromatic but the W side chain of mutant was left behind the substrate channel groove (Joo *et al.*, 2016), thus hydrophobic interaction between substrate and enzyme was even lower than that of Y418A mutant leading to extremely low enzyme activity.

Kinetics of disproportionation reaction by G3 substrate were also investigated by ITC. Curve fitting analysis was performed on the thermal power profile (Jeoh *et al.*, 2005) and the endothermic heat rate production of the enzyme-catalyzed reaction was converted to the kinetic parameters of the enzyme (Todd and Gomez, 2001). The pseudo steady state assumptions at high substrate to enzyme ratio was used to determine kinetic parameters of the enzyme (Bianconi, 2007). The thermogram of WT and Y418A/W mutated CgAMs showed that the thermal power signal was higher when concentration of G3 was increased (Appendix 22). V_{max}/K_m values were in the order of WT > Y418A > Y418W at 10 mM G3 (Table 3.6). This suggested that each enzyme had different efficiency in catalysis. Moreover, all results showed that when concentration of G3 was increased, the product inhibition was occurred, V_{max}/K_m values

were decreased when G3 was changed from 10 to 30 mM (Figure 3.30). This may result from higher production of glucose, a main product from disproportionation reaction, that can also act as substrate for CgAM or glucose itself can be an inhibitor to the enzyme (Jeoh *et al.*, 2005). Similar situation had been reported in ITC analysis of β -D-glucosidase whereby high glucose product produced at high cellobiose substrate could inhibit enzyme activity, V_{max}/K_m values observed at high substrate concentration were decreased (Jeoh *et al.*, 2005).

DSC is one of the most frequently used techniques to determine thermal stability of protein. Its fundamental principle is to measure the heat capacity (C_p) when molecules unfold due to the increase in temperature, generally performed at -10 °C to 130 °C. The transition midpoint or melting temperature (T_m) is considered as a temperature, where 50% of the proteins own its native conformation, and the rest remain denatured. Higher T_m values would be representative of a more stable molecule. Besides T_m , T_p value which represents the DSC peak temperature is easily obtained and also can be used to designate thermostability of the molecules (Jelesarov and Bosshard, 1999). In this work, DSC was investigated to determine the thermal stability of WT and Y418A/W mutated CgAMs. At every scanning rate (0.75, 1.0 and 1.5 °C .min⁻¹), all CgAMs showed the irreversible transition state in accordance with our previous report on the WT enzyme (Nimpiboon *et al.*, 2016a). When compared the thermal transition curves (Figure 3.31), the heat capacity profiles of WT and Y418A were similar while a shift of peak temperature (T_p) of Y418W towards 4 °C lower was observed (Table 3.7). DSC results thus support that CgAM is not a thermostable enzyme in accordance with our previous studies (Nimpiboon *et al.*, 2016a). Moreover, the WT was more stable to temperature than Y418W, which suggested that the aromatic side chain especially

tyrosine at position 418 is involved in controlling thermal stability of CgAM through the aromatic hydrophobic interaction at the substrate entrance.

4.4 The proposed model structures of mutated CgAMs

In the attempt to relate changes in properties of CgAM observed upon mutations to changes in enzyme structure, the X-ray structure of the WT CgAM (PDB code 5B68) (Joo *et al.*, 2016) was compared with the model structures of all mutants (Figure 3.32, 3.42 and 3.54). Possible H-bonding and hydrophobic interaction with residues closed by the mutated residues was analyzed and compared with WT. In addition, H-bond interactions between position 461 and 287 with acarbose molecule were also investigated.

Six model structures of Y418 mutated (Y418A/S/D/R/W/F mutants) CgAMs were constructed (Figure 3.32). In the 410s loop, eight residues including D416, G417, N419, Q420, R577, V582, Q662 and P663 are within 5 Å away from Y418. It is known that side chain-side chain H-bond can be formed within 3.5 Å (Barlow and Thornton, 1983; McDonald and Thornton, 1994; Sokalingam *et al.*, 2012). We found that only the R mutant had one H-bond forming between R418 and D416 while no H-bond was found in WT and other mutants (Figure 3.32-1E). Difference in H-bonding observed here was not corresponded to the difference in properties of Y418 mutated enzymes. When the molecular surfaces of aromatic edge of CgAMs were determined, WT-CgAM showed rather strong hydrophobic interaction (gold color in Figure 3.32-2A) between Y418 and F534 residues that are proposed to form the channel for substrate entering, as similar to situation in *TbAM* (Jung *et al.*, 2011) described below. Moderate interaction was found

in Y418F/W mutants which might be due to the inward direction of F/W side chain. For the Y418A/S/D/R mutants, low or no interaction was observed (grey color in Figure 3.32 2B-2F). Thus, hydrophobic interactions around the loop area were different between the WT and mutated enzymes, and this difference is likely to be responsible for change in properties of Y418 mutated enzymes. It was reported that the decrease in hydrophobicity of the environment led to non-optimal binding of the incoming oligosaccharide acceptor substrate (Tang *et al.*, 2006). Transglucosylation activities of amylomaltases, as similar to cyclodextrin glycosyltransferases, are facilitated by hydrophobic interaction at the acceptor binding site (van der Veen *et al.*, 2001). From sequence alignment of *CgAM* and *TbAM*, Y418 and F534 in 410s loop of *CgAM* corresponded to F251 and F366 in 250s loop of *TbAM* that have been proposed to form the hydrophobic stacking interaction between substrate and enzyme (Jung *et al.*, 2011). The mutants F251G in *TbAM* (Jung *et al.*, 2011) and F366L in *TtAM* showed a significant decrease in the activity of both enzymes (Kaper *et al.*, 2007). We here propose that upon losing the hydrophobic interaction at the loop entrance, the mutated *CgAMs* could not stabilize the extended loop due to less suitable conformation that leads to less enzyme activities and product yield.

From the model structure, the substrate entering channel in Y418A was larger (Figure 3.32-2B) while those of Y418R and Y418W were smaller (Figure 3.32-2E, 2F) when compared to the WT ((Figure 3.32-2A)). The distances between the residue position 418 and F534 which form the channels were predicted (Table 3.8); 1.0 Å longer and 4.5 Å shorter than that of the WT were observed in the A and R mutants, respectively. The R and W mutants provided the shorter distances due to having charged and bulky functional groups (Nelson *et al.*, 2008; Voet *et al.*, 1999), thus

resulting in difficulty of substrate, especially those long polysaccharides, to enter the loop area. In contrast, the distance in the F mutant did not change much (0.4 Å shorter), in accordance with the insignificant change of catalytic activity and product formation compared to the WT. The loop movement is important, as similarly proposed in 250s loop of *TbAM* (Jung *et al.*, 2011). Y418 having proper hydrophobic interaction with F534 might make the 410s loop in closed form, the acceptor substrate was then oriented to the active site and the conformation of *CgAM* was suitable for catalysis. While in the R and W mutants, the loop might be in open form resulting in activity lost.

The model structures of H461 mutated *CgAMs* were also constructed. The H461 residue is in the active site area, twelve residues including Y23, G412, W425, D460, V462, L463, G464, L465, R467, L468 and E508 are within 5 Å away from H461 position. In the WT and the H461A/D/R/W mutants, no hydrogen bond was formed with those residues, but the S mutants had one H-bond with D460 (Figure 3.42-C). From our study, we found that H461 is essential for *CgAM* activity, nearly total loss of all transglucosylation activities were observed upon mutation, especially cyclization whereby LR-CDs formation was nil. Analysis of H-bonding between residue 461 and closed by residues was not totally accounted for changes in activities except for the S mutant which had one H-bonds that might cause local conformational change around active site. From the previous report in *TtAM*, the model for substrate binding site in active site area showed the interaction of H294 residue with maltoheptaose (G7) substrate at subsite +1 (Kaper *et al.*, 2007). Moreover, from multiple amino acid sequence alignment, we observed that this histidine is highly conserved among amyloamylases and disproportionating enzymes (DPE-1) from bacteria and plants, respectively (Appendix 18). When H-bond interactions between position 461 and

acarbose molecule were investigated (Figure 3.42), we found only WT and H461D mutated CgAMs could form two and one H-bond with acarbose molecule at subsite +1 (Figure 3.42A and D) These results suggested that H-bond of H461 with substrate at subsite +1 is essential for CgAM catalysis.

Around N287 residues, ten amino acids residues including E225, P228, P229, T230, D285, R286, D288, V289, Y290 and A291 are within 5 Å away from N287 position. Hydrogen bonds could be formed between residues at position 287 and three residues (T230, Y290 and D285) (Figure 3.54). And only N287D mutant had one hydrogen bond with glucose unit C of acarbose bound at the active site (Figure 3.54-D). The previous study from our group reported that the change in hydrophobicity at this position in N287Y mutants led to decrease in enzyme activity (Nimpiboon *et al.*, 2016b). Moreover, mutation at Y101 of *TaAM* (corresponded to our N287) showed lower disproportionation activity similar to our results. We conclude here that position 287 requires positively charged side group for high CgAM activity.

After we nearly finished mutation experiments at N287, the X-ray structure of CgAM was published by a Korean research group (Joo *et al.*, 2016) and deposited as PDB 5B68 around mid 2016 as earlier mentioned. We then used this structure to superimpose with X-ray structure of *TaAM* (PDB 1CWY) and surprisingly found that N287 of CgAM is corresponding to G98, not Y101 of *TaAM*. And Y101 of *TaAM* corresponded to Y290 of CgAM, the same result as we had obtained from our amino acid sequence alignment (Figure 3.1). Our resolved X-ray structure and the PDB 5B68 structure seem to show a three amino acid - shift in the helix turn around the positions 287 to 290. The difference may be due to different based structure used when electron density map was resolved into each X-ray structure of CgAM. At present, we think

Y290 of *CgAM* is corresponding to Y101 of *TaAM*. So which residue in *TaAM* corresponded to N287 of *CgAM*, sequence alignment suggested G98 (Figure 3.1). The residue G98 is closed to glucose unit A and also one of the important residues in the second glucan binding site of *TaAM* (Figure 4.2) However, from our results we found that N287 was closer to glucose unit C than unit A (Figure.3.54) Therefore, effects from N287 mutations reflect the importance of second glucan binding site of *CgAM*.

In early 2017, Roth *et al.* reported the X-ray crystal structure of *TaAM* in complex with cycloamylose (CA34) at resolution range of 1.73-37 Å. The result showed that 250s loop (F251 residue) and the second glucan binding site (Y54 and Y101 residues) which are close to 460s loop are important for LR-CD formation and enzyme activity via the hydrophobic interaction of amino acid residues around the loops of *TaAM* (Roth *et al.*, 2017). This work thus supports our results in terms of the importance of the unique loops and the second glucan binding site on their functions involving transglucosylation activity and LR-CD product formation of *CgAM*

CHAPTER V

CONCLUSIONS

Three target amino acid residues of CgAM consisting of Y418 (at the tip of 410s loop which lies over the active site), H461 (in active site) and N287 (in second glucan binding site) were selected for site-directed mutagenesis. Y418, H461 and N287 mutated CgAMs were constructed, expressed and purified by His-trap column chromatography. The major protein band of 84 kDa similar to WT - CgAM was observed. All mutated CgAMs showed significantly lower transglucosylation activities than WT enzyme, except the Y418F mutant. Interestingly, H461 mutated CgAMs lost an intramolecular transglucosylation (cyclization) activity since LR-CD products could not be detected.

The optimum temperatures and pHs of mutated enzymes were similar to WT, at 40 °C, pH 6.0 and 30 °C, pH 6.0 for disproportionation and cyclization reactions, respectively. Thermostability at 30, 35 and 40 °C and pH stability at pH 7.0 and 8.0 of all mutated CgAMs were significantly decreased when compared to WT. Substrate specificity in disproportionation reaction showed that G3 was the best substrate for WT, Y418 and N287 mutated CgAMs while H461 mutants preferred G2. The catalytic efficiency, k_{cat}/K_m of all mutated CgAMs was lower than that of WT, mainly due to the significant decrease in k_{cat} for both disproportionation and cyclization reactions. The K_m values for G3 of Y418 mutated CgAMs were not changed much while those of H461 and N287 mutated enzymes were higher than WT. In cyclization, K_m values for pea starch substrate of Y418 and N287 mutated CgAMs were higher than WT. Product analysis demonstrated that all mutated enzymes gave a lower product yield in comparison to WT. Y418A/S/D mutated CgAMs provided a larger LR-CD size (CD36-

CD40) while N287/A/S/D/R/W gave a smaller size (CD26-CD28) compared to WT (CD29-CD33). While Y418R/W showed a broad product pattern.

The secondary structure observed from CD spectra was not significantly changed upon mutations. In biophysical characterization, heat production in disproportionation reaction by WT was higher than those of Y418A and Y418W as observed in ITC. And product inhibition was observed at high maltotriose. From DSC, heat capacity profile of Y418W showed the lowest peak temperature (T_p) than WT and Y418A CgAM. The model structures of all mutated CgAMs were constructed and compared to WT structure to help explain mutation effect on changes in properties of CgAM. From overall results, changes in enzyme activities, biochemical & biophysical properties and LR-CD product pattern resulted from local conformation change caused by alteration in hydrophobicity or hydrogen bonding interactions around mutated residues. Y418 in 410s loop not only contributes to transglucosylation activities but also controls the amount and size of LR-CD products through the proposed hydrophobic stacking interaction and the suitable distance (418 - F534 residue) of loop channel for substrate entering, the shift in product pattern is likely to be the result of the difference of preferable oligosaccharides substrates between WT and mutated CgAMs. H461 is essential for enzyme catalysis, especially in cyclization reaction and N287 could also be involved in enzyme activity and LR-CD products pattern by retaining positively charge side chain.

REFERENCES

- Alting A.C., Van de Velde F., Kanning M.W., Burgering M., Mulleners L., Sein A., Buwalda P. (2009) Improved creaminess of low-fat yoghurt: The impact of amyloamylase-treated starch domains. *Food Hydrocolloids* 23:980-987.
- Baek H.H., Kwon S.Y., Rho S.J., Lee W.S., Yang H.J., Hah J.M., Choi H.G., Kim Y.R., Yong C.S. (2011) Enhanced solubility and bioavailability of flurbiprofen by cycloamylose. *Archives of Pharmacal Research* 34:391-397.
- Banner D., Bloomer A., Petsko G., Phillips D., Pogson C., Wilson I., Corran P., Furth A., Milman J., Offord R. (1975) Structure of chicken muscle triose phosphate isomerase determined crystallographically at 2.5 Å resolution: using amino acid sequence data. *Nature* 255:609-614.
- Barends T.R., Bultema J.B., Kaper T., van der Maarel M.J., Dijkhuizen L., Dijkstra B.W. (2007) Three-way stabilization of the covalent intermediate in amyloamylase, an α -amylase-like transglycosylase. *Journal of Biological Chemistry* 282:17242-17249.
- Barends T.R.M., Korf, H., Kaper, T., van der Maarel, M.J.E.C., Dijkhuizen, L., Dijkstra, B.W. (2005) Structural influences on product specificity in amyloamylase from *Aquifex aeolicus* <http://www.rcsb.org/pdb/explore/explore.do?structureId=1TZ7>
- Barlow D.J., Thornton J. (1983) Ion-pairs in proteins. *Journal of Molecular Biology* 168:867-885.
- Bender H., Lehmann J., Wallenfels K. (1959) Pullulan, ein extracelluläres glucan von *Pullularia pullulans*. *Biochimica et Biophysica Acta* 36:309-316.

- Bhuiyan S.H., Kitaoka M., Hayashi K. (2003) A cycloamylose-forming hyperthermostable 4- α -glucanotransferase of *Aquifex aeolicus* expressed in *Escherichia coli*. *Journal of Molecular Catalysis B: Enzymatic* 22:45-53.
- Bianconi M.L. (2007) Calorimetry of enzyme-catalyzed reactions. *Biophysical Chemistry* 126:59-64.
- Bollag D.M., Rozycki M.D., Edelstein S.J. (1996) *Protein methods* Wiley-Liss New York.
- Boos W., Shuman H. (1998) Maltose/maltodextrin system of *Escherichia coli*: transport, metabolism, and regulation. *Microbiology and Molecular Biology Reviews* 62:204-229.
- Chikan N.A., Bhavaniprasad V., Anbarasu K., Shabir N., Patel T.N. (2013) From natural products to drugs for epimutation computer-aided drug design. *Applied Biochemistry and Biotechnology* 170:164-175.
- Coutinho P.M., Deleury E., Davies G.J., Henrissat B. (2003) An evolving hierarchical family classification for glycosyltransferases. *Journal of Molecular Biology* 328:307-317.
- Del Valle E.M. (2004) Cyclodextrins and their uses: a review. *Process Biochemistry* 39:1033-1046.
- Endo T. (2011) Large-ring cyclodextrins. *Trends in Glycoscience and Glycotechnology* 23:79-92. DOI: 10.4052/tigg.23.79.
- Freire E. (1995) Differential scanning calorimetry. *Protein Stability and Folding: Theory and Practice*:191-218.

- Freyer M.W., Lewis E.A. (2008) Isothermal titration calorimetry: experimental design, data analysis, and probing macromolecule/ligand binding and kinetic interactions. *Methods in Cell Biology* 84:79-113.
- Fujii K., Minagawa H., Terada Y., Takaha T., Kuriki T., Shimada J., Kaneko H. (2005) Use of random and saturation mutageneses to improve the properties of *Thermus aquaticus* amylomaltase for efficient production of cycloamyloses. *Applied and Environmental Microbiology* 71:5823-5827.
- Fujii K., Minagawa H., Terada Y., Takaha T., Kuriki T., Shimada J., Kaneko H. (2007) Function of second glucan binding site including tyrosines 54 and 101 in *Thermus aquaticus* amylomaltase. *Journal of Bioscience and Bioengineering* 103:167-173.
- Gessler K., Usón I., Takaha T., Krauss N., Smith S.M., Okada S., Sheldrick G.M., Saenger W. (1999) V-Amylose at atomic resolution: X-ray structure of a cycloamylose with 26 glucose residues (cyclomaltohexaicosaoase). *Proceedings of the National Academy of Sciences* 96:4246-4251.
- Gill P., Moghadam T.T., Ranjbar B. (2010) Differential scanning calorimetry techniques: applications in biology and nanoscience. *J Biomol Tech* 21:167-193.
- Goda S.K., Eissa O., Akhtar M., Minton N.P. (1997) Molecular analysis of a *Clostridium butyricum* NCIMB 7423 gene encoding 4- α -glucanotransferase and characterization of the recombinant enzyme produced in *Escherichia coli*. *Microbiology* 143:3287-3294.

- Hansen L.D., Transtrum M.K., Quinn C., Demarse N. (2016) Enzyme-catalyzed and binding reaction kinetics determined by titration calorimetry. *Biochimica et Biophysica Acta (BBA)-General Subjects* 1860:957-966.
- Harata K. (1981) Induced circular dichroism of cycloamylose complexes with meta- and para-disubstituted benzenes. *Bioorganic Chemistry* 10:255-265.
- Holm L., Sander C. (1998) Touring protein fold space with Dali/FSSP. *Nucleic Acids Research* 26:316-319.
- Jelesarov I., Bosshard H.R. (1999) Isothermal titration calorimetry and differential scanning calorimetry as complementary tools to investigate the energetics of biomolecular recognition. *Journal of Molecular Recognition* 12:3-18.
- Jeoh T., Baker J.O., Ali M.K., Himmel M.E., Adney W.S. (2005) β -d-glucosidase reaction kinetics from isothermal titration microcalorimetry. *Analytical Biochemistry* 347:244-253.
- Jeon B.S., Taguchi H., Sakai H., Ohshima T., Wakagi T., Matsuzawa H. (1997) 4- α -glucanotransferase from the hyperthermophilic archaeon *Thermococcus litoralis*. *European Journal of Biochemistry* 248:171-178.
- Johnson C.M. (2013) Differential scanning calorimetry as a tool for protein folding and stability. *Archives of Biochemistry and Biophysics* 531:100-109.
- Joo S., Kim S., Seo H., Kim K.-J. (2016) Crystal structure of amylomaltase from *Corynebacterium glutamicum*. *Journal of Agricultural and Food Chemistry* 64:5662-5670.

- Jung J.H., Jung T.Y., Seo D.H., Yoon S.M., Choi H.C., Park B.C., Park C.S., Woo E.J. (2011) Structural and functional analysis of substrate recognition by the 250s loop in amyloamylase from *Thermus brockianus*. *Proteins: Structure, Function, and Bioinformatics* 79:633-644.
- Kaewpathomsri P., Takahashi Y., Nakamura S., Kaulpiboon J., Kidokoro S.-i., Murakami S., Krusong K., Pongsawasdi P. (2015) Characterization of amyloamylase from *Thermus filiformis* and the increase in alkaline and thermostability by E27R substitution. *Process Biochemistry* 50:1814-1824.
- Takefuda G., Duke S.H. (1989) Characterization of pea chloroplast D-enzyme (4- α -D-glucanotransferase). *Plant Physiology* 91:136-143.
- Kaper T., Leemhuis H., Uitdehaag J.C., Van Der Veen B.A., Dijkstra B.W., van der Maarel M.J., Dijkhuizen L. (2007) Identification of acceptor substrate binding subsites+ 2 and+ 3 in the amyloamylase from *Thermus thermophilus* HB8. *Biochemistry* 46:5261-5269.
- Kaper T., Talik B., Ettema T.J., Bos H., van der Maarel M.J., Dijkhuizen L. (2005) Amyloamylase of *Pyrobaculum aerophilum* IM2 produces thermoreversible starch gels. *Applied and Environmental Microbiology* 71:5098-5106.
- Kelly S.M., Jess T.J., Price N.C. (2005) How to study proteins by circular dichroism. *Biochimica et Biophysica Acta (BBA)-Proteins and Proteomics* 1751:119-139.
- Kim J.H., Wang R., Lee W.H., Park C.S., Lee S., Yoo S.H. (2011) One-pot synthesis of cycloamyloses from sucrose by dual enzyme treatment: Combined reaction of amylosucrase and 4- α -glucanotransferase. *Journal of Agricultural and Food chemistry* 59:5044-5051.

- Larsen K.L. (2002) Large Cyclodextrins. *Journal of Inclusion Phenomena and Macrocyclic Chemistry* 43:1-13. DOI: 10.1023/a:1020494503684.
- Lee B.H., Oh D.K., Yoo S.H. (2009) Characterization of 4- α -glucanotransferase from *Synechocystis* sp. PCC 6803 and its application to various corn starches. *New Biotechnology* 26:29-36.
- MacGregor E.A., Janeček Š., Svensson B. (2001) Relationship of sequence and structure to specificity in the α -amylase family of enzymes. *Biochimica et Biophysica Acta (BBA)-Protein Structure and Molecular Enzymology* 1546:1-20.
- Machida S., Ogawa S., Xiaohua S., Takaha T., Fujii K., Hayashi K. (2000) Cycloamylose as an efficient artificial chaperone for protein refolding. *FEBS letters* 486:131-135.
- Manners D., Rowe K.L. (1969) Studies on carbohydrate-metabolising enzymes: Part XXI. The α -glucosidase and d-enzyme activity of extracts of carrots and tomatoes. *Carbohydrate Research* 9:441-450.
- McDonald I.K., Thornton J.M. (1994) Satisfying hydrogen bonding potential in proteins. *Journal of Molecular Biology* 238:777-793.
- Miwa I., Okuda J., Maeua K., Okuda G. (1972) Mutarotase effect on colorimetric determination of blood glucose with β -D-glucose oxidase. *Clinica Chimica Acta* 37:538-540.
- Mun S., Rho S.J., Kim Y.R. (2009) Study of inclusion complexes of cycloamylose with surfactants by isothermal titration calorimetry. *Carbohydrate Polymers* 77:223-230.

- Nelson D.L., Lehninger A.L., Cox M.M. (2008) *Lehninger Principles of Biochemistry* Macmillan.
- Nimpiboon P., Kaulpiboon J., Krusong K., Nakamura S., Kidokoro S.-i., Pongsawasdi P. (2016a) Mutagenesis for improvement of activity and thermostability of amyloamylase from *Corynebacterium glutamicum*. *International Journal of Biological Macromolecules* 86:820-828.
- Nimpiboon P., Krusong K., Kaulpiboon J., Kidokoro S.-i., Pongsawasdi P. (2016b) Roles of N287 in catalysis and product formation of amyloamylase from *Corynebacterium glutamicum*. *Biochemical and Biophysical Research Communications*.
- O'Neill E.C., Stevenson C.E., Tantanarat K., Latousakis D., Donaldson M.I., Rejzek M., Nepogodiev S.A., Limpaseni T., Field R.A., Lawson D.M. (2015) Structural dissection of the maltodextrin disproportionation cycle of the arabidopsis plastidial disproportionating enzyme 1 (DPE1). *Journal of Biological Chemistry* 290:29834-29853.
- Okita T.W., Greenberg E., Kuhn D.N., Preiss J. (1979) Subcellular localization of the starch degradative and biosynthetic enzymes of spinach leaves. *Plant Physiology* 64:187-192.
- Park J.H., Kim H.J., Kim Y.H., Cha H., Kim Y.W., Kim T.J., Kim Y.R., Park K.H. (2007) The action mode of *Thermus aquaticus* YT-1 4- α -glucanotransferase and its chimeric enzymes introduced with starch-binding domain on amylose and amylopectin. *Carbohydrate Polymers* 67:164-173.

- Peat S., Whelan W., Rees W. (1956) 10. The enzymic synthesis and degradation of starch. Part XX. The disproportionating enzyme (D-enzyme) of the potato. *Journal of the Chemical Society (Resumed)*:44-53.
- Przylas I., Terada Y., Fujii K., Takaha T., Saenger W., Sträter N. (2000a) X-ray structure of acarbose bound to amylomaltase from *Thermus aquaticus*. *European Journal of Biochemistry* 267:6903-6913.
- Przylas I., Tomoo K., Terada Y., Takaha T., Fujii K., Saenger W., Sträter N. (2000b) Crystal structure of amylomaltase from *Thermus aquaticus*, a glycosyltransferase catalysing the production of large cyclic glucans. *Journal of Molecular Biology* 296:873-886.
- Rachadech W., Nimpiboon P., Naumthong W., Nakapong S., Krusong K., Pongsawasdi P. (2015) Identification of essential tryptophan in amylomaltase from *Corynebacterium glutamicum*. *International Journal of Biological Macromolecules* 76:230-235.
- Robyt J.F., Ackerman R.J. (1971) Isolation, purification, and characterization of a maltotetraose-producing amylase from *Pseudomonas stutzeri*. *Archives of Biochemistry and Biophysics* 145:105-114.
- Roth C., Weizenmann N., Bexten N., Saenger W., Zimmermann W., Maier T., Sträter N. (2017) Amylose recognition and ring-size determination of amylomaltase. *Science advances* 3:e1601386.
- Roujeinikova A., Raasch C., Sedelnikova S., Liebl W., Rice D.W. (2002) Crystal structure of *Thermotoga maritima* 4- α -glucanotransferase and its acarbose complex: implications for substrate specificity and catalysis. *Journal of Molecular Biology* 321:149-162.

- Rudeekulthamrong P., Sawasdee K., Kaulpiboon J. (2013) Production of long-chain isomaltooligosaccharides from maltotriose using the thermostable amyloamylase and transglucosidase enzymes. *Biotechnology and Bioprocess Engineering* 18:778-786.
- Saehu S., Srisimarat W., Prousoontorn M.H., Pongsawasdi P. (2013) Transglucosylation reaction of amyloamylase for the synthesis of anticariogenic oligosaccharides. *Journal of Molecular Catalysis B: Enzymatic* 88:77-83.
- Sambrook J., Russell D.W. (2006) Transformation of *E. coli* by electroporation. *Cold Spring Harbor Protocols* 2006:pdb. prot3933.
- Seibold G., Dempf S., Schreiner J., Eikmanns B.J. (2007) Glycogen formation in *Corynebacterium glutamicum* and role of ADP-glucose pyrophosphorylase. *Microbiology* 153:1275-1285.
- Seibold G.M., Eikmanns B.J. (2007) The *glgX* gene product of *Corynebacterium glutamicum* is required for glycogen degradation and for fast adaptation to hyperosmotic stress. *Microbiology* 153:2212-2220.
- Seibold G.M., Wurst M., Eikmanns B.J. (2009) Roles of maltodextrin and glycogen phosphorylases in maltose utilization and glycogen metabolism in *Corynebacterium glutamicum*. *Microbiology* 155:347-358.
- Smith S.M., Fulton D.C., Chia T., Thorneycroft D., Chapple A., Dunstan H., Hylton C., Zeeman S.C., Smith A.M. (2004) Diurnal changes in the transcriptome encoding enzymes of starch metabolism provide evidence for both transcriptional and posttranscriptional regulation of starch metabolism in arabidopsis leaves. *Plant Physiology* 136:2687-2699.

- Sokalingam S., Raghunathan G., Soundrarajan N., Lee S.-G. (2012) A study on the effect of surface lysine to arginine mutagenesis on protein stability and structure using green fluorescent protein. *PLOS ONE* 7:e40410.
- Srisimararat W., Kaulpiboon J., Krusong K., Zimmermann W., Pongsawasdi P. (2012) Altered large-ring cyclodextrin product profile due to a mutation at Tyr-172 in the amyloamylase of *Corynebacterium glutamicum*. *Applied and Environmental Microbiology* 78:7223-7228.
- Srisimararat W., Murakami S., Pongsawasdi P., Krusong K. (2013) Crystallization and preliminary X-ray crystallographic analysis of the amyloamylase from *Corynebacterium glutamicum*. *Acta Crystallographica Section F: Structural Biology and Crystallization Communications* 69:1004-1006.
- Srisimararat W., Powviriyakul A., Kaulpiboon J., Krusong K., Zimmermann W., Pongsawasdi P. (2011) A novel amyloamylase from *Corynebacterium glutamicum* and analysis of the large-ring cyclodextrin products. *Journal of Inclusion Phenomena and Macrocyclic Chemistry* 70:369-375.
- STASsI D.L., Lopez P., Espinosa M., Lacks S.A. (1981) Cloning of chromosomal genes in *Streptococcus pneumoniae*. *Proceedings of the National Academy of Sciences* 78:7028-7032.
- Strater N., Przylas I., Saenger W., Terada Y., Fuji K., Takaha T. (2002) Structural basis of the synthesis of large cycloamyloses by amyloamylase. *Biologia-Bratislava* - 57:93-100.

- Taira H., Nagase H., Endo T., Ueda H. (2006) Isolation, Purification and Characterization of Large-Ring Cyclodextrins (CD36-CD39). *Journal of Inclusion Phenomena and Macrocyclic Chemistry* 56:23-28. DOI: 10.1007/s10847-006-9055-8.
- Takaha T., Smith S.M. (1999) The functions of 4- α -glucanotransferases and their use for the production of cyclic glucans. *Biotechnology and Genetic Engineering Reviews* 16:257-280.
- Tang S.Y., Yang S.J., Cha H., Woo E.J., Park C., Park K.H. (2006) Contribution of W229 to the transglycosylation activity of 4- α -glucanotransferase from *Pyrococcus furiosus*. *Biochimica et Biophysica Acta (BBA)-Proteins and Proteomics* 1764:1633-1638.
- Tantanarat K., O'Neill E.C., Rejzek M., Field R.A., Limpaseni T. (2014) Expression and characterization of 4- α -glucanotransferase genes from *Manihot esculenta* Crantz and *Arabidopsis thaliana* and their use for the production of cycloamyloses. *Process Biochemistry* 49:84-89.
- Terada Y., Fujii K., Takaha T., Okada S. (1999) *Thermus aquaticus* ATCC 33923 amyloamylase gene cloning and expression and enzyme characterization: production of cycloamylose. *Applied and Environmental Microbiology* 65:910-915.
- Todd M.J., Gomez J. (2001) Enzyme kinetics determined using calorimetry: a general assay for enzyme activity *Analytical Biochemistry* 296:179-187.
- Transtrum M.K., Hansen L.D., Quinn C. (2015) Enzyme kinetics determined by single-injection isothermal titration calorimetry. *Methods* 76:194-200.

- Van der Maarel M., Euverink G., Binnema D., Bos H.T.P., Bergsma J. (2000) Amylomaltase from the hyperthermophilic bacterium *Thermus thermophilus*: enzyme characteristics and application in the starch industry. Mededelingen-Faculteit Landbouwkundige en Toegepaste Biologische Wetenschappen, Universiteit Gent 65:231-234.
- Van der Maarel M.J., Van Der Veen B., Uitdehaag J.C., Leemhuis H., Dijkhuizen L. (2002) Properties and applications of starch-converting enzymes of the α -amylase family. Journal of Biotechnology 94:137-155.
- van der Veen B.A., Leemhuis H., Kralj S., Uitdehaag J.C., Dijkstra B.W., Dijkhuizen L. (2001) Hydrophobic amino acid residues in the acceptor binding site are main determinants for reaction mechanism and specificity of cyclodextrin-glycosyltransferase. Journal of Biological Chemistry 276:44557-44562.
- Vertès A.A., Inui M., Yukawa H. (2005) Manipulating corynebacteria, from individual genes to chromosomes. Applied and Environmental Microbiology 71:7633-7642.
- Voet D., Voet J.G., Pratt C.W. (1999) Fundamentals of Biochemistry Wiley New York.
- Weiss S.C., Skerra A., Schiefner A. (2015) Structural basis for the interconversion of maltodextrins by MalQ, the amyloamylase of *Escherichia coli*. Journal of Biological Chemistry 290:21352-21364.
- Wolf A., Krämer R., Morbach S. (2003) Three pathways for trehalose metabolism in *Corynebacterium glutamicum* ATCC13032 and their significance in response to osmotic stress. Molecular Microbiology 49:1119-1134. DOI: 10.1046/j.1365-2958.2003.03625.x.

- Xavier K.B., Peist R., Kossmann M., Boos W., Santos H. (1999) Maltose metabolism in the hyperthermophilic archaeon *Thermococcus litoralis*: purification and characterization of key enzymes. *Journal of Bacteriology* 181:3358-3367.
- Zheng M., Endo T., Zimmermann W. (2002) Enzymatic synthesis and analysis of large-ring cyclodextrins. *Australian Journal of Chemistry* 55:39-48.
- Zhu H.X., Shi Y., Zhang Q.N., Chen Y.L. (2005) Applying 3, 5-dinitrosalicylic Acid (DNS) Method to Analyzing the Content of Potato Reducing Sugar [J]. *Chinese Potato* 5.



APPENDICES



จุฬาลงกรณ์มหาวิทยาลัย
CHULALONGKORN UNIVERSITY

APPENDIX 1: Preparation of polyacrylamide gel electrophoresis**1) Stock reagents****30% acrylamide, 0.8% bis-acrylamide, 100 ml**

Acrylamide 29.2 g

N, N-methylene-bis-acrylamide 0.8 g

Adjusted volume to 100 ml with distilled water

1.5 M Tris-HCl pH 8.8

Tris (hydroxymethyl)-aminomethane 18.2 g

Adjusted pH to 8.8 with 1 M HCl and adjusted volume to 100 ml with distilled water

2 M Tris-HCl pH 8.8

Tris (hydroxymethyl)-aminomethane 24.2 g

Adjusted pH to 8.8 with 1 M HCl and adjusted volume to 100 ml with distilled water

0.5 M Tris-HCl pH 6.8

Tris (hydroxymethyl)-aminomethane 6.06 g

Adjusted pH to 6.8 with 1 M HCl and adjusted volume to 100 ml with distilled water

1 M Tris-HCl pH 6.8

Tris (hydroxymethyl)-aminomethane 12.1 g

Adjusted pH to 6.8 with 1 M HCl and adjusted volume to 100 ml with distilled water

Solution B (SDS-PAGE)

2 M Tris-HCl pH 8.8	75 ml
10% SDS	4 ml
Distilled water	21 ml

Solution C (SDS-PAGE)

1 M Tris-HCl pH 6.8	50 ml
10% SDS	4 ml
Distilled water	46 ml

2) Denaturing PAGE (SDS-PAGE)**10% separating gel**

30% Acrylamide solution	2.50 ml
Solution B (SDS-PAGE)	2.50 ml
Distilled water	2.39 ml
10% $(\text{NH}_4)_2\text{S}_2\text{O}_8$	100 μl
TEMED	10 μl

5% stacking gel

30% Acrylamide solution	0.84 ml
Solution C (SDS-PAGE)	1.0 ml
Distilled water	3.1 ml
10% $(\text{NH}_4)_2\text{S}_2\text{O}_8$	50 μl
TEMED	10 μl

5X sample buffer

1 M Tris-HCl pH 6.8	0.6 ml
50% Glycerol	5.0 ml
10% SDS	2.0 ml
2-Mercaptoethanol	0.5 ml
1% Bromophenol blue	1.0 ml
Distilled water	0.9 ml

One part of sample buffers was added to four parts of sample. The mixture was boiled for 5 min prior to loading to the gel.

Electrophoresis (TBE) buffer, 1 litre

Tris (hydroxymethyl)-aminomethane	3 g
Glycine	14.4 g
SDS	1.0 g

Adjusted volume to 1 litre with distilled water (pH should be approximately 8.3)

Coomassie Gel Stain, 1 litre

Coomassie Blue R-250	1 g
Methanol	450 ml
Distilled water	450 ml
Glacial acetic acid	100 ml

Coomassie Gel Destain, 1 liter

Methanol	100 ml
Glacial acetic acid	100 ml
Distilled water	800 ml

Adjusted volume to 100 ml with distilled water, adjusted to pH 4.0, 5.0 or 6.0 by 0.2 M acetic acid.

APPENDIX 2: Preparation of agarose electrophoresis**Stock Tris-boric acid (TBE) solution (10X)**

Tris (hydroxymethyl)-aminomethane	108 g
Boric acid	55 g
0.5 M EDTA	40 ml

Adjusted volume to 1 litre with distilled water

APPENDIX 3: Preparation for buffers solutions**0.2 M Sodium Acetate pH 4.0, 5.0 and 6.0**

CH ₃ COONa	1.21 g
-----------------------	--------

Adjusted volume to 100 ml with distilled water and adjusted pH to pH 4.0, 5.0 and 6.0 by 0.2 M acetic acid

0.2 M Phosphate buffer pH 6.0

KH_2PO_4	3.28 g
K_2HPO_4	0.16 g
Distilled water	100 ml

0.2 M Phosphate buffer pH 7.0

KH_2PO_4	1.35 g
K_2HPO_4	1.67 g
Distilled water	100 ml

0.2 M Phosphate buffer pH 8.0

KH_2PO_4	0.48 g
K_2HPO_4	2.34 g
Distilled water	100 ml

0.2 M Tris-Glycine NaOH pH 8.0, 9.0 and 10.0

Glycine	1.5 g
---------	-------

Adjusted to pH 8.0, 9.0 and 10.0 by 1 M NaOH and adjusted volume to 100 ml with distilled water

APPENDIX 4: Preparation of solution for cell preparation and enzyme purification

1) Stock solution

1 M Monopotassium phosphate 100 ml

The pellet of Monopotassium phosphate 13.6 g was dissolved in distilled water to final volume 100 ml

1 M Dipotassium hydrogen phosphate 100 ml

The pellet of Dipotassium hydrogen phosphate 87.1 g was dissolved in distilled water to final volume 500 ml

1 M Potassium phosphate buffer, pH 7.4

1 M Potassium phosphate buffer, pH 7.4 was prepared by mixing 1 M of monopotassium phosphate and 1 M dipotassium hydrogen phosphate and then pH was adjusted to pH 7.4.

2) Extraction buffer

1 M Potassium phosphate buffer, pH 7.4	5.0 ml
0.1 M PMSF in 95% absolute ethanol	0.1 ml
100% (v/v) β -mercaptoethanol	10 μ l
0.5 M EDTA	0.2 ml
Adjusted volume to 100 ml with distilled water	

3) 0.85% NaCl

Sodium chloride	0.85 g
Adjusted volume to 100 ml with distilled water	

4) Binding buffer

Imidazole	0.3 g
Sodium chloride	5.8 g
1 M Potassium phosphate buffer, pH 7.4	4.0 ml
Adjusted pH to pH 7.4 with 1 N HCl and adjusted volume to 200 ml with distilled water	

5) Elution buffer

Imidazole	6.8 g
Sodium chloride	5.8 g
1 M Potassium phosphate buffer, pH 7.4	4.0 ml
Adjusted pH to pH 7.4 with 1 N HCl and adjusted volume to 200 ml with distilled water	

APPENDIX 5: Preparation of Iodine solution**10X Iodine stock solution 100 ml**0.2% (w/v) I₂ in 2.0% (w/v) KI

Potassium iodide	2 g
Iodine	0.2 g

1X Iodine solution 100 ml

0.2% (w/v) I ₂ in 2.0% (w/v) KI	10 ml
Distilled water	90 ml

APPENDIX 6: Preparation of Bradford solution (Bollag and Edelstein, 1999)

1) Stock solution

Ethanol	100 ml
Phosphoric acid	200 ml
Coomassie blue G-250	350 mg

Stable indefinite at room temperature with stirring overnight and filtration by Whatman No.1 paper.

2) Working solution

Ethanol	15 ml
Phosphoric acid	30 ml
Stock solution	30 ml
Distilled water	425 ml

Store at room temperature in brown glass bottle.

APPENDIX 7: Preparation for Bicinchoninic acid (BCA) assay

Bicinchoninic acid reagent

Solution A

4, 4'-dicarboxy-2, 2'-biquinoline	0.130 g
-----------------------------------	---------

Dissolved in 85 ml of distilled water

Na ₂ CO ₃	6.221 g
---------------------------------	---------

Adjusted to 100 ml with distilled water

Solution B

Component 1

L-aspartic acid 0.642 g

Na₂CO₃ 0.868 g

Dissolved in 15 ml of distilled water

Component 2

CuSO₄ 0.174 g

Dissolved in 5 ml of distilled water

Mixed component 1 and 2, then adjusted volume to 25 ml with distilled water

Mixed 24 ml of solution A and 1 ml of solution B and used within 24 h

APPENDIX 8: Preparation for DNS reagent**DNS reagent**

2-hydroxy-3, 5'-dinitrobenzoic acid 5 g

2 N NaOH 100 ml

Potassium sodium tartrate 150 g

Adjusted volume to 500 ml with distilled water

APPENDIX 9: Bacterial media culture**LB (Luria-Bertani) medium and plate**

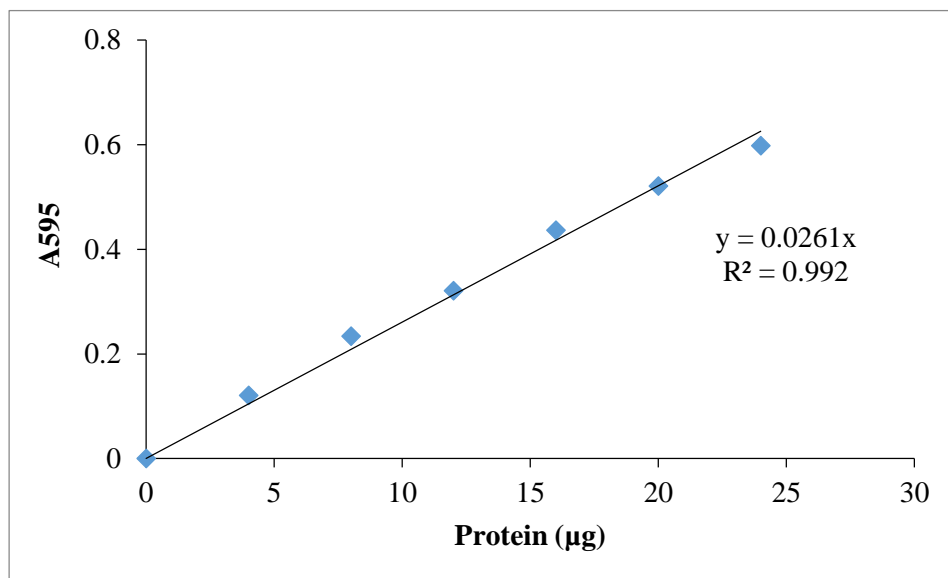
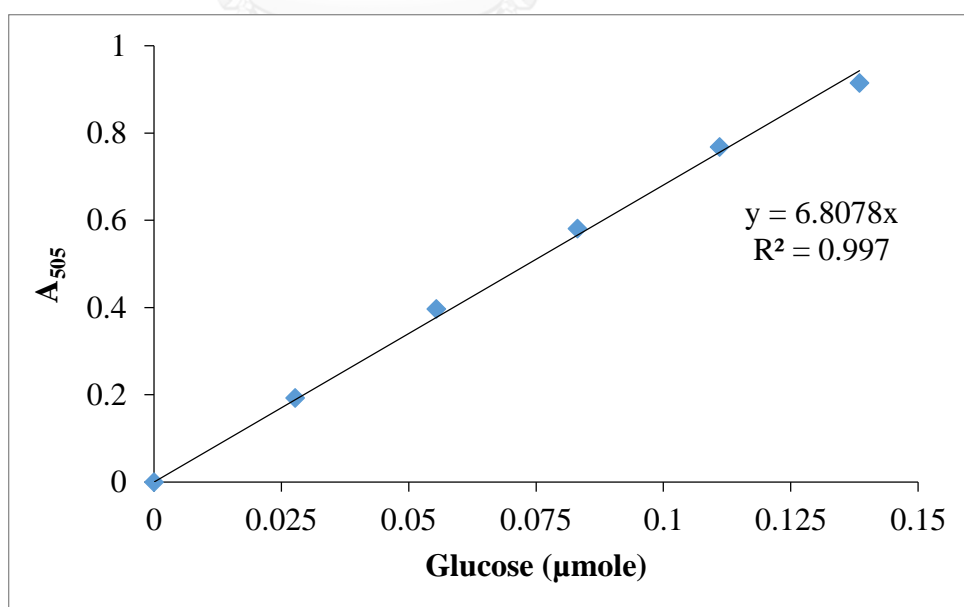
Tryptone	10 g
Yeast extract	5 g
NaCl	5 g

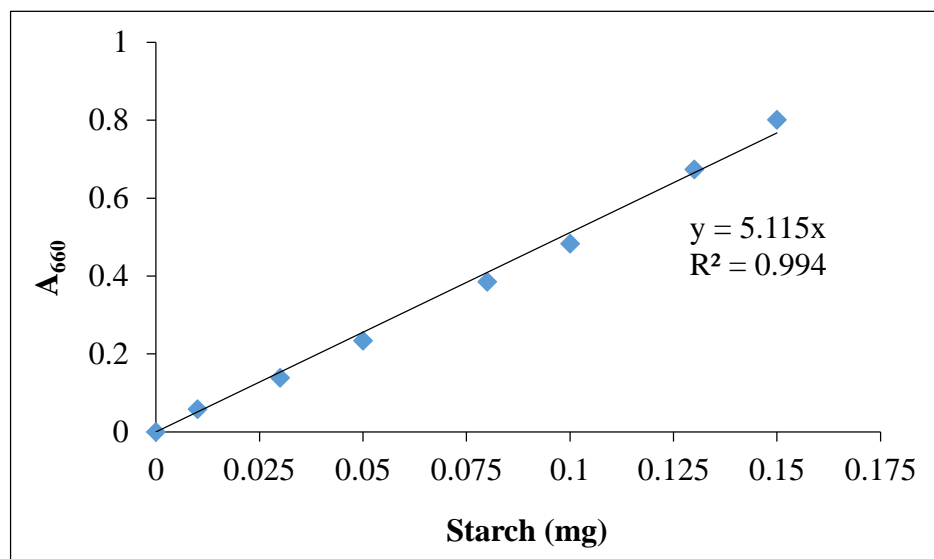
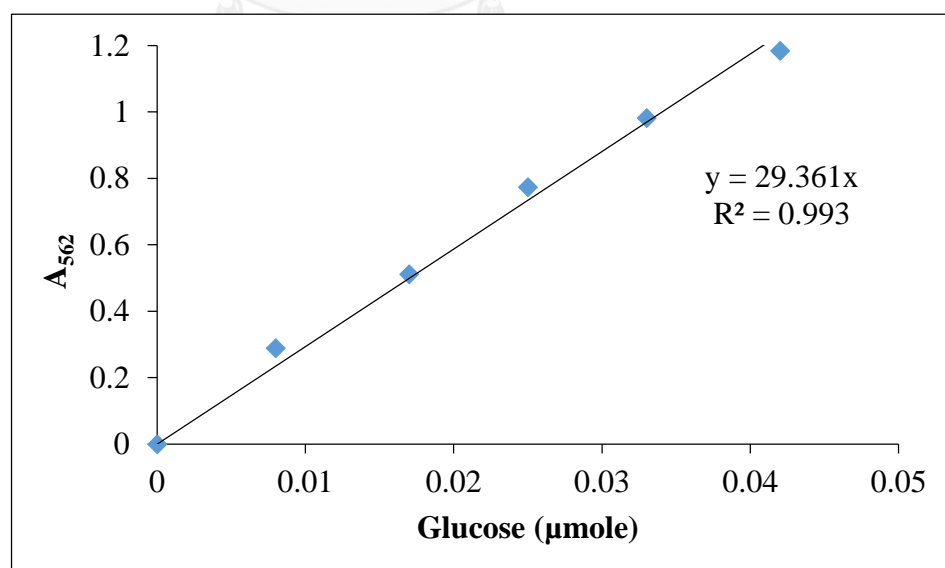
Adjusted volume to 1,000 ml with distilled water (15 g/l of bacteria agar was added for plate). The medium were sterilized by autoclaving at 15 lb/in² for 15 min.

APPENDIX 10: Ampicillin antibiotic**100 mg/ml of ampicillin**

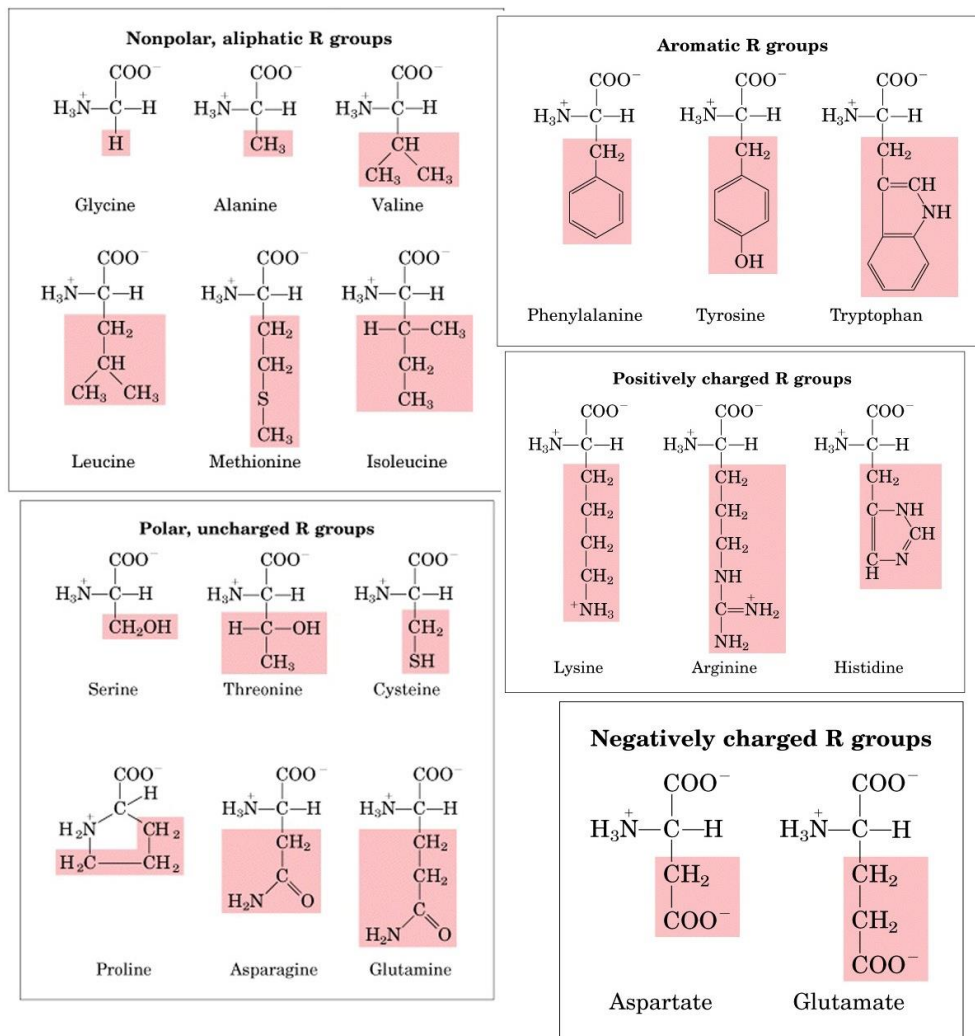
Ampicillin	1 g
Autoclaved distilled water	10 ml

An aliquot of 100 mg/ml of ampicillin was stored at -20 °C for long time.

APPENDIX 11: Standard curve for protein determination by Bradford's method**APPENDIX 12: Standard curve for glucose determination by glucose oxidase assay**

APPENDIX 13: Standard curve for starch degrading activity assay**APPENDIX 14: Standard curve for glucose determination by Bicinchoninic acid assay**

APPENDIX 16: Structure of amino acids commonly found in protein



APPENDIX 17: Abbreviation of amino acid residues (Voet, 1990)

Amino acid	3 Letter-Abbreviation	1 Letter-Abbreviation
Alanine	Ala	A
Arginine	Arg	R
Asparagine	Asn	N
Aspartic acid	Asp	D
Cysteine	Cys	C
Glutamine	Gln	Q
Glutamic acid	Glu	E
Glycine	Gly	G
Histidine	His	H
Isoleucine	Ile	I
Leucine	Leu	L
Lysine	Lys	K
Methionine	Met	M
Phenylalanine	Phe	F
Proline	Pro	P
Serine	Ser	S
Threonine	Thr	T
Tryptophan	Try	W
Tyrosine	Trp	Y
valine	val	V
Unknown	-	X

APPENDIX 18: Amino acid sequences alignment of amyломaltases

<i>StDPE1</i>	-----	0
<i>AtDPE1</i>	-----	0
<i>SpAM</i>	-----	0
<i>TaAM</i>	-----	0
<i>TtAM</i>	-----	0
<i>CgAM</i>	MTARRFLNELADLYGVATS YTDYKGAHIEVSDDTLVKILRALGVNLDTSNLPNDDAIQRQ	60
<i>EcAM</i>	MESKR-LDNAALAAGISPNYINAHGKPKQSISAETKRRL-----	38
<i>StDPE1</i>	-----MA-----IHTCFSLIPSSFSFKLPYPKNTTFQSP-----	30
<i>AtDPE1</i>	-----MSILLRPSSSPSLCSSLKFLRLLSPDS-----LIDAAV-----	33
<i>SpAM</i>	-----	0
<i>TaAM</i>	-----	0
<i>TtAM</i>	-----	0
<i>CgAM</i>	IALFHDRE---FTRPLPPSVV-----AVEGDELVFPVHVHDGSPADVHIELEDGTQR	109
<i>EcAM</i>	-DAMHQRTATKVAVTPVPMVMV-----YTSKKM--PMVVEGSGEYSWLLTTE-----	83
<i>StDPE1</i>	----IPKLSRPTFMFDRKG-SFQNGTAAVPAVGEDFPIDYAD-----	67
<i>AtDPE1</i>	----LRNRTKPSQSFMRMEVSSNSTCLSSISVGEDFPSEYEQ-----	71
<i>SpAM</i>	-----	0
<i>TaAM</i>	-----	0
<i>TtAM</i>	-----	0
<i>CgAM</i>	DVSQVENWTAPREI---DGIR---WGEASFKIPGDLPLGWHKHLKSNERSAECGLIITP	163
<i>EcAM</i>	-----EGTQY---KGHV---TGGKAFNLPTKLPYHTLTLTQEDQRAHCRVIVAP	128
<i>StDPE1</i>	---WLPKRDPNDRRRAGILLHPTSFPG--PYGIGDLGFPQAFKFLDWLHLAGCSLWQVLPL	122
<i>AtDPE1</i>	---WLPVPDPESRRRAGVLLHPTSFRG--PHGIGDLGEEAFRFIDWLHSTGCSVWQVLPL	126
<i>SpAM</i>	-----MKKRQSGVLMHISLSPG--AYGIGSFGQSAYDFVDFLVRTKQRYWQILPL	48
<i>TaAM</i>	-----MELPRAFGLLLHPTSPLG--PYGVVGLGLEARDFLRFLKGAGGRFVQVLPL	49
<i>TtAM</i>	-----MELPRAFGLLLHPTSPLG--PYGVVGLGREARDFLRFLKEAGGRYVQVLPL	49
<i>CgAM</i>	ARLSTADKYLDSP-RSGVMAQIYSVRSTLSWGMGDFNDLGNLAS-VVAQDGADFLINPM	221
<i>EcAM</i>	KRCYEPQALLNKQKLGACVQLYTLRSEKNWIGDFGDLKAMLV-DVAKRGGSFIGLNP I	187
*	: : . . * : * : . . : : * :	
<i>StDPE1</i>	VPPGKRGNEGSPYSGQDANCGNTLLISLEELVDDGLLKMEEL-----P---EPLPT	171
<i>AtDPE1</i>	VPPD---EGGSPYAGQDANCGNTLLISLDELVKDGLLIKDEL-----P---QPIDA	171
<i>SpAM</i>	GATS---YGDSPYQSFSAFAGNTHFIDLDELVEQGLEASDL-----EGVDFGSDA	96
<i>TaAM</i>	GPTG---YGDSPYQAFSAFAGNPYLIDLRPLAEKGYLVLKD-----PGFPQ	92
<i>TtAM</i>	GPTG---YGDSPYQSFSAFAGNPYLIDLRPLAERGYVRLD-----PGFPQ	92
<i>CgAM</i>	HAAEPLPPTEDSPYLPTRRFINPIYIRVEDIPEFNQLEIDLRRDIAEMAAEFRRNLTS	281
<i>EcAM</i>	HALYPANPESASPYSPSSRRWLNVIYIDVNAVEDFHLSEEAQAWWQLPPTQQTQQARDA	247
***	* * : : . .	

StDPE1 = Disproportionating enzyme from *Solonum tuberculsum*, *AtDPE1* = Disproportionating enzyme from *Arabidopsis thaliana*, *SpAM* = Amylomaltase from *Streptococcus pneumonia*, *TaAM* = Amylomaltase from *T. aquaticus*, *TtAM* = Amylomaltase from *T. thermophilus*, *CgAM* = Amylomaltase from *C. glutamicum* and *EcAM* = Amylomaltase from *E.coli*

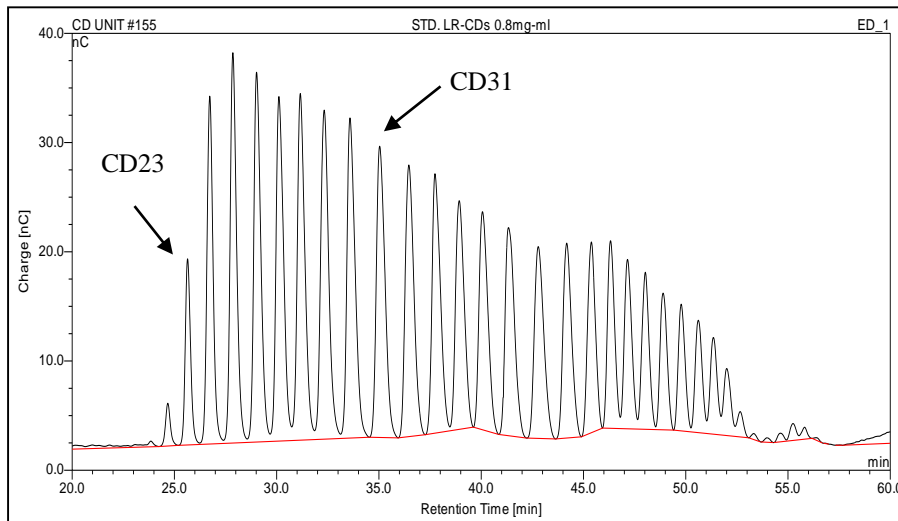
<i>StDPE1</i>	DRVNYSTISEIKDPLITKAAKRLLSSEGE-LKDQLENFRDPN-ISSWLEDAAYFAA--I	227
<i>AtDPE1</i>	DSVNYQTANKLKSPLITKAAKRLIDGNGE-LSKLLDFRNDPS-ISCWLEDAAYFAA--I	227
<i>SpAM</i>	SEVDYAKIYYARRPILLEKAVKRFEEVGD--VKDFEKFAQ--D-NQSWLELFAEYMA--I	148
<i>TaAM</i>	GRVDYGLWLYAWKWPALKAAAYQGFLKAPRKEREDFPAPQE--K-EASWLKDYALFMA--L	147
<i>TtAM</i>	GRVDYGLLYAWKWPALKEAFRGFKKASPEEREAFAAFRE--R-EAWWLEDYALFMA--L	147
<i>CgAM</i>	DI IERNVDVYAAKLQVLRIFE--MPSRSEER-EANFVSVFVQREGQGLI-----	325
<i>EcAM</i>	DWVDYSTVTALKMTALRMAWKGFQRDDEQ-MAAFRQFVADHGDSLFWQAALHAHQV	306
	. : : . : : . : *	
<i>StDPE1</i>	DNSVNTISWYDWPEPLK-NRHLSALEEIVYQSEKDFIDIFIAQQFLFQRQWKKVRDYARSK	286
<i>AtDPE1</i>	DNTLNAYSWFEWPEPLK-NRHLSALEAIYESQKEFIDLFIKQFLFQRQWQKVRDYARRQ	286
<i>SpAM</i>	KEYFDNLAWTEWPDADARARKSALESYREQLADKLVYHRVTQYFFFQWLKLYAYANDN	208
<i>TaAM</i>	KAQHGGFLPWNRWPLPLR-RREEKAMKEAEAAALAEVAFHAWTQWLFFEAWKALKEEAEAL	206
<i>TtAM</i>	KGAHGGLPWNRWPLPLR-KREKALREAKSALAEVAFHAWTQWLFFRQWGLKAEAEAL	206
<i>CgAM</i>	-----DFATWCADRE-TAQSESVHGTEPDRDELTMFYMWLQWLCDEQLAAAQKRAVDA	377
<i>EcAM</i>	KEDEMWRGWPAWPEMYQ-NVDSPEVRQFCEEHRDDVDFYLWLQWLAYSQFAACWEISQGY	365
	: * . : . : * : :	
<i>StDPE1</i>	--GISIMGDMP IYVGYHSADVWANKKQFLLRKGFPLIVSGVPPDAFSETGQLWGSPLYD	344
<i>AtDPE1</i>	--GVDIMGDMP IYVGYHSADVWANKKHFLLNKKGFPLLVSGVPPDLFSETGQLWGSPLYD	344
<i>SpAM</i>	--HIEIVGDMP IYVAEDSSDMWANPHLFKTDVNGKATCIAGCPPDEFVSTGQLWGNPIYD	266
<i>TaAM</i>	--GIQIIGDMP IFVAEDSAEVWAHPWFHLDDEGRPLVVAGVPPDYFSETGQRWGNPLYR	264
<i>TtAM</i>	--GIRIIGDMP IFVAEDSAEVWAHPWFHLDDEGRPTVVAGVPPDYFSETGQRWGNPLYR	264
<i>CgAM</i>	GMSIGIMADLAVGVHPGGADAQNLSHVLAPD-----ASVGAPPDGYNQGGDWSQPPWH	431
<i>EcAM</i>	EMPIGLYRDLAVGVAEGGAETWCDRELYCLK-----ASVGAPPDILGPLGQNWGLPPMD	419
	: : * : * . : : . * * * * . * * * . *	
<i>StDPE1</i>	WKAMEKDGFSWVWRRIQRATDLDFDEFRIDHFRGFAGFWAVPSEEKIAILGRWKVGP GKPL	404
<i>AtDPE1</i>	WKAMESDQYSWVWNRIIRAQDLYDECRIDHFRGFAGFWAVPSEAKVAMVGRWKVGP GKSL	404
<i>SpAM</i>	WEAMDKDGYKWWIERLRESFKIYDIVRIDHFRGFESYWEIPAGSDTAAPGEWVKGPGYKL	326
<i>TaAM</i>	WDVLEREGFSFWIARLAKALELPHLVRVDHFRGFAYWEIPASCPTAVEGRWVKASGEKL	324
<i>TtAM</i>	WDVLEREGFSFWIRRLEKALELPHLVRVDHFRGFAYWEIPASCPTAVEGRWVKAPGEKL	324
<i>CgAM</i>	PVRLAEEGYIPWRNLLRTVLRHSGGIRVDHVLGLFRLFVMPRMQ-SPATGTYIRFDHNAL	490
<i>EcAM</i>	PHIITARAYEPFIELLRANMONGALRIDHVMMLRLWVWIPYGE-TADQGAYVHYPVDDL	478
	: : : : * : * . : : * * :	
<i>StDPE1</i>	FD--AILQAVGKINIIAEDLGVITEDVVQLRKSIEAPGMAVLQFAFGSDAENPHLPHNHE	462
<i>AtDPE1</i>	FD--AISKGVGKIKIIAEDLGVITKDVVELRKSIGAPGMAVLQFAFGGADNPHLPHNHE	462
<i>SpAM</i>	FA--AVKEELGELNIIAEDLGFMTDEVIELRERTGFPGMKILQFAFNPEDESIDSPLHAP	384
<i>TaAM</i>	FD--RIQEVFGEVPIAEDLGVITPEVEPLRDRYGLPGMKVLQFAFDHGMENPFLPHNYP	382
<i>TtAM</i>	FQ--KIQEVFGEVPIAEDLGVITPEVEALRDRFGLPGMKVLQFAFDHGMENPFLPHNYP	382
<i>CgAM</i>	VGILALEAEALAGAVVIGEDLGTFFPWWQDALAQRGIMGTSILWFEHSPPQPPRRQEEYR	550
<i>EcAM</i>	LSILALESKRHRMVGEDLGTVPVEIVGKLRSSGVYSYKVLVYFENDHEK-TFRSPKAYP	537
	. : : : * * * * . : : * * .	

(Continued) *StDPE1* = Disproportionating enzyme from *Solonum tuberculsum*, *AtDPE1* = Disproportionating enzyme from *Arabidopsis thaliana*, *SpAM* = Amylomaltase from *Streptococcus pneumonia*, *TaAM* = Amylomaltase from *T. aquaticus*, *TtAM* = Amylomaltase from *T. thermophilus*, *CgAM* = Amylomaltase from *C. glutamicum* and *EcAM* = Amylomaltase from *E.coli*

<i>StDPE1</i>	Q--NQVVYTGTHDNDTIRGWWDTLPQE-EKSNVLKYLNS-----IEEEEISR-----	506
<i>AtDPE1</i>	V--NQVVYSGTHDNDTIRGWWDTLDQE-EKSKAMKYLSI-----AGEDDISW-----	506
<i>SpAM</i>	A--NSVMYTGTHDNDTTLGWYRNEIDDATREYMARYTNR-----KEYETVVH-----	429
<i>TaAM</i>	AHGRVVVYTGTHDNDTTLGWYRTASPH-ERAFLELYLADWGISFRQEEVVPW-----	433
<i>TtAM</i>	AHGRVVVYTGTHDNDTTLGWYRTATPH-EKAFMARYLADWGITFREEEVPW-----	433
<i>CgAM</i>	P--LALTVTTHDLPPTAGYLEGEHIALR-ERLGVLNTPAAE-L-AEDLQW-QAEILDV	604
<i>EcAM</i>	E--QSMAVAATHDLPPLRGYWESGDLTLG-KTLGLYPDEVVLR-GLYQDRELAKQGLLDA	593
	: *** *:	
<i>StDPE1</i>	-----GLIEGAVSSVARIAIIPMQDVLGLGSDSRMNI	538
<i>AtDPE1</i>	-----SVIQAAFSSSTAQTAIIPMQDILGLGSSARMNT	538
<i>SpAM</i>	-----AMLRVTFSSVSFMAIATMQDLLELDEAARMNF	461
<i>TaAM</i>	-----ALMGLCLKSVARLAIYPVQDVLALGSEARMNY	465
<i>TtAM</i>	-----ALMHLGMKSVARLAVYPVQDVLALGSEARMNY	465
<i>CgAM</i>	AASANALPAREYVGLERDQRGELAELEGLHTFVAK--TPSALTCVCLVDMVGKRAQNQ	662
<i>EcAM</i>	LHKYGCLLKR--AGHKASLMSMTPTLNRLQRYIAD--SNSALLGLQPEDWLDMAEPVNI	649
	.: . : * : : : . *	
<i>StDPE1</i>	PATQ---FGNWSWRIPSSTSFNDLDAEAKKLR---DILATYGR-----	576
<i>AtDPE1</i>	PATE---VGNWGWRIPSSTSFNDLETSRDLR---DLSLYGR-----	576
<i>SpAM</i>	PSTL---GGNWSWRMTEDQLTP---AVEEGLL---DLTTIYRRINENLVDLKK	505
<i>TaAM</i>	PGRP---SGNWAWRLLPGQLTQ---EHAARLL---AMAEATGRT-----	500
<i>TtAM</i>	PGRP---SGNWAWRLLPGELSP---EHGARLR---AMAEATERL-----	500
<i>CgAM</i>	PGTTRDMYPNWCIPLCDSE-----GNSVLIESLRENELYHRVAKASKRD--	706
<i>EcAM</i>	PGTS-YQYKNWRKLSATLETMFADDGVNKLLKDLDRR---RR-AAAKKK---	694
	*. ** : * *	

(Continued) *StDPE1* = Disproportionating enzyme from *Solonum tuberculsum*, *AtDPE1* = Disproportionating enzyme from *Arabidopsis thaliana*, *SpAM* = Amylomaltase from *Streptococcus pneumonia*, *TaAM* = Amylomaltase from *T. aquaticus*, *TtAM* = Amylomaltase from *T. thermophilus*, *CgAM* = Amylomaltase from *C. glutamicum* and *EcAM* = Amylomaltase from *E.coli*

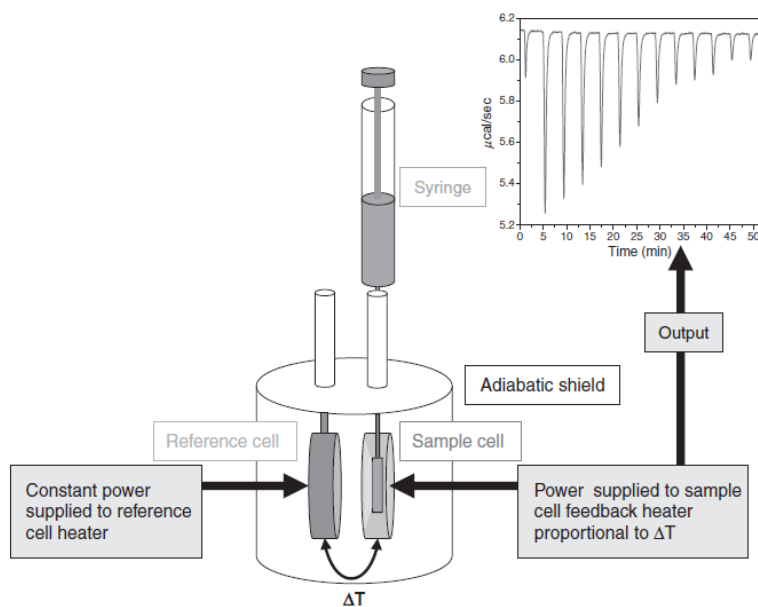


APPENDIX 19: HPAEC profile of standard 0.8 mg/ml LR-CD

APPENDIX 20: Isothermal titration calorimetry (ITC)

ITC is the direct method to measure the heat change that occurs when two molecules are interacted at a constant temperature (Jelesarov and Bosshard, 1999). Heat is released or absorbed as a result of the redistribution of non-covalent bonds when the interacting molecules go from free to the bound state. The experiment is performed by titrating one binding partner (titrant or L) in syringe into a solution containing the other binding partner (titrand or M) in the sample cell of the calorimeter. After each addition of a small aliquot of L, the heat released or absorbed in the sample cell is measured with respect to a reference cell filled with buffer or control sample. The heat change is expressed as the electrical power ($\mu\text{cal/sec}$) required to maintain a constant small temperature difference between sample cell and reference cell, which are both placed in adiabatic jacket (Freyer and Lewis, 2008).

ITC is a one particular type of calorimeter of several that can be used for enzyme kinetic analysis (Hansen *et al.*, 2016). In general, kinetic data obtained from ITC are in the form of the rate of heat production, $(dQ_{\text{measured}}/dt)$ (Hansen *et al.*, 2016). Two types of kinetics of enzyme-catalyzed reactions by ITC was divided into 2 method; multiple injection method and single injection method. The multiple injection method is done by successive injections of substrate solution into an enzyme solution which is commonly used to investigate binding property of biomolecules and enzyme kinetics (Jelesarov and Bosshard, 1999). While single injection method is used for determining enzyme activity which usually requires less experiment time than multiple injection method (Transtrum *et al.*, 2015).

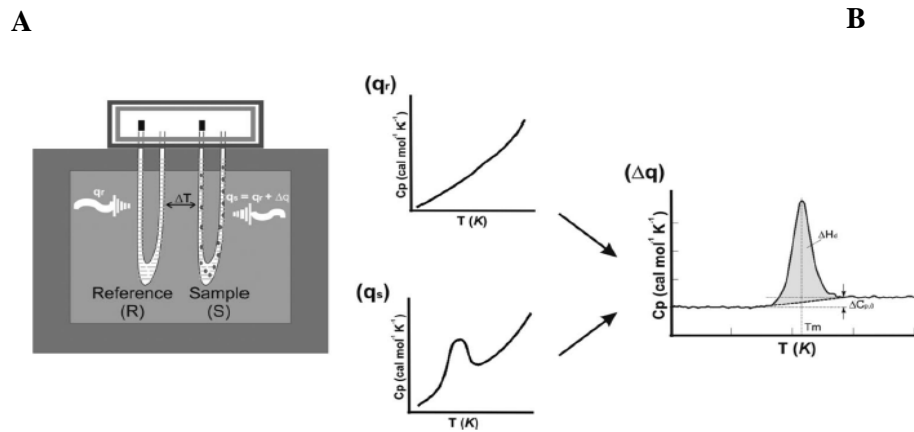


Represent diagram of ITC instrument. Major features of instrument such as the references and sample cells, syringe for adding titrant and the adiabatic shield are noted in figure. This diagram shows an oversimplification how the power applied by the instrument to maintain constant temperature between the references and sample cells is measured resulting instrument signal (Freyer and Lewis, 2008).

APPENDIX 21: Differential scanning calorimetry (DSC)

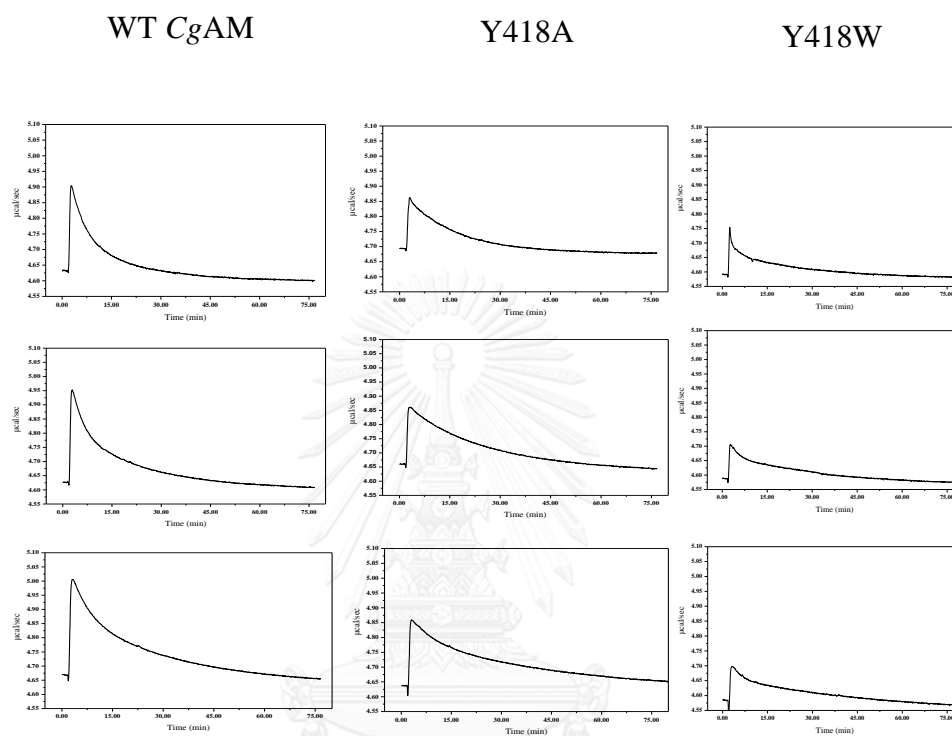
DSC is used to study thermal transitions of biological macromolecules such as protein when temperature increases (Freire, 1995). DSC instrument monitors a small temperature difference between a reference cell that is filled with water or buffer and sample cell that contains the protein of interest in an identical solvent (Johnson, 2013). As the temperature of both cells is increased thermally induced process occurring in the sample cell resulted in heat being absorbed and this produces a change in the temperature difference relative to the reference cell (Jelesarov and Bosshard, 1999). Heaters on the sample cell surface in a feedback circuit input additional electrical power to return the temperature difference to its initial value. This is additional heat is proportional to the excess heat capacity of the thermally induced process. For simple proteins a single heat absorption peak is often observed in the scan.

DSC experiment gives the partial specific heat capacity and transition midpoint or melting temperature (T_m) which is considered as the temperature that half of the protein structure is in native stage and another is denatured (Johnson, 2013). Beside T_m , T_p or peak temperature can be determined. T_p represents the highest value of DSC peak temperature which is easily obtained and also be designated as the thermal stability of molecules (Gill *et al.*, 2010).



Represent diagram for a DSC experiment. The amount of heat required to increase the temperature by the same increments (ΔT) of a sample cell (q_s) is higher than that required for the reference cell (q_r) by the excess heat absorbed by the molecules in the sample (Δq) (A). The resulting DSC scans with the reference subtracted from the sample show how this excess heat changes as a function of temperature. T (K), temperature Kelvin; ΔH_d , change in enthalpy; $\Delta C_{p,d}$, change in C_p ; T_m , transition and melting point; d , denatured (B) (Gill *et al.*, 2010).

APPENDIX 22: Heat production of amylo maltase from disproportionation reaction detected by ITC technique



VITA

Miss Suthipapun Tumhom was born on April 16th, 1985. She graduated with the first class honors in Bachelor degree of Science (Biology) from Faculty of Science, Silpakorn University in 2007. Then she is studying in Ph. D program of the Biochemistry and Molecular Biology, Department of Biochemistry, Faculty of Science, Chulalongkorn University in 2011. She has received Science Achievement Scholarship of Thailand since her undergraduate study till Doctoral degree.

Publications:

Suthipapun Tumhom, Kuakarun Krusong, and Piamsook Pongsawasdi, Y418 in 410s loop is required for high transglucosylation activity and large-ring cyclodextrin production of amylomaltase from *Corynebacterium glutamicum*, *Biophysical and Biochemical Research Communication*, 488 (2017), 515-521.

Suthipapun Tumhom, Kuakarun Krusong, Shun-ichi Kidokoro, Etsuko Katoh and Piamsook Pongsawasdi, Biophysical characterization of wild type and Y418 mutated amylomaltases from *Corynebacterium glutamicum* (under submission to *PIOSONE*).

Awards:

2015 The 1st Runner up for poster presentation in “Cell and Molecular Biology” theme in the 20th Biological Science Graduate Congress, Chulalongkorn University, Bangkok, Thailand

2016 Outstanding Oral Presentation Award in “The 5th International Biochemistry and Molecular Biology Conference, Prince of Songkla University”, Songkla, Thailand.

Grants and fellowships:

2003 - 2006 Science Achievement Scholarship of Thailand (SAST) for Bachelor degree of Science in Biology, Silpakorn University, Thailand

2011 - 2016 Science Achievement Scholarship of Thailand (SAST) for Doctorate degree of Science in Biochemistry and Molecular biology, Chulalongkorn University

2016 Research Grant “Japan Student Service Organization (JASSO)” at Nagaoka University of Technology, Nagaoka, Japan

2016 The 90th anniversary of Ratchadaphiseksomphot Endowment Fund of Chulalongkorn University

2017 The oversea research experience scholarship, Graduate school and Faculty of Science, Chulalongkorn University